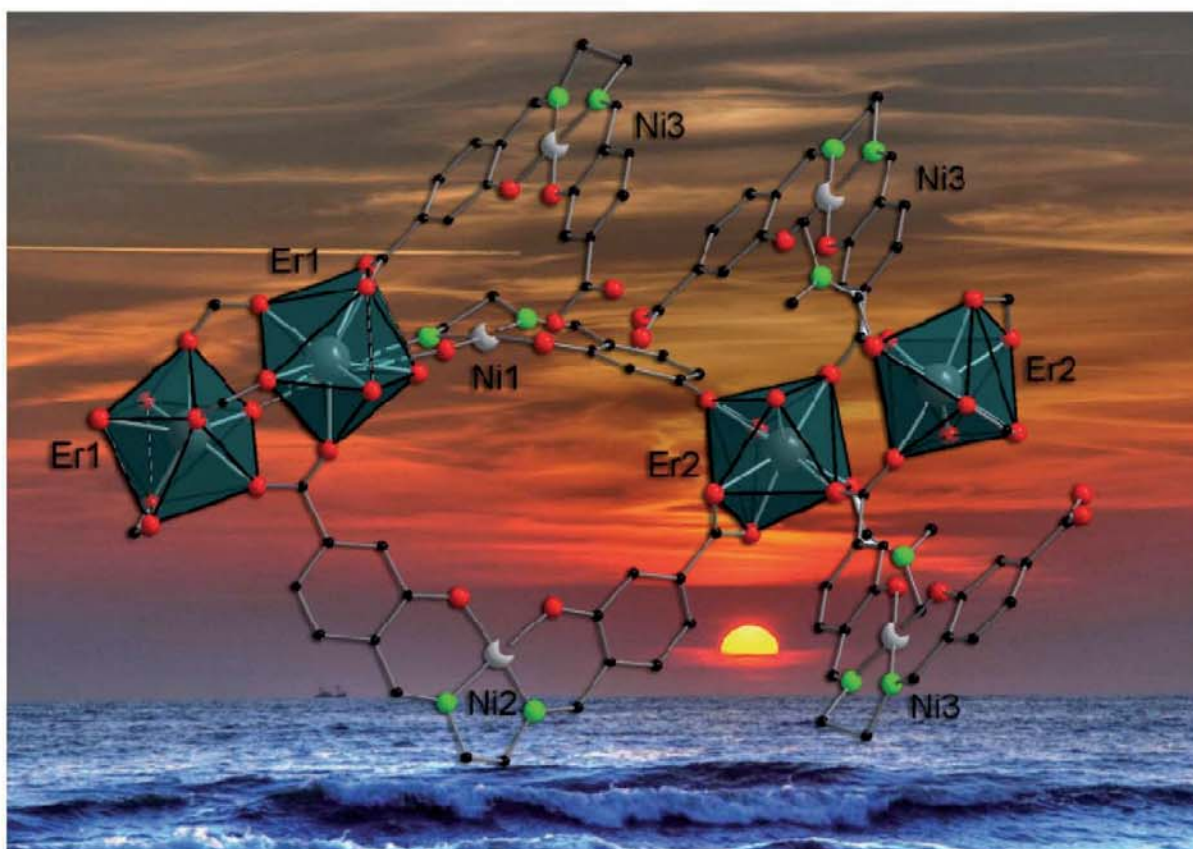


**Functionalized 3d/4f Coordination Oligomers and Polymers.**





# Functionalized 3d/4f Coordination Oligomers and Polymers

Zur Erlangung des akademischen Grades eines

DOKTORS DER NATURWISSENSCHAFTEN

(Dr. rer. nat.)

Fakultät für Chemie und Biowissenschaften

Karlsruher Institut für Technologie (KIT) - Universitätsbereich

vorgelegte

DISSERTATION

von

M. S.-Chem. Asamanjoy Bhunia

aus

Midnapore, Indien

Dekan: Prof. Dr. S. Bräse

Referent: Prof. Dr. P. W. Roesky

Korreferent: Prof. A. K. Powell

Tag der mündlichen Prüfung: 15.07.2011

**Bibliografische Information der Deutschen Nationalbibliothek**

Die Deutsche Nationalbibliothek verzeichnet diese Publikation in der Deutschen Nationalbibliografie; detaillierte bibliografische Daten sind im Internet über <http://dnb.d-nb.de> abrufbar.

1. Aufl. - Göttingen : Cuvillier, 2011  
Zugl.: Karlsruhe, Univ., Diss., 2011

978-3-86955-877-6

© CUVILLIER VERLAG, Göttingen 2011  
Nonnenstieg 8, 37075 Göttingen  
Telefon: 0551-54724-0  
Telefax: 0551-54724-21  
[www.cuvillier.de](http://www.cuvillier.de)

Alle Rechte vorbehalten. Ohne ausdrückliche Genehmigung des Verlages ist es nicht gestattet, das Buch oder Teile daraus auf fotomechanischem Weg (Fotokopie, Mikrokopie) zu vervielfältigen.

1. Auflage, 2011  
Gedruckt auf säurefreiem Papier

978-3-86955-877-6

*Dedicated to my Grandpa and parents*



# Table of contents

<b>1</b>	<b>Introduction.....</b>	<b>1</b>
1.1	The rare earth elements.....	1
1.2	Metal organic frameworks (MOFs).....	3
1.2.1	History and scope.....	3
1.2.2	Salen frameworks.....	5
1.3	Single molecule magnets (SMMs).....	10
<b>2</b>	<b>Research objectives.....</b>	<b>13</b>
<b>3</b>	<b>Results and discussion.....</b>	<b>15</b>
3.1	Salen-based infinite coordination polymers.....	15
3.1.1	N,N'-bis(4-carboxysalicylidene)ethylenediamine with alkali and transition metals.....	16
3.1.1.1	Thermogravimetric analysis of compounds <b>1-3</b> .....	20
3.1.1.2	Magnetic property of compound <b>2</b> .....	21
3.1.2	N,N'-bis (4-carboxysalicylidene)propanediamine (H <sub>4</sub> L <sup>2</sup> ) and N,N'-bis (4-carboxysalicylidene)-1,3-diamino-2-propanol (H <sub>5</sub> L <sup>3</sup> ) ligands with alkali and transition metal.....	22
3.1.2.1	Thermogravimetric analysis of compounds <b>4</b> and <b>5</b> .....	27
3.1.2.2	Magnetic property of compound <b>4</b> .....	28
3.2	Salen-based metal organic frameworks.....	29
3.2.1	Nickel and lanthanide based MOFs.....	29
3.2.1.1	Thermogravimetric analysis of compounds <b>6-11</b> .....	36
3.2.1.2	Gas adsorption of compounds <b>6</b> and <b>9</b> .....	38
3.2.1.3	Magnetic properties of compounds <b>6, 7</b> and <b>10</b> .....	39

3.2.2	Manganese and lanthanides based MOFs.....	42
3.2.2.1	Thermogravimetric analysis of compounds <b>12-16</b> .....	46
3.2.3	Iron and lanthanides based MOFs.....	48
3.2.3.1	Thermogravimetric analysis of compounds <b>17-21</b> .....	53
3.2.3.2	Magnetic properties of compounds <b>19-21</b> .....	54
3.3	Trinuclear Mn(III) and Ni(II) complexes.....	57
3.3.1	Magnetic properties of compounds <b>22</b> and <b>23</b> .....	60
3.4	Lanthanide complexes of hitherto unknown cage ligand ( <i>N,N'</i> -Bis{[2-hydroxy-3-carboxybenzylidene]aminoethylaminoethyl} aminoethylamine) ( $H_4L^5$ ).....	62
3.4.1	<i>Ab initio</i> calculation of compound <b>26</b> .....	65
3.4.2	Magnetic properties of compounds <b>25</b> and <b>26</b> .....	66
3.5	Heterometallic 3d-4f metal complexes.....	71
3.5.1	Trinuclear manganese and lanthanide metal complexes.....	72
3.5.1.1	ESI-MS spectral studies of compounds <b>29-31</b> .....	74
3.5.1.2	<i>Ab initio</i> calculation of compound <b>31</b> .....	79
3.5.1.1	Magnetic properties of compounds <b>30</b> , <b>31</b> and <b>32</b> .....	80
3.5.2	Trinuclear nickel and lanthanide metal complexes.....	85
3.2.1	Magnetic property of compound <b>34</b> .....	87
<b>4</b>	<b>Experimental section</b> .....	<b>88</b>
4.1	Spectroscopic studies.....	88
4.2	Synthesis.....	88
4.2.1	Ligand synthesis.....	89



4.2.1.1	Synthesis of <i>N,N'</i> -Bis (4-carboxysalicylidene)ethylenediamine (H <sub>4</sub> L).....	89
4.2.1.2	Synthesis of <i>N,N'</i> -bis (4-carboxysalicylidene)propanediamine (H <sub>4</sub> L <sup>2</sup> ).....	89
4.2.1.3	Synthesis of <i>N,N'</i> -bis (4-carboxysalicylidene)-1,3-diamino-2-propanol (H <sub>5</sub> L <sup>3</sup> ).....	89
4.2.1.4	Synthesis of <i>N,N'</i> -bis (4-hydroxysalicylidene)-1,3-diamino-2-propanol (H <sub>5</sub> L <sup>4</sup> ).....	90
4.2.2	Synthesis of novel compounds.....	90
4.2.2.1	General procedure for the synthesis of complexes <b>1-2</b> .....	90
4.2.2.1.1	[Na <sub>4</sub> (NiL) <sub>2</sub> ·(H <sub>2</sub> O) <sub>9</sub> ] <sub>n</sub> ( <b>1</b> ).....	91
4.2.2.1.2	[Na <sub>4</sub> (CuL) <sub>2</sub> ·(H <sub>2</sub> O) <sub>9</sub> ] <sub>n</sub> ( <b>2</b> ).....	91
4.2.2.2	Synthesis of [Li(NiHL)(DMSO)] <sub>n</sub> ( <b>3</b> ).....	91
4.2.2.3	Synthesis of [Na <sub>5</sub> {(NiL <sup>2</sup> )(HCOO)(H <sub>2</sub> O) <sub>11</sub> }·(H <sub>2</sub> O) <sub>4</sub> ] <sub>n</sub> ( <b>4</b> ).....	92
4.2.2.4	Synthesis of [Na <sub>4</sub> {(CuHL <sup>3</sup> ) <sub>2</sub> (MeOH) <sub>2</sub> (H <sub>2</sub> O)·(Et <sub>2</sub> O)] <sub>n</sub> ( <b>5</b> ).....	92
4.2.2.5	General procedure for the synthesis of complexes <b>6-9</b> .....	92
4.2.2.5.1	[{Er <sub>2</sub> (NiL) <sub>3</sub> (DMF)(H <sub>2</sub> O) <sub>3</sub> }·(DMF) <sub>4</sub> ·(H <sub>2</sub> O) <sub>10</sub> ] <sub>n</sub> ( <b>6</b> ).....	93
4.2.2.5.2	[{Tm <sub>2</sub> (LNi) <sub>3</sub> (DMF)(H <sub>2</sub> O) <sub>3</sub> }·(DMF) <sub>4</sub> ·(H <sub>2</sub> O) <sub>10</sub> ] <sub>n</sub> ( <b>7</b> ).....	93
4.2.2.5.3	[{Yb <sub>2</sub> (NiL) <sub>3</sub> (DMF)(H <sub>2</sub> O) <sub>3</sub> }·(DMF) <sub>4</sub> ·(H <sub>2</sub> O) <sub>10</sub> ] <sub>n</sub> ( <b>8</b> ).....	93
4.2.2.5.4	[{Lu <sub>2</sub> (NiL) <sub>3</sub> (DMF)(H <sub>2</sub> O) <sub>3</sub> }·(DMF) <sub>4</sub> ·(H <sub>2</sub> O) <sub>10</sub> ] <sub>n</sub> ( <b>9</b> ).....	93
4.2.2.6	Synthesis of [Dy{(NiL)(DMSO)(NO <sub>3</sub> )}(H <sub>2</sub> O) <sub>2</sub> ·(DMSO)] <sub>n</sub> ( <b>10</b> ).....	94
4.2.2.7	Synthesis of [Na <sub>3</sub> Yb{(NiL)(H <sub>2</sub> O)} <sub>3</sub> ·(DMF)] <sub>n</sub> ( <b>11</b> ).....	94
4.2.2.8	General procedure for the synthesis of complexes <b>12-16</b> .....	95
4.2.2.8.1	[Nd <sub>2</sub> (MnLCl) <sub>2</sub> (NO <sub>3</sub> ) <sub>2</sub> (DMF) <sub>5</sub> ·(DMF) <sub>4</sub> ] <sub>n</sub> ( <b>12</b> ).....	95
4.2.2.8.2	[Eu <sub>2</sub> (MnLCl) <sub>2</sub> (NO <sub>3</sub> ) <sub>2</sub> (DMF) <sub>5</sub> ·(DMF) <sub>4</sub> ] <sub>n</sub> ( <b>13</b> ).....	95

4.2.2.8.3	$[\text{Gd}_2(\text{MnLCl})_2(\text{NO}_3)_2(\text{DMF})_5 \cdot (\text{DMF})_4]_n$ ( <b>14</b> ).....	96
4.2.2.8.4	$[\text{Tb}_2(\text{MnLCl})_2(\text{NO}_3)_2(\text{DMF})_5 \cdot (\text{DMF})_4]_n$ ( <b>15</b> ).....	96
4.2.2.8.5	$[\text{Dy}_2(\text{MnLCl})_2(\text{NO}_3)_2(\text{DMF})_5 \cdot (\text{DMF})_4]_n$ ( <b>16</b> ).....	96
4.2.2.9	General procedure for the synthesis of complexes <b>17-21</b> .....	97
4.2.2.9.1	$[\text{Y}_2(\text{FeLCl})_2(\text{NO}_3)_2(\text{DMF})_5 \cdot (\text{DMF})_4]_n$ ( <b>17</b> ).....	97
4.2.2.9.2	$[\text{Eu}_2(\text{FeLCl})_2(\text{NO}_3)_2(\text{DMF})_5 \cdot (\text{DMF})_4]_n$ ( <b>18</b> ).....	97
4.2.2.9.3	$[\text{Gd}_2(\text{FeLCl})_2(\text{NO}_3)_2(\text{DMF})_5 \cdot (\text{DMF})_4]_n$ ( <b>19</b> )... ..	97
4.2.2.9.4	$[\text{Tb}_2(\text{FeLCl})_2(\text{NO}_3)_2(\text{DMF})_5 \cdot (\text{DMF})_4]_n$ ( <b>20</b> )... ..	98
4.2.2.9.5	$[\text{Dy}_2(\text{FeLCl})_2(\text{NO}_3)_2(\text{DMF})_5 \cdot (\text{DMF})_4]_n$ ( <b>21</b> )... ..	98
4.2.2.10	Synthesis of $[\text{Mn}_3\{(\text{H}_2\text{L}^4)(\text{HL}^4)_2(\text{OMe})_2(\text{MeOH})_2\} \cdot (\text{MeOH})_4]$ ( <b>22</b> ).....	98
4.2.2.11	Synthesis of $[\text{Ni}_3(\text{H}_3\text{L}^4)_2(\text{OAc})_2(\text{DMF})_2 \cdot (\text{H}_2\text{O})_3]$ ( <b>23</b> ).....	99
4.2.2.12	General procedure for the synthesis of complexes <b>24-29</b> .....	99
4.2.2.12.1	$[\text{Eu}(\text{H}_2\text{L}^5)_2 \cdot (\text{NO}_3) \cdot (\text{EtOH}) \cdot (\text{H}_2\text{O})_8]$ ( <b>24</b> ).....	99
4.2.2.12.2	$[\text{Tm}(\text{H}_2\text{L}^5)_2 \cdot (\text{NO}_3) \cdot (\text{EtOH}) \cdot (\text{H}_2\text{O})_8]$ ( <b>25</b> ).....	100
4.2.2.12.3	$[\text{Dy}(\text{H}_2\text{L}^5)_2 \cdot (\text{NO}_3) \cdot (\text{EtOH}) \cdot (\text{H}_2\text{O})_8]$ ( <b>26</b> ).....	100
4.2.2.12.4	$[\text{Er}(\text{H}_2\text{L}^5)_2 \cdot (\text{NO}_3) \cdot (\text{EtOH}) \cdot (\text{H}_2\text{O})_8]$ ( <b>27</b> ).....	100
4.2.2.12.5	$[\text{Tm}(\text{H}_2\text{L}^5)_2 \cdot (\text{NO}_3) \cdot (\text{EtOH}) \cdot (\text{H}_2\text{O})_8]$ ( <b>28</b> ).....	101
4.2.2.13	General procedure for the synthesis of complexes <b>29-33</b> .....	101
4.2.2.13.1	$[\text{NH}_2\text{Et}]_2[\text{Eu}(\text{MnL}^5)_2 \cdot (\text{H}_2\text{O})_2 \cdot (\text{ClO}_4)]$ ( <b>29</b> ).....	101
4.2.2.14.2	$[\text{NH}_2\text{Et}]_2[\text{Gd}(\text{MnL}^5)_2 \cdot (\text{H}_2\text{O})_2 \cdot (\text{ClO}_4)]$ ( <b>30</b> ).....	102
4.2.2.14.2	$[\text{NH}_2\text{Et}]_2[\text{Dy}(\text{MnL}^5)_2 \cdot (\text{H}_2\text{O})_2 \cdot (\text{ClO}_4)]$ ( <b>31</b> ).....	102
4.2.2.14.3	$[\text{NH}_2\text{Et}]_2[\text{Tm}(\text{MnL}^5)_2 \cdot (\text{H}_2\text{O})_4 \cdot (\text{ClO}_4)]$ ( <b>32</b> ).....	102
4.2.2.14.4	$[\text{NH}_2\text{Et}]_2[\text{Lu}(\text{MnL}^5)_2 \cdot (\text{H}_2\text{O})_2 \cdot (\text{ClO}_4)]$ ( <b>33</b> ).....	102

4.2.2.15	Synthesis of complex $\text{Dy}\{\text{Ni}(\text{H}_2\text{L}^5)(\text{tren})\}_2\cdot(\text{H}_2\text{O})_{14}\cdot(\text{NO}_3)_3$ ( <b>34</b> ).....	103
<b>5</b>	<b>Crystal structure measurement.....</b>	<b>104</b>
5.1	Data collection with refinement.....	104
5.2	Crystallographic data.....	106
5.2.1	$[\text{Na}_4(\text{NiL})_2\cdot(\text{H}_2\text{O})_9]_n$ ( <b>1</b> ).....	106
5.2.1	$[\text{Na}_4(\text{CuL})_2\cdot(\text{H}_2\text{O})_9]_n$ ( <b>2</b> ).....	106
5.2.3	$[\text{Li}(\text{NiHL})(\text{DMSO})]_n$ ( <b>3</b> ).....	107
5.2.4	$[\text{Na}_5\{(\text{NiL}^2)(\text{HCOO})(\text{H}_2\text{O})_{11}\}\cdot(\text{H}_2\text{O})_4]_n$ ( <b>4</b> ).....	107
5.2.5	$[\text{Na}_2(\text{CuHL}^3)(\text{MeOH})(\text{H}_2\text{O})\cdot(\text{Et}_2\text{O})]_n$ ( <b>5</b> ).....	108
5.2.6	$[\{\text{Er}_2(\text{NiL})_3(\text{DMF})(\text{H}_2\text{O})_3\}\cdot(\text{DMF})_4\cdot(\text{H}_2\text{O})_{10}]_n$ ( <b>6</b> ).....	108
5.2.7	$[\{\text{Tm}_2(\text{NiL})_3(\text{DMF})(\text{H}_2\text{O})_3\}\cdot(\text{DMF})_4\cdot(\text{H}_2\text{O})_{10}]_n$ ( <b>7</b> ).....	109
5.2.8	$[\{\text{Yb}_2(\text{NiL})_3(\text{DMF})(\text{H}_2\text{O})_3\}\cdot(\text{DMF})_4\cdot(\text{H}_2\text{O})_{10}]_n$ ( <b>8</b> ).....	109
5.2.9	$[\{\text{Lu}_2(\text{NiL})_3(\text{DMF})(\text{H}_2\text{O})_3\}\cdot(\text{DMF})_4\cdot(\text{H}_2\text{O})_{10}]_n$ ( <b>9</b> ).....	110
5.2.10	$[\text{Dy}\{(\text{NiL})(\text{DMSO})(\text{NO}_3)\}(\text{H}_2\text{O})_2\cdot(\text{DMSO})]_n$ ( <b>10</b> ).....	110
5.2.11	$[\text{Na}_3\text{Yb}\{(\text{NiL})(\text{H}_2\text{O})\}_3\cdot(\text{DMF})]_n$ ( <b>11</b> ).....	111
5.2.12	$[\text{Nd}_2(\text{MnLCl})_2(\text{NO}_3)_2(\text{DMF})_5\cdot(\text{DMF})_4]_n$ ( <b>12</b> ).....	111
5.2.13	$[\text{Eu}_2(\text{MnLCl})_2(\text{NO}_3)_2(\text{DMF})_5\cdot(\text{DMF})_4]_n$ ( <b>13</b> ).....	112
5.2.14	$[\text{Gd}_2(\text{MnLCl})_2(\text{NO}_3)_2(\text{DMF})_5\cdot(\text{DMF})_4]_n$ ( <b>14</b> ).....	112
5.2.15	$[\text{Tb}_2(\text{MnLCl})_2(\text{NO}_3)_2(\text{DMF})_5\cdot(\text{DMF})_4]_n$ ( <b>15</b> ).....	113
5.2.16	$[\text{Dy}_2(\text{MnLCl})_2(\text{NO}_3)_2(\text{DMF})_5\cdot(\text{DMF})_4]_n$ ( <b>16</b> ).....	113
5.2.17	$[\text{Y}_2(\text{FeLCl})_2(\text{NO}_3)_2(\text{DMF})_5\cdot(\text{DMF})_4]_n$ ( <b>17</b> ).....	114
5.2.18	$[\text{Eu}_2(\text{FeLCl})_2(\text{NO}_3)_2(\text{DMF})_5\cdot(\text{DMF})_4]_n$ ( <b>18</b> ).....	114
5.2.18	$[\text{Gd}_2(\text{FeLCl})_2(\text{NO}_3)_2(\text{DMF})_5\cdot(\text{DMF})_4]_n$ ( <b>19</b> ).....	115
5.2.20	$[\text{Tb}_2(\text{FeLCl})_2(\text{NO}_3)_2(\text{DMF})_5\cdot(\text{DMF})_4]_n$ ( <b>20</b> ).....	115
5.2.21	$[\text{Dy}_2(\text{FeLCl})_2(\text{NO}_3)_2(\text{DMF})_5\cdot(\text{DMF})_4]_n$ ( <b>21</b> ).....	116

5.2.22	[Mn <sub>3</sub> {(H <sub>2</sub> L <sup>4</sup> )(HL <sup>4</sup> )(OMe)(MeOH) <sub>2</sub> }·(MeOH) <sub>4</sub> ] ( <b>22</b> ).....	116
5.2.23	[Ni <sub>3</sub> (H <sub>3</sub> L <sup>4</sup> ) <sub>2</sub> (OAc) <sub>2</sub> (DMF) <sub>2</sub> ·(H <sub>2</sub> O) <sub>3</sub> ] ( <b>23</b> ).....	117
5.2.24	[Eu(H <sub>2</sub> L <sup>5</sup> ) <sub>2</sub> ·(EtOH)·(H <sub>2</sub> O) <sub>8</sub> ·(NO <sub>3</sub> )] ( <b>24</b> ).....	117
5.2.25	[Tb(H <sub>2</sub> L <sup>5</sup> ) <sub>2</sub> ·(EtOH)·(H <sub>2</sub> O) <sub>8</sub> ·(NO <sub>3</sub> )] ( <b>25</b> ).....	118
5.2.26	[Dy(H <sub>2</sub> L <sup>5</sup> ) <sub>2</sub> ·(EtOH)·(H <sub>2</sub> O) <sub>8</sub> ·(NO <sub>3</sub> )] ( <b>26</b> ).....	118
5.2.27	[Er(H <sub>2</sub> L <sup>5</sup> ) <sub>2</sub> ·(EtOH)·(H <sub>2</sub> O) <sub>8</sub> ·(NO <sub>3</sub> )] ( <b>27</b> ).....	119
5.2.28	[Tm(H <sub>2</sub> L <sup>5</sup> ) <sub>2</sub> ·(EtOH)·(H <sub>2</sub> O) <sub>8</sub> ·(NO <sub>3</sub> )] ( <b>28</b> ).....	119
5.2.30	[NHEt] <sub>2</sub> [Eu(MnL <sup>5</sup> ) <sub>2</sub> ·(H <sub>2</sub> O) <sub>2</sub> ·(ClO <sub>4</sub> )] ( <b>29</b> ).....	120
5.2.31	[NHEt] <sub>2</sub> [Dy(MnL <sup>5</sup> ) <sub>2</sub> ·(H <sub>2</sub> O) <sub>2</sub> ·(ClO <sub>4</sub> )] ( <b>31</b> ).....	120
5.2.32	[NHEt] <sub>2</sub> [Tm(MnL <sup>5</sup> ) <sub>2</sub> ·(H <sub>2</sub> O) <sub>4</sub> ·(ClO <sub>4</sub> )] ( <b>32</b> ).....	121
5.2.33	[NHEt] <sub>2</sub> [Lu(MnL <sup>5</sup> ) <sub>2</sub> ·(H <sub>2</sub> O) <sub>2</sub> ·(ClO <sub>4</sub> )] ( <b>33</b> ).....	121
5.2.34	[[Dy{Ni(H <sub>2</sub> L <sup>5</sup> )(tren)} <sub>2</sub> ·(H <sub>2</sub> O) <sub>14</sub> ·(NO <sub>3</sub> ) <sub>3</sub> ] ( <b>34</b> ).....	122
<b>6</b>	<b>Summary.....</b>	<b>123</b>
6.1	Summary.....	123
6.2	Zusammenfassung.....	126
<b>7</b>	<b>Reference.....</b>	<b>130</b>
<b>8</b>	<b>Appendix.....</b>	<b>137</b>
A.1	Directory of abbreviations.....	137
A.1.1	General.....	137
A.1.2	NMR abbreviations.....	138
A.1.3	IR abbreviations.....	138
A.1.4	Magnetic abbreviations.....	139
A.2	Directory of compounds.....	140

# 1 Introduction

## 1.1 The Rare Earth Elements

Lanthanides are the first period of f-block elements ranging from Cerium to lutetium (La-Lu,  $Z = 57-71$ ) in the periodic table. Together with scandium and yttrium, they are called rare earth elements (REEs). Lanthanides have traditionally been divided into two groups: the light rare earth elements (LREEs), lanthanum to europium ( $Z = 57-63$ ), and the heavy rare earth elements (HREEs), gadolinium to lutetium ( $Z = 64-71$ ). When they were first discovered and isolated, they were called "rare earth" elements due to the assumption that they are less abundant compared to other elements. Indeed, all lanthanides (except radioactive promethium) including the least common element, thulium, are more abundant in earth's crust than bismuth, arsenic, cadmium, mercury and other precious metals.<sup>[1]</sup>

**Table 1.1** Some properties of lanthanide atoms and ions.

Atomic number	Name	Symbol	Electronic configuration		$E^0(\text{V})^{[2]}$
			Atom	$M^{3+}$	
57	Lanthanum	La	$[\text{Xe}]5d^16s^2$	$[\text{Xe}]$	-2.38
58	Cerium	Ce	$[\text{Xe}]4f^15d^16s^2$	$4f^1$	-2.34
59	Praseodymium	Pr	$[\text{Xe}]4f^36s^2$	$4f^2$	-2.35
60	Neodymium	Nd	$[\text{Xe}]4f^46s^2$	$4f^3$	-2.32
61	Promethium	Pm	$[\text{Xe}]4f^56s^2$	$4f^4$	-2.29
62	Samarium	Sm	$[\text{Xe}]4f^66s^2$	$4f^5$	-2.30
63	Europium	Eu	$[\text{Xe}]4f^76s^2$	$4f^6$	-1.99
64	Gadolinium	Gd	$[\text{Xe}]4f^75d^16s^2$	$4f^7$	-2.28
65	Terbium	Tb	$[\text{Xe}]4f^96s^2$	$4f^8$	-2.31
66	Dysprosium	Dy	$[\text{Xe}]4f^{10}6s^2$	$4f^9$	-2.29
67	Holmium	Ho	$[\text{Xe}]4f^{11}6s^2$	$4f^{10}$	-2.33
68	Erbium	Er	$[\text{Xe}]4f^{12}6s^2$	$4f^{11}$	-2.32
69	Thulium	Tm	$[\text{Xe}]4f^{13}6s^2$	$4f^{12}$	-2.32
70	Ytterbium	Yb	$[\text{Xe}]4f^{14}6s^2$	$4f^{13}$	-2.22
71	Lutetium	Lu	$[\text{Xe}]4f^{14}5d^16s^2$	$4f^{14}$	-2.30

<sup>[2]</sup> $\text{Ln}^{3+} + 3e^- = \text{Ln}$

The rare earth elements along with some of their principal characteristics are listed in Table 1.1. Going from lanthanum to lutetium, fourteen 4f-electrons are added, causing the electronic configuration to change from  $[\text{Xe}]5d^16s^2$  to  $[\text{Xe}]4f^{14}5d^16s^2$ , with slight irregularities in the case of some elements (Table 1.1). Also, the highly electropositive character of lanthanide elements is comparable to that of alkali and alkaline earth metals. The formation of predominantly ionic compounds is expected, and the +3 oxidation state is the most stable. In fact, the energy of the 4f orbitals is lower than that of the 6s and 5d orbitals; therefore, two 6s electrons and one 5d electron are easier to remove than the 4f electrons leading to a +3 oxidation state. The +2 and +4 oxidation states also exist, but they can revert to +3 *e.g.* Sm(II), Eu(II) and Yb(II) lose one electron to become +3. Thus, these divalent lanthanides are good reducing agents. Eu(II) and Yb(II) are the most stable divalent species<sup>[3]</sup> because they are somewhat stabilized by the  $4f^7$  and  $4f^{14}$  configuration (from exchange energy) and enjoy the stability of half-filled and filled subshells.<sup>[4]</sup> In contrast, the tetravalent lanthanide ions can be reduced to adopt the +3 oxidation state, making them good oxidizing agents. Generally, an oxidation state +4 is exhibited by cerium, praseodymium, and terbium but in aqueous solution only cerium(IV) is stable (kinetically). Some of its salts are cerium(IV) ammonium nitrate, cerium(IV) sulfate, etc.

The lanthanides exhibit a feature, called lanthanide contraction,<sup>[5]</sup> which refers to the penetration of the 4f subshell by the 5s and 5p, such that the 4f orbital is not shielded from the increasing nuclear charge. An atomic radius decreases throughout the lanthanide series with increase in atomic number; hence, the ionic radii of lanthanide ions decrease from lanthanum to lutetium. To illustrate this concept, ionic radii of the nine coordinate trivalent lanthanides and yttrium are shown in Table 1.2.

The 4f orbitals of the lanthanides have less radial extension than the filled  $5s^2$  and  $5p^6$  orbitals and are thus shielded from external perturbations. The 4f electrons have little involvement in covalent interactions upon the formation of chemical bonds, therefore, Ln(III) ions display large and variable coordination numbers (CN = 8–12).<sup>[6]</sup>

**Table 1.2.** Ionic radii of trivalent nine-coordinate rare earth metal ions.

Ln <sup>3+</sup>	Ionic radius [Å]	Ln <sup>3+</sup>	Ionic radius [Å]
La	1.216	Tb	1.095
Ce	1.196	Dy	1.083
Pr	1.179	Y	1.075
Nd	1.163	Ho	1.072
Pm	1.144	Er	1.062
Sm	1.132	Tm	1.052
Eu	1.120	Yb	1.042
Gd	1.107	Lu	1.032

The variable and versatile coordinating behavior of lanthanide ion, Ln<sup>3+</sup>, limits its selective introduction into organized molecular or supramolecular architectures.<sup>[7]</sup> Several types of lanthanide-based complexes have been successfully developed into functional molecular devices, such as luminescence sensors and light converters, nuclear magnetic resonance (NMR),<sup>[7],[8],[9]</sup> magnetic resonance imaging (MRI),<sup>[10],[11]</sup> catalysts in organic synthesis and biological reactions,<sup>[12],[13]</sup> gas adsorption<sup>[14]</sup> and magnetism<sup>[15]</sup> in the fields of chemistry, biology, medicine and materials science, respectively. Recent interest in coordination chemistry to synthesize lanthanide-based metal organic frameworks (MOFs) has been sparked because of their unique properties, offering a wide range potential applications including nonlinear optics, gas storage and catalysis.

## 1.2 Metal Organic Frameworks (MOFs)

### 1.2.1 History and Scope

One of the very first MOFs was isolated in 1943, formulated as [Ag<sub>2</sub>(C<sub>2</sub>O<sub>4</sub>)]<sub>n</sub>, although similar studies from the early 1930s are also known.<sup>[16]</sup> In 1965, Tomic *et al.* synthesized a series of metal complexes from an aromatic carboxylic acid, which would nowadays be called MOFs.<sup>[17]</sup> In the late 1980s and early 1990s, this field was further developed by Robson after he initiated his famous "node-and-spacer" concept.<sup>[18]</sup> Then, in the late 1990s, the concept of

reticular design was initiated by Yaghi *et al.*<sup>[19],[20]</sup> The development of these two concepts has caused this field to become a hot topic in chemistry, and now a plethora of MOFs are known.

MOFs are a type of coordination polymer constructed from metal ions or metal ion clusters and organic bridging ligands.<sup>[21],[22],[23],[24],[25]</sup> The organic ligands act as linkers and are considered "struts" that bridge metal centers. The combination of a metal center and a linker are regarded as inorganic secondary building units (SBUs), which act as joints in the resulting MOF architecture.<sup>[23],[26],[27]</sup> The metal centers and ligands are connected to each other by coordination bonds, which, together with other intermolecular interactions, form a network with a definite topology. In most cases, the organic linkers are multidentate ligands - usually carboxylates, azoles, nitriles, etc. The metal centers used for this purpose are mainly 3d metal ions such as zinc, nickel, iron, copper, manganese and cobalt ions.<sup>[26]</sup> For example, **MOF-5**, reported by Yaghi *et al.* is formulated as  $[\text{Zn}_4\text{O}(\text{BDC})_3 \cdot (\text{DMF})_8 \cdot (\text{C}_6\text{H}_5\text{Cl})]$  ( $\text{H}_2\text{BDC}$  = 1,4-benzenedicarboxylate).<sup>[28]</sup>

Due to the size of the ligands, inorganic connecting points and network connectivity, the porosity of MOFs can be readily tuned to afford open channels and pores with dimensions from several angstroms to several nanometers. Because of their stability, MOFs can be used for gas storage,<sup>[29],[30]</sup> separation,<sup>[31],[32]</sup> magnetic materials,<sup>[33]</sup> luminescence,<sup>[34]</sup> drug storage and drug delivery.<sup>[35],[36]</sup>

Usually, MOFs are synthesized by a common method known as the solvent evaporation process,<sup>[37]</sup> in which a saturated solution is slowly evaporated or cooled, resulting in crystalline or amorphous materials. A wide variety of other methods such as diffusion, microwave reaction and ultrasonication have also been established.<sup>[38],[39],[40]</sup> Another very useful method for the synthesis of MOFs is the hydro(solvo)thermal process. Usually, the temperature that is used in this approach ranges from 80-260°C (*i.e.* higher than the boiling point of the solvent molecule). Frameworks, regardless of their synthetic method, are heavily influenced by factors such as structural characteristics of the ligands, the coordination nature of the metal ions, the solvent systems, the template, the pH value of the solution, steric requirement of the counterion, reaction temperature and the metal to ligand ratio.

Although many MOFs have been synthesized so far, it is still a challenge to explore successful synthetic strategies that lead to MOFs with promising applications and intriguing structures. In this thesis, attempts were made to design new MOFs using the self-assembly of metal ions (mainly manganese, iron, nickel and copper with lanthanides) and salen ligands.



## 1.2.2 Salen Frameworks

Salen ligands are common ligands in coordination chemistry. The name "salen" is abbreviated from the contraction of "salicylaldehyde" and "ethylenediamine" (*i.e.* salen = 2sal + en). This type of ligand is synthesized by a simple condensation reaction of a salicylaldehyde and ethylenediamine. In contrast to salen ligand, the schiff base ligand which contain the azomethine group (-CH=N-) and it is synthesized by the condensation reaction of a primary amine with carbonyl compound. Salen ligands form complexes with metal ions *via* nitrogen and oxygen donor atoms.<sup>[41]</sup> Steric and electronic effects around the metal core can be finely turned through the appropriate selection of electron-withdrawing or electron-donating substituents of different size in the salen ligands (Figure 1.1). The nitrogen and oxygen atoms induce two opposite electronic effects: the phenolate oxygen atoms are regarded as a hard donor, which stabilizes higher oxidation states of the metal ion, while the imine nitrogen atoms are softer donors and will stabilize lower oxidation states.<sup>[42]</sup> As a result, these ligands can stabilize many different metals in various oxidation states; therefore, metallosalens have the potentials to be used in different areas such as catalysis, zeolite matrices, luminescence, magnetism.<sup>[43],[44],[45],[46]</sup>

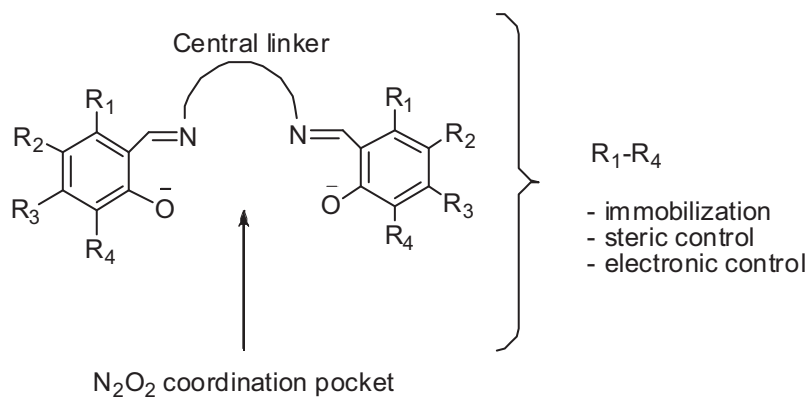
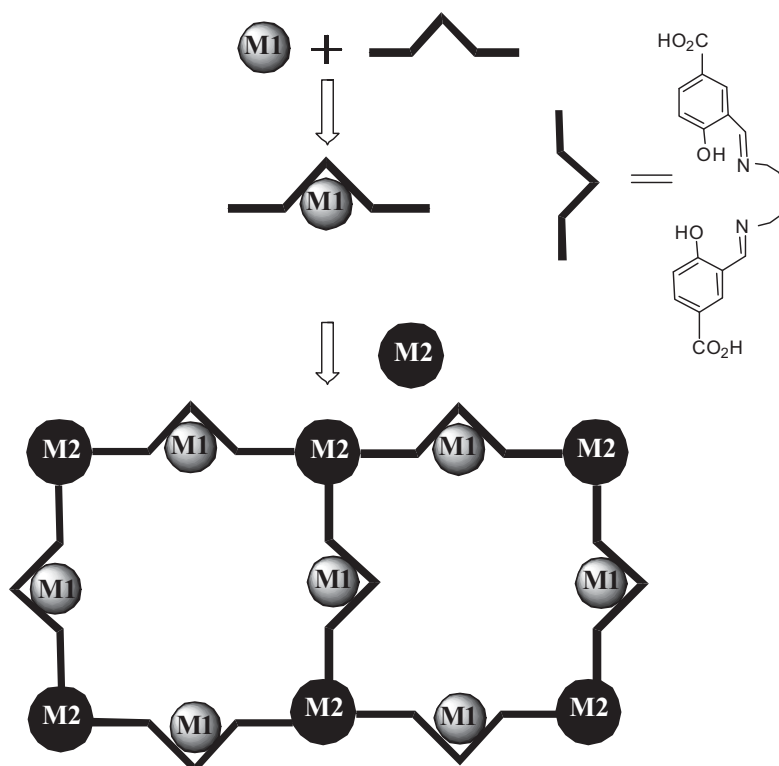


**Figure 1.1** General structure of a symmetrical salen. The substitution at the phenyl rings may be used for immobilization and/or easy control over the ligand properties.

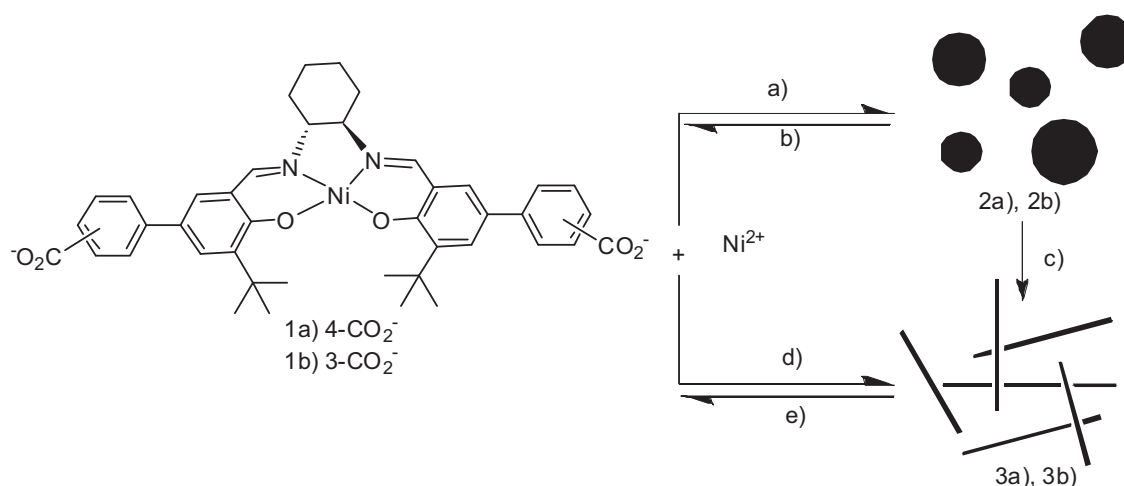
Some previously reported work demonstrate the various features of the chemistry of salen ligands. These examples are compared to the results obtained during this thesis work. Kitagawa and coworkers reported microporous coordination polymers (MCPs) with unsaturated metal centers (UMCs) using metalloligand (ML) systems. The assembly of the MCPs is a two step process: (1) synthesis of ML by the reaction of well-defined salen ligands and metal ions (mainly 3d metal ions) that together act as a linker (M1), and (2) reaction of

ML with another metal ion (M2), which acts as a nodal unit in a framework.<sup>[47],[48]</sup> Thus, two types of metal centers are present in MCPs which shown in Scheme 1.1.



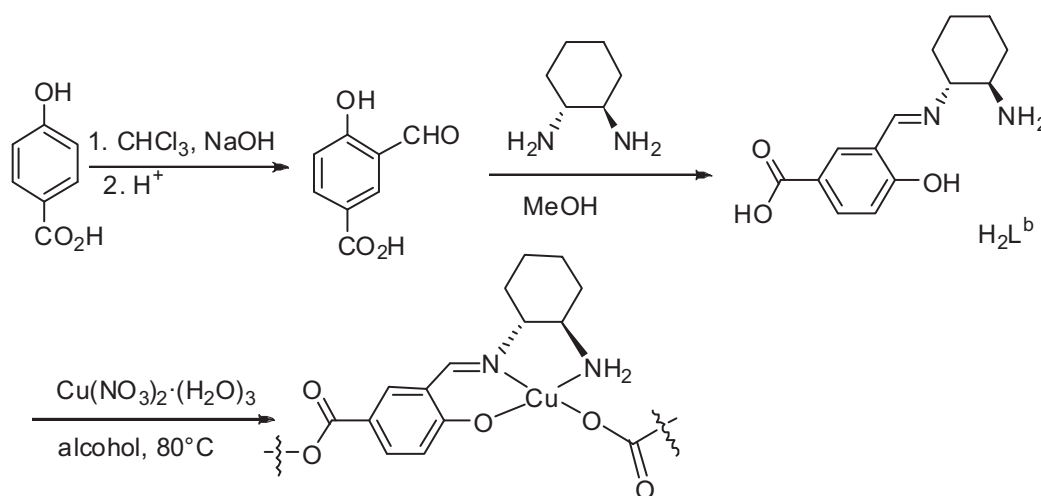
**Scheme 1.1** MCPs formed upon addition of M2 from metalloligand system.

In 2007, Mirkin *et al.* studied the interconversion between amorphous and crystalline microparticles that are built from Ni-salen-dicarboxylic acid and an excess amount of Ni(OAc)<sub>2</sub>·(H<sub>2</sub>O)<sub>4</sub> (Scheme 1.2).<sup>[49]</sup> The same authors synthesized the chiral building block (*S*)-H<sub>4</sub>L<sup>a</sup> by using an imine coupling reaction of the enantiopure (*S*)-binaphthyl diamine and 4-formyl-3-hydroxybenzoic acid. This (*S*)-H<sub>4</sub>L<sup>a</sup> ligand was further reacted with Cu(OAc)<sub>2</sub>·(H<sub>2</sub>O)<sub>6</sub> to form homochiral triangular macrocycles and helical coordination polymers.<sup>[50]</sup>



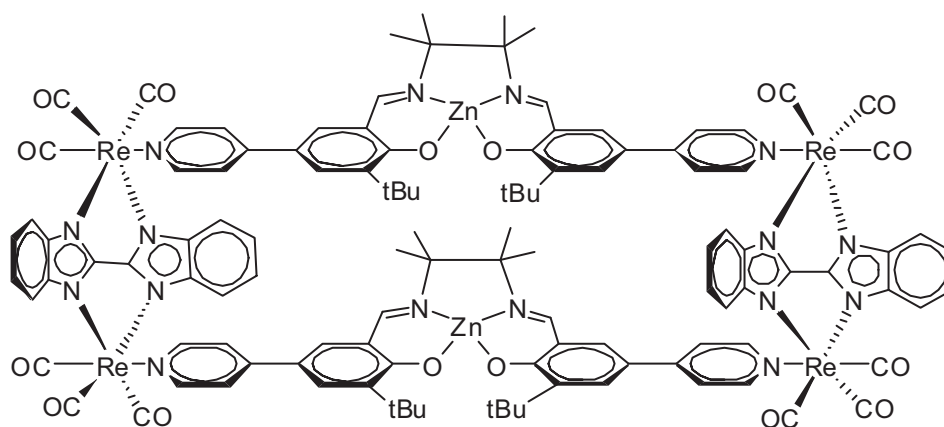
**Scheme 1.2** Synthesis of salen based microparticles and their dynamic solvent-triggered crystallization process: (a) pyridine / ether, (b) pyridine, (c) methanol, (d) pyridine / methanol, (e) pyridine. Amorphous microparticle: 2a, 2b; crystalline rod: 3a, 3b

Cui *et al.* carried out chiral recognition and separation using a 2D coordination polymer built from unsymmetrical chiral Schiff base metal complexes (Scheme 1.3).<sup>[51]</sup>



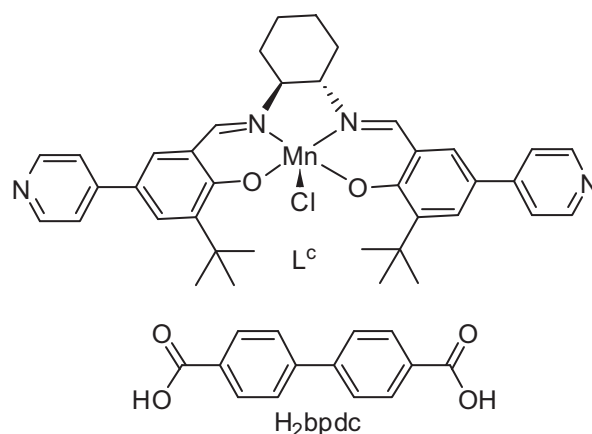
**Scheme 1.3** Synthesis of the H<sub>2</sub>L<sup>b</sup> ligand and copper polymer.

Nguyen and Hupp established a salen-containing loop-type structure synthesized from a platinum precursor.<sup>[52]</sup> A subsequent ligand rigidification, either by post-metalation or direct use of the respective Zn-salen precursors, favors the formation of box-like structures. Moreover, Hupp *et al.* reported a box-assembled coordination polymer, in which Zn-salen coordinates to a rhenium center (Scheme 1.4). This compound exhibits photophysical properties.<sup>[53]</sup>



**Scheme 1.4** Scheme of the box like assemble for zinc-rhenium complex.

Hupp and coworkers also reported a homochiral MOF constructed from chiral Mn-salen, biphenyl-4,4'-dicarboxylic acid ( $H_2bpdC$ ) and  $Zn^{2+}$  ions (Scheme 1.5). The framework,  $[Zn_2(bpdC)_2(L^c) \cdot (DMF)_{10} \cdot (H_2O)_8]_n$  (abbreviated  $[Zn_2L^c(bpdC)]_n$ ), was obtained under solvothermal conditions and shows a two-fold interpenetrating 3D network with 57% solvent accessible volume (Figure 1.2).<sup>[54]</sup> The channels in the  $a$  and  $c$  directions possess dimensions of  $6.2 \times 6.2 \text{ \AA}$  and  $6.2 \times 15.7 \text{ \AA}$ , respectively. Due to the diagonal displacement of the network, all Mn(III) ion sites are accessible through the channels. This homochiral MOF was examined for asymmetric olefin epoxidation reactions, and it was shown to effectively catalyze the epoxidation in 82% ee (Scheme 1.6).



**Scheme 1.5** Chiral bridging Mn-salen complex and the achiral ligand  $H_2bpdC$ .

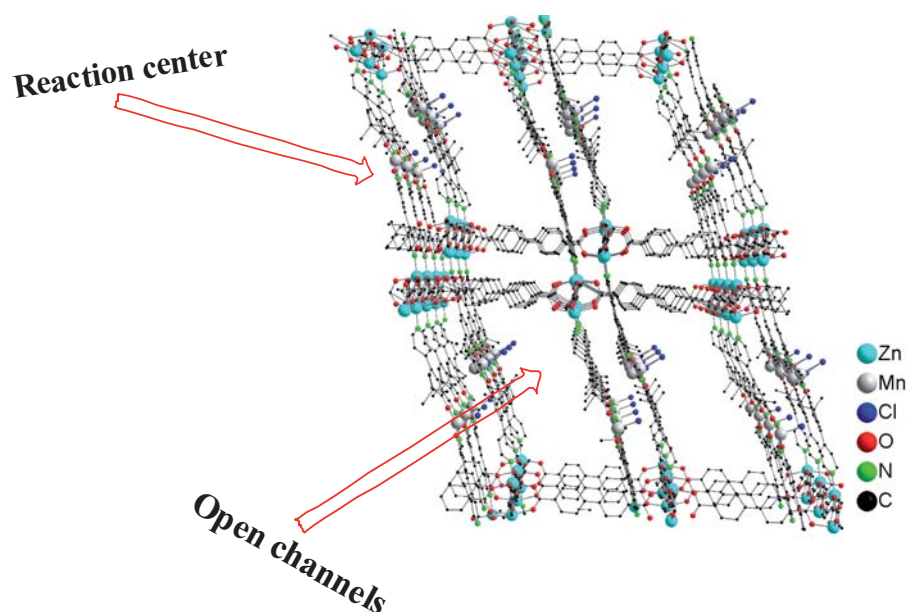
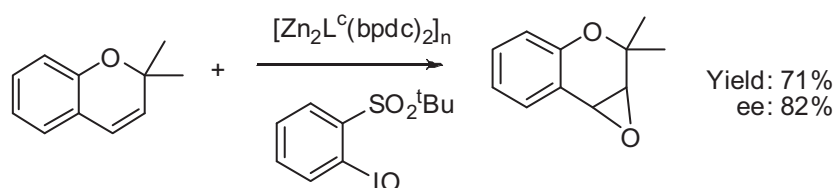
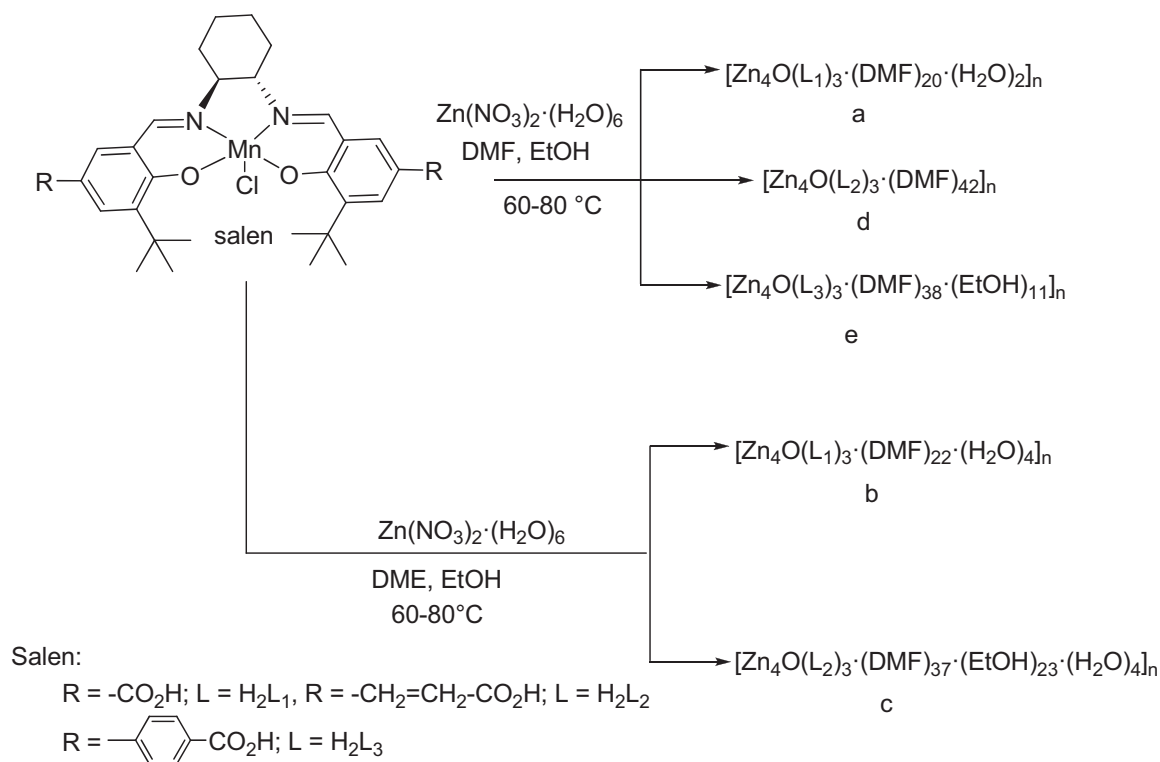


**Figure 1.2** Pictorial representation of the open channels and catalytic active sites of compound  $[\text{Zn}_2\text{L}^a(\text{bpdc})]_n$



**Scheme 1.6** Asymmetric epoxidation catalysed by the homochiral MOF  $[\text{Zn}_2\text{L}^c(\text{bpdc})]_n$ .

Chen *et al.* reported a mixed metal organic framework (M'MOF), formulated as  $[\text{Zn}_3(\text{BDC})_3\{\text{Cu}(\text{Pyen})\} \cdot (\text{DMF})_5 \cdot (\text{H}_2\text{O})_5]_n$  ( $\text{H}_2\text{BDC}$  = 1,4 benzenedicarboxylic acid and  $\text{H}_2\text{Pyen}$  = 5-methyl-4-oxo-1,4-dihydro-pyridine-3-carbaldehyde), containing 36 tessellated  $\text{Zn}_3(\text{BDC})_3$  2D sheets that are pillared by  $\text{Cu}(\text{Pyen})$  to form a 3D network.<sup>[55]</sup> This compound has slightly greater  $\text{D}_2$ -surface than  $\text{H}_2$ -surface interactions, while  $\text{D}_2$ - $\text{D}_2$  interactions are lower than  $\text{H}_2$ - $\text{H}_2$  interactions. Interestingly, Lin *et al.* reported isoreticular chiral metal organic frameworks (CMOFs) which are constructed from  $[\text{Zn}_4(\mu_4\text{-O})(\text{O}_2\text{CR})_6]$  ( $\text{R}$  = organic linker) SBUs and systematically elongated dicarboxylate struts that are derived from chiral Mn-salen catalytic subunits (Scheme 1.7).<sup>[56]</sup>



**Scheme 1.7** Synthetic scheme of compounds **a-e**.

Compounds **a-e** are highly effective catalysts for the asymmetric epoxidation of a variety of unfunctionalized olefins up to 92% ee. The rate of the epoxidation reaction depends on the dimensions of the open channel of the CMOFs. These compounds can be reused after catalytic transformations.

### 1.3 Single Molecule Magnets (SMMs)

In the early 1990s, the discovery of single molecule magnets (SMMs) created a new research field in physics and chemistry.<sup>[57],[58]</sup> The final goal of this research activity is to modulate the quantum properties of these nanosized magnets in order to store and address a large amount of information in specialized devices and to provide basic components for future quantum computers.<sup>[59],[60]</sup>

SMMs are nanoscale magnetic molecules that exhibit slow relaxation of magnetization at low temperatures, *i.e.* below their blocking temperature,  $T_B$ .<sup>[61],[62]</sup> The main requirements for observing such behavior in molecules are a high spin ground state ( $S$ ) and a significant negative zero-field splitting ( $D$ ) of that ground state. The negative axial anisotropy ( $D < 0$ )

removes the degeneracy in the  $M_s$  levels of the ground spin state, placing higher magnitude levels at lower energies. The selection rule,  $\Delta M_s = \pm 1$ , for allowed transitions results in an energy barrier ( $U$ ), separating the two lowest energy levels,  $M_s = \pm S$ . The spin reversal energy barrier will be  $U = S^2 |D|$  and  $U = (S^2 - 1/4) |D|$  for integer and half-integer  $S$  values, respectively. A positive  $D$  value causes  $M_s = 0$  levels to be lowest in energy, such that there is no energy cost for losing direction of the spin (*i.e.* in going from  $M_s = +S$  to  $M_s = 0$ ). This means that for a molecule to behave as a SMM, it should have a negative  $D$  value. Experimentally, a SMM shows superparamagnet-like properties, exhibiting both a frequency-dependent out-of-phase alternating current (ac) magnetic susceptibility signal and a hysteresis plot of magnetization versus applied direct current (dc) magnetic field.

The field of SMMs, or molecular nanomagnets, started with the mixed-valence complex,  $[\text{Mn}_{12}\text{O}_{12}(\text{OAc})_{16}(\text{H}_2\text{O})_4] \cdot (\text{HOAc})_2 \cdot (\text{H}_2\text{O})_4$  (abbreviated  $\text{Mn}_{12}\text{Ac}$ ).<sup>[63],[64],[65],[66],[67]</sup>  $\text{Mn}_{12}\text{Ac}$  contains twelve manganese ions, in which there are four Mn(IV) ions and eight Mn(III) ions. All of these Mn(IV) and Mn(III) ions are independently ferromagnetically coupled with  $S = 3/2$  and  $S = 2$ , respectively. Since four Mn(IV) ions are coupled antiferromagnetically with eight Mn(III) ions in the cluster, the total spin is  $S = 8 \times 2 - 4 \times 3/2 = 10$  and it therefore possesses  $M_s = +10$  to  $-10$ , which is divided by a potential energy barrier of around  $50 \text{ cm}^{-1}$  (as  $U = S^2|D|$ ) (Figure 1.3).

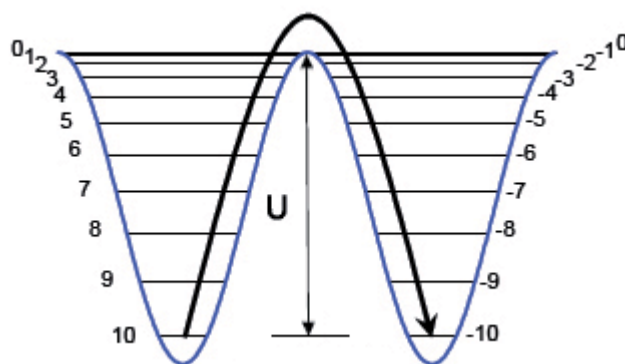


**Figure 1.3** Energy of a classical  $S = 10$  magnetic moment as a function of the angle between the moment and the main anisotropy axis (green). The horizontal lines are the energies of the spin microstates belonging to the  $S = 10$  multiplet.<sup>[57]</sup>

The ac magnetic susceptibility measurements enable the measurement of the relaxation rate. In this process, the susceptibility of a sample is measured using a small ac magnetic field that switches direction at a fixed frequency. As the switching frequency starts to approach the

relaxation rate for the magnetization of the molecules, the in-phase, or real component, of the ac susceptibility ( $\chi'$ ) starts to decrease, while the out-of-phase, or imaginary component, of the ac susceptibility ( $\chi''$ ) increases. Since the energy levels are thermally activated, the energy barrier ( $U_{eff}$ ) and the relaxation rate ( $\tau$ ) of the molecule can be estimated by using an Arrhenius plot according to the Arrhenius expression,

$$\tau = \tau_0 e^{(U_{eff}/K_B T)}$$

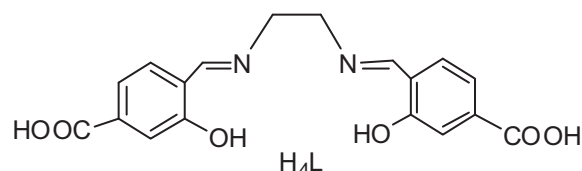
where  $\tau_0$  is a pre-exponential factor and  $U_{eff}$  is the energy barrier to reverse the direction of magnetization in the molecule. A plot of  $\ln(\tau)$  versus  $1/T$  ( $T$  = temperature) of this molecule is linear, and the slope and intercept obtained correspond to  $U_{eff}$  and  $\tau_0$ , respectively.

Although most SMMs are based on polynuclear transition metal complexes, trivalent lanthanides also play a special role because of their unique magnetic properties.<sup>[68]</sup> Some lanthanide ions have a significant spin and/or a large intrinsic single-ion anisotropy arising from the large, unquenched orbital angular momentum; therefore, lanthanide ions have become attractive candidates for constructing new SMMs.<sup>[69]</sup> Murugesu *et al.* have recently reported a Dy<sub>4</sub> butterfly compound that displays the largest anisotropy barrier (~170 K) reported for a polynuclear species.<sup>[70]</sup> Interestingly, even mononuclear complexes can show strong, slow relaxation behaviour at relatively high temperatures, as reported by the Ishikawa group.<sup>[71]</sup> In this regard, clusters of mixed 3d-4f metals are of considerable interest because a combination of properties may allow the observation of high spin clusters with a large anisotropy resulting from magnetic interactions between the ions. For this reason, a number of polynuclear heterometallic 3d-4f clusters have recently been reported,<sup>[72],[73]</sup> some of which display SMM behavior.<sup>[73],[74]</sup>



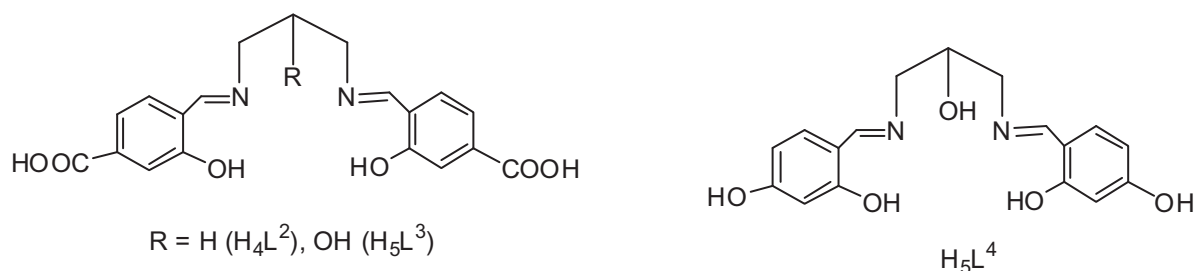
## 2 Research Objectives

The general aim of this project is to synthesize MOFs and coordination clusters using salen ligands. The initial strategy was to synthesize the salen ligand, *N,N'*-bis(4-carboxysalicylidene)ethylenediamine ( $H_4L$ ), which contains carboxylic acids group as linkers (Scheme. 2.1).



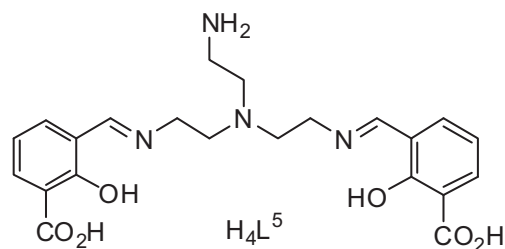
**Scheme 2.1** Chemical structure of the ligand  $H_4L$ .

In the  $H_4L$  ligand, the carboxylic groups are in the *meta* position with respect to the phenoxylate group. Similar ligands were used in transition metal chemistry with promising results,<sup>[47],[49-50]</sup> but the  $H_4L$  ligand was previously unknown in coordination chemistry. The first target was to synthesize the 3d metal salen (ML) complexes. Since 3d-4f-block MOFs have recently gained considerable attention due to their potential applications in hydrogen storage and catalysis. Therefore, another goal was to synthesize such compounds *via* the reaction of the metallosalen compounds with lanthanide ions. Several reports have shown that coordinatively unsaturated metal centers embedded within the MOFs can participate directly in the binding of  $H_2$ . The plan of this work is to study the gas adsorption properties of the porous 3d-4f-block MOFs. Additionally, incorporation of lanthanides also offers the possibility to study the magnetic properties due to their large number of unpaired electrons and considerable single-ion anisotropy. Furthermore, there was interest to change the amine part as well as the aldehyde part of the  $H_4L$  ligand in order to vary the porosity and size of the MOFs. To pursue this interest, we have synthesized the *N,N'*-bis(4-carboxysalicylidene)propanediamine ( $H_4L^2$ ), *N,N'*-bis(4-carboxysalicylidene)-1,3-diamino-2-propanol ( $H_5L^3$ ) and *N,N'*-bis(4-hydroxysalicylidene)-1,3-diamino-2-propanol ( $H_5L^4$ ) ligands (Scheme 2.2), which used to make metal complexes.



**Scheme 2.2** Chemical structure of ligands  $H_4L^2$ ,  $H_5L^3$  and  $H_5L^4$ .

The next goal is to prepare the polypodal ligand, (*N,N'*-bis{[2-hydroxy-3-carboxybenzylidene]-aminoethyl}aminoethylamine) ( $H_4L^5$ ) (Scheme 2.3), in order to synthesize oligomeric compounds. In contrast to  $H_4L$ , the  $H_4L^5$  ligand is more flexible, and the carboxylate group is present in ortho position with respect to the phenoxylate group. Also, the amine part of  $H_4L^5$  is different from the  $H_4L$  ligand (Scheme 2.3), the  $H_4L^5$  ligand contains multiple coordination sites that are in close proximities. Each coordination site possesses a different affinity towards transition metals and lanthanides, which might be facilitate the synthesis of cluster compounds. Thus, the target is the synthesis of mononuclear lanthanide and trinuclear 3d-4f heterometallic cluster compounds in order to examine their magnetic properties.



**Scheme 2.3** Chemical structure of the polypodal ligand ( $H_4L^5$ ).

## 3 Results and Discussions

### 3.1 Salen-Based Infinite Coordination Polymers<sup>1</sup>

Infinite coordination polymers (ICPs) are an area of growing interest in chemistry. In material science recently ICPs particles with micro- or nanostructural dimensions were reported.<sup>[75],[76]</sup> In contrast to MOFs,<sup>[23],[77],[78],[79],[80]</sup> ICPs were reported to show a higher level of structural tailorability.<sup>[76]</sup> The structures of these kinds of compounds were usually synthesized from the appropriate metal salts and bifunctional ligands. Among others one successful strategy in the synthesis of ICPs and MOFs was the use of metal-based ligands<sup>[41],[76],[81],[82],[83],[84]</sup> such as  $[(\eta^6\text{-1,4-benzenedicarboxylate})\text{Cr}(\text{CO})_3]$ ,<sup>[85]</sup> carboxylate functionalized salen (*N,N'*-phenylenebis(salicylideneimine)) templates,<sup>[86]</sup> and functionalized salen (*N,N'*-bis(salicylidene)ethylenediamine) ligands.<sup>[87]</sup> In this metalloligand approach, functionalized salen ligands coordinate to a transition metal center, forming a metalloligand (ML; M = metal) which is suitable for the construction of higher dimensional homo- or heterometallic ICPs or MOFs by reaction with further metal centers. Interest in such metalloligands comes from the fact that metal can have an unsaturated environment of M center, which might be useful for hydrogen storage.<sup>[81]</sup> Another potential application could be homogeneous catalytic transformations such as the epoxidation of olefins, lactide polymerization, asymmetric ring opening of epoxides, and Michael reactions.<sup>[54],[88]</sup> Until now, various ICPs and MOFs with an additional functional group such as carboxylates,<sup>[86]</sup> *p*-pyridyl groups,<sup>[54]</sup> and *p*-benzoic acid groups<sup>[89],[49]</sup> in the *para* position to the hydroxyl group have been reported. Additionally, it has been theoretically investigated and proposed that the capability for hydrogen storage of ICPs or MOFs can be increased by including unsaturated  $\text{Na}^+$  or  $\text{Li}^+$ .<sup>[90],[91]</sup>

A different approach to construct the ICPs or MOFs by using the ligand *N,N'*-bis(4-carboxysalicylidene)ethylenediamine ( $\text{H}_4\text{L}$ ), which is a salen ligand having carboxylate groups in the *meta* position to the hydroxyl groups. The different stereochemistry compared to the established systems results in different angles which are expected to have a significant influence on the shape of the coordination polymer. The ligand  $\text{H}_4\text{L}$  was synthesized

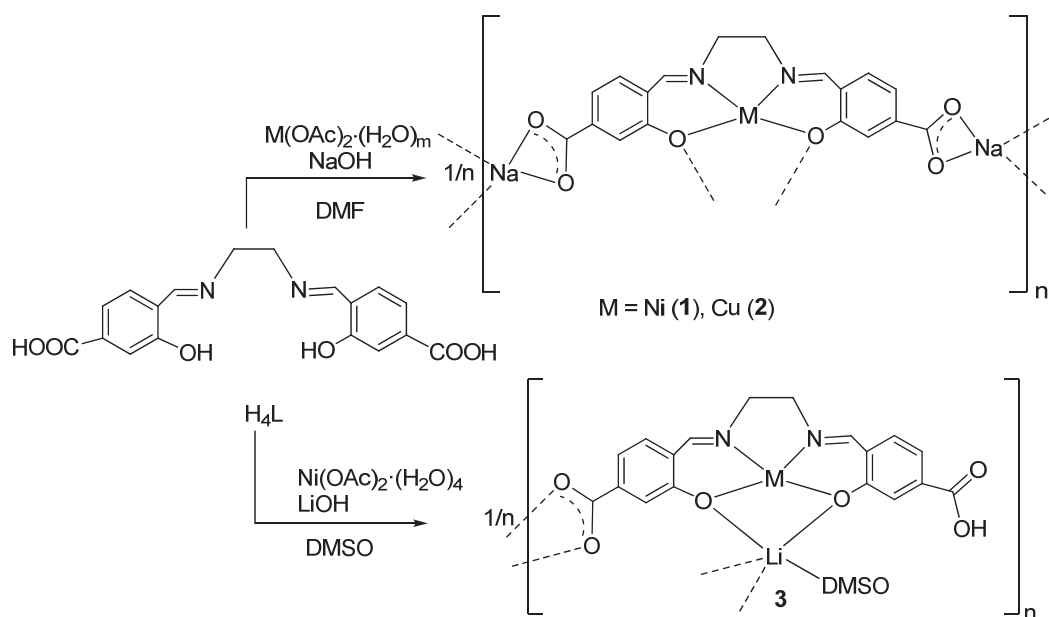
---

<sup>1</sup> Reproduced in part with permission from A. Bhunia, P. W. Roesky, Y. Lan, G. E. Kostakis, A. K. Powell, *Inorg. Chem.* 2009, 48, 10483. Copyright 2009 American Chemical Society.

according to a literature procedure by a condensation reaction of ethylenediamine with 4-formyl-3-hydroxybenzoic acid.<sup>[92]</sup> The obtained crude product, which contained some ethylenediamine as impurity, was used without further purification. In addition, the salen ligands  $N,N'$ -bis(4-carboxysalicylidene)propanediamine ( $H_4L^2$ ) and  $N,N'$ -bis(4-carboxysalicylidene)-1,3-diamino-2-propanol ( $H_5L^3$ ), which have carboxylate groups in the *meta* position to the hydroxy groups, were also synthesized according to a literature procedure.<sup>[92]</sup> The metalations of such ligands are given in the following sections.

### 3.1.1 $N,N'$ -Bis(4-carboxysalicylidene)ethylenediamine with Alkali and Transition Metals<sup>1</sup>

Reaction of ligand  $H_4L$  with  $M(OAc)_2 \cdot (H_2O)_m$  ( $m = 4$ ;  $M = Ni$  and  $m = 1$ ;  $M = Cu$ ) in the presence of NaOH in DMF resulted, after crystallization, in the polymeric compounds  $[Na_4(ML)_2 \cdot (H_2O)_9]_n$  ( $M = Ni$  (**1**), Cu (**2**)) (Scheme 3.1).



**Scheme 3.1** Synthetic scheme of compounds **1-3**

Compounds **1** and **2** were obtained as red crystals. Both compounds were characterized by standard analytical / spectroscopic techniques, and the solid state structures were determined by single crystal X-ray diffraction (Figure 3.1). In both compounds the transition metal is

coordinated by the salen ligand resulting in a distorted square planar geometry. Owing to this coordination mode, the  $d^8$  nickel compound **1** is diamagnetic and thus could also be characterized by NMR. The NMR signals are in the expected range.  $^{13}\text{C}\{\text{H}\}$  NMR spectrum clearly showed, compared to the free ligand, a significant downfield shift of the carboxyl group ( $\delta$  175.25 ppm (**1**) vs. 167.86 ppm in  $\text{H}_4\text{L}$ ), indicating that the Ni-salen unit is also deprotonated at the acid function. To balance the charge, two sodium cations are bound to the Ni-salen framework. These cations bridge the salen units by forming infinite structures. Also, four differently coordinated sodium atoms are localized in the solid state structure.

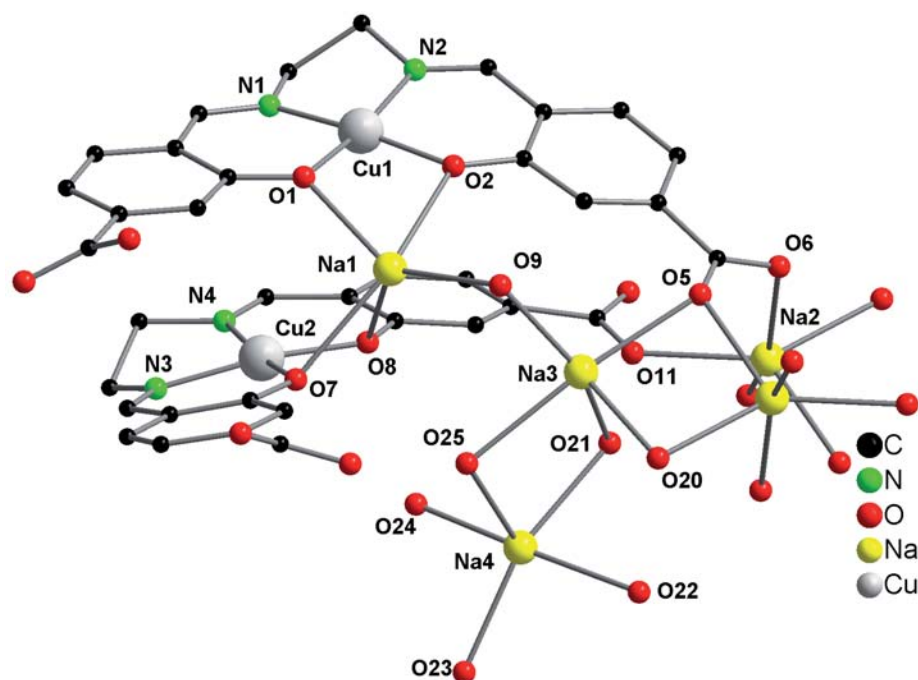


**Figure 3.1** Solid state structure of **2**, omitting hydrogen atoms. Compounds **1** and **2** are isostructural. Selected bond lengths [ $\text{\AA}$ ] and bond angles [ $^\circ$ ]:

**1:** Ni1-N1 1.847(2), Ni1-N2 1.850(3), Ni1-O1 1.854(2), Ni1-O2 1.863(2), Ni2-N3 1.836(3), Ni2-N4 1.863(3), Ni2-O7 1.863(2), Ni2-O8 1.855(2), Na1-O1 2.295(2), Na2-O5 2.371(3), Na2-O20 2.344(3), Na2-O23 2.442(3), Na3-O5 2.450(3), Na3-O20 2.317(3), Na3-O21 2.443(3), Na3-O25 2.483(3), Na4-O21 2.414(3), Na4-O22 2.441(3), Na4-O23 2.352(3), Na4-O24 2.296(3), Na4-O25 2.373(3), N1-Ni1-N2 85.84(12), N1-Ni1-O2 173.63(11), N2-Ni1-O2 94.74(11), O1-Ni1-O2 85.56(10), O1-Na1-O2 63.20(8), O2-Na1-O8 91.96(9), O2-Na1-O10 116.13(9), O1-Na1-O7 101.39(9), O7-Na1-O8 60.63(8), O23-Na4-O25 112.57(11), O21-Na4-O23 159.86(11), O21-Na4-O25 87.32(11).

**2:** Cu1-N1 1.929(2), Cu1-N2 1.925(2), Cu1-O1 1.888(2), Cu1-O2 1.902(2), Cu2-N3 1.913(2), Cu2-N4 1.940(2), Cu2-O7 1.896(2), Na2-O5 2.367(2), Na3-O5 2.503(3), Na2-O6 2.489(3), Na3-O9 2.234(2), Na3-O21 2.415(3), Na4-O21 2.439(3), Na4-O22 2.423(3), Na4-O23 2.365(3), N1-Cu1-N2 84.80(9), N3-Cu2-N4 84.74(10), N3-Cu2-O8 171.31(10), N4-Cu2-O8 94.18(9), O7-Cu2-O8 86.31(8), O5-Na3-O9 104.01(9), O5-Na3-O20 89.01(8), O9-Na3-O25 84.47(9), O20-Na3-O21 89.36(9), O20-Na3-O25 90.55(9), O21-Na4-O22 78.74(8), O21-Na4-O23 158.58(10), O23-Na4-O25 114.12(10), O24-Na4-O25 81.41(10).

In the asymmetric unit two M-salen complexes ( $M = \text{Ni}, \text{Cu}$ ) are bridged *via* the phenol oxygen atoms and Na1. Moreover, Na2 bridges the metal centers using the carboxylate groups

(Figure 3.1). All sodium atoms are six-fold coordinated. Vacant coordination sites are filled with water molecules; *e.g.*, Na4 is surrounded by five water molecules and one carboxylate group. Connecting the asymmetric units results in zig-zag chains (Figure 3.2), which were previously not observed. The zig-zag chains (Figure 3.2) arise from the substitution pattern of the salen phenol ring where the phenolate and the carboxylate group are in the *meta* position. Thus, compounds **1** and **2** can be considered as one-dimensional (1D) metal functionalized ICPs. Between different chains, water molecules are localized in the solid state structure.

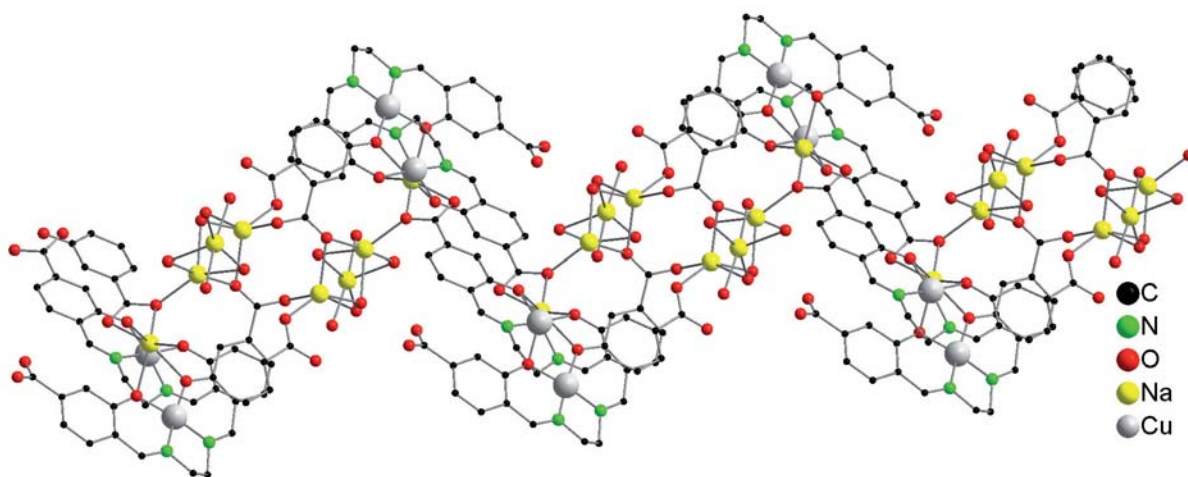


**Figure 3.2** Solid state structure of **2**, omitting hydrogen atoms. Cut out of the polymeric structure.

In contrast to the results described above, the reaction of ligand H<sub>4</sub>L with Ni(OAc)<sub>2</sub>·(H<sub>2</sub>O)<sub>4</sub> in the presence of LiOH·H<sub>2</sub>O in DMSO resulted, after crystallization, in the polymeric compound, [Li(NiHL)(DMSO)]<sub>n</sub> (**3**) (Scheme 3.1). Compound **3** was fully characterized by standard analytical techniques, and the solid state structure was established by single crystal X-ray diffraction (Figure 3.3). Compound **3** is almost insoluble in any solvent we tried. Thus, no useful NMR data could be acquired. In contrast to compounds **1** and **2**, only one alkaline metal cation was localized as the center ion in the Ni-salen fragment, indicating that the ligand is not fully deprotonated. As result of the bent ligand geometry and the deprotonation of only one carboxylate group, the [Li(NiHL)(DMSO)] units assemble into a helical chain (Figure 3.4). The nickel atoms are, as expected, coordinated in the center of the salen ligand in a distorted square planar mode, *e.g.*, N1-Ni-N2 86.77(11)° and N1-Ni-O1 95.28(10)°. The lithium atom is coordinated in a chelating fashion by the two phenol oxygen atoms of a Ni-salen subunit having Li-O bond distances of Li-O1 1.986(5) Å and Li-O2 1.992(5) Å. Moreover, the lithium atom is coordinated by one equivalent of DMSO and one carboxylate

group of a neighboring [Li(NiHL)(DMSO)] unit. The latter coordination is the reason for the formation of the helical structure setup.

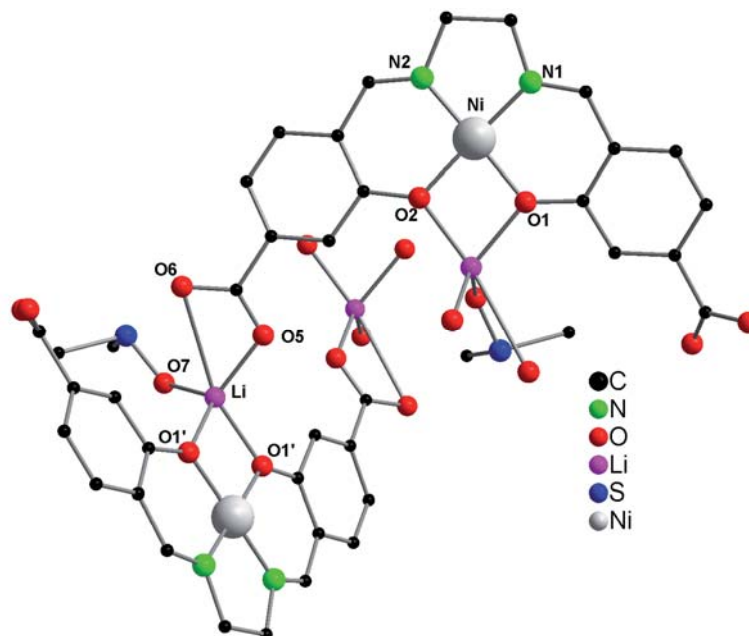


**Figure 3.3** Solid state structure of compound **3**, omitting hydrogen atoms. Selected bond lengths [Å] and bond angles [°]: Ni-N1 1.851(2), Ni-N2 1.839(2), Ni-O1 1.858(2), Ni-O2 1.864(2), Li-O1 1.986(5), Li-O2 1.991(5), Li-O5 1.930(5), Li-O7 1.907(5), N1-Ni-N2 86.76(11), N1-Ni-O2 176.43(10), N2-Ni-O2 95.46(10), O1-Ni-O2 82.64(9), O1-Li-O2 76.3(2), O2-Li-O7 111.8(3), O5-Li-O6 51.59(8), O5-Li-O7 118.1(3).

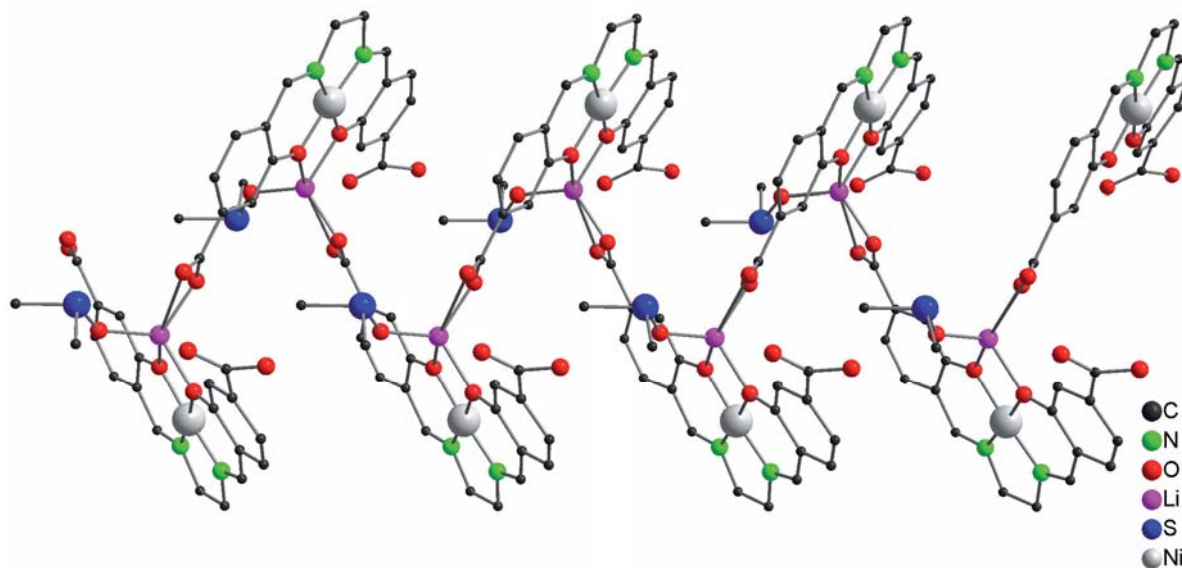


**Figure 3.4** Solid state structure of **3**, omitting hydrogen atoms. Cut out of the polymeric structure.

### 3.1.1.1 Thermogravimetric Analysis (TGA) of Compound 1-3

TGA measurements were performed for all compounds **1-3** as shown in Figure 3.5. At room temperature they retain their crystalline behavior for a couple of months.

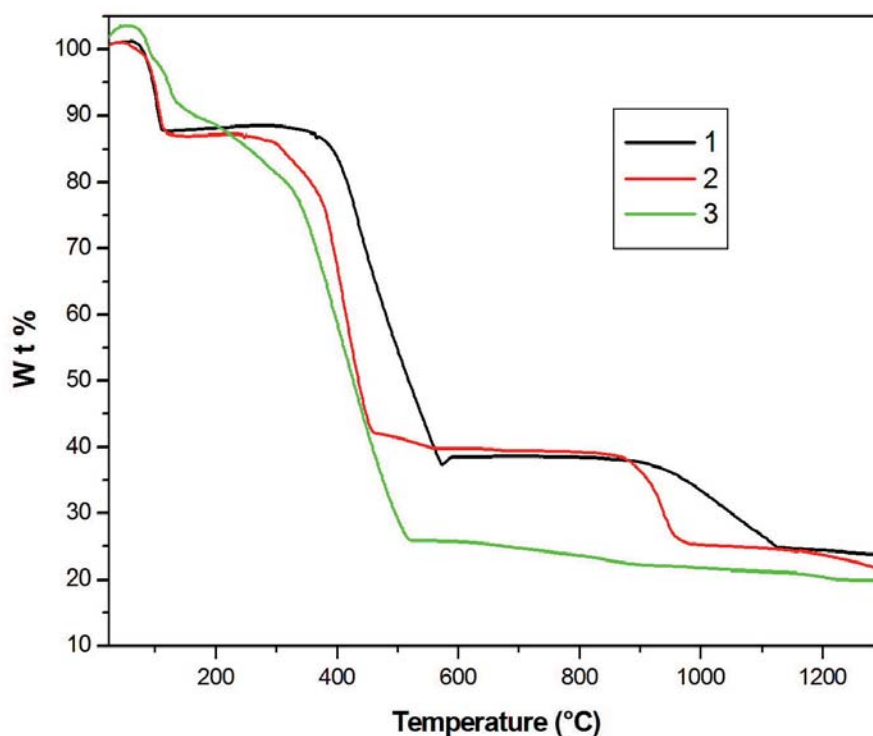


**Figure 3.5** TGA for **1-3** in temperature range from 25°C to 1350°C at a heating rate of 5°C / min under N<sub>2</sub> atmosphere.

The TGA curve of compound **1** shows that seven water molecules are lost in the temperature range of 70°C to 115°C (obsd 12.14%, calcd 11.71%). Then it is stable up to 330°C. At higher temperature, decomposition starts and two weight losses are observed, one from 300°C to 570°C (obsd 37.67%) and the other from 830°C to 1130°C. As the final product, we suggest a mixture of NiO and Na<sub>2</sub>O (obsd 24.97%, calcd 25.40%) (Figure 3.5). Compound **2** shows a similar TGA curve. Eight water molecules are lost in the temperature range from 60°C to 128 °C (obsd 12.87%, calcd 13.26%). The dehydrated product is stable up to 260°C. Above this temperature, decomposition of the organic ligands starts, leading to a weight loss in the range of 260°C to 560°C (obsd 39.98%) and another weight loss in the range from 850°C to 990°C (obsd 25.49%, calcd 26.06%), leading to the formation of CuO and Na<sub>2</sub>O (Figure 3.5). The TGA curve of compound **3** is different. A gradual decomposition occurs up to 520°C resulting in weight loss of observed 74%. We suggest a formation of LiOH and



Ni(OH)<sub>2</sub> (calcd 76.53%). Finally, a slight weight loss up to 1230°C is observed, giving a mixture of NiO and Li<sub>2</sub>O (obsd 20.18%; calcd 18.03%) (Figure 3.5).

### 3.1.1.2 Magnetic Properties of Compound 2

Magnetic susceptibility measurements were performed by Dr. Yanhua Lan (Prof. A. K. Powell) in the temperature range from 1.8 K to 300 K only for paramagnetic compound **2**. The evolution of  $\chi T$  as a function of temperature is shown in Figure 3.6.

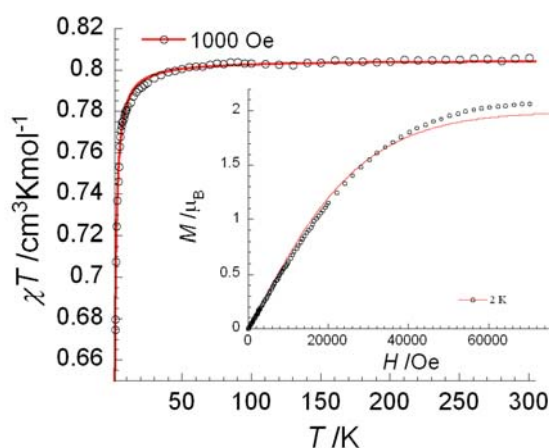


**Figure 3.6** The magnetic susceptibility product ( $\chi T$  vs  $T$  plot) at 1000 Oe; inset: field dependence of magnetization ( $M$  vs  $H$  plot) at 2 K for compound **2**. Open circles are experimental data; red solid lines indicate the calculated curves discussed in text.

The magnetic superexchange interaction between the two Cu(II) centres within each repeating unit is mediated by the phenol oxygen atoms from each ligand strand through one sodium atom. However, no interaction could be possible between each unit, which is connected by three double sodium atoms along with the 1D chain. At room temperature, the  $\chi T$  product is  $0.81\text{cm}^3\text{K/mol}$ . This value is in very good agreement with the theoretical value resulting from the presence of two Cu(II) ions ( $S = \frac{1}{2}$ ). The  $g$  value can thus be estimated at 2.07. Decreasing the temperature, the  $\chi T$  product at 1000 Oe stays almost constant till 40 K and then continuously decreases to reach  $0.67\text{cm}^3\text{K/mol}$  at 1.8 K indicating the presence of weak antiferromagnetic interactions. The data have been analyzed using the isotropic spin Hamiltonian  $H = -2JS_1S_2$  with quantum numbers  $S_1 = S_2 = \frac{1}{2}$ . Using the the Bleaney–Bowers equation,<sup>[93]</sup> the fit to the experimental data leads to the best set of parameters as  $J = -0.53(1)$  K and  $g = 2.07(1)$  (Figure 3.6). The sign and magnitude of the magnetic interactions imply that the two Cu(II) ions are weakly interacting through the oxygen atoms and sodium atoms.

Furthermore, the field dependence of the magnetization of compound **2** almost saturates to  $2.1 \mu_B$  at 2 K above 6 T (Figure 3.6, inset) corresponding to two uncoupled  $S = \frac{1}{2}$  spins. This is also confirmed by simulation of the Brillouin function with  $g = 2.06$  for two non-interacting  $S = \frac{1}{2}$ , further suggesting weak antiferromagnetic interactions present in each dinuclear motif.

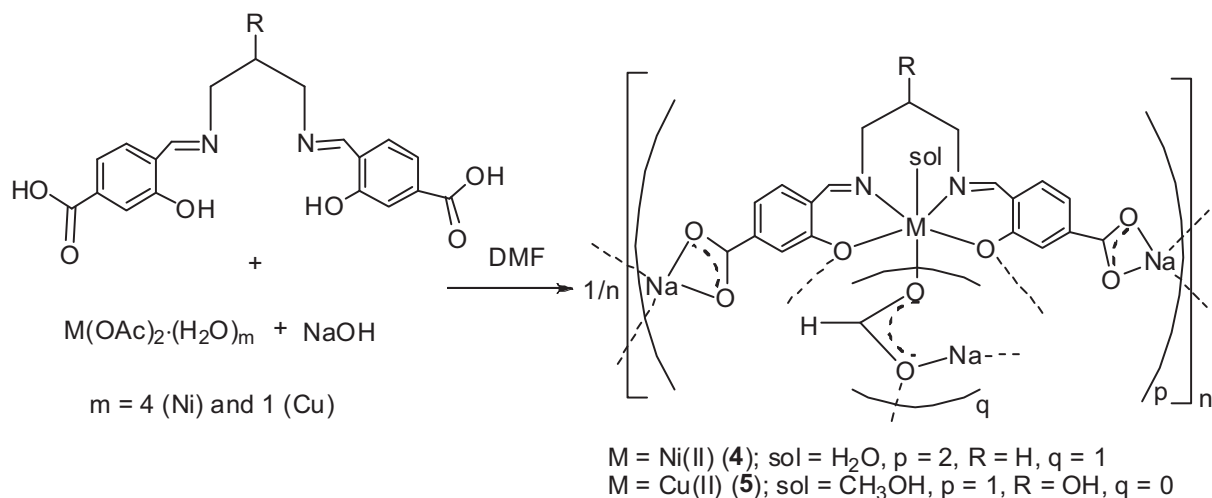
In conclusion, it has been shown that the ligand  $H_4L$ , which is a salen type compound that has carboxylate groups in the position *meta* to the hydroxyl groups, is suitable to build up new kinds of ICPs. By coordination of nickel and copper in the central salen unit, different types of metal-functionalized 1D ICPs were built up. The shape of the coordination polymers depends on the alkaline metal that is coordinated to the carboxylate function. The coordination polymers are thermally very robust. For the copper compound, a weak antiferromagnetic interaction was observed between the Cu(II) ions.

### 3.1.2 *N,N'*-Bis(4-carboxysalicylidene)propanediamine ( $H_4L^2$ ) and *N,N'*-Bis(4-carboxysalicylidene)-1,3-diamino-2-propanol ( $H_5L^3$ ) with Alkali and Transition Metal

Treatment of  $H_4L^2$  with  $Ni(OAc)_2 \cdot (H_2O)_4$  in the presence of aqueous NaOH in DMF at room temperature afforded the compound,  $[Na_5\{(NiL^2)(HCOO)(H_2O)_{11}\} \cdot (H_2O)_4]_n$  (**4**) (Scheme 3.2). It was noted that the formate ligand arises from the *in situ* hydrolysis of DMF; without DMF molecules the synthesis of compound **4** was not successful. Compound **4** was obtained as green crystals and characterized by standard analytical / spectroscopic techniques. The solid state structures were determined by single crystal X-ray diffraction (Figure 3.7). The IR spectrum of compound **4** shows strong absorption bands at about  $1620 \text{ cm}^{-1}$  and  $1397 \text{ cm}^{-1}$ , which are assigned to the asymmetric and symmetric vibration of the carboxylate groups. The absence of the characteristic absorption band in the range of  $1700 \text{ cm}^{-1}$  indicates complete deprotonation of salen ligands and coordinates to metal ions.

Compound **4** crystallizes in the monoclinic space group  $P2_1/m$ . The asymmetric unit of this compound consists of half of two salen ligands, one fully occupied sodium atom, three half occupied sodium atoms, one formate ion, two Ni(II) ions and 7.5 water molecules. The unit cell contains two different kinds of  $NiL^2$  units that are bridged by the phenoxy oxygen atoms, Na1, the formate ion and Na2. Since the carboxylate oxygen atoms and phenoxy oxygen

atoms are involved in the coordination to the sodium atoms (Na1, Na2, Na3 and Na4), 2D ICPs are formed (Figure 3.7).



**Scheme 3.2** Synthetic scheme of compounds 4 and 5.

Both sodium atoms Na1 and Na2 adopt an octahedral geometry by coordinating to two oxygen atoms from the salen unit (Na1: O1 and O1', and Na2: O2 and O2'), three oxygen atoms from water molecules (Na1: O8, O16 as well as O16' and Na2: O11, O11' as well as O12) and one formate oxygen atom (Na1: O10 and Na2: O9). In contrast, the sodium atoms Na3 and Na4 are five-fold coordinated. The sodium atom Na3 is surrounded by two carboxylic oxygen atoms (O4 and O4') and three water molecules (O13, O14 and O14'), and Na4 is coordinated by one carboxylate oxygen atom (O6) and four oxygen atoms (O14, O15, O17 and O18) from four water molecules. Ni1 is coordinated in a square pyramidal arrangement with two imine nitrogen atoms and two phenoxy oxygen atoms from the chelating salen ligand ( $L^2$ )<sup>4-</sup> localized in the square plane and one oxygen atom from a water molecule localized in the apex (Figure 3.7). Ni2 is coordinated in an elongated octahedral geometry with two imine nitrogen atoms and two phenoxy oxygen atoms of ( $L^2$ )<sup>4-</sup> localized in the square plane, one oxygen atom from a formate ion and one oxygen atom from a water molecule localized in the apex. The Ni-O and Ni-N bond distances are in the expected range of 2.017(2) Å to 2.225(3) Å and 2.054(2) Å to 2.059(2) Å, respectively, for salen complexes.

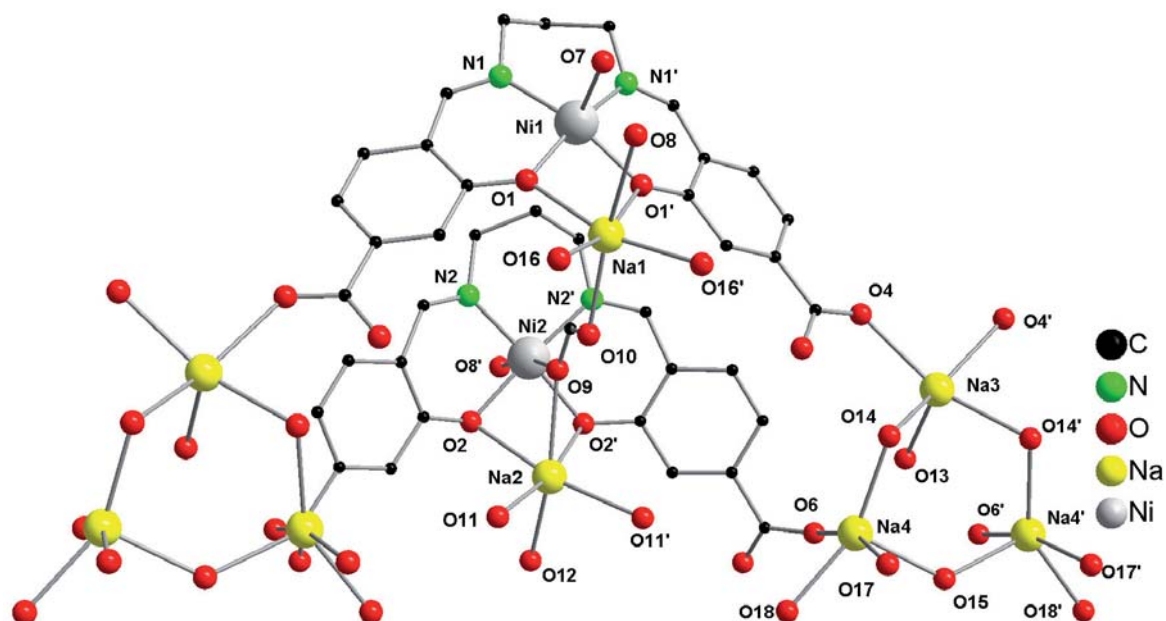


**Figure 3.7** Solid state structure of compound **4**, omitting hydrogen atoms. Selected bond lengths [ $\text{\AA}$ ] and angles [ $^\circ$ ]: Ni1-N1 2.054(2), Ni1-O1 2.017(2), Ni1-O7 2.076(2), Ni2-N2 2.059(2), Ni2-O2 2.025(2), Ni2-O8 2.225(3), Na1-O1 2.372(2), Na1-O8 2.662(3), Na1-O10 2.374(3), Na1-O16 2.336(2), Na2-O2 2.473(2), Na2-O9 2.457(3), Na2-O11 2.449(2), Na2-O12 2.316(3), Na3-O4 2.471(2), Na3-O13 2.305(3), Na3-O14 2.392(2), Na4-O14 2.387(2), Na4-O15 2.380(2), Na4-O17 2.524(2), Na4-O18 2.344(2), N1-Ni1-N1' 93.52(11), N1-Ni1-O1 90.29(7), N1-Ni1-O7 95.09(7), O1-Ni1-O1' 82.92(9), O1-Ni1-O7 98.14(7), N2-Ni2-N2' 93.78(12), O2-Ni2-O2' 85.12(9), N2-Ni2-O2 90.55(8), N2-Ni2-O8 94.17(8), N2-Ni2-O9 94.21(7), O2-Ni2-O8 86.32(7), O8-Ni2-O9 167.72(10), O2-Ni2-O9 84.65(7), O1-Na1-O1' 68.51(9), O2-Na2-O2' 67.26(8).

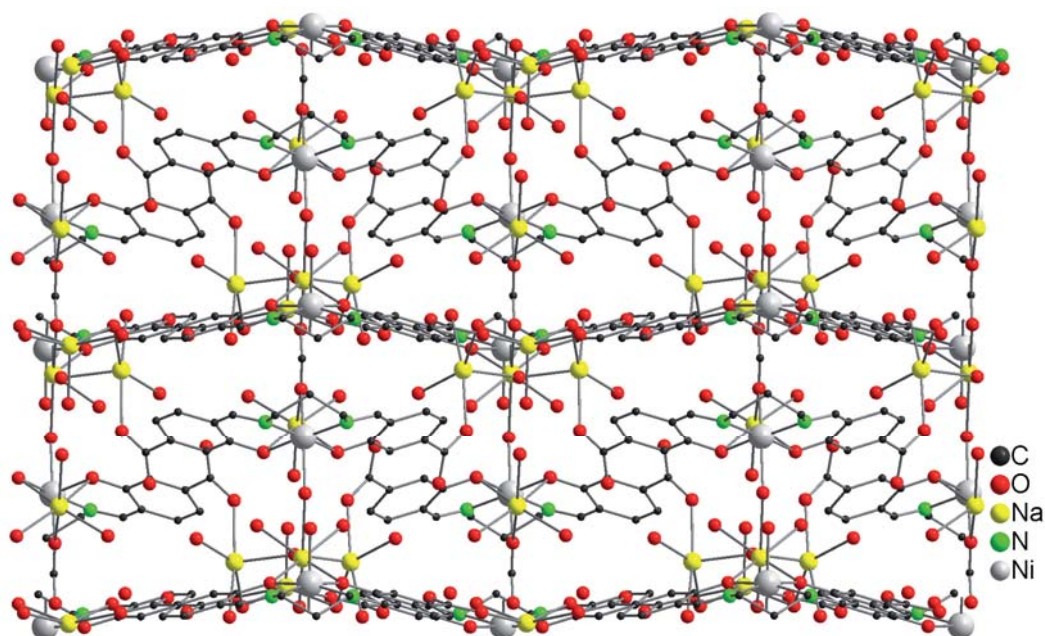


**Figure 3.8** Solid state structure of **4**, omitting hydrogen atoms. Cut out of the polymeric structure.

Reaction of  $\text{H}_5\text{L}^3$  with  $\text{Cu}(\text{OAc})_2 \cdot \text{H}_2\text{O}$  in the presence of aqueous  $\text{NaOH}$  in methanol followed by crystallization from ether diffusion resulted in a compound formulated as  $[\text{Na}_4(\text{CuHL}^3)_2(\text{MeOH})_2(\text{H}_2\text{O}) \cdot (\text{Et}_2\text{O})]_n$  (**5**) (Scheme 3.2). The IR spectrum of compound **5** shows the characteristic absorption peaks of the functional groups. The broad band of compound **5** at  $3415 \text{ cm}^{-1}$  is assigned to the O-H stretching vibrations of water molecules, while the strong absorption bands at about  $1617 \text{ cm}^{-1}$  and  $1386 \text{ cm}^{-1}$  are assigned to the asymmetric and symmetric vibration of the carboxylate groups. The absence of a characteristic absorption band around  $1700 \text{ cm}^{-1}$  indicates the complete deprotonation of the salen ligands and coordination to metal ions. Compound **5** was characterized by standard analytical / spectroscopic techniques, and the solid state structure was analyzed by single crystal X-ray diffraction (Figure 3.9). It crystallizes in the monoclinic space group  $C2/c$  and forms a 2D network in the solid state (Figure 3.10). The selected bond lengths and bond angles are given in the caption of Figure 3.9. The asymmetric unit contains one Cu(II) ion, one  $(\text{HL}^3)^4-$  ligand, two sodium atoms, one methanol, half a diethyl ether molecule and half a water molecule. The Cu(II) ion is coordinated in a square pyramidal geometry by two imine nitrogen atoms and two phenoxy oxygen atoms from  $(\text{HL}^3)^4-$  localized in the square plane and one oxygen atom from methanol localized in the apex. The Cu-O and Cu-N bond distances are in the normal range of  $1.933(2) \text{ \AA}$  to  $2.396(3) \text{ \AA}$  and  $1.986(3) \text{ \AA}$  to  $2.013(3) \text{ \AA}$ , respectively. The carboxylate oxygen atoms and the phenoxy oxygen atoms are involved in the coordination to the sodium atoms (Na1 and Na2). Both of the sodium atoms, Na1 and Na2, are five-fold coordinated (Figure 3.9). The Na1 atom is surrounded by two phenoxy oxygen atoms from one salen unit (O1' and O2'), two carboxylate oxygen atoms (O4 and O6') and one water molecule (O9). In contrast, the Na2 atom is coordinated by five carboxylate oxygen atoms (O4', O5, O5', O6, O6'') from neighboring salen units, resulting in a 2D network structure (Figure 3.10). The Na-O bond lengths and O-Na-O bond angles are in the range of  $2.219(3) \text{ \AA}$  to  $2.695(3) \text{ \AA}$  and  $64.52(8)^\circ$  to  $165.42(10)^\circ$ , respectively.

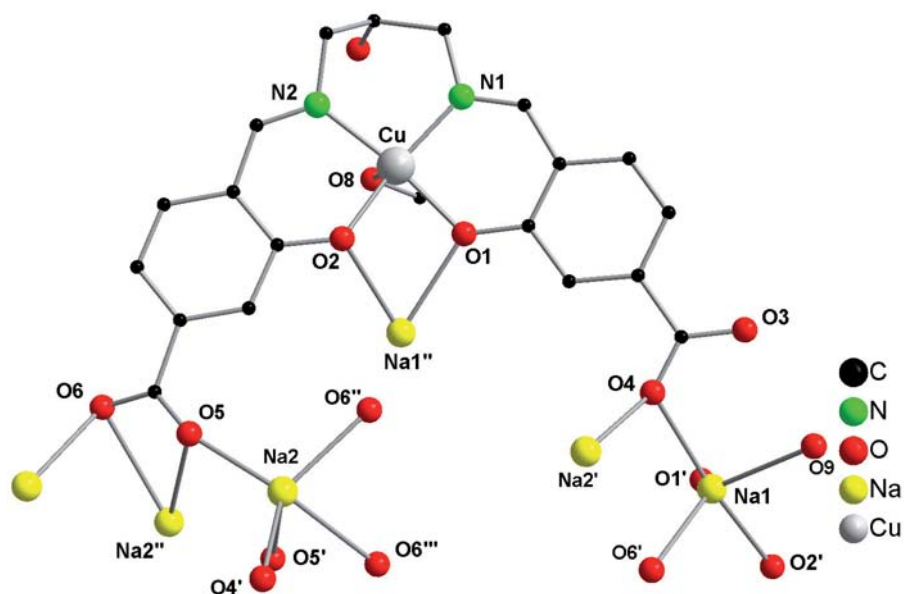


**Figure 3.9** Solid state structure of **5**, omitting hydrogen atoms. Selected bond lengths [ $\text{\AA}$ ] and angles [ $^\circ$ ]: Cu-N1 1.986(2), Cu-N2 2.011(2), Cu-O1 1.948(2), Cu-O2 1.932(2), Cu-O8 2.394(3), Na1-O1' 2.377(2), Na1-O2' 2.342(2), Na1-O4 2.346(2), Na1-O6' 2.446(2), Na1-O9 2.483(12), Na2-O4' 2.220(2), Na2-O5 2.222(2), Na2-O6'' 2.692(2), N1-Cu-N2 95.91(10), N1-Cu-O2 169.02(9), N2-Cu-O2 90.76(9), N1-Cu-O8 91.10(9), N2-Cu-O8 86.30(9), O1-Cu-O2 80.97(8), O1-Cu-O8 96.80(9), O2-Cu-O8 98.05(9), O1-Na1-O2 64.51(7), O2''-Na1-O4 165.44(8), O5-Na2''-O6 50.51(7).

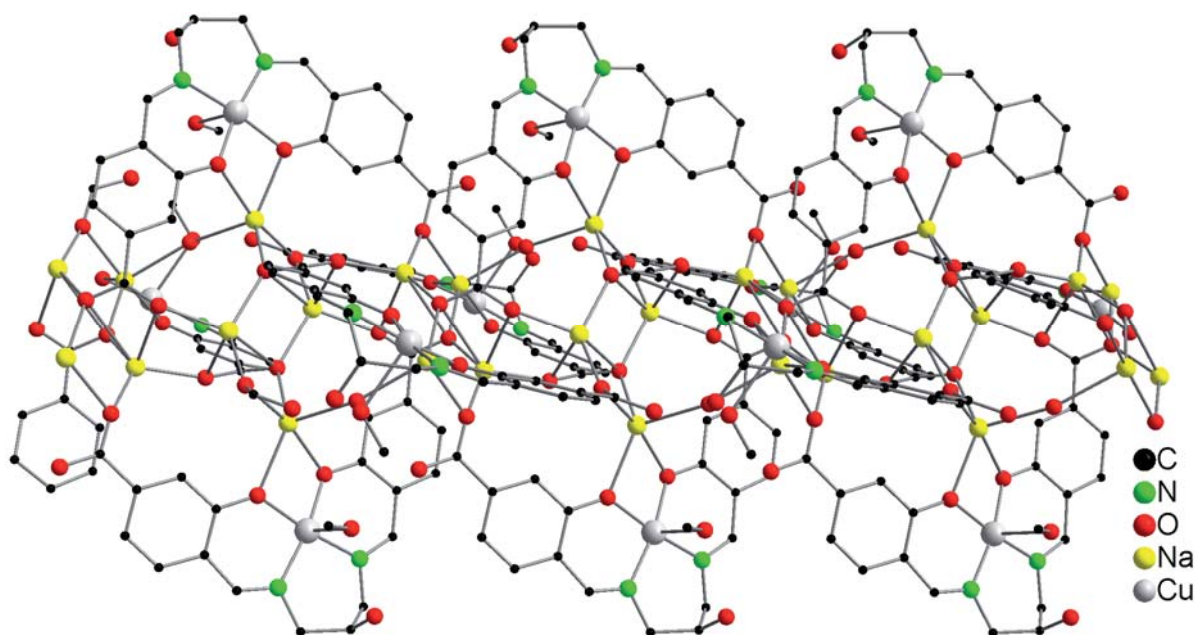


**Figure 3.10** Solid state structure of **5**, omitting hydrogen atoms. Cut out of the polymeric structure.

### 3.1.2.1 Thermogravimetric Analysis of Compounds 4 and 5

The TGA of compound **4** shows that the twelve water molecules are lost at a temperature of 133°C (obsd 16.33%, calcd 16.87%) (Figure 3.11), after which the compound is stable up to 250°C. The residual guest solvent molecules are lost in the temperature range of 250°C to 365°C (obsd 20.13%, calcd 21.08%). At higher temperatures, the networks began to decompose with a continuous weight loss and finally form NiO and Na<sub>2</sub>O (2 : 2.5) (obsd 27.57%, calcd 23.76%). The TGA curve of complex **5** shows a weight loss of 11.06% around 124°C, corresponding to the release of two coordinated MeOH and one non-coordinated Et<sub>2</sub>O (calcd 12.12%) (Figure 3.11), after which the framework is stable up to 250°C. Another weight loss occurs around 270°C (obsd 1.72%, calcd 1.58%) due to the loss of one coordinated water molecule. Afterwards, decomposition of the residue starts. Finally, weight loss at a temperature of 1100°C (obsd 26.89%, calcd 26.16%) leads to the suggested formation of CuO and Na<sub>2</sub>O.

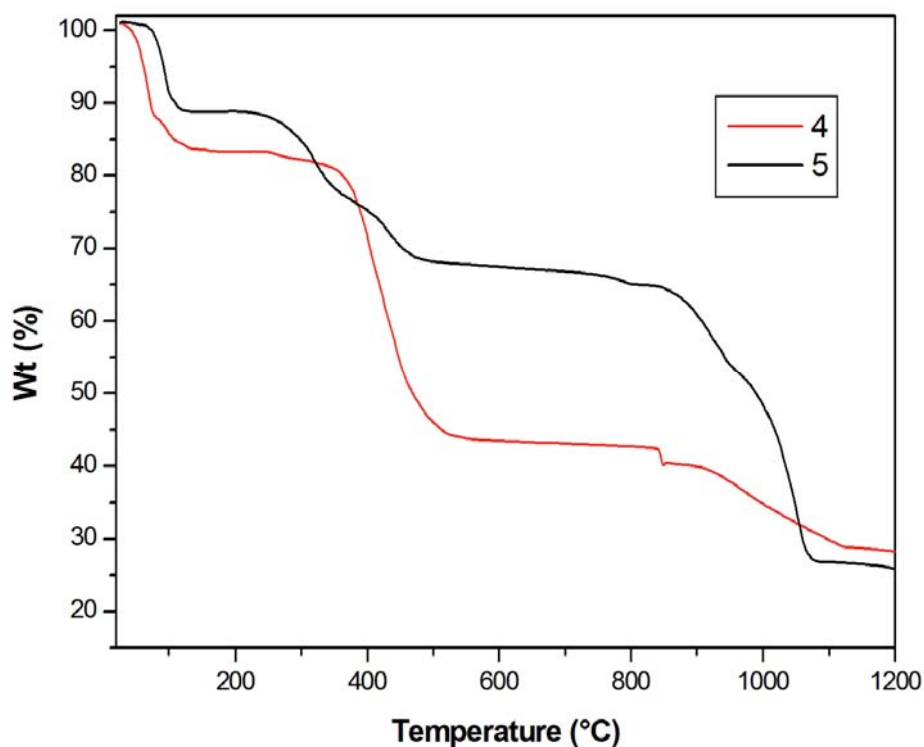


**Figure 3.11** TGA for **4** and **5** in temperature range of 25-1350°C at the heating rate of 5°C / min under the N<sub>2</sub> atmosphere.

### 3.1.2.2 Magnetic Properties of Compound 4

The magnetic susceptibility of **4** was investigated by Dr. Yanhua Lan (Prof. A. K Powell) in the temperature range of 300 K to 1.8 K at 1000 Oe (Figure 3.12). The magnetic exchange interaction between the two Ni(II) centers within each repeating unit is mediated by the phenol oxygen atoms from each  $(L^2)^4$ , which stand through the sodium atom and formate ion (details are in structural description text). At room temperature, the  $\chi T$  product at 1000 Oe is  $2.4 \text{ cm}^3\text{K/mol}$ , which agrees with the expected value for the presence of two Ni(II) ions with  $S = 1$  and  $g = 2.19$ . Upon decreasing the temperature, the  $\chi T$  product at 1000 Oe stays almost constant until 50 K and below which it continuously decreases to reach  $0.45 \text{ cm}^3\text{K/mol}$  at 1.8 K, indicating the presence of weak antiferromagnetic interactions. The data have been analyzed using the isotropic spin Hamiltonian  $H = -2J(S_1 \cdot S_2)$ ,<sup>[93]</sup> with quantum numbers  $S_1 = S_2 = 1$ . The fitting of the experimental data leads to the best-fit parameters of  $g = 2.213(3)$  and  $J/k_B = -2.12(3) \text{ K}$ .

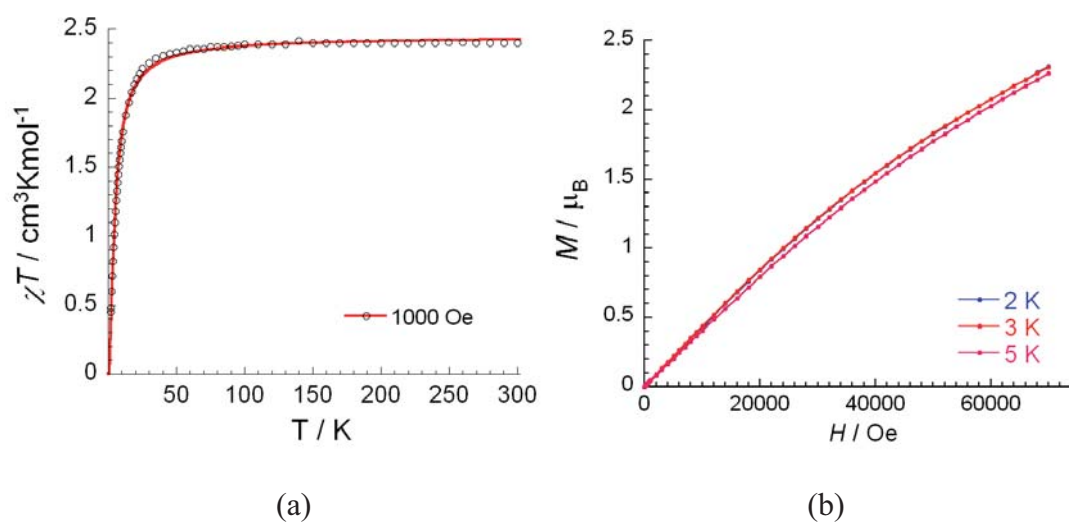


**Figure 3.12** (a) Magnetic susceptibility product ( $\chi T$  vs  $T$  plot) at 1000 Oe for compound **4**. (b) Field dependence of magnetization ( $M$  vs  $H$  plot) from 2-5 K for compound **4**.

The field dependence of the magnetization of compound **4** at low temperatures reveals a gradual increase with the absence of a true saturation of the magnetization. The  $M$  value reaches  $2.3 \mu_B$  at 7 T, as shown in Figure 3.12. This behavior suggests the presence of low-lying excited states that might be populated when a field is applied. This is also in agreement with the fact that the only weak antiferromagnetic interactions present in the coordination polymer can be easily overcome by the external field.



In conclusion, the two salen ligands, *N,N'*-bis(4-carboxysalicylidene)propanediamine ( $H_4L^2$ ) and *N,N'*-bis(4-carboxysalicylidene)-1,3-diamino-2-propanol ( $H_3L^3$ ), yield the 2D ICPs  $[Na_5\{(NiL^2)(HCOO)(H_2O)_{11}\} \cdot (H_2O)_4]_n$  (**4**) and  $[Na_4\{(CuL^3)_2(MeOH)_2(H_2O)\} \cdot (Et_2O)]_n$  (**5**) based on transition and alkali metal atoms. In compound **4**, the formate ion acts as a bridging ligand, suggesting that the shape of the coordination polymer depends on the metal center and the ligand systems. The TGA study shows that **4** and **5** are stable at room temperature. Additionally, a weak antiferromagnetic interaction was observed in compound **4** between the Ni(II) centers.

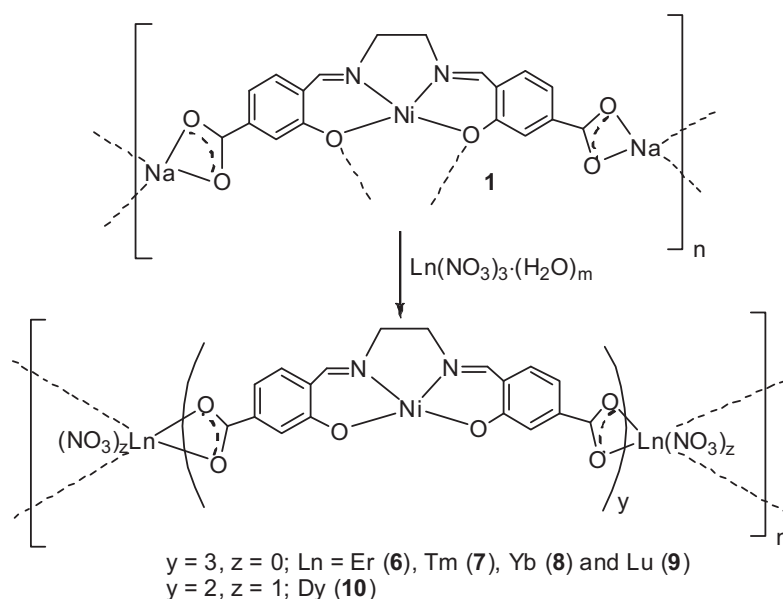
## 3.2 Salen-Based Metal Organic Frameworks

The *N,N'*-bis(4-carboxysalicylidene)ethylenediamine ( $H_4L$ ) ligand<sup>[92]</sup> can be used as a building block to assemble metal-functionalized MOFs. By using lanthanide ions, functionalized d-f-block metals MOFs are obtained.

### 3.2.1 Nickel and Lanthanide-Based MOFs<sup>[94]</sup>

Treatment of a DMF / water solution of compound **1** with  $Ln(NO_3)_3 \cdot (H_2O)_m$  ( $m = 4$  (Lu), 5 (Er, Dy) and 6 (Yb, Tm)) leads to, after work-up and crystallization, the formation of 2D polymeric lanthanide-nickel compounds,  $[\{Ln_2(NiL)_3(DMF)(H_2O)_3\} \cdot (DMF)_4 \cdot (H_2O)_{10}]_n$  ( $Ln = Er$  (**6**), Tm (**7**), Yb (**8**) and Lu (**9**)) (Scheme 3.3). Compounds **6-9** were obtained as red crystals and characterized by standard analytical and spectroscopic techniques. The solid state structures were determined by single crystal X-ray diffraction (Figure 3.13). Compounds **6-9** crystallize in the triclinic space group *P*-1. Since they are isostructural to each other, only the solid state structure of **6** will be described in detail.

The solid state structure of **6** results from the influence of two different secondary building units (SBUs) (Figure 3.13). One SBU, which is based on a  $[(Er)_2(\mu-O_2CR)_4(\eta^2-O_2CR)_2]$  building block, is formed around Er1. This SBU can be regarded as a distorted octahedron built from two lanthanide ions bridged by four carboxylates. Each Er1 atom is eight-fold coordinated by two water molecules, two oxygen atoms of the chelating carboxylate groups, and four oxygen atoms of the four bridging carboxylates.



**Scheme 3.3** Synthetic scheme of compounds **6-10**.

The other SBU is formed around Er<sub>2</sub>. This SBU consists of a [(Er)<sub>2</sub>(μ-O<sub>2</sub>CR)<sub>2</sub>(η<sup>2</sup>-O<sub>2</sub>CR)<sub>4</sub>] building block. The second SBU is a distorted hexagon, which was observed previously in [Er<sub>2</sub>(anth)<sub>6</sub>(H<sub>2</sub>O)<sub>4</sub>]·(H<sub>2</sub>O)<sub>2</sub> (anth = anthranilate).<sup>[95]</sup> In this structural motif, Er<sub>2</sub> is also eight-fold coordinated by four oxygen atoms of two chelating carboxylate groups, two oxygen atoms of two metal bridging carboxylate groups, one water molecule and one molecule of DMF.

The asymmetric unit comprises metalloligands, which all coordinate in a chelating fashion with one carboxylate group and in a metal bridging mode with the other carboxylate group. The nickel atoms in compound **6** is coordinated by the salen ligand, displaying a distorted square planar geometry, meaning that, in contrast to other MOFs, the connecting organic struts are not absolutely rigid. The salen unit is slightly bent at the nickel center, which can be seen by different torsion angles of the ONNO-units (e.g. for **6**: 6.43(3)° around Ni1, 7.28(3)° around Ni2, and 2.68(3)° around Ni3). Within the cavities, water and DMF molecules are localized in the single crystal X-ray structures (Figure 3.13). The void space of compound **6-9**, which is filled with DMF and water molecules, were calculated by PLATON to be 37.7%.

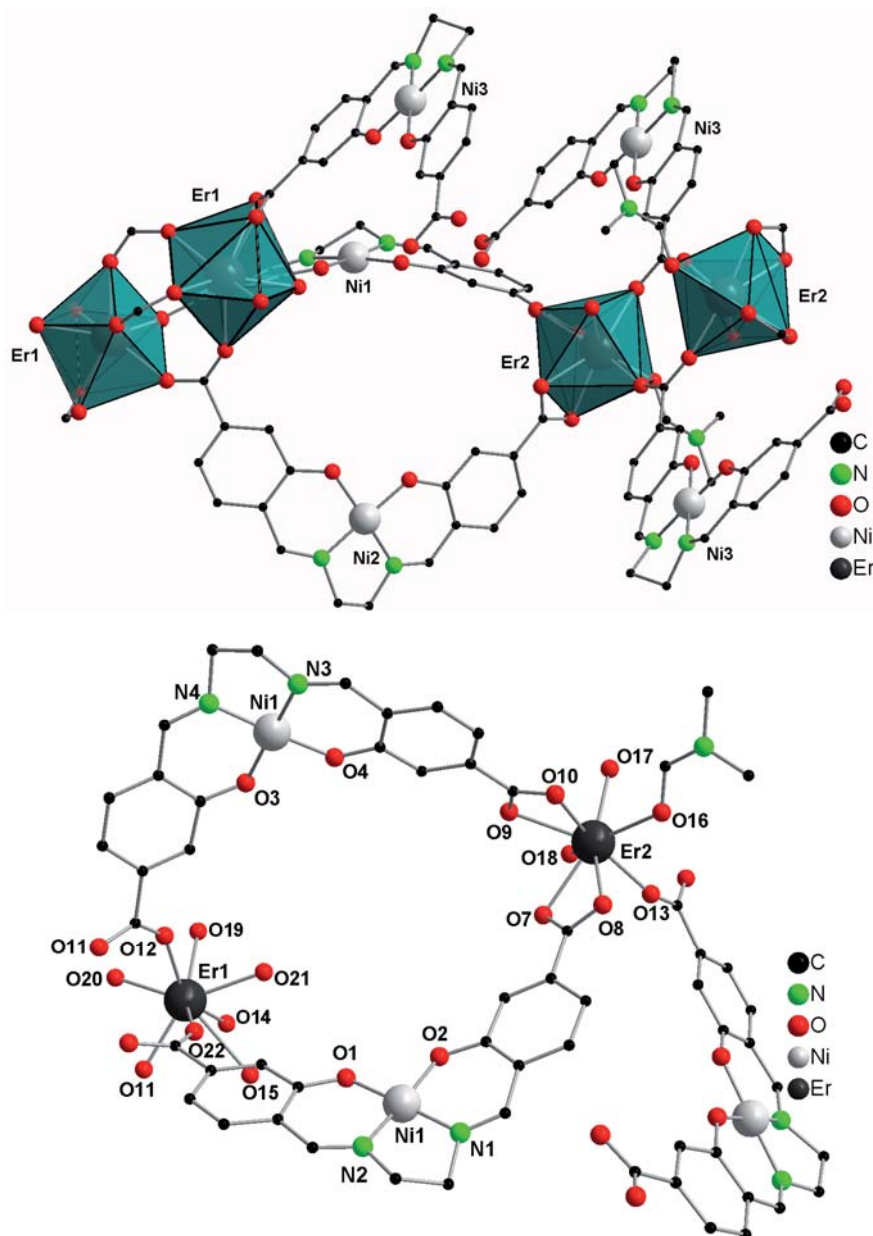


**Figure 3.13** Solid state structure of **6**, omitting hydrogen atoms. Top: SBU unit. Bottom: asymmetric unit. Compounds **6-9** are isostructural. Selected bond lengths [Å] and angles [°]:

**6:** Ni1-N1 1.860(8), Ni1-N2 1.844(9), Ni1-O1 1.861(7), Ni1-O2 1.868(7), Er1-O11 2.253(7), Er1-O12 2.271(8), Er1-O14 2.292(8), Er1-O15 2.786(9), Er1-O19 2.418(7), Er1-O20 2.288(7), Er1-O21 2.373(8), Er1-O22 2.233(7), Er2-O7 2.397(7), Er2-O8 2.421(7), Er2-O9 2.426(7), Er2-O10 2.378(8), Er2-O13 2.250(7), Er2-O16 2.352(7), Er2-O17 2.228(6), Er2-O18 2.318(7), N1-Ni1-N2 86.3(4), O1-Ni1-O2 84.9(3), N1-Ni1-O2 94.0(3), O11-Er1-O12 127.2(3), O11-Er1-O21 140.6(3), O11-Er1-O22 80.5(4), O14-Er1-O15 49.4(2), O19-Er1-O21 74.3(3), O7-Er2-O8 54.1(3), O8-Er2-O13 75.2(2), O9-Er2-O17 83.7(3), O16-Er2-O17 76.6(3), O17-Er2-O18 78.1(3).

**7:** Ni1-N1 1.857(5), Ni1-N2 1.852(4), Ni1-O1 1.851(4), Ni1-O2 1.875(4), Tm1-O11 2.250(4), Tm1-O12 2.272(4), Tm1-O14 2.276(4), Tm1-O15 2.819(6), Tm1-O19 2.406(4), Tm1-O20 2.290(5), Tm1-O21 2.364(4), Tm1-O22 2.235(4), Tm2-O7 2.390(4), Tm2-O8 2.402(4), Tm2-O9 2.427(4), Tm2-O10 2.369(4), Tm2-O13 2.259(4), Tm2-O16 2.344(4), Tm2-O17 2.221(4), Tm2-O18 2.335(4), N1-Ni1-N2 85.9(2), N1-Ni1-O2 94.3(2), O1-Ni1-O2 85.0(2), O11-Tm1-O12 126.2(2), O11-Tm1-O21 140.6(2), O11-Tm1-O22 80.5(2), O14-Tm1-O15 49.54(15), O19-Tm1-O21 74.9(2), O7-Tm2-O8 54.27(14), O7-Tm2-O16 129.99(15), O8-Tm2-O13 75.33(15), O9-Tm2-O13 150.8(2), O13-Tm2-O17 106.0(2), O16-Tm2-O17 76.82(1), O16-Tm2-O18 140.8(2), O17-Tm2-O18 77.5(2). (See next page for compound **8**).

**8:** Ni1-N1 1.80(2), Ni1-N2 1.864(6), Ni1-O1 1.858(12), Ni1-O2 1.875(13), Yb1-O11 2.248(14), Yb1-O12 2.276(12), Yb1-O14 2.285(10), Yb1-O15 2.82(2), Yb1-O19 2.389(13), Yb1-O20 2.252(14), Yb1-O21 2.356(13), Yb1-O22 2.249(12), Yb2-O7 2.384(14), Yb2-O8 2.397(14), Yb2-O9 2.419(13), Yb2-O10 2.349(10), Yb2-O13 2.236(11), Yb2-O16 2.324(14), Yb2-O17 2.221(14), Yb2-O18 2.325(12), N1-Ni1-N2 86.9(7), N1-Ni1-O2 93.5(7), O1-Ni1-O2 84.6(6), O11-Yb1-O12 126.9(5), O11-Yb1-O21 139.6(6), O11-Yb1-O22 80.8(6), O14-Yb1-O22 124.2(4), O19-Yb1-O21 74.8(5), O7-Yb2-O8 54.5(5), O8-Yb2-O13 74.7(5), O16-Yb2-O17 75.6(5), O17-Yb2-O18 77.2(5).

**9:** Ni-N1 1.854(7), Ni-N2 1.856(6), Ni-O1 1.862(6), Ni-O2 1.856(5), Lu1-O11 2.240(6), Lu1-O12 2.242(6), Lu1-O14 2.249(6), Lu1-O19 2.380(6), Lu1-O20 2.272(6), Lu1-O21 2.336(6), Lu1-O22 2.223(6), Lu2-O7 2.366(6), Lu2-O8 2.394(6), Lu2-O9 2.412(6), Lu2-O10 2.351(6), Lu2-O13 2.229(5), Lu2-O16 2.316(6), Lu2-O17 2.196(5), Lu2-O18 2.319(6), N1-Ni1-N2 85.8(3), O1-Ni1-O2 84.9(2), N1-Ni1-O2 94.6(3), O11-Lu1-O12 126.6(2), O11-Lu1-O21 139.2(2), O11-Lu1-O22 80.0(3), O14-Lu1-O22 123.1(2), O19-Lu1-O21 75.3(2), O7-Lu2-O8 54.8(2), O8-Lu2-O13 75.3(2), O16-Lu2-O17 76.7(2), O17-Lu2-O18 77.3(2).

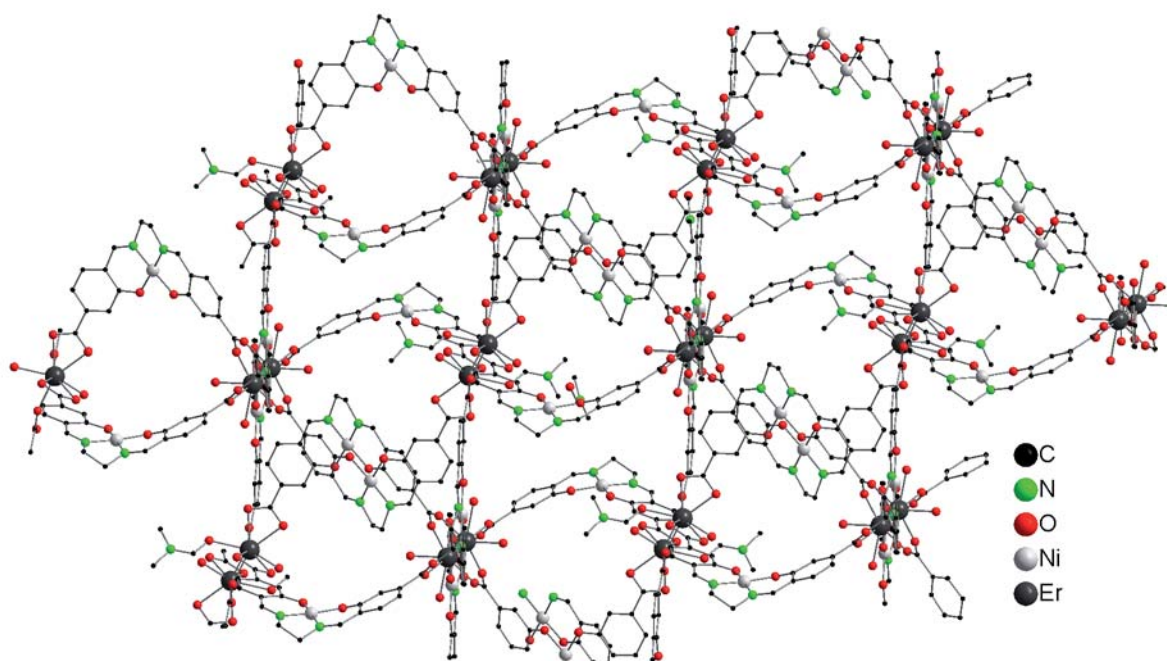


**Figure 3.14** Solid state structure of **6**, omitting hydrogen atoms. Cut out of the polymeric structure. Compounds **6-9** are isostructural.

Reaction of *in situ* prepared compound **1** in DMSO / THF with an aqueous solution of  $\text{Dy}(\text{NO}_3)_3 \cdot (\text{H}_2\text{O})_5$ , resulted in the polymeric dysprosium-nickel compound,  $[\text{Dy}\{(\text{NiL})(\text{DMSO})(\text{NO}_3)\} \cdot (\text{H}_2\text{O})_2 \cdot (\text{DMSO})]_n$  (**10**) (Scheme 3.3). Compound **10**, which has been obtained as red needle-shaped crystals, was characterized by standard analytical / spectroscopic techniques, and the solid state structure was determined by single crystal X-ray diffraction (Figure 3.15). It crystallizes in the monoclinic space group  $P2_1/n$  as polymeric 3D structure. In contrast to compound **6**, only one SBU is formed by a  $[(\text{Dy})_2(\mu\text{-O}_2\text{CR})_2(\eta\text{-O}_2\text{CR})_2]$  building block. This SBU consists of parallelogram having only four points of extension.<sup>[79]</sup> The difference in the SBU of compound **10** compared to **6** is probably due to the

larger ionic radius of dysprosium compared to erbium. The dysprosium atoms are eight-fold coordinated, forming a distorted dodecahedron. This coordination polyhedron is built from four oxygen atoms of two chelating carboxylates, two oxygen atoms of two metal bridging carboxylate groups, one  $\mu\text{-}\eta^2\text{-O}_2\text{NO}$  ion and one molecule of DMSO.

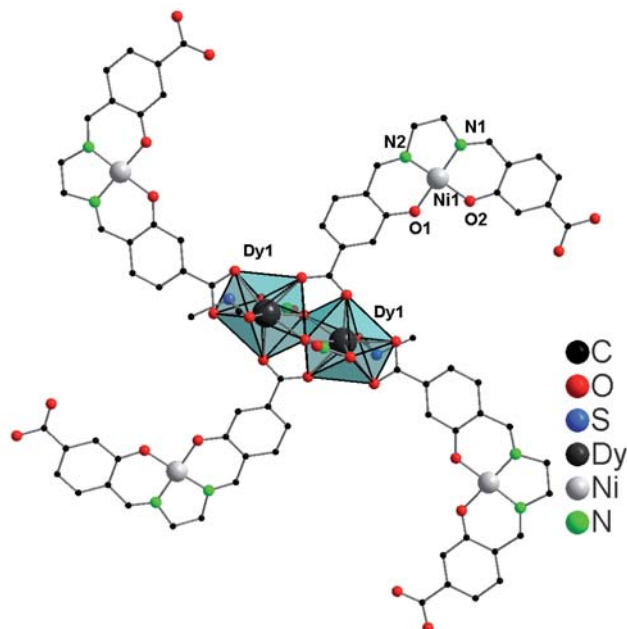


**Figure 3.15** Solid state structures of **10**, omitting hydrogen atoms. The SBU is representing. Selected bond lengths [ $\text{\AA}$ ] and angles [ $^\circ$ ]: Ni1-N1 1.842(7), Ni1-N2 1.855(7), Ni1-O1 1.864(5), Ni1-O2 1.855(5), Dy1-O3 2.395(5), Dy1-O4 2.403(5), Dy1-O5 2.319(5), Dy1-O6 2.299(5), Dy1-O7 2.432(6), Dy1-O8 2.323(5), Dy1-O10 2.298(6), N1-Ni1-N2 85.8(3), N1-Ni1-O1 178.1(3), N1-Ni1-O2 95.0(3), O1-Ni1-O2 84.3(2), O3-Dy1-O4 54.7(2), O5-Dy1-O6 140.8(2), O5-Dy1-O10 105.6(2), O6-Dy1-O10 92.8(2), O7-Dy1-O8 52.9(2).

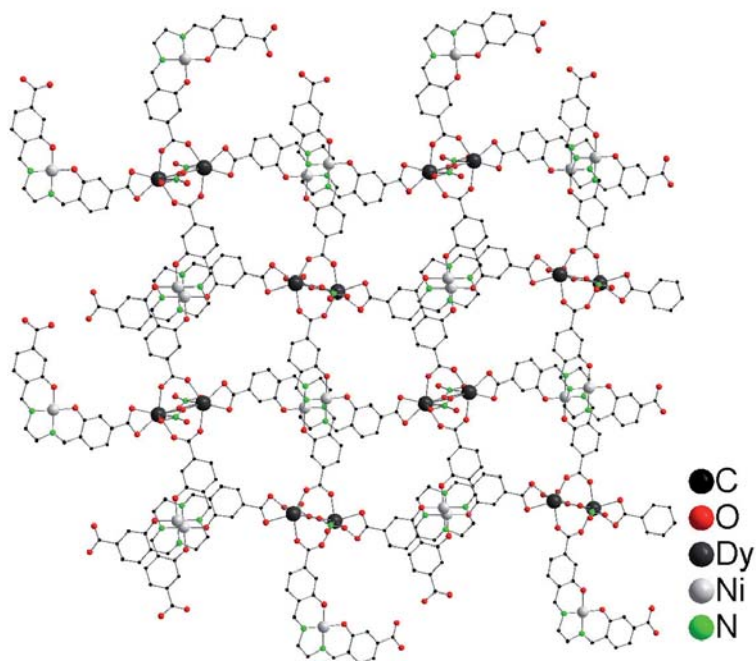


**Figure 3.16** Solid state structure of **10**, omitting hydrogen atoms and solvent molecules. Cut out of polymeric structure.

In contrast to compounds **6-9** the salen unit is almost planar. These rigid struts form a three-dimensional porous network (3.16). The void space of compound **10**, which is filled with DMSO and water, was calculated by PLATON to be 22.1%. The size of the pores is thus estimated to be  $8.4 \times 11.8 \text{ nm}^2$ .

Treatment of  $\text{H}_4\text{L}$ , aqueous NaOH, and  $\text{Ni}(\text{OAc})_2 \cdot (\text{H}_2\text{O})_4$  with  $\text{Yb}(\text{NO}_3)_3 \cdot (\text{H}_2\text{O})_6$  in the presence of DMF / water resulted in a compound formulated as  $[\text{Na}_3\text{Yb}\{(\text{NiL})(\text{H}_2\text{O})\}_3 \cdot (\text{DMF})]_n$  (**11**). Due to different solvent used for metalation leads to the different structural network compare to compound **10**. Compound **11** was isolated as red crystals and characterized by standard analytical / spectroscopic techniques. The solid state structure was determined by single crystal X-ray diffraction (Figure 3.17).

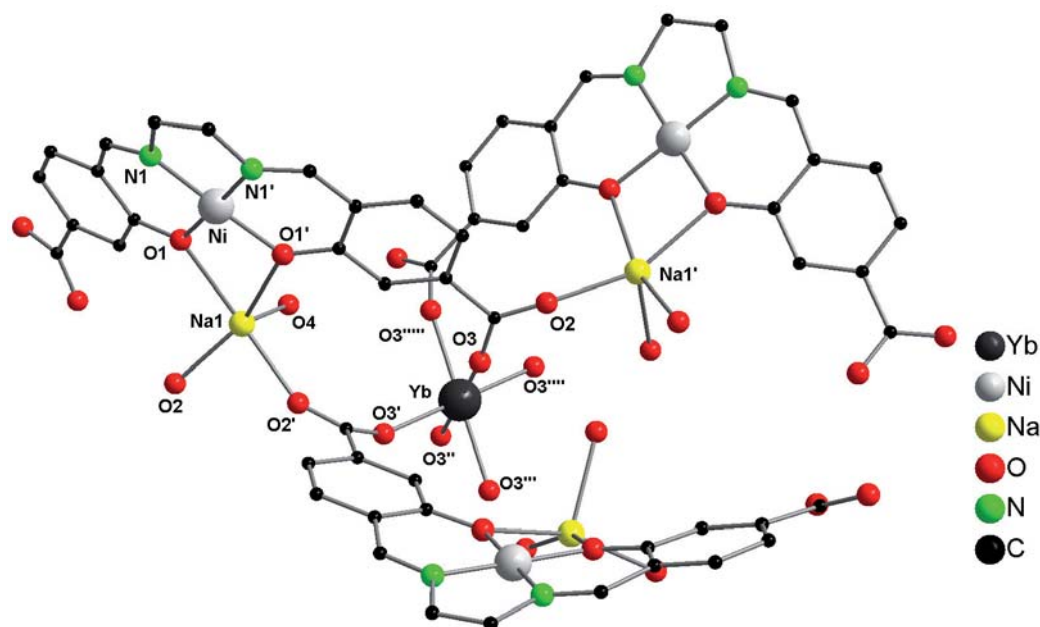


**Figure 3.17** Solid state structure of **11**, omitting hydrogen atoms. Sodium atom is disordered; and selected bond lengths and angles [ $^\circ$ ] are given for both position Na1A and Na1B: Ni-N1 1.843(5), Ni-O1 1.863(4), Yb-O3 2.208(5), Na1A-O1' 2.414(5), Na1B-O1' 2.365(7), Na1A-O2' 2.291(6), Na1B-O2' 2.187(7), Na1A-O4 2.186(11), Na1B-O4 2.795(13), O3-Yb1-O3'' 80.20(2), O3-Yb1-O3''' 180.0(3), O3-Yb-O3'''' 99.80(2), N1-Ni-N1' 84.6(3), N1-Ni-O1 94.1(2), O1-Ni-O1' 87.2(2), O1-Na1A-O1' 64.3(2), O1-Na1B-O1' 65.8(3), O1-Na1A-O2 148.2(3), O1-Na1B-O2 167.5(3), O1-Na1A-O4 112.7(3), O1-Na1B-O4 95.5(3), O2-Na1A-O2' 85.6(3), O2-Na1B-O2' 90.8(4), O2'-Na1A-O4 98.1(3), O2'-Na1B-O4 84.6(3).

Compound **11** crystallizes in the hexagonal space group  $P6_3/m$  with one-sixth of the molecule in the asymmetric unit. The selected bond angles and bond lengths are given in the caption of Figure 3.17. The ytterbium ion is six-fold coordinated; ligated to six carboxylate oxygen atoms (Yb: O3, O3', O3'', O3''', O3'''' and O3''''') from six different  $\text{L}^{4-}$  anions. Thus, the coordination polyhedron can be best described as a distorted octahedron. The Yb-O bond length and O-Yb-O bond angle are 2.208(5) Å and 80.20(2)-180.0(3) $^\circ$ , which are comparable

to those found in other reported Yb(III) complexes.<sup>[96],[97]</sup> The sodium atom is five-fold coordinated with a distorted square pyramidal arrangement.<sup>[98],[99]</sup> Sodium atom Na1 is coordinated to two phenoxy oxygen atoms (O1 and O1'), two carboxylate oxygen atoms (O2 and O2') from two different L<sup>4-</sup> anions and one oxygen atom (O4) from one water molecule. The Na-O bond lengths and O-Na-O bond angles range from 2.186(11) Å to 2.795(13) Å and 64.3(2)° to 167.5(3)°, respectively. The Na1 is disordered over two sites (Na1A and Na1B), both of which have site occupancy factors of 0.5. The Ni(II) ion is hosted in the inner N2O2 compartment of L<sup>4-</sup>, resulting in a square planar arrangement with similar Ni-N and Ni-O bond lengths (Ni-N 1.843(5) Å, Ni-O 1.863(4) Å).<sup>[100]</sup> The two carboxylate groups of each Ni-salen unit exhibit the metal bridging mode: each carboxylate group is bound to the ytterbium ion as well as to sodium ion in a bridging mode. Thus, the network in compound **11** is built from direct interaction among the carboxylate group of the Ni-salen unit with ytterbium ion, resulting in a 1D infinite structure (Figure 3.18). In fact, the Ni-salen unit acts as a linker. All the ytterbium ions and sodium ions in the chain are coplanar with the shortest Yb...Na distance being 5.461(12) Å. The distance between adjacent ytterbium atoms found in compound **11** is 8.261(2) Å. Overall, the 1D chains are interacting through weak interchain  $\pi\cdots\pi$  interactions of the Ni-salen units to create a 2D layer polymer (Figure 3.18).<sup>[101]</sup> In contrast to compound **6** and **10**, compound **11** shows a different structural motif due to less steric demand around the lanthanide ion when the carboxylate group adopts chelating mode rather than a bridging mode. The void space is calculated by the PLATON program to be 9.1%.

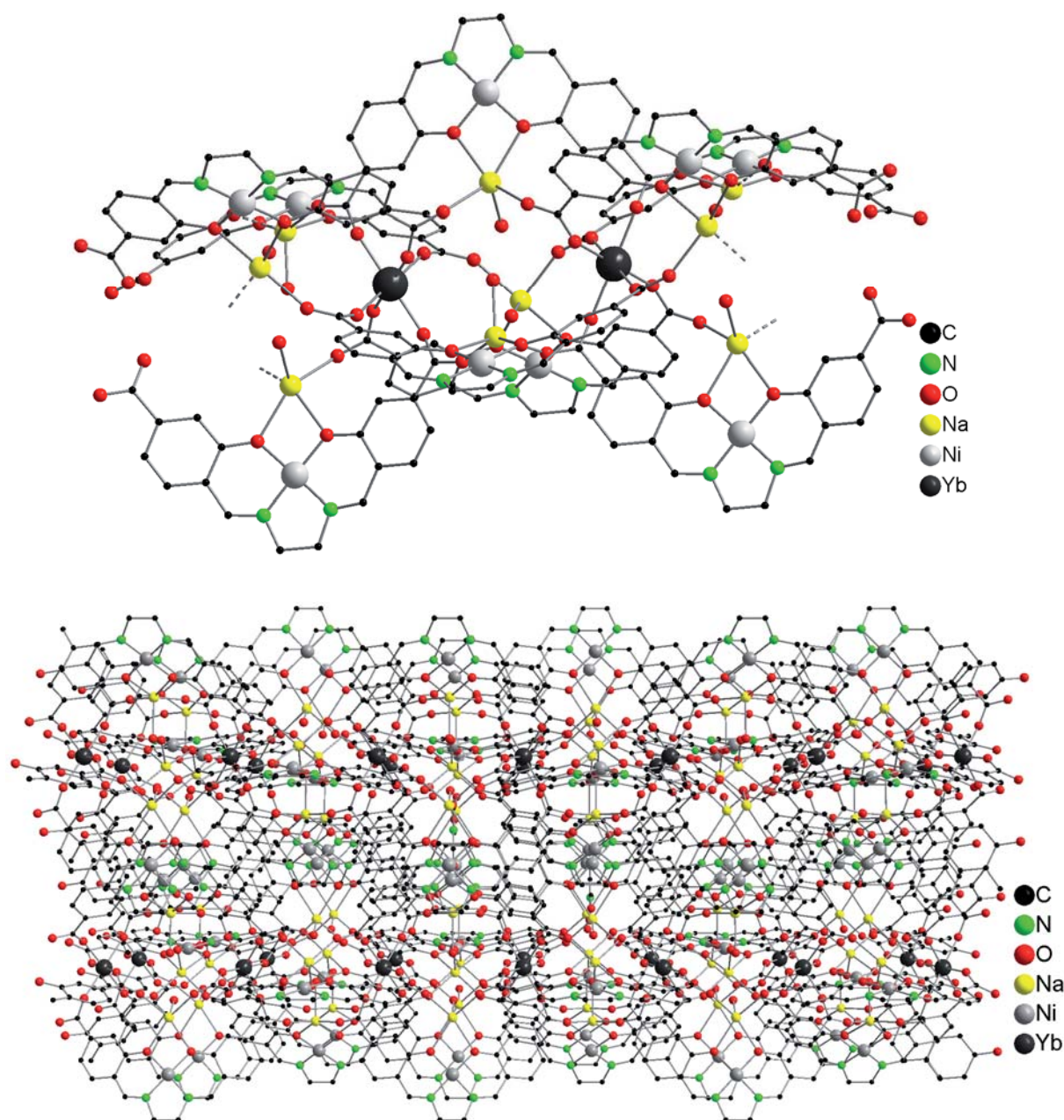


**Figure 3.18** Solid state structure of **11**, omitting hydrogen atoms. Top: Shown is the 1D coordination polymeric structures. Bottom: Shown is the 2D layer polymer.

### 3.2.1.1 Thermogravimetric Analysis of Compounds 6-11

TGA measurements were performed for compounds **6-11** (Figure 3.19). At room temperature they retain their crystalline behavior for a couple of months. The TGA of complex **6** shows that eight of the lattice water molecules are lost in the temperature range of 45°C to 102°C (obsd 6.08%, calcd 6.6%), after which the compound is stable up to 160°C. The other guest solvent molecules (four DMF and two water molecules) are lost in the temperature range of



160°C to 360°C (obsd 14.31%, calcd 15.13%). After the loss of guest solvent molecules, the network begins to decompose with a continuous weight loss up to 450°C. The TGA curve of complex **7** is different. The lattice water molecules are lost in the temperature range of 90°C to 270°C (obsd 6.97%, calcd 7.88%), after which the compound starts to decompose with continuous weight loss up to 550°C. The TGA of complex **8** shows that the lattice water molecules are lost in the temperature range of 42°C to 92°C (obsd 6.55%, calcd 7.88%). The other four DMF lattice solvent molecules are lost in the temperature range of 90°C to 362°C (obsd 14.36%, calcd 13.46%). After the loss of guest solvent molecules, the network begins to decompose with a continuous weight loss up to 650°C. Compound **9** shows a slightly different TGA curve. Eight lattice water molecules are lost in the temperature range of 55°C to 140°C (obsd 6.52%, calcd 6.6%). The other two water molecules and the four DMF lattice solvent molecules are lost in the temperature range of 140°C to 326°C (obsd 13.44%, calcd 14.98%). After the loss of guest solvent molecules, the network begins to decompose with a continuous weight loss up to 450°C.

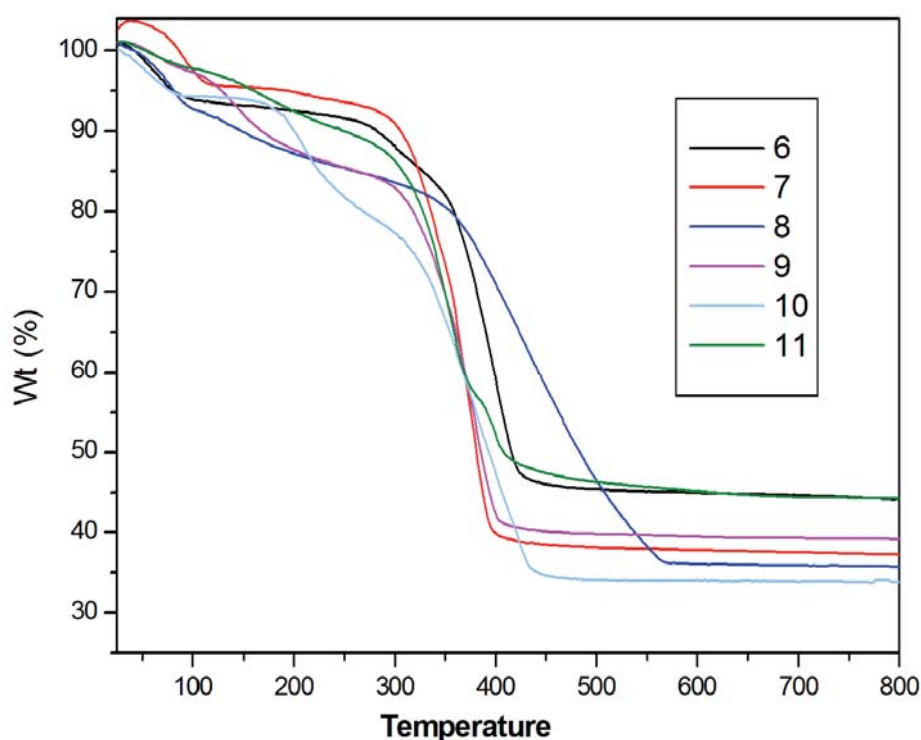


**Figure 3.19** TGA for **6-11** in temperature range of 25-800°C at the heating rate of 5°C / min under the N<sub>2</sub> atmosphere.

A weight loss of 4.3% was observed in the temperature range of 30°C to 90°C, which corresponds to the loss of the coordinated water molecules (calcd 5.27%) in compound **10**. After the initial weight loss, the compound is stable up to 160°C. The two DMSO molecules are lost in the temperature range of 160°C to 310°C (obsd 19.38%, calcd 18.87%). Finally, the compound starts to decompose with continuous weight loss up to 450°C. The TGA curve of complex **11** shows that the three water molecules and one DMF molecule are lost in the temperature range of 140°C to 208°C (obsd 7.92%, calcd 7.9%). Then the organic ligands start to decompose and finally a weight loss was noted at 415°C (obsd 50.82%, calcd 50.18%) due to the loss of one equivalent of  $\text{Yb}_2\text{O}_3$ , three equivalents of  $\text{Na}_2\text{O}$  and three equivalents of  $\text{NiO}$ .

### 3.2.1.2 Gas Adsorption of Compounds **6** and **9**

The  $\text{N}_2$  adsorption / desorption profiles of compounds **6** and **9**, determined by Prof. S. Kureti, refer to the isotherm type III associated with nonporous solids. As a consequence, the derived BET surface areas were found to be low, *e.g.* 2  $\text{m}^2/\text{g}$  for compound **6** (Figure 3.20) and 3  $\text{m}^2/\text{g}$  for compound **9** (Figure 3.21). Obviously, the guest solvent molecules block the existing pores of the samples; hence, they are not accessible for the  $\text{N}_2$  adsorbate. The thermal removal of these solvent molecule leads to decomposition of the framework structure, as shown by the TGA investigations.

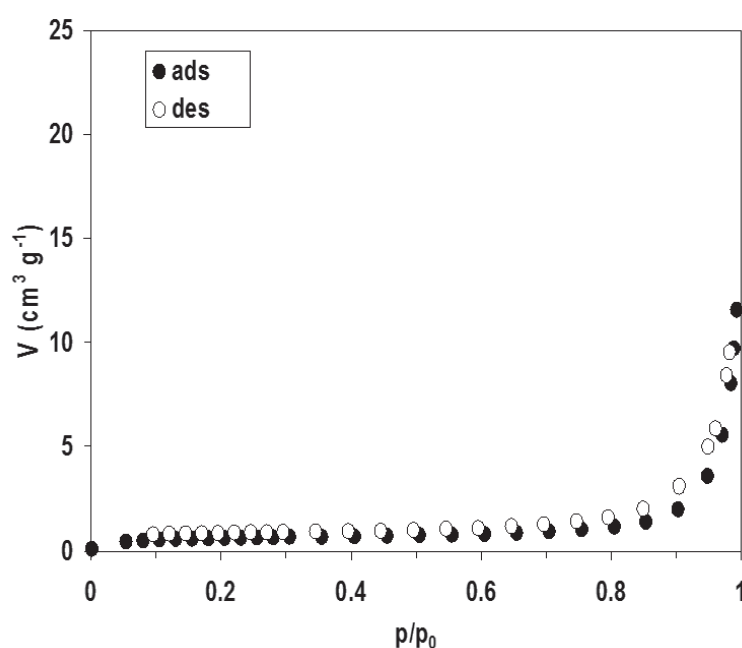


**Figure 3.20**  $\text{N}_2$  adsorption / desorption isotherm of compound **6** at  $-196^\circ\text{C}$ .

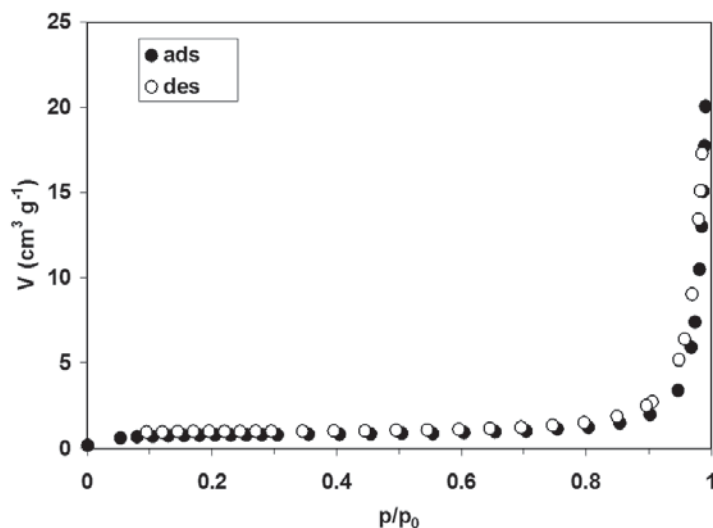
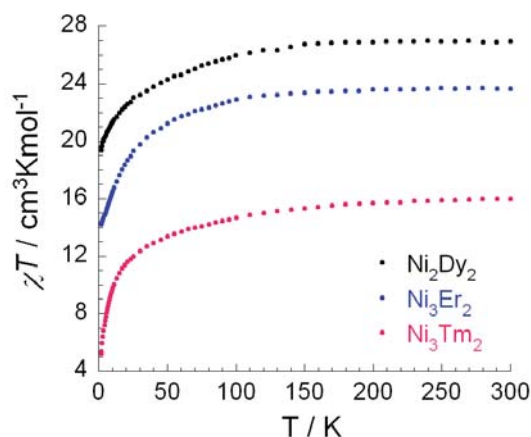


Figure 3.21 N<sub>2</sub> adsorption / desorption isotherm of compound **9** at -196°C.

### 3.2.1.3 Magnetic Properties of Compounds **6**, **7** and **10**

Magnetic studies for compounds **6**, **7** and **10** were performed by Dr. Yanhua Lan (Prof. AK. Powell) using a SQUID magnetometer operating in the 1.8-300 K temperature range with applied magnetic field of 0.1 T. To facilitate comparison with the dimeric moiety in **6** and **9**, the molar susceptibility data for **10** was calculated using a doubled formula weight, 1655.6 g/mol, corresponding to the molecule containing the building block, [(Dy)<sub>2</sub>(μ-O<sub>2</sub>CR)<sub>2</sub>(η<sup>2</sup>-O<sub>2</sub>CR)<sub>2</sub>]. Looking at the structures, the two Ln(III) ions in each building unit are bridged by carboxylates, and pairs of Ln(III) ions are well isolated by diamagnetic metalloligand linkers. Consequently, the magnetic properties of the frameworks can essentially be ascribed to each building unit itself. The temperature dependence of susceptibility for compounds **6**, **7** and **10** shows similar thermal evolution indicating a similarity in their static properties. Upon cooling from room temperature, the  $\chi T$  product of **6**, **7** and **10** monotonically decreases from a value of 23.66, 15.98 and 26.93 cm<sup>3</sup>K/mol, which compares well to two non-interacting Ln(III) ions,<sup>[102]</sup> to a minimum of 14.17, 5.18 and 19.31 cm<sup>3</sup>K/mol at 1.8 K, respectively (Figure 3.22). This behavior suggests the presence of weak antiferromagnetic interactions between the Ln(III) ions, but the decrease in  $\chi T$  probably partially results also from anisotropic effects arising from the Ln(III) centers and from the thermal depopulation of the Ln(III) excited states, as often seen in anisotropic lanthanide-based complexes.



**Figure 3.22** Temperature dependence of the  $\chi T$  product for compounds **6**, **7** and **10** at 0.1 T (with  $\chi$  being the molar susceptibility defined as  $M/H$ ).

The field dependence of magnetization measurements at low temperatures reveals that the magnetization has a relatively rapid increase below 1 T and then follows a weak linear increase to reach a value of 11.2, 7.3 and 10.7  $\mu_B$  at 7 T for **6**, **7** and **10** (Figure 3.23).

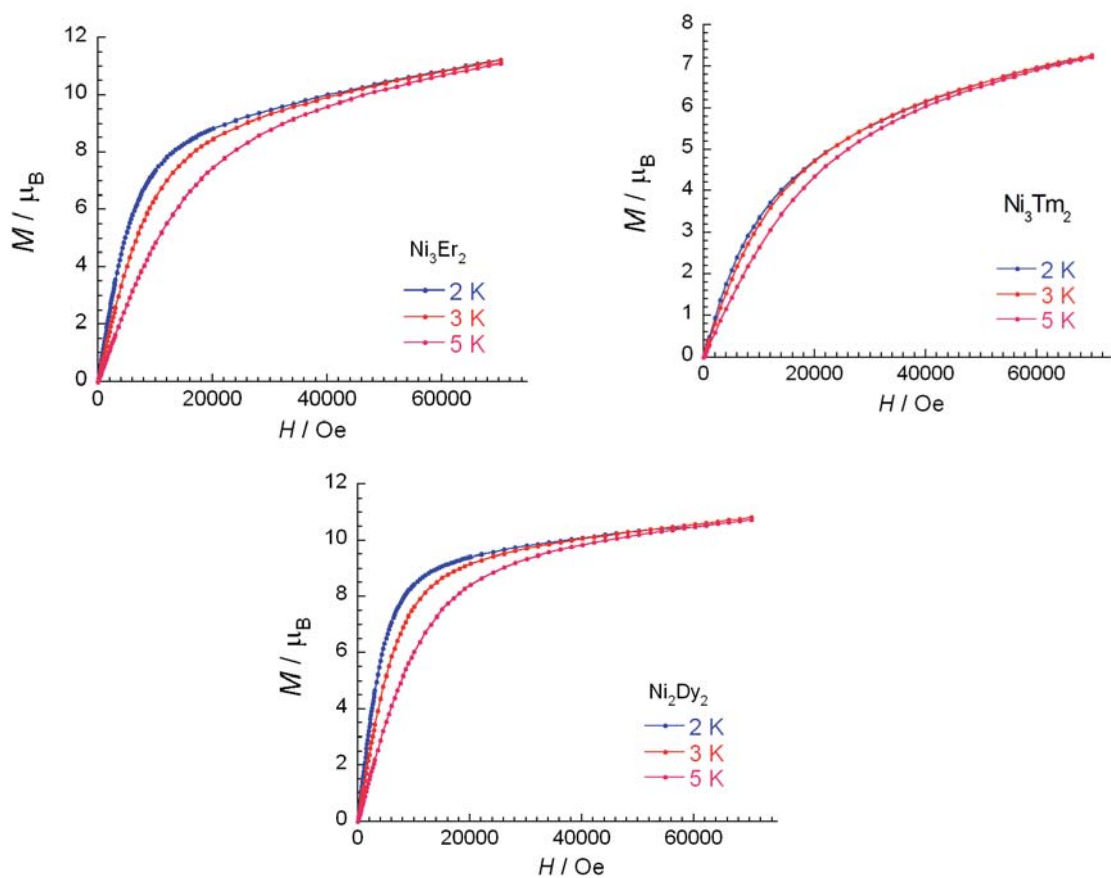


**Figure 3.23** Field dependence of the magnetization from 2-5 K for **6** (top, left), **7** (top, right) and **10** (bottom, center) respectively.

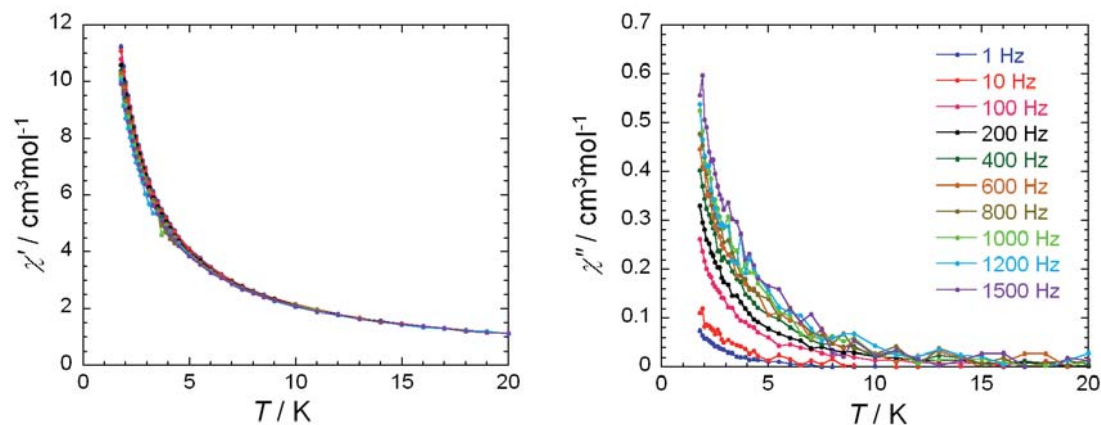


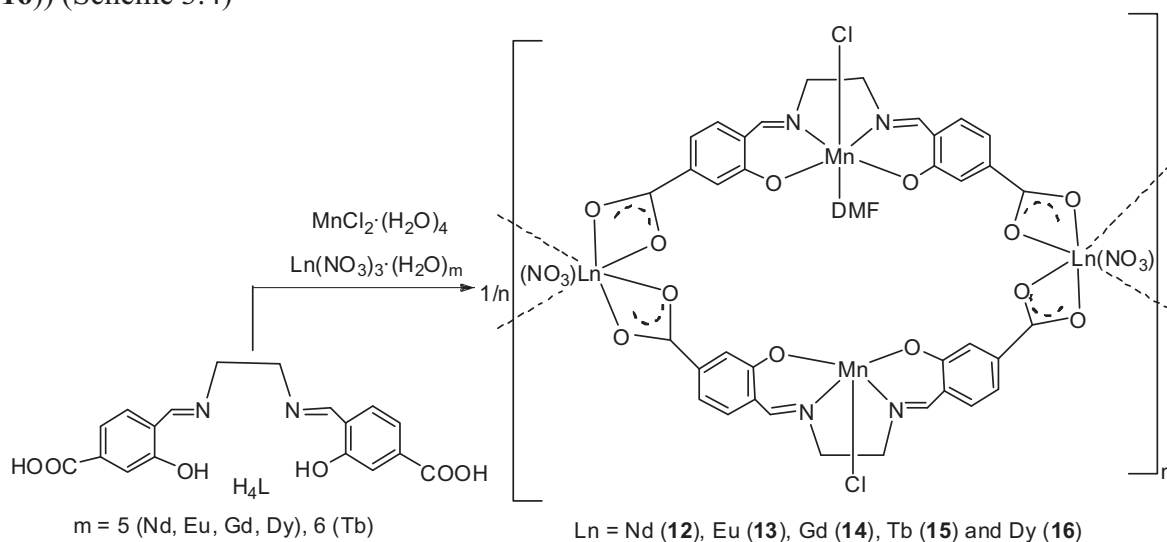
**Figure 3.24** Temperature dependence of the in-phase (left) and out-of-phase (right) components of ac magnetic susceptibility at indicated frequencies for compound **10** under zero dc field.

This behavior indicates the presence of magnetic anisotropy and/or the lack of a well-defined ground state, suggesting the presence of low-lying excited states that might be populated when a field is applied. The magnetic relaxation of compounds **6**, **7** and **10** were tested using ac susceptibility measurements under a zero dc field. We found that only compound **10** exhibits a non-zero frequency dependence of out-of-phase components below 12 K, indicating slow relaxation of its magnetization under these conditions (Figure 3.24). However, the energy barrier for spin-reversal in magnetization can not be determined from this set of data because the maxima of the  $\chi''$  peaks are out of the available ranges on the SQUID (lowest temperature is 1.8 K and highest frequency is 1500 Hz). The barrier for the reversal of the magnetization is undoubtedly generated by the presence of magnetic anisotropy of Dy(III) ions, as often observed in many such types of compounds, but it is impossible to discuss it more based on the obtained data.<sup>[103]</sup>

In conclusion, well defined salen-nickel complexes as a metalloligand in lanthanide-based MOFs have been introduced. By using this strategy, unique structures were obtained, in which the Ni-salen unit acts as flexible strut. The shape of the network is strongly influenced by the ionic radius of the lanthanide element. Magnetic susceptibility measurements under zero dc field showed that the nickel-dysprosium compound exhibits a non-zero frequency dependence of out-of-phase components below 12 K, indicating slow relaxation of its magnetization under these conditions. The presented strategy now offers a new area to prepare new MOF, in which the 3d metals as well as 4f metals can be varied over a wide range.

### 3.2.2 Manganese and Lanthanide Based MOFs

The reaction of  $H_4L$ ,  $MnCl_2 \cdot (H_2O)_4$  and  $Ln(NO_3)_3 \cdot (H_2O)_m$  ( $m = 5$  (Nd, Eu, Gd, Dy) and 6 (Tb)), in the presence of DMF / pyridine resulted in crystalline materials formulated as  $[Ln_2(MnLCl)_2(NO_3)_2(DMF)_5 \cdot (DMF)_4]_n$  ( $Ln = Nd$  (**12**), Eu (**13**), Gd (**14**), Tb (**15**) and Dy (**16**)) (Scheme 3.4)



**Scheme 3.4** Synthetic scheme of compounds **12-16**.

Compounds **12-16** have been characterized by standard analytical / spectroscopic techniques and the solid state structures were established by single X-ray diffraction (Figure 3.25). The IR spectrum of compounds **12-16** show the asymmetric and symmetric stretching bands of the carboxylate groups at around 1593, 1476 and 1386  $cm^{-1}$  for **12**; 1645, 1476 and 1386  $cm^{-1}$  for **13**; 1600, 1464 and 1402  $cm^{-1}$  for **14**; 1617, 1472 and 1386  $cm^{-1}$  for **15**; and 1616, 1470 and 1404  $cm^{-1}$  for **16**. The differences between asymmetric and symmetric stretching bands are 210 and 157  $cm^{-1}$  for **12**; 259 and 169  $cm^{-1}$  for **13**; 198 and 136  $cm^{-1}$  for **14**; 241 and 145  $cm^{-1}$  for **15**; and 212 and 146  $cm^{-1}$  for **16**. This finding indicates that the carboxylate group coordinates to the metal atom in a bridging fashion. The absence of a characteristic absorption band around 1700  $cm^{-1}$  indicates the complete deprotonation of the salen ligands and coordination to the metal ions. Moreover, characteristic stretching vibration bands ( $\nu_1$ - $\nu_4$ ) of the nitrate group are observed (experimental section) in compounds **12-16**, and the difference in wave number between  $\nu_1$  and  $\nu_2$  is about 200  $cm^{-1}$ , indicating that the nitrate group coordinates to the metal in a bidentate chelating mode. Compounds **12-16** are insoluble in common solvents; thus, no NMR data could be acquired.

Suitable crystals of **12-16** were measured by single X-ray diffraction. Compounds **12-16** crystallize in the triclinic space group *P*-1. The selected bond lengths and bond angles are given in the caption of Figure 3.26. Single crystal X-ray diffraction analysis reveals that compounds **12-16** are isostructural; thus, only the structure of **14** is presented in detail. In the asymmetric unit, two gadolinium ions (Gd1 and Gd2), two Mn-salen units ([Mn1LC11](DMF)] and [Mn2LC12]), two nitrate groups, five coordinating DMF molecules and four non-coordinating DMF molecules are found (Figure 3.25). Gd1 is ligated to eight oxygen atoms: four oxygen atoms (O5, O6', O9 and O10') from  $\mu_2$  bidentate bridging carboxylate groups of different Mn-Salen unit, two oxygen atoms (O14 and O15) from one nitrate group and two oxygen atoms (O20 and O21) from DMF molecules. The coordination geometry around the Gd1 ion can be described as a distorted square antiprism. The adjacent gadolinium ions (Gd1 and Gd1') are associated *via* four  $\mu_2$  bidentate bridging carboxylate groups of different Mn-salen units to create the paddlewheel unit I. Gd2 is coordinated by five carboxylate oxygen atoms (O7, O8', O11, O11', O12) of four different Mn-salen units *via* the  $\mu_2$  bidentate as well as  $\mu_3$  tridentate binding mode of carboxylate groups, two oxygen atoms (O17 and O18) from nitrate group and two oxygen atoms (O22 and O23) from two DMF molecules. The coordination polyhedron of Gd2 can be described as a distorted tricapped trigonal prism. This Gd2 ion again creates a paddlewheel unit II with the adjacent gadolinium ion. The Gd-O bond lengths and O-Gd-O bond angles range from 2.278(2) Å to 2.798(2) Å and 49.37(6)° to 154.13(6)°, respectively. These bond lengths and bond angles around the lanthanide ions are comparable with the reported values in the lanthanide polymer.<sup>[104],[105]</sup> In the Mn-salen unit [Mn1LC11](DMF)], the manganese ion adopts a distorted octahedral environment that is built by ONNO atoms of the salen ligand, one chloride ion and one DMF molecule. The chloride ion and DMF molecule occupy the apical position with Mn1-Cl1 and Mn1-O13 bond lengths of 2.521(12) Å and 2.323(2) Å, respectively. The ONNO atoms of the salen ligand form an equatorial plane around the Mn1 atom with Mn-N and Mn-O bond lengths of 1.996(2) Å to 1.998(2) Å and 1.882(2) Å to 1.897(2) Å, respectively. The Mn1 atom and the equatorial plane (O1, N1, N2, and O2) are coplanar with a mean deviation from the plane of 0.095 Å. In contrast to Mn1, Mn2 is bonded to donor ONNO atoms of the salen ligand and one chloride ion. Thus, the Mn2 ion is five-fold coordinated in the Mn-salen unit [Mn2LC12] with square bipyramidal geometry. The equatorial plane around the Mn2 is built from two phenoxy oxygen atoms and two imine nitrogen atoms of the salen ligand (Mn-N and Mn-O equatorial bond lengths are 1.984(2) Å, 1.993(2) Å, 1.866(2) Å and 1.871(2) Å, respectively). The apical position is occupied by a chloride ion with a Mn2-Cl2 bond length

of 2.375(11) Å. The Mn2 atom and the equatorial plane (O3, N3, N4, O4) are coplanar with a mean deviation of 0.307 Å from the plane; thus, Mn2 is further away from the plane with respect to Mn1. The dihedral angle between the two planes (around Mn1 and around Mn2) is 87.50°. The carboxylate groups of the Mn-salen units display two kind of metal bridging modes: (1)  $\mu_2$  bidentate bridging mode where two oxygen atoms of one carboxylate group bind to two gadolinium atoms, and (2)  $\mu_3$  tridentate binding mode, in which one oxygen atom binds to two gadolinium ions and other oxygen atom binds to only one gadolinium ion. The latter kind of binding mode is reported by Ouchi *et al.*<sup>[106]</sup>

The network in compound **14** is built from direct interaction among the salen units and gadolinium ions, resulting in a 1D chain along the *a* axis containing alternating paddlewheel units I and II (Figure 3.25). These 1D chains further interact *via* weak  $\pi \cdots \pi$  interaction to create a 2D network (Figure 3.27). The solvent accessible void space in compound **14** calculated by the PLATON program is 27.9%. The guest DMF molecules occupy the void space, resulting in a microporous framework.

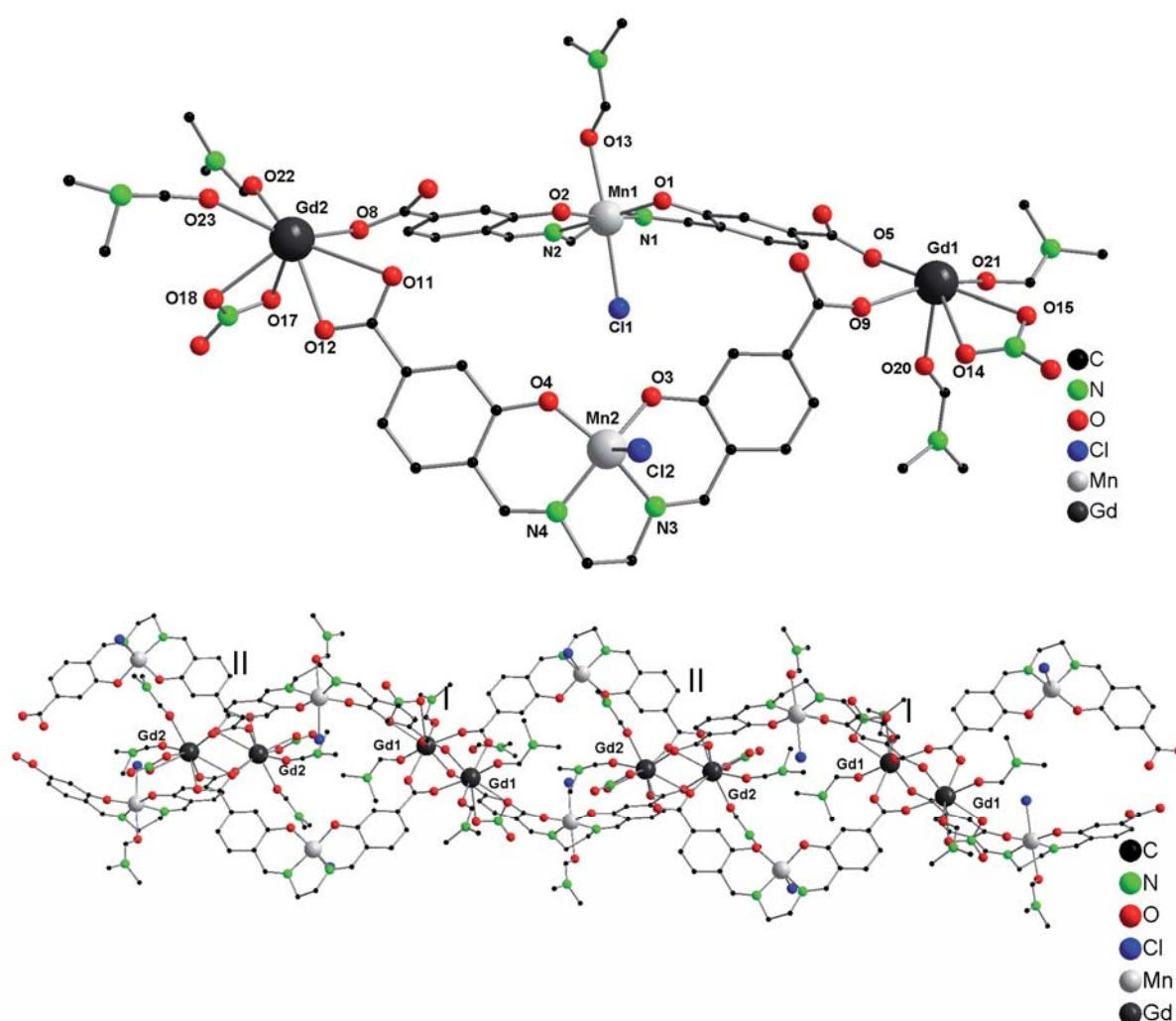


**Figure 3.25** Solid state structures of **14**, omitting hydrogen atoms. Top: asymmetric unit. Bottom: shown is the paddlewheel unit. Compounds **12-16** are isostructural.



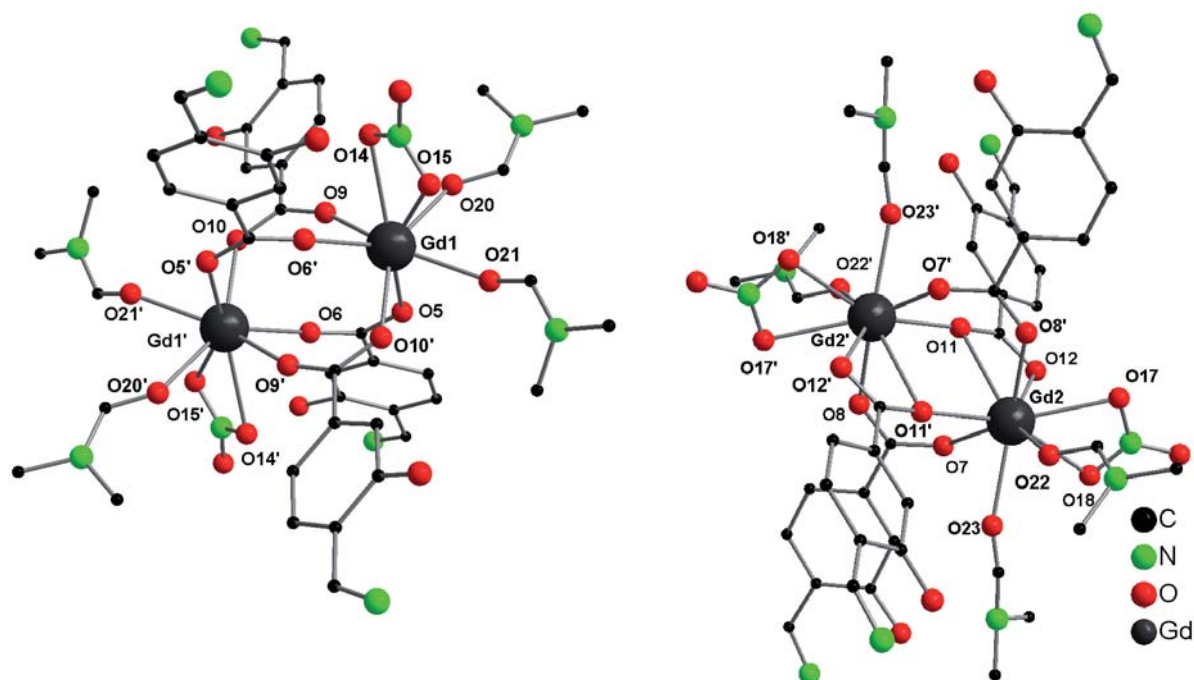


**Figure 3.26:** Coordination arrangements of dysprosium dimers of compound **14**. Compounds **12-16** are isostructural. Selected bond lengths [ $\text{\AA}$ ] and bond angles [ $^\circ$ ]:

**12:** Mn1-N1 1.998(4), Mn1-N2 1.997(4), Mn1-O1 1.881(3), Mn1-O2 1.901(3), Mn1-O13 2.327(4), Mn1-C11 2.524(2), Mn2-C12 2.375(2), Nd1-O5 2.438(4), Nd1-O6' 2.340(4), Nd1-O9 2.325(3), Nd1-O10' 2.440(3), Nd1-O14 2.656(4), Nd1-O15 2.562(4), Nd1-O20 2.448(4), Nd1-O21 2.433(4), Nd2-O7 2.378(3), Nd2-O8' 2.430(3), Nd2-O11 2.778(3), Nd2-O11' 2.412(3), Nd2-O12 2.499(3), Nd2-O17 2.608(4), Nd2-O18 2.556(3), Nd2-O22 2.400(3), Nd2-O23 2.504(4), N1-Mn1-N2 81.35(15), N1-Mn1-O1 90.35(14), N1-Mn1-O2 170.1(2), N1-Mn1-C11 93.60(12), N2-Mn1-O13 86.6(2), O1-Mn1-O2 95.18(13), O1-Mn1-O13 90.42(15), O1-Mn1-C11 93.35(11), O13-Mn1-C11 176.20(11), N3-Mn2-C12 95.54(12), O3-Mn2-C12 98.84(13), O5-Nd1-O10' 83.03(14), O6'-Nd1-O10' 71.15(14), O9-Nd1-O10' 125.79(14), O10'-Nd1-O20 147.46(14), O10'-Nd1-O21 73.05(14), O14-Nd1-O15 48.98(13), O20-Nd1-O21 75.46(15), O7-Nd2-O12 73.33(11), O11-Nd2-O12 49.21(9), O11'-Nd2-O12 124.40(10), O12-Nd2-O22 143.09(12), O12-Nd2-O23 124.35(12), O17-Nd2-O18 49.42(12), O22-Nd2-O23 72.14(12).

**13:** Mn1-N1 1.997(3), Mn1-N2 1.993(3), Mn1-O1 1.881(2), Mn1-O2 1.894(2), Mn1-O13 2.307(3), Mn1-C11 2.524(13), Mn2-C12 2.374(12), Eu1-O5 2.386(2), Eu1-O6' 2.303(3), Eu1-O9 2.285(3), Eu1-O10' 2.390(3), Eu1-O14 2.617(3), Eu1-O15 2.515(3), Eu1-O20 2.394(3), Eu1-O21 2.379(3), Eu2-O7 2.330(2), Eu2-O8' 2.381(3), Eu2-O11 2.765(2), Eu2-O11' 2.359(2), Eu2-O12 2.444(3), Eu2-O17 2.576(3), Eu2-O18 2.503(3), Eu2-O22 2.351(3), Eu2-O23 2.469(3), N1-Mn2-N2 81.49(11), N1-Mn1-O1 90.27(11), N1-Mn1-O2 170.61(11), N1-Mn1-C11 92.90(9), N2-Mn1-O13 86.44(12), O1-Mn1-O2 95.17(10), O1-Mn1-O13 90.71(11), O13-Mn1-C11 176.05(8), O1-Mn1-C11 93.24(9), N3-Mn2-C12 95.38(9), O3-Mn2-C12 98.92(9), O5-Eu1-O10' 82.25(10), O6'-Eu1-O10' 71.79(10), O9-Eu1-O10' 125.12(11), O10'-Eu1-O20 147.51(10), O10'-Eu1-O21 73.07(11), O14-Eu1-O15 49.70(9), O20-Eu1-O21 75.65(11), O7-Eu2-O12 73.31(9), O11-Eu2-O12 49.65(7), O11'-Eu2-O12 124.72(8), O12-Eu2-O22 143.01(9), O12-Eu2-O23 124.79(9), O17-Eu2-O18 50.33(9), O22-Eu2-O23 71.93(9).

**14:** Mn1-N1 1.998(2), Mn1-N2 1.996(2), Mn1-O1 1.882(2), Mn1-O2 1.897(2), Mn1-O13 2.323(2), Mn1-C11 2.521(12), Mn2-C12 2.375(11), Gd1-O5 2.375(2), Gd1-O6' 2.298(2), Gd1-O9 2.278(2), Gd1-O10' 2.381(2), Gd1-O14 2.617(3), Gd1-O15 2.498(2), Gd1-O20 2.393(2), Gd1-O21 2.378(2), Gd2-O7 2.330(2), Gd2-O8' 2.369(2), Gd2-O11 2.798(2), Gd2-O11' 2.340(2), Gd2-O12 2.429(2), Gd2-O17 2.574(2), Gd2-O18 2.499(2), Gd2-O22 2.342(2), Gd2-O23 2.469(2), N1-Mn1-N2 81.51(9), N1-Mn1-O1 90.23(9), N1-Mn1-O2 170.11(9), N1-Mn1-C11 93.41(7), N2-Mn1-O13 86.37(10), O1-Mn1-O2 95.33(8), O1-Mn1-O13 90.53(9), O1-Mn1-C11 93.50(7), O13-Mn1-C11 175.95(7), N3-Mn2-C12 95.63(8), O3-Mn2-C12 99.13(8), O5-Gd1-O10' 82.13(9), O6'-Gd1-O10' 72.06(9), O9-Gd1-O10' 125.06(9), O10'-Gd1-O20 147.60(8), O10'-Gd1-O21 72.88(8), O14-Gd1-O15 49.82(8), O20-Gd1-O21 75.98(9), O7-Gd2-O12 74.07(7), O11-Gd2-O12 49.34(6), O11'-Gd2-O12 124.83(7), O12-Gd2-O22 142.81(7), O12-Gd2-O23 125.90(7), O17-Gd2-O18 50.29(8), O22-Gd2-O23 71.67(7). (See next page for compound **15**).

**15:** Mn1-N1 1.998(4), Mn1-N2 1.999(4), Mn1-O1 1.881(3), Mn1-O2 1.900(4), Mn1-O13 2.313(4), Mn1-C11 2.524(2), Mn2-Cl2 2.374(2), Tb1-O5 2.355(3), Tb1-O6' 2.272(3), Tb1-O9 2.258(4), Tb1-O10' 2.361(4), Tb1-O14 2.597(4), Tb1-O15 2.475(4), Tb1-O20 2.365(4), Tb1-O21 2.354(4), Tb2-O7 2.314(3), Tb2-O8' 2.347(3), Tb2-O11 2.784(3), Tb2-O11' 2.319(4), Tb2-O12 2.423(4), Tb2-O17 2.552(4), Tb2-O18 2.478(4), Tb2-O22 2.316(3), Tb2-O23 2.451(4), N1-Mn1-N2 81.6(2), N1-Mn1-O1 90.37(15), N1-Mn1-O2 170.5(2), N1-Mn1-C11 92.95(14), N2-Mn1-O13 86.4(2), O1-Mn1-O2 95.15(14), O1-Mn1-O13 90.6(2), O1-Mn1-C11 93.32(12), O13-Mn1-C11 176.02(11), N3-Mn2-Cl2 95.42(12), O3-Mn2-Cl2 99.16(13), O5-Tb1-O10' 82.17(14), O6'-Tb1-O10' 72.26(14), O9-Tb1-O10' 124.80(15), O10'-Tb1-O20 147.53(15), O10'-Tb1-O21 72.92(15), O14-Tb1-O15 49.93(14), O20-Tb1-O21 75.9(2), O7-Tb2-O12 73.39(12), O11-Tb2-O12 49.67(11), O11'-Tb2-O12 125.00(11), O12-Tb2-O23 125.60(13), O12-Tb2-O22 142.87(12), O17-Tb2-O18 50.88(13), O22-Tb2-O23 71.82(13).

**16:** Mn1-N1 2.000(5), Mn1-N2 1.995(5), Mn1-O1 1.883(4), Mn1-O2 1.900(4), Mn1-O13 2.326(5), Mn1-C11 2.523(2), Mn2-Cl2 2.378(2), Dy1-O5 2.352(5), Dy1-O6' 2.265(5), Dy1-O9 2.245(5), Dy1-O10' 2.360(5), Dy1-O14 2.606(6), Dy1-O15 2.467(5), Dy1-O20 2.363(5), Dy1-O21 2.353(6), Dy2-O7 2.301(4), Dy2-O8' 2.341(5), Dy2-O11 2.813(4), Dy2-O11' 2.299(4), Dy2-O12 2.395(4), Dy2-O17 2.554(5), Dy2-O18 2.466(5), Dy2-O22 2.313(5), Dy2-O23 2.452(5), N1-Mn1-N2 81.7(2), N1-Mn1-O1 90.2(3), N1-Mn1-O2 170.2(2), N1-Mn1-C11 93.5(2), N2-Mn1-O13 86.2(2), O1-Mn1-O2 95.1(2), O1-Mn1-O13 90.9(2), O1-Mn1-C11 93.28(15), O13-Mn1-C11 175.86(14), N3-Mn2-Cl2 95.4(2), O3-Mn2-Cl2 99.3(2), O5-Dy1-O10' 81.7(2), O6'-Dy1-O10' 73.0(2), O9-Dy1-O10' 126.0(2), O10'-Dy1-O20 147.3(2), O10'-Dy1-O21 72.3(2), O14-Dy1-O15 50.1(2), O20-Dy1-O21 76.2(2), O7-Dy2-O12 74.6(2), O11-Dy2-O12 49.30(12), O11'-Dy2-O12 124.96(15), O12-Dy2-O22 142.4(2), O12-Dy2-O23 127.5(2), O17-Dy2-O18 50.2(2), O22-Dy2-O23 71.4(2).

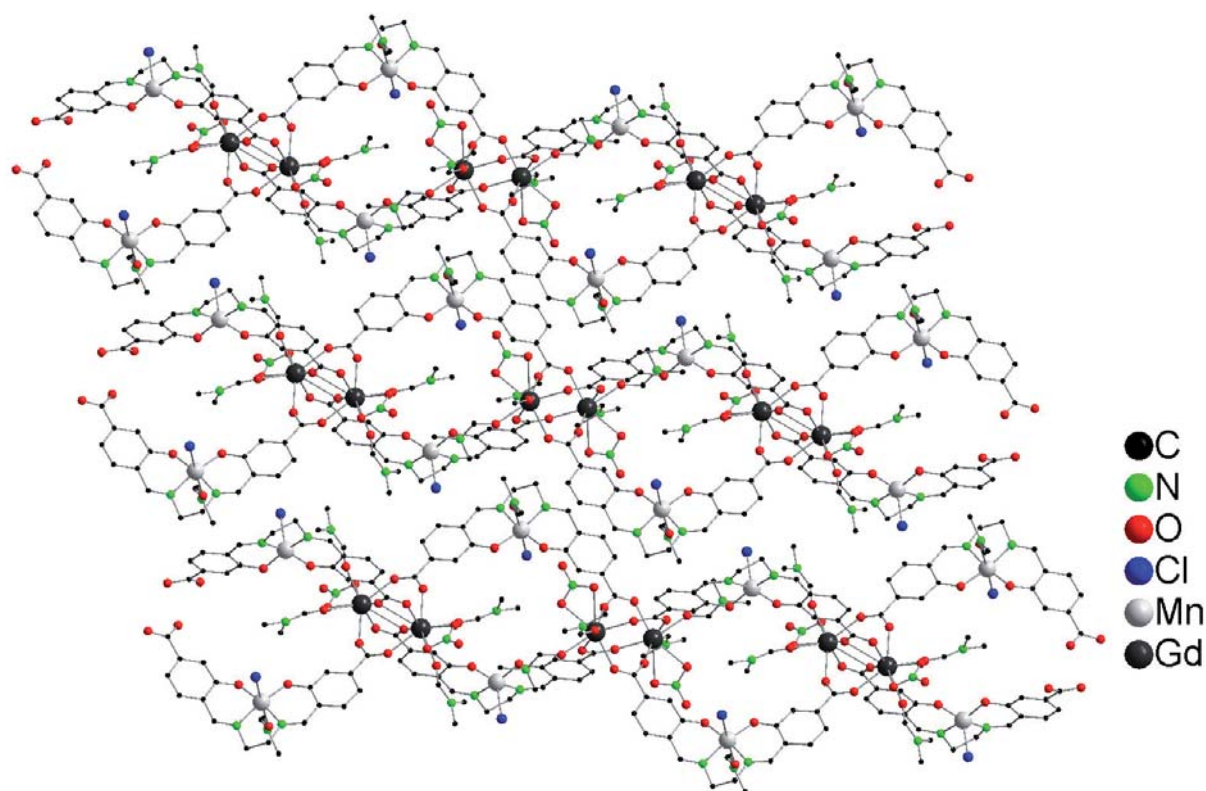


**Figure 3.27** Solid state structures of **14**, omitting hydrogen atoms. Cut out of the polymeric structure. Compounds **12-16** are isostructural.

### 3.2.2.1 Thermogravimetric Analysis of Compounds 12-16

Compounds **12-16** were investigated by TGA measurements (Figure 3.28). In compound **12** there is a weight loss around 240°C (obsd 18.3%, calcd 18.69%) arising from the lose of five

DMF molecules, followed by the loss of three DMF molecules in the temperature range of 280°C to 330°C (obsd 11.23%, calcd 11.21%). The remaining DMF molecule and the organic linker start to decompose with a continuous weight loss up to 500°C. The TGA of **13** shows that the four non-coordinated DMF molecules of the lattice are lost in the temperature range of 100°C to 230°C (obsd 14.13%, calcd 14.83%). The five coordinated DMF molecules in complex **13** are lost in the temperature range of 270°C to 360°C (obsd 19.52%, calcd 18.54%). In the case of **14**, a weight loss is found due to the release of five DMF molecules in the temperature range of 90°C to 160°C (obsd 18.71%, calcd 18.44%), and the remaining four DMF molecules are lost in the temperature range of 190°C to 322°C (obsd 14.27%, calcd 14.27%). Finally, the network decomposes at a temperature of 500°C.

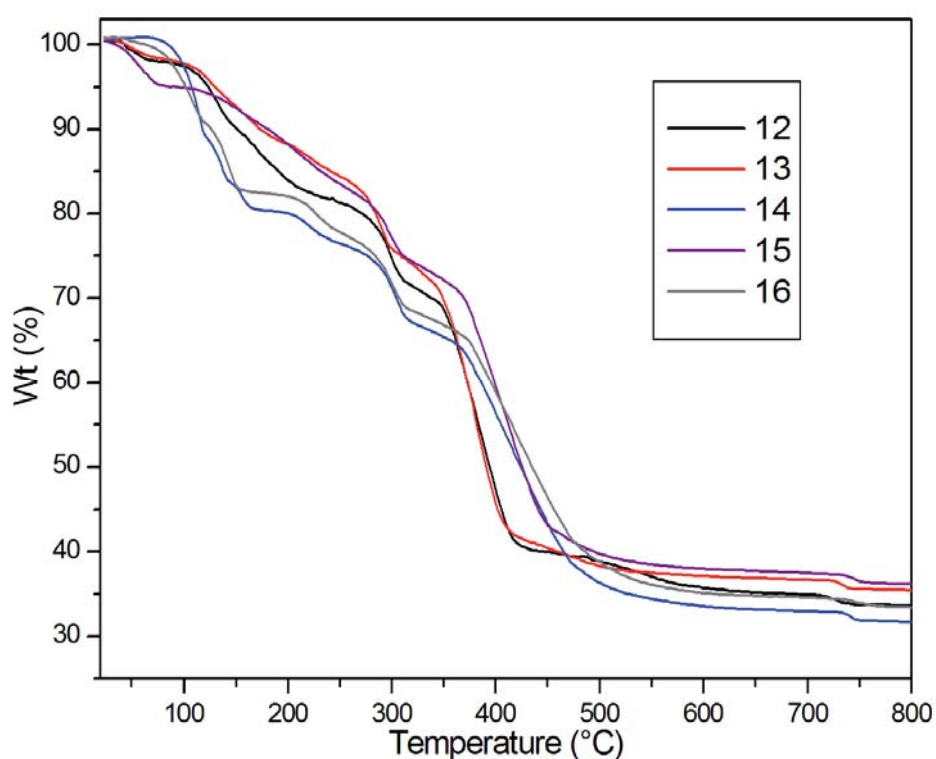


**Figure 3.28** TGA for compounds **12-16** in temperature range of 20 to 800°C at the heating rate of 5°C / min under the N<sub>2</sub> atmosphere.

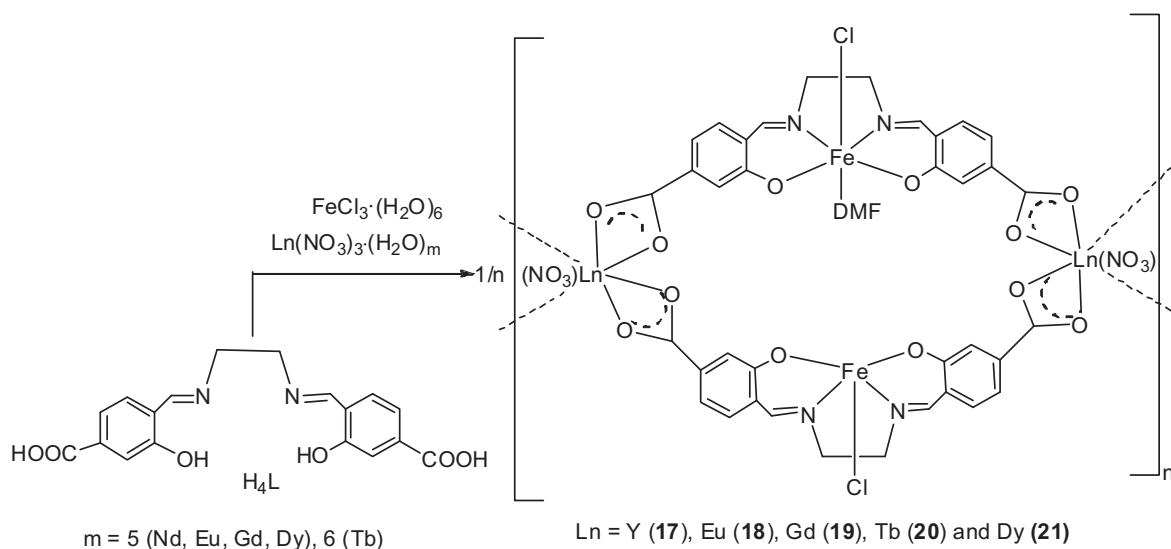
The weight loss of compound **15** is different from the others. First, one DMF molecule is lost at a temperature of 70°C (obsd 4.17%, calcd 3.68%), and then seven more DMF molecules are lost in the temperature range of 120°C to 364°C (obsd 24.97%, calcd 25.75%). Finally, the remaining DMF molecule and the organic frameworks begin to decompose with continuous weight loss up to 550°C. For complex **16**, a weight loss is observed from 70°C to 160°C, which is attributed to the loss of five DMF molecules, a weight loss of 14.88%

(calcd 14.82%). The remaining four DMF molecules decompose in the temperature range of 200°C to 346°C, and then the frameworks collapse at 500°C.

In summary, a series of manganese-lanthanide MOFs have been synthesized by solvothermal reactions. Compounds **12-16** represent infinite 1D chains, which, further extended, result in 2D frameworks in the solid state. Notably, the two different metalloligand systems are connected to trivalent lanthanides to form an infinite chain structure. The guest solvent molecules occupy the void space in the framework. The TGA analysis reveals that compounds **12-16** are robust. A heterogeneous catalytic study of compound **14** is in process.

### 3.2.3 Iron and Lanthanide Based MOFs

The reaction of  $H_4L$ ,  $FeCl_3 \cdot (H_2O)_6$  and  $Ln(NO_3)_3 \cdot (H_2O)_m$  ( $m = 5$  (Eu, Gd, Dy), 6 (Y, Tb)) in the presence of DMF / pyridine under solvothermal conditions results in the isolation of compounds formulated as  $[Ln_2(FeLCl)_2(NO_3)_2(DMF)_5 \cdot (DMF)_4]_n$  ( $Ln = Y$  (**17**), Eu (**18**), Gd (**19**), Tb (**20**) and Dy (**21**)) (Scheme 3.5).



**Scheme 3.5** Synthetic scheme of compounds **17-21**.

All compounds were obtained as red crystalline material and characterized by standard analytical and spectroscopic techniques. In the IR spectra, the asymmetric and symmetric stretching bands for carboxylate groups are observed at around 1614, 1477 and 1403  $cm^{-1}$  for **17**; 1597, 1462 and 1401  $cm^{-1}$  for **18**; 1600, 1475 and 1402  $cm^{-1}$  for compound **19**; 1611, 1480 and 1385  $cm^{-1}$  for **20**; and 1616, 1475 and 1404  $cm^{-1}$  for **21**. The differences between

asymmetric and symmetric stretching bands, 211 and 74  $\text{cm}^{-1}$  for **17**; 196 and 61  $\text{cm}^{-1}$  for **18**; 198 and 73  $\text{cm}^{-1}$  for **19**; 226 and 95  $\text{cm}^{-1}$  for **20**; 212 and 71  $\text{cm}^{-1}$  for **21**, indicate that the carboxylate group is coordinated to the metal ions through a bridging as well as a chelating fashion. The absence of a characteristic absorption band in the range of 1700  $\text{cm}^{-1}$  indicates the complete deprotonation of the salen ligands and coordination to metal ions. Moreover, the characteristic stretching vibrations bands ( $\nu_1$  to  $\nu_4$ ) of the nitrate group are observed (experimental section) in compounds **17-21**, and the difference in the wave number between  $\nu_1$  and  $\nu_2$  is about 200  $\text{cm}^{-1}$ , indicating that the nitrate group is coordinating to the metal ion in a bidentate chelating mode.

The solid state structures were determined by single crystal X-ray diffraction (Figure 3.29). Compounds **17-21** crystallize in the triclinic space group *P*-1. They are isostructural; thus, only the structure of **21** will be described in detail. Selected bond length and bond angles are listed in the caption of Figure 3.30. The asymmetric unit of compound **21** contains two dysprosium ions (Dy1 and Dy2), two different Fe-salen units ((Fe1LC11)(DMF)) and (Fe2LC12)), two nitrate groups, four coordinating DMF molecules, and five non-coordinating DMF molecules. Two neighboring dysprosium ions (Dy1 and Dy1') are connected together *via* four carboxylate groups from four different Fe-salen units to form the paddlewheel unit I (Figure 3.29). Each Dy1 is nine-fold coordinated; they are ligated to four carboxylate groups from four different Fe-salen units, one nitrate group and two molecules of DMF. The coordination polyhedron of Dy1 can be described as a distorted tricapped trigonal prism. Dy2 is connected *via* four  $\mu_2$  bidentate carboxylate groups from four different Fe-salen units to form the paddlewheel unit II (Figure 3.29). In contrast to Dy1, Dy2 is ligated to eight oxygen atoms: four oxygen atoms (O5, O6', O9 and O10') from  $\mu_2$  bidentate bridging carboxylate groups of the Fe-salen unit, two oxygen atoms (O14 and O15) from one nitrate group and two oxygen atoms (O20 and O21) from two DMF molecules. This polyhedron can be described as distorted square antiprism. The Dy-Dy distances in the paddlewheel units I and II are 4.0496(9) Å and 4.1996(10) Å, respectively. The Dy-O bond distances are in the range of 2.280(5) Å to 2.860(5) Å, which is comparable to reported dysprosium coordination polymers.<sup>[107],[108],[109]</sup> In the first Fe-salen unit ((Fe1LC11)(DMF)), Fe1 is coordinated to the salen ligand, one chloride ion and one DMF molecule, resulting in a distorted octahedral geometry with the chloride ion and the oxygen atom of the DMF molecule in apical positions.<sup>[110]</sup> In the second Fe-salen unit (Fe2LC12), Fe2 adopts a square-pyramidal geometry with a chloride ion in the apical position. The Fe-N and Fe-O bond lengths range from 2.078(5) Å to 2.120(7) Å and 1.876(5) Å to 1.910(5) Å, respectively, which is common for

the Fe-salen unit.<sup>[111]</sup> The Fe-Cl bond distances in compound **21** are 2.368(2) Å and 2.231(3) Å for Fe1 and Fe2, respectively. Connecting the asymmetric units results in a 1D chain along *a* axis having alternating paddlewheel units I and II (Figure 3.29). Carefully examining the structure of compound **21**, we found that the Fe-salen units act as a linker to form the infinite chain, and this linker is not likely to be rigid. This 1D chain also interacts with neighboring 1D chains *via*  $\pi$ - $\pi$  interactions, resulting in a 2D porous structure that possesses large free void space (Figure 3.31). The solvent DMF molecules occupy the void space. The total potential solvent accessible void volume of compound **21** calculated by PLATON is 28%.

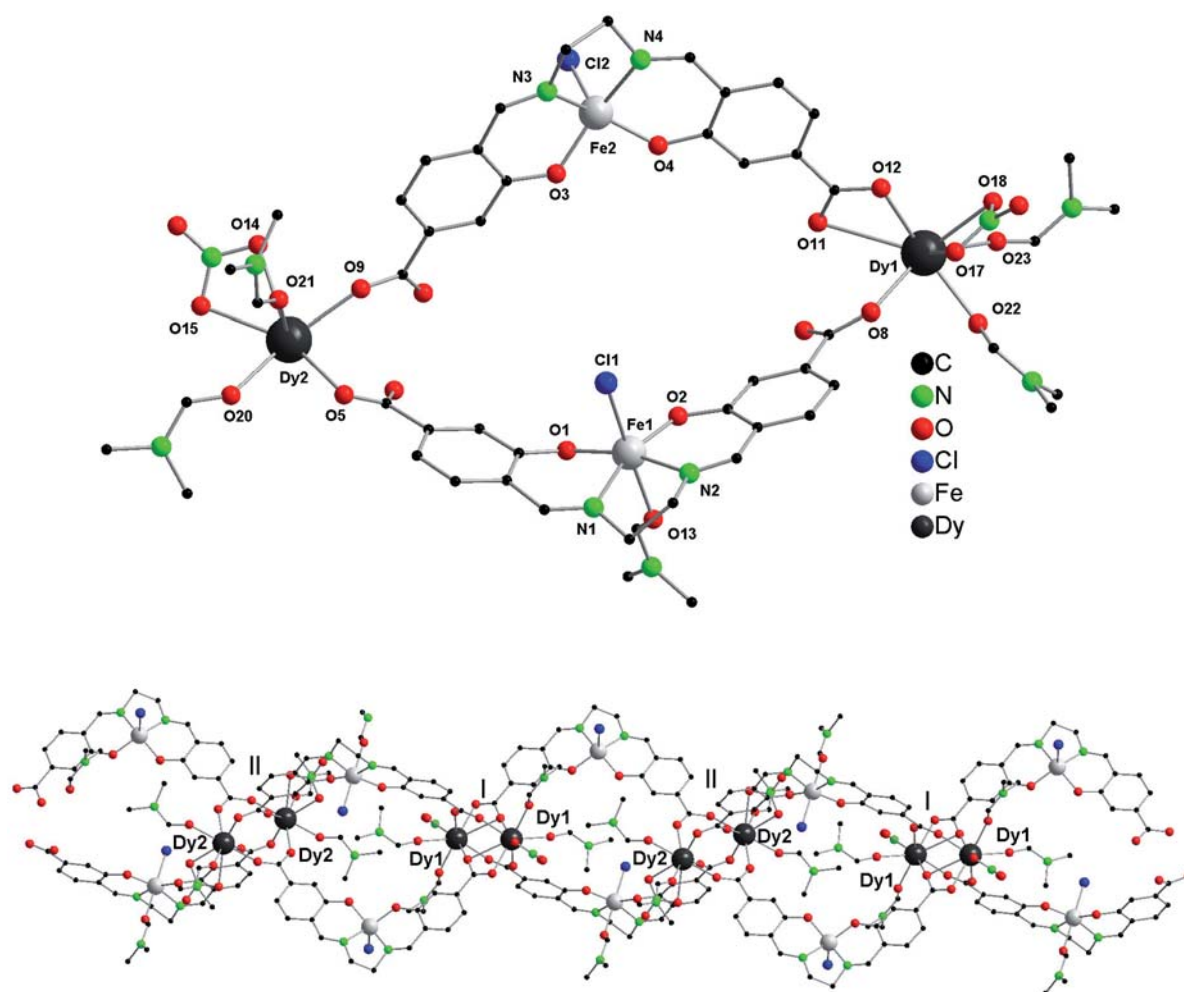


**Figure 3.29** Solid state structures of **21**, omitting hydrogen atoms. Top: asymmetric unit. Bottom: Paddlewheel unit. Compounds **17-21** are isostructural.

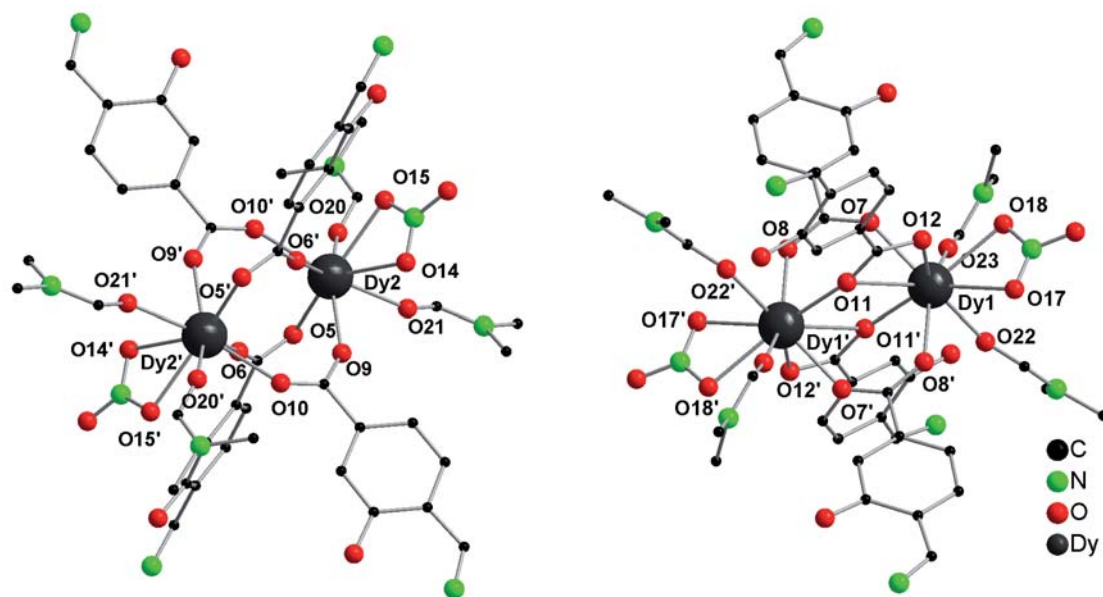


**Figure 3.30** Solid state structures of **21**, shown is the coordination arrangements of dysprosium dimers, omitting hydrogen atoms. Compounds **17-21** are isostructural. Selected bond lengths [Å] and bond angles [°]:

**17:** Fe1-N1 2.114(6), Fe1-N2 2.113(5), Fe1-O1 1.908(5), Fe1-O2 1.897(4), Fe1-O13 2.144(5), Fe1-C11 2.365(2), Fe2-C12 2.225(3), Y1-O7 2.262(5), Y1-O8 2.314(5), Y1-O11 2.892(5), Y1-O11' 2.264(5), Y1-O12 2.372(5), Y1-O17 2.548(6), Y1-O18 2.450(6), Y1-O22 2.289(6), Y1-O23 2.418(5), Y2-O5 2.334(4), Y2-O6' 2.266(5), Y2-O9 2.265(4), Y2-O10' 2.327(5), Y2-O14 2.582(5), Y2-O15 2.426(5), Y2-O20 2.373(5), Y2-O21 2.337(6), N1-Fe1-N2 77.5(2), N1-Fe1-O1 89.4(2), N1-Fe1-O2 164.4(2), N1-Fe1-C11 90.3(2), N2-Fe1-O13 84.70(2), O1-Fe1-O13 84.7(2), O1-Fe1-C11 96.8(2), O13-Fe1-C11 174.86(15), N3-Fe2-C12 97.8(2), O3-Fe2-C12 111.6(2), O7-Y1-O8' 129.8(2), O7-Y1-O11 65.92(15), O7-Y1-O11' 76.3(2), O7-Y1-O12 75.4(2), O7-Y1-O17 133.3(2), O7-Y1-O18 91.3(2), O7-Y1-O22 140.2(2), O7-Y1-O23 72.4(2), O11'-Y1-O12 125.2(2), O17-Y1-O18 51.4(2), O22-Y1-O23 70.8(2), O5-Y2-O6' 124.1(2), O6'-Y2-O9 77.3(2), O6'-Y2-O20 138.0(2), O6'-Y2-O21 139.0(2), O9-Y2-O10' 130.1(2), O14-Y2-O15 50.4(2).

**18:** Fe1-N1 2.119(3), Fe1-N2 2.126(4), Fe1-O1 1.907(3), Fe1-O2 1.909(3), Fe1-O13 2.166(3), Fe1-C11 2.367(15), Fe2-C12 2.232(2), Eu1-O7 2.328(3), Eu1-O8' 2.385(3), Eu1-O11 2.836(3), Eu1-O11' 2.348(3), Eu1-O12 2.427(3), Eu1-O17 2.591(4), Eu1-O18 2.506(4), Eu1-O22 2.348(3), Eu1-O23 2.481(3), Eu2-O5 2.400(3), Eu2-O6' 2.340(3), Eu2-O9 2.313(3), Eu2-O10' 2.388(3), Eu2-O14 2.620(3), Eu2-O15 2.495(3), Eu2-O20 2.429(3), Eu2-O21 2.409(4), N1-Fe1-N2 77.08(13), N1-Fe1-O1 87.60(13), N1-Fe1-O2 163.04(14), N1-Fe1-C11 93.32(10), N2-Fe1-O13 85.44(14), O1-Fe1-O13 90.81(14), O1-Fe1-C11 93.58(10), O13-Fe1-C11 174.92(11), N3-Fe2-C12 100.60(12), O3-Fe2-C12 105.37(13), O7-Eu1-O8' 130.69(10), O7-Eu1-O11 66.04(9), O7-Eu1-O11' 75.26(10), O7-Eu1-O12 74.85(10), O7-Eu1-O17 133.70(11), O7-Eu1-O18 94.05(13), O7-Eu1-O22 140.47(10), O7-Eu1-O23 72.36(10), O11'-Eu1-O12 124.95(10), O17-Eu1-O18 49.92(12), O22-Eu1-O23 71.47(11), O5-Eu2-O6' 123.85(11), O6'-Eu2-O9 76.44(12), O6'-Eu2-O20 137.70(13), O6'-Eu2-O21 139.31(12), O9-Eu2-O10' 130.93(10), O14-Eu2-O15 49.64(12).

**19:** Fe1-N1 2.109(4), Fe1-N2 2.129(4), Fe1-O1 1.905(3), Fe1-O2 1.908(3), Fe1-O13 2.174(4), Fe1-C11 2.367(2), Fe2-C12 2.232(2), Gd1-O7 2.322(3), Gd1-O8' 2.378(3), Gd1-O11 2.848(3), Gd1-O11' 2.329(3), Gd1-O12 2.414(3), Gd1-O17 2.588(4), Gd1-O18 2.492(4), Gd1-O22 2.340(4), Gd1-O23 2.466(4), Gd2-O5 2.390(3), Gd2-O6' 2.326(4), Gd2-O9 2.307(3), Gd2-O10' 2.380(3), Gd2-O14 2.621(4), Gd2-O15 2.489(4), Gd2-O20 2.420(4), Gd2-O21 2.389(4), N1-Fe1-N2 77.35(15), N1-Fe1-O1 87.34(14), N1-Fe1-O2 162.88(15), N1-Fe1-C11 93.35(12), N2-Fe1-O13 84.9(2), O1-Fe1-O13 90.77 (15), O1-Fe1-C11 93.66(11), O13-Fe1-C11 174.88(11), N3-Fe2-C12 100.72(13), O3-Fe2-C12 105.60(14), O7-Gd1-O8' 130.20(11), O7-Gd1-O11 65.54(11), O7-Gd1-O11' 75.56(12), O7-Gd1-O12 74.71(12), O7-Gd1-O17 133.71(13), O7-Gd1-O18 93.93(14), O7-Gd1-O22 140.67(13), O7-Gd1-O23 72.40(12), O11'-Gd1-O12 125.00(11), O17-Gd1-O18 49.06(15), O22-Gd1-O23 71.59(13), O5-Gd2-O6' 124.11(13), O6'-Gd2-O9 77.19(13), O6'-Gd2-O20 137.43(15), O6'-Gd2-O21 139.05(15), O9-Gd2-O10' 130.64(12), O14-Gd2-O15 49.80(14). (See next page for compound **20**)

**20:** Fe1-N1 2.116(3), Fe1-N2 2.125(4), Fe1-O1 1.907(3), Fe1-O2 1.907(3), Fe1-O13 2.168(4), Fe1-Cl1 2.366(2), Fe2-Cl2 2.232(2), Tb1-O7 2.305(3), Tb1-O8' 2.353(3), Tb1-O11 2.870(3), Tb1-O11' 2.308(3), Tb1-O12 2.400(3), Tb1-O17 2.573(4), Tb1-O18 2.478(4), Tb1-O22 2.323(3), Tb1-O23 2.460(3), Tb2-O5 2.367(3), Tb2-O6' 2.304(3), Tb2-O9 2.289(3), Tb2-O10' 2.370(3), Tb2-O14 2.607(4), Tb2-O15 2.470(4), Tb2-O20 2.394(4), Tb2-O21 2.370(4), N1-Fe1-N2 77.16(14), N1-Fe1-O1 87.43(13), N1-Fe1-O2 163.14(14), N1-Fe1-Cl1 93.34(11), N2-Fe1-O13 84.86(15), O1-Fe1-O13 90.70(14), O1-Fe1-Cl1 93.66(10), O13-Fe1-Cl1 174.89(11), N3-Fe2-Cl2 100.99(12), O3-Fe2-Cl2 105.77(14), O7-Tb1-O8' 130.26(11), O7-Tb1-O11 65.80(10), O7-Tb1-O11' 75.88(11), O7-Tb1-O12 75.13(11), O7-Tb1-O17 133.43(12), O7-Tb1-O18 93.02(14), O7-Tb1-O22 140.60(11), O7-Tb1-O23 72.28(11), O11'-Tb1-O12 125.27(11), O17-Tb1-O18 50.12(14), O22-Tb1-O23 71.51(12), O5-Tb2-O6' 123.93(12), O6'-Tb2-O9 77.36(13), O6'-Tb2-O20 137.27(14), O6'-Tb2-O21 139.37(13), O9-Tb2-O10' 130.36(11), O14-Tb2-O15 50.22(13).

**21:** Fe1-N1 2.109(6), Fe1-N2 2.120(7), Fe1-O1 1.898(6), Fe1-O2 1.910(5), Fe1-O13 2.154(6), Fe1-Cl1 2.368(2), Fe2-Cl2 2.231(3), Dy1-O7 2.290(5), Dy1-O8' 2.348(5), Dy1-O11 2.860(5), Dy1-O11' 2.288(5), Dy1-O12 2.393(5), Dy1-O17 2.571(6), Dy1-O18 2.460(6), Dy1-O22 2.309(5), Dy1-O23 2.445(5), Dy2-O5 2.362(5), Dy2-O6' 2.287(5), Dy2-O9 2.280(5), Dy2-O10' 2.351(5), Dy2-O14 2.604(6), Dy2-O15 2.462(6), Dy2-O20 2.384(6), Dy2-O21 2.354(6), N1-Fe1-N2 77.3(2), N1-Fe1-O1 87.5(2), N1-Fe1-O2 163.6(2), N1-Fe1-Cl1 92.9(2), N2-Fe1-O13 85.4(2), O1-Fe1-O13 90.2(2), O1-Fe1-Cl1 93.8(2), O13-Fe1-Cl1 175.3(2), N3-Fe2-Cl2 100.3(2), O3-Fe2-Cl2 105.7(2), O7-Dy1-O8' 129.6(2), O7-Dy1-O11 65.1(2), O7-Dy1-O11' 76.1(2), O7-Dy1-O12 74.5(2), O7-Dy1-O17 133.7(2), O7-Dy1-O18 93.9(2), O7-Dy1-O22 141.2(2), O7-Dy1-O23 72.3(2), O11'-Dy1-O12 125.5(2), O17-Dy1-O18 50.8(2), O22-Dy1-O23 72.1(2), O5-Dy2-O6' 123.5(2), O6'-Dy2-O9 77.3(2), O6'-Dy2-O20 137.2 (2), O6'-Dy2-O21 138.5(2), O9-Dy2-O10' 129.1(2), O14-Dy2-O15 50.5(2).

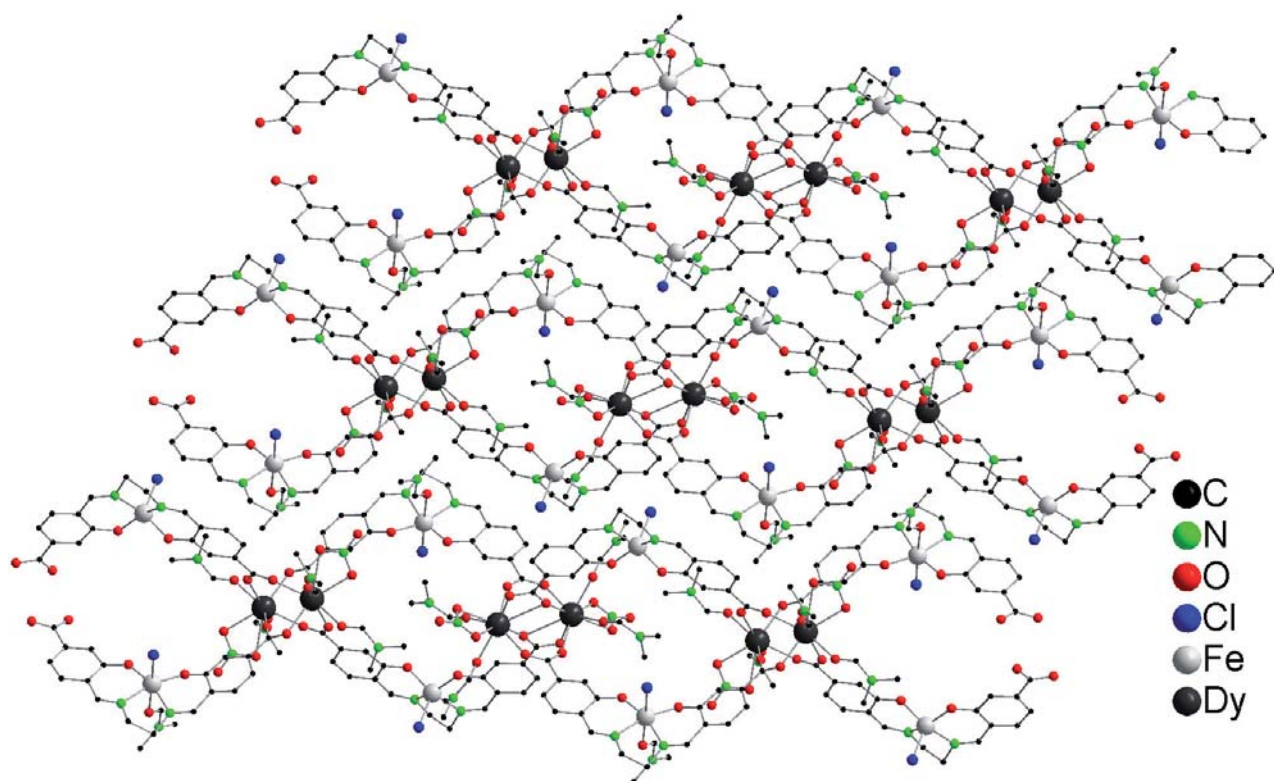


**Figure 3.31** Solid state structure of **21**, omitting hydrogen atoms and guest solvent molecules. Cut out of the polymeric structure. Compounds **17-21** are isostructural.



### 3.2.3.1 Thermogravimetric Analysis of Compounds 17-21

The TGA of compounds **17-21** are depicted in Figure 3.32. The TGA of complex **17** shows that five DMF molecules are lost in the temperature range of 70°C to 180°C (obsd 19.93%, calcd 19.79%). The remaining four DMF molecules are lost in the temperature range of 230°C to 312°C (obsd 14.94%, calcd 15.83%). The framework begins to decompose with a continuous weight loss up to 450°C. Compound **18** shows a weight loss of 14.88% around 128°C, corresponding to the release of four non-coordinated DMF molecules (calcd 14.82%); one coordinated DMF molecule is lost around 200°C (obsd 4.31%, calcd 3.70%). The other four coordinated DMF molecules are released in the temperature range of 240°C to 310°C, and the rotting of the residue occurs at 550°C. The TGA of compound **19** is similar to that of compound **18**: there is a weight loss in the temperature range of 75°C to 126°C from the loss of four non-coordinated DMF molecules, a second weight loss arises in the temperature range of 170°C to 196°C from the loss of one coordinated DMF molecule, and a weight loss in the temperature range of 220°C to 310°C from the loss of four coordinated DMF molecules. The residues decompose up to 450°C.

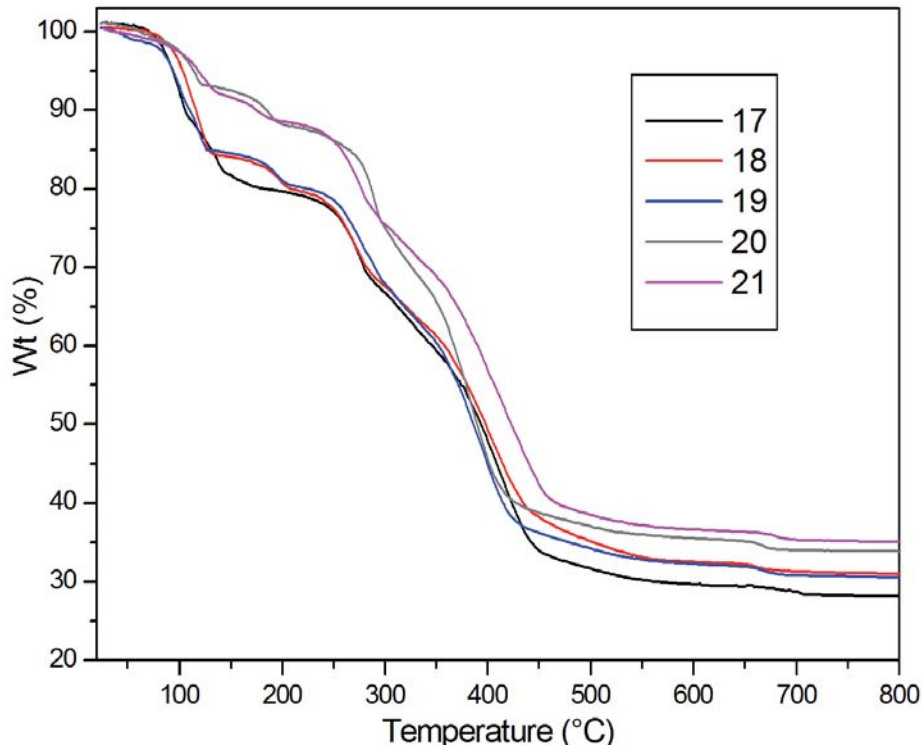


**Figure 3.32** TGA for **17-21** in temperature range of 20 to 800°C at the heating rate of 5°C / min under the N<sub>2</sub> atmosphere.

For **20**, the weight loss at 134°C corresponds to the loss of two DMF molecules (obsd 6.78%, calcd 7.36%). Subsequently, five DMF molecules are lost in the temperature range of 280°C to 342°C (obsd 18.97%, calcd 18.39%). After loss of all lattice solvent molecules, the framework begins to decompose. For **21**, the weight loss at around 136°C corresponds to the loss of two non-coordinated DMF molecules (obsd 7.92%, calcd 7.33%), followed by the release of two non-coordinated DMF molecules in the temperature range of 160°C to 260°C (obsd 7.56%, calcd 7.33%). Additionally, a weight loss of 18.8% at 270°C to 370°C corresponds to the loss of five coordinated DMF molecules (calcd 18.33%). Finally, the framework begins to disintegrate with continuous weight loss up to 450°C.

### 3.2.3.2 Magnetic Properties of Compounds 19-21

The magnetic susceptibility of compounds **19-21**, studied by Dr. Yanhua Lan (Prof. A. K. Powell), were measured from 300 K to 1.8 K at 1000 Oe. At 300 K,  $\chi T$  products of **19-21** are 25.30, 33.06 and 37.67  $\text{cm}^3\text{K/mol}$ , respectively (Figure 3.33).

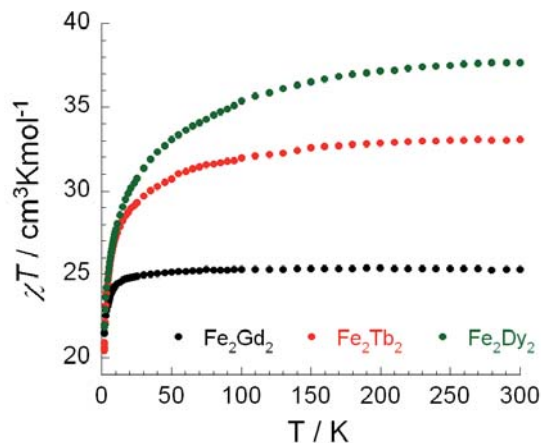


**Figure 3.33** Temperature dependence  $\chi T$  products for **19**, **20** and **21** at 1 kOe.

These values are in good agreement with the expected values (24.5  $\text{cm}^3\text{K/mol}$  for **19**, 32.39  $\text{cm}^3\text{K/mol}$  for **20** and 37.09  $\text{cm}^3\text{K/mol}$  for **21**) for two Fe(III) ions ( $S = 5/2$ ,  $g = 2$ ,  $C = 4.375 \text{ cm}^3\text{K/mol}$ ) and two lanthanide atoms (Ln = Gd(III);  $S = 5/2$ ,  $L = 0$ ,  $g = 2$ ,  ${}^8\text{S}_{7/2}$ ,  $C = 7.875 \text{ cm}^3\text{K/mol}$ , Ln = Tb(III);  $S = 3$ ,  $L = 5$ ,  $g = 3/2$ ,  ${}^7\text{F}_6$ ,  $C = 11.82 \text{ cm}^3\text{K/mol}$  and Ln = Dy(III);  $S = 5/2$ ,  $L = 5$ ,  $g = 4/3$ ,  ${}^6\text{H}_{15/2}$ ,  $C = 14.17 \text{ cm}^3\text{K/mol}$ ).<sup>[102]</sup> Upon decreasing the temperature, the  $\chi T$  products continuously decrease until 21.53, 20.48 and 21.85  $\text{cm}^3\text{K/mol}$  at

1.8 K for compounds **19-21**, respectively, indicating the presence of weak intramolecular antiferromagnetic interactions. From a structural point of view, the magnetic interaction between the paramagnetic centers mainly originates from the pair of lanthanide ions. The interaction of Fe-Ln is likely to be very weak or negligible. The  $\chi T$  product of compound **19** as a function of temperature is almost temperature independent above 30 K, indicating paramagnetic behavior in the temperature range of 30 K to 300 K and weakly antiferromagnetic interactions between Gd-Gd below 30 K, which might be true for analogous compounds **20** and **21**.

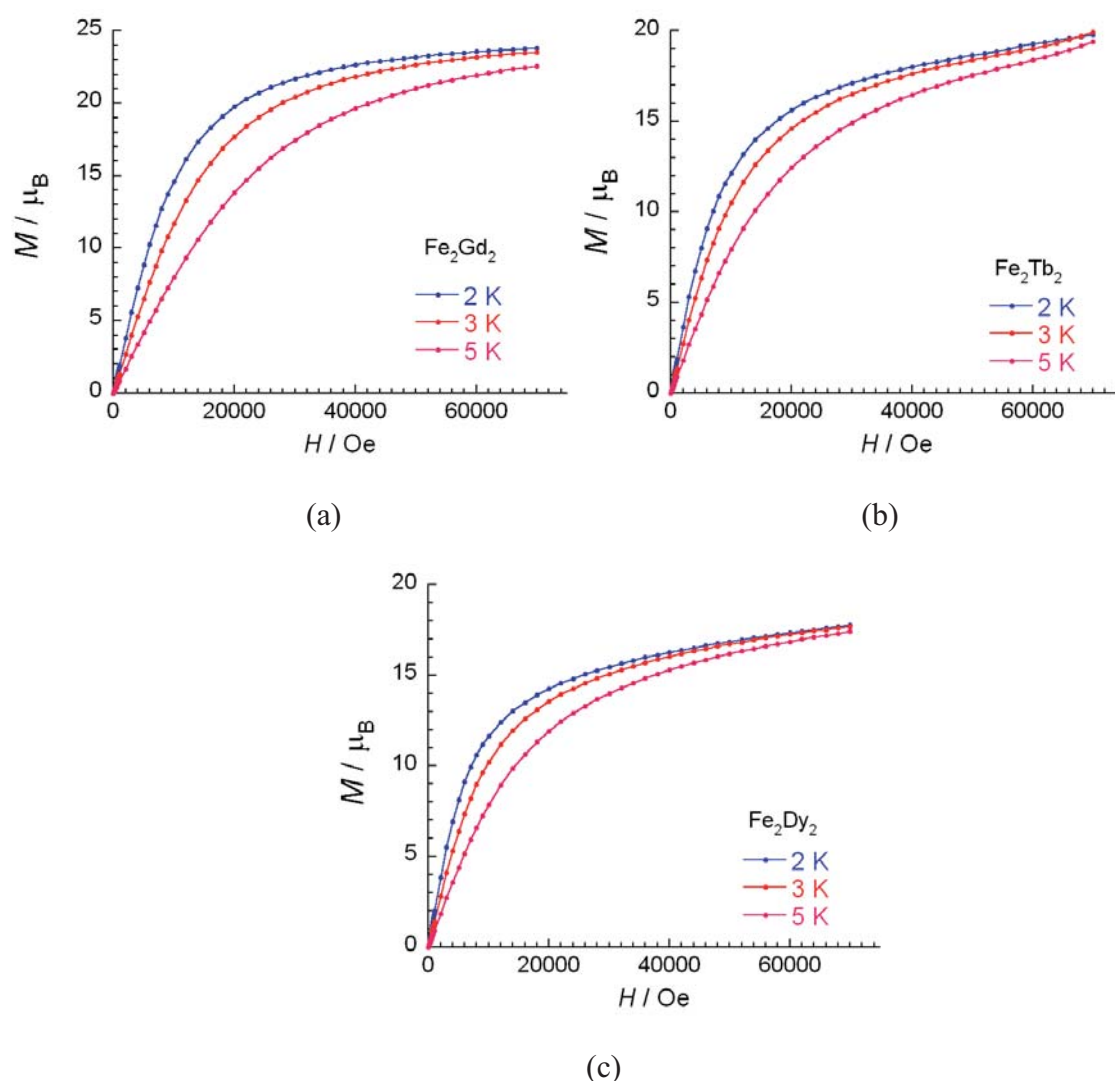


**Figure 3.34** (a) Field dependence of magnetization for **19** from 2 K to 5 K; (b)  $M$  vs  $H$  plot for **20** from 2 K to 5 K; (c)  $M$  vs  $H$  plot for **21** from 2 K to 5 K.

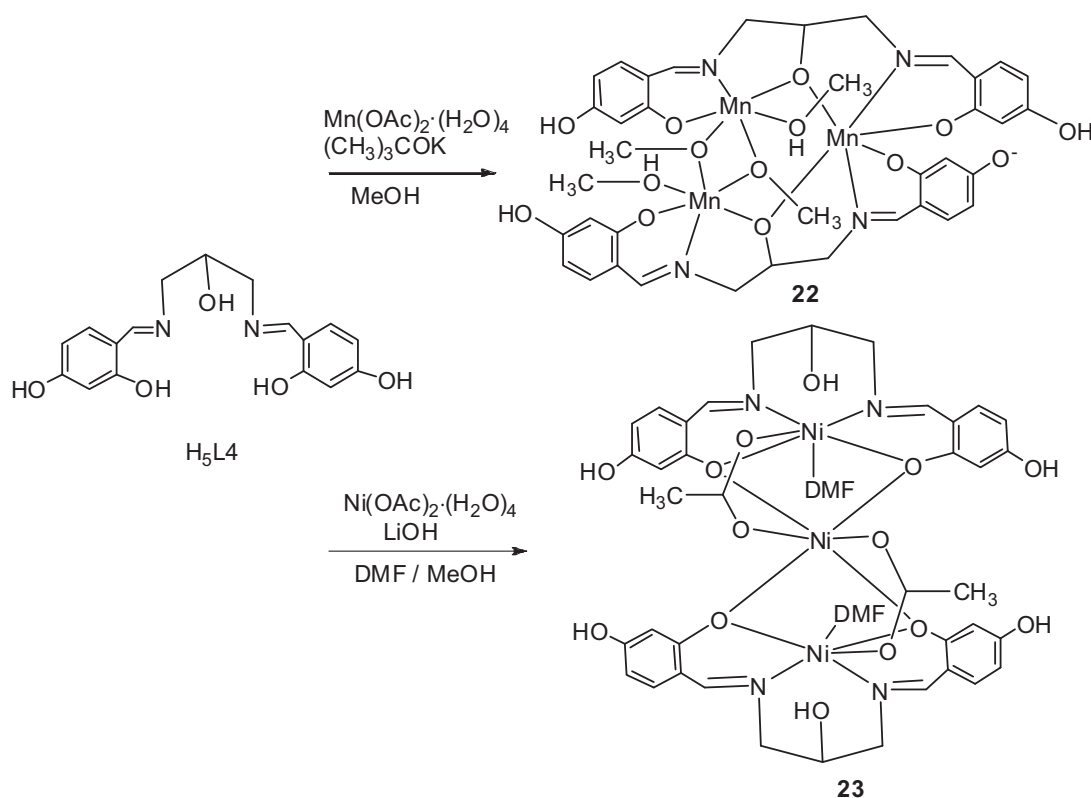
The field dependence of the magnetization at low temperatures shows that the magnetization smoothly increases with the applied dc field (Figure 3.34). At 7 T, it reaches values of 23.8, 19.8 and 17.8  $\mu_B$  for compounds **19-21**, respectively. There is no clear saturation for all three

compounds, suggesting the presence of magnetic anisotropy and/or the population of low-lying excited states. The magnetic relaxations of compounds **19-21** were investigated using ac susceptibility measurements under zero dc field; no frequency dependence of out-of-phase signals was detected.

In summary, a series of iron and lanthanide containing MOFs have been successfully prepared using trivalent lanthanide and iron salts along with the salen ligand (H<sub>4</sub>L) by solvothermal reactions. The novel iron-lanthanide compounds, [Ln<sub>2</sub>(FeLCl)<sub>2</sub>(NO<sub>3</sub>)<sub>2</sub>(DMF)<sub>5</sub>·(DMF)<sub>4</sub>]<sub>n</sub> (Ln = Y (**17**), Eu (**18**), Gd (**19**), Tb (**20**) and Dy (**21**)), are 2D microporous materials (Figure 3.31). This is the first example in which iron, used in metallosalen-based moieties, have carboxylate linkers connected to a lanthanide to form a 1D chain structure. These chains are also interacting with neighboring chains through π-π-stacking to form the 2D network. The magnetic studies of compounds **19-21** exhibit antiferromagnetic interactions. The TGA analysis of compounds **17-21** shows that the frameworks are stable at room temperature.

### 3.3 Trinuclear Mn(III) and Ni(II) Complexes

The treatment of  $H_5L^4$  with  $Mn(OAc)_2 \cdot (H_2O)_4$  in the presence of potassium tertiary butoxide in methanol resulted, after crystallization, in the trinuclear complex formulated as  $[Mn_3\{(H_2L^4)(HL^4)(OMe)_2(MeOH)_2\} \cdot (MeOH)_4]$  (**22**) (Scheme 3.6). A different reaction pathway was also used for the synthesis of compound **22** by reaction of  $H_5L^4$ ,  $Mn(OAc)_2 \cdot (H_2O)_4$ , LiOH and  $C_6H_5COONa$  in methanol. Compound **22** has been characterized by standard analytical / spectroscopic techniques, and the solid state structure has been established by single crystal X-ray diffraction (Figure 3.35). This compound is paramagnetic and could therefore not be characterized by NMR spectroscopy.



**Scheme 3.6** Synthetic scheme of compounds **22-23**.

Compound **22** crystallizes in the tetragonal space group  $P4_1$  with four formula units and sixteen methanol molecules in the unit cell. Compound **22** contains three manganese ions, one trianionic salen ligands  $(H_2L^4)^{3-}$ , one tetra anionic salen ligand  $(HL^4)^{4-}$ , two methoxide groups (OMe) and six methanol molecules (Figure 3.35). All the manganese ions are in the +3 oxidation state, which is established by inspection of the Mn-O and Mn-N bond distances and confirmed by the bond valence sum (BVS) calculations (Table 3.1).<sup>[112],[113]</sup> These three

manganese atoms (Mn1, Mn2 and Mn3) form a trinuclear core, which is very common in the literature.<sup>[114],[115],[116],[117]</sup> The Mn1 is octahedrally coordinated by four oxygen atoms (O1, O3, O7 and O8) and two nitrogen atoms (N1 and N4) from the salen ligand. The Mn2 and Mn3 are also octahedrally coordinated by three oxygen atoms (Mn2: O11, O12, O13 and Mn3: O11, O12, O14) from three methanol molecules, two oxygens atoms (O2, O3 for Mn2 and O6, O8 for Mn3) and one nitrogen atom (N2 for Mn2 and N3 for Mn3) from the salen ligand (Figure 3.35). The Mn-O and Mn-N bond lengths range from 1.872(3) Å to 2.287(3) Å and 1.973(4) Å to 2.025(4) Å, respectively, which is comparable to reported trinuclear manganese complexes.<sup>[114],[115],[116],[117]</sup> Since, all the Mn(III) ions display an octahedral geometry, they exhibit a Jahn–Teller (JT) distortion as expected for high-spin  $d^4$  ions with this geometry. The axial Mn-O bonds are longer than the equatorial Mn-O bonds, therefore, the JT axes are along O11-Mn2-O13 and O12-Mn3-O14 for Mn2 and Mn3 (Figure 3.35). The JT axes for Mn1 are not clear because, it is disordered by the ligand field. The three manganese ions are at the apices of an scalene triangle, since the Mn1⋯Mn2, Mn2⋯Mn3, and Mn3⋯Mn1 distances are 3.7487(5) Å, 3.1642(4) Å and 3.6426(7) Å, respectively.

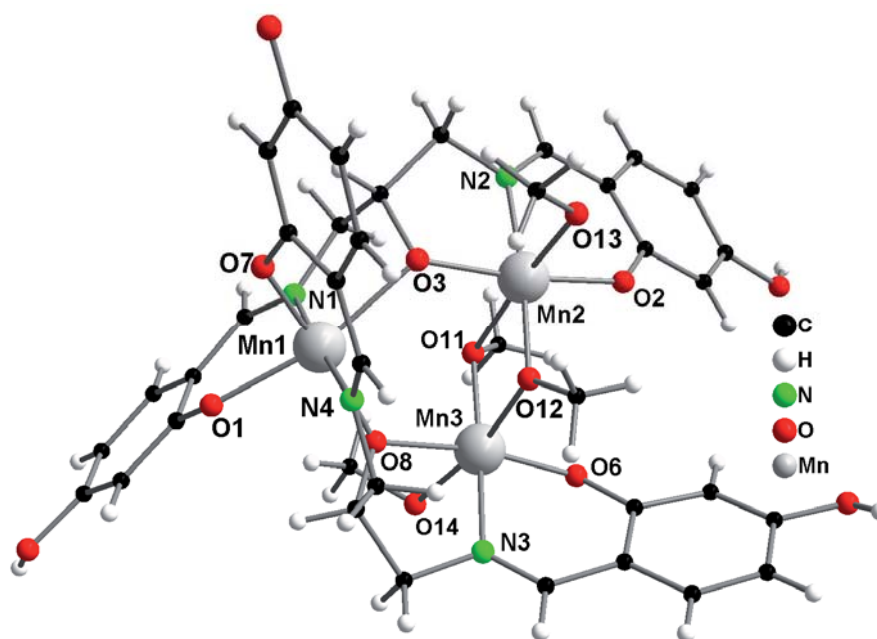


**Figure 3.35** Solid state structure of **22**, Selected bond lengths [Å] and bond angles [°]: Mn1-N1 2.025(4), Mn1-N4 1.973(4), Mn1-O1 2.085(3), Mn1-O3 2.226(3), Mn1-O7 1.938(3), Mn1-O8 2.014(3), Mn2-N2 1.988(4), Mn2-O2 1.901(4), Mn2-O3 1.938(4), Mn2-O11 2.287(3), Mn2-O12 1.909(3), Mn2-O13 2.235(3), Mn3-N3 1.979(4), Mn3-O6 1.911(4), Mn3-O8 2.008(4), Mn3-O11 1.872(3), Mn3-O12 2.175(3), Mn3-O14 2.304(3), Mn1-O3-Mn2 128.2(2), Mn1-O8-Mn3 129.8(2), Mn2-O11-Mn3 98.57(14), Mn2-O12-Mn3 101.37(14), N4-Mn1-O7 88.03(15), O1-Mn1-O7 87.80(14), O7-Mn1-O8 168.15(14), O3-Mn1-O7 86.27(14), O3-Mn1-O8 99.36(13), N2-Mn2-O2 88.6(2), N2-Mn2-O3 83.5(2), N2-Mn2-O12 174.2(2), O2-Mn2-O11 92.03(14), O3-Mn2-O11 89.11(14), O3-Mn2-O12 92.16(15), O12-Mn2-O13 93.72(13), N3-Mn3-O8 82.0(2), N3-Mn3-O14 90.7(2), O6-Mn3-O8 169.5(2), O6-Mn3-O11 95.6(2), O6-Mn3-O12 95.2(2), O11-Mn3-O14 91.11(14).

**Table 3.1** Bond Valence Sum (BVS) calculations for Mn in compound **22**.

Atom	Mn(II)	Mn(III)	Mn(IV)
Mn1	3.48	3.03	2.98
Mn2	3.40	3.14	3.08
Mn3	3.40	3.13	3.08

In contrast to the results described above, the reaction of  $H_3L^4$  ligand with  $Ni(OAc)_2 \cdot (H_2O)_4$  in the presence of lithium hydroxide in a mixture of MeOH / DMF (2:1) results, after crystallization, in the trinuclear compound formulated as  $[Ni_3(H_3L^4)_2(OAc)_2(DMF)_2 \cdot (H_2O)_3]$  (**23**) (Scheme 3.6). Compound **23** was characterized by standard analytical techniques, and the solid state structure was established by single crystal X-ray diffraction (Figure 3.36). The characteristic IR stretching frequency was observed (see experimental section) for compound **23**. Compound **23** crystallizes in the monoclinic space group  $P2_1/n$  and with five molecules of compound **23** and fifteen molecules of water present in the unit cell. In the trinuclear cluster, there are two crystallographically distinct nickel ions present. The two terminal nickel ions (Ni1 and Ni1') are equivalent due to the inversion center passing through the central Ni2 ion (Figure 3.36). To balance the charge we consider each salen ligand to have a double negative charged; therefore, each nickel ion is in the +2 oxidation state. In the trinuclear cluster, the Ni1 ion is six-fold coordinated: it is ligated to two nitrogen atoms (N1 and N2) and two phenoxy oxygen atoms (O1 and O2) from the  $(H_3L^4)^{2-}$  ligand, one oxygen atom (O6) from an acetate group and other oxygen atom (O7) from a DMF molecule. The Ni1 exhibits a distorted octahedral arrangement. The equatorial plane (O1, N1, N2 and O2) is almost coplanar with 0.102 Å deviations for the Ni1 ion. In contrast to Ni1, the central Ni2 ion is coordinated with four phenoxy oxygen atoms (O1, O2, O1' and O2') from two different  $(H_3L^4)^{2-}$  ligand and two bridging oxygen atoms (O8 and O8') from acetate groups; thus, the geometry around the Ni2 is distorted octahedral (Figure 3.36). The Ni-O and Ni-N bond lengths range from 2.000(3) Å to 2.182(3) Å and 2.029(3) Å to 2.034(4) Å, respectively, which are comparable in the trinuclear Ni(II)-salen complex.<sup>[118]</sup> The four donor oxygen atoms (O1, O2, O1' and O2') and Ni2 ion are almost in planar arrangement. The dihedral angle between the plane (O1, Ni1 and O2) and (O1, Ni2 and O2) is 21.37°. The central and terminal nickel ions are non-equivalent with a Ni1...Ni2 distance of 3.0468(6) Å, which shows the close proximity of the nickel ions.

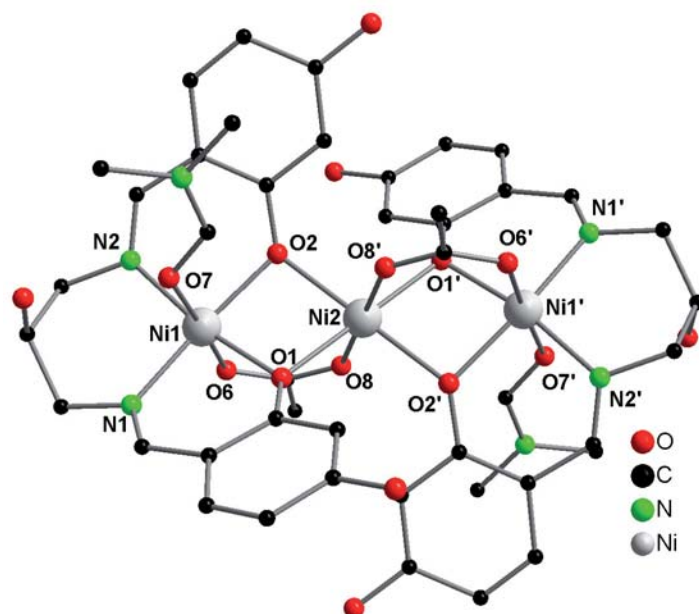


**Figure 3.36** Solid state structure of **23**, omitting hydrogen atoms. Selected bond lengths [ $\text{\AA}$ ] and bond angles [ $^\circ$ ]: Ni1-N1 2.034(4), Ni1-N2 2.029(3), Ni1-O1 2.000(3), Ni1-O2 2.016(3), Ni1-O6 2.101(3), Ni1-O7 2.182(3), Ni2-O1 2.054(2), Ni2-O2 2.072(2), Ni2-O8 2.039(3), Ni1-O1-Ni2 97.45(10), Ni1-O2-Ni2 96.36(10), N1-Ni1-N2 96.2(2), N1-Ni1-O1 91.08(13), N1-Ni1-O2 171.79(12), N1-Ni1-O6 95.15(13), N1-Ni1-O7 83.37(13), N2-Ni1-O1 169.82(15), N2-Ni1-O6 93.22(13), O1-Ni1-O2 82.11(11), O1-Ni1-O6 93.14(11), O1-Ni1-O7 89.92(11), O2-Ni1-O6 89.83(11), O6-Ni1-O7 176.63(12), O1-Ni2-O1' 180.0, O1-Ni2-O2 79.48(10), O1-Ni2-O8 87.86(10), O1'-Ni2-O8 92.14(10), O2'-Ni2-O8 92.61(11), O8-Ni2-O8' 180.0(15).

### 3.3.1 Magnetic Properties of Compounds 22-23

The temperature dependence of magnetic susceptibilities of compounds **22** and **23** are shown in the Figure 3.37.

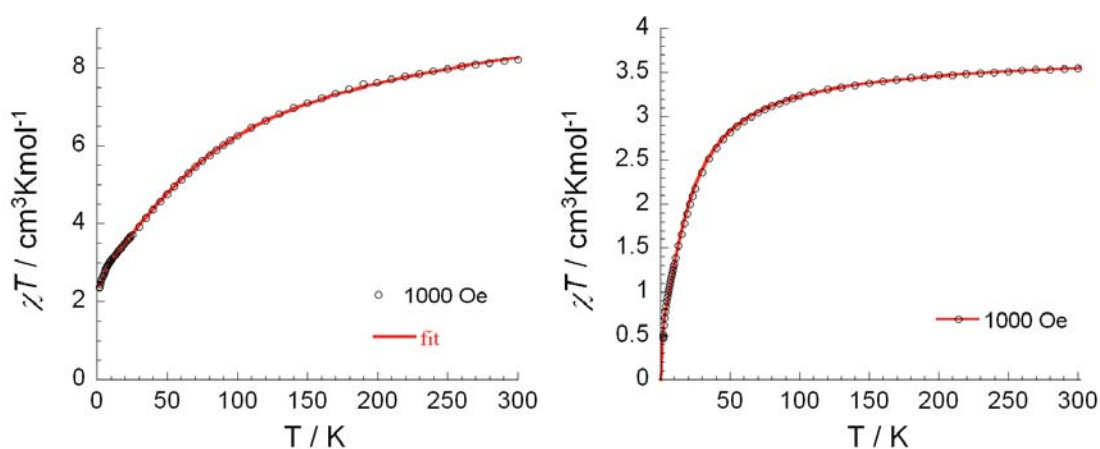
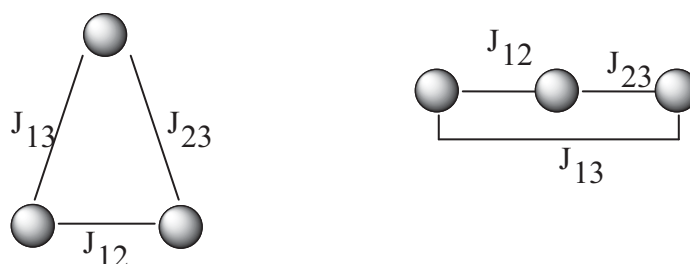


**Figure 3.37** Temperature dependence of the  $\chi_M T$  product for **22** (left) and **23** (right) at 1000 Oe.



The  $\chi T$  values at room temperature are 8.21 and 3.54 cm<sup>3</sup>K/mol for **22** and **23**, respectively. These values are in good agreement with the expected values of three Mn(III) ions ( $S = 2$  and  $g = 2$ ) for compound **22** and three Ni(II) ( $S = 1$  and  $g = 2$ ) for compound **23**. As the temperature decreases,  $\chi T$  values gradually decrease to 2.36 and 0.47 cm<sup>3</sup>K/mol at 1.8 K for **22** and **23**, respectively, indicating the presence of antiferromagnetic coupling between the neighboring metal ions.



**Scheme 3.7** Schematic diagrams representing the exchange interactions within complexes **22** (left) and **23** (right).

To determine exchange parameters (Scheme 3.7, left) between the paramagnetic Mn(III) ( $S = 2$ ) pairs in **22**, the susceptibility data were simulated based on spin Hamiltonian  $H = -2J_{13} (S_1 \cdot S_3 + S_2 \cdot S_3) - 2J_{12} (S_1 \cdot S_2)$  (where  $J_{13} = J_{23}$ ). The magnetic data could be reproduced well by the following parameters:  $g = 1.92$  (fixed),  $J_{12}/k_B = 0.48(7)$  K,  $J_{13}/k_B = -7.93(8)$  K,  $zJ/k_B = -0.047(3)$  K,  $N_a = 0.00265$  cm<sup>3</sup>/mol. The sign and magnitude of magnetic interactions imply that the antiferromagnetic interactions are dominant among the three Mn(III) ions. On the other hand, the structure of **23** consists of isolated linear Ni(II) trimer units and, assuming that the exchange coupling within the cluster is isotropic (Scheme 3.7, right), the Heisenberg Hamiltonian for the trimer system can be written as:  $H = -2J_{12} (S_1 \cdot S_2 + S_2 \cdot S_3) - 2J_{13} (S_1 \cdot S_3)$  (where  $J_{12} = J_{23}$ ).<sup>[119]</sup> The magnetic data could be reproduced well by the following parameters:  $g = 2.218(2)$ ,  $J_{12}/k_B = -5.51(5)$  K,  $J_{13}/k_B = -3.43(3)$  K.<sup>[119]</sup> The negative  $J$  value indicates antiferromagnetic coupling between Ni(II) ions. The  $M$  versus  $H$  measurements (Figure 3.38) at low temperature reveals slow increase in the magnetization, which reaches the values of 4.2 and 1.9  $\mu_B$  at 7 T for compounds **22** and **23**, respectively. A true saturation of the magnetization values was not observed, suggesting the presence of low-lying excited states that might be populated when the dc field is increased. At a higher field, when the antiferromagnetic interactions are overcome, there should be a saturation of the magnetization at 12  $\mu_B$  for **22** (Mn(III) with  $S = 2$  and  $g = 2.0$ ) and 6  $\mu_B$  for **23** (Ni(II) with  $S = 1$  and  $g = 2.0$ ) because all spins will be parallel.

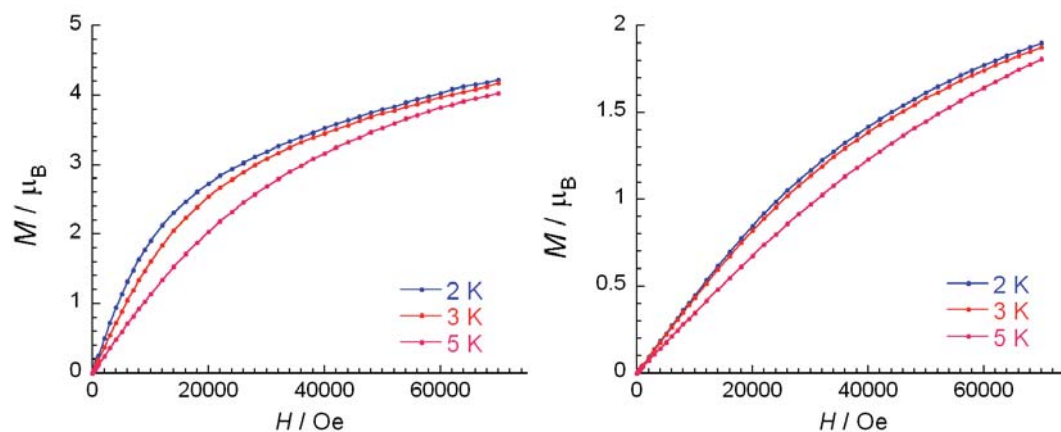


**Figure 3.38** Field dependence of the magnetization from 2-5 K for **22** (left) and **23** (right).

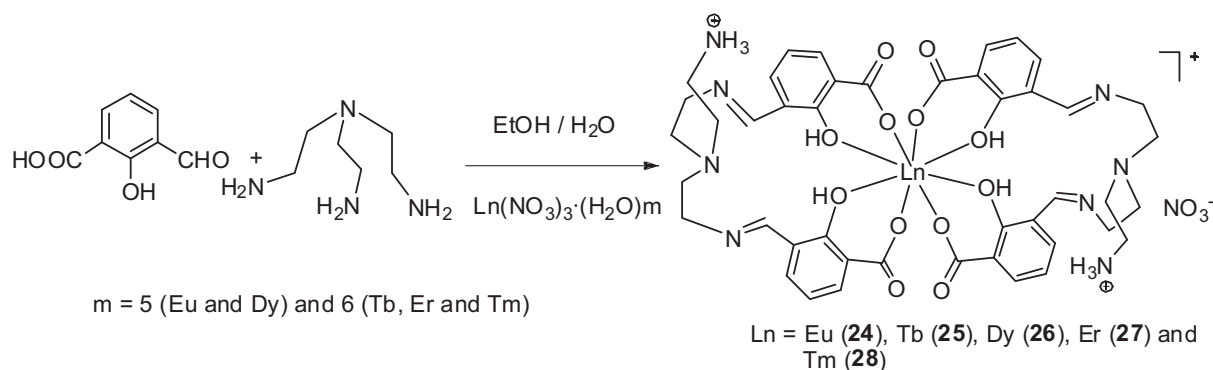
In summary, the ligand  $H_3L^4$  has been successfully used to generate the trinuclear compounds **22-23**  $[Mn_3\{(HL^4)(L^4)(OMe)_2(MeOH)_2\} \cdot (MeOH)_4]$  and  $[Ni_3(H_3L^4)_2(OAc)_2(DMF)_2 \cdot (H_2O)_3]$ , respectively. Both compounds arise from a self-assembly process, which is controlled by donor atoms of the ligand moieties. The solid state structure of compounds **22-23** shows that three Mn(III) ions are at the apices of a scalene triangle whereas three Ni(II) ions are in a linear fashion. The magnetic studies of compounds **22** and **23** shows that overall antiferromagnetic interactions are present.

### 3.4 Lanthanide Complexes of Hitherto Unknown Cage Ligand (*N,N'*-Bis{[2-hydroxy-3-carboxybenzylidene]aminoethylaminoethyl}aminoethylamine) ( $H_4L^5$ )

One of the research efforts was to prepare mononuclear lanthanide complexes by using a poly podal ligand. Due to the sticky nature of the unmetallated ligand, the ligand was synthesized *in situ* by mixing 3-formylsalicylic acid and tris-(2-aminoethyl)amine during the reactions with lanthanide salts. This  $H_4L^5$  ligand has three potential coordination pockets: one oxygen donor pocket and two nitrogen donor pockets. Although this ligand has three donor pockets, lanthanides prefer the oxygen donor pockets leading to mononuclear lanthanide metal complexes.

As shown in Scheme 3.8, the reaction of 3-formylsalicylic acid, tris-(2-aminoethyl)amine and  $Ln(NO_3)_3 \cdot (H_2O)_m$  ( $m = 5$  (Eu and Dy) and 6 (Tb, Er and Tm) in ethanol / water (3:1) results

in the complexes formulated as  $[\text{Ln}(\text{H}_2\text{L}^5)_2 \cdot (\text{EtOH}) \cdot (\text{H}_2\text{O})_x \cdot (\text{NO}_3)]$  ( $x = 9$ ; Ln = Eu (**24**) and  $x = 8$ ; Ln = Tb (**25**), Dy (**26**), Er (**27**) and Tm (**28**)). Independent of the ionic radii of the lanthanides, all complexes are monomeric in the solid state together with an uncoordinated nitrate ion, water molecules and an ethanol molecule.



**Scheme 3.8** Synthetic scheme of compounds **24-28**.

Complexes **24-28** were characterized by standard analytical / spectroscopic techniques, and the solid state structures were analyzed by single crystal X-ray diffraction. The IR spectra of these compounds **24-28** show the characteristic absorption peaks for the functional groups. The broad band around  $3238\text{ cm}^{-1}$  for **24**,  $3420\text{ cm}^{-1}$  for **25**,  $3447\text{ cm}^{-1}$  for **26**,  $3264\text{ cm}^{-1}$  for **27** and  $3328\text{ cm}^{-1}$  for **28** is associated with the O-H stretching vibration of water molecules. The absence of the characteristic band around  $1700\text{ cm}^{-1}$  for compounds **24-28** indicates the deprotonation of carboxylate groups. There are strong absorption bands of asymmetric and symmetric vibrations at around  $1602$  and  $1374\text{ cm}^{-1}$  for **24**;  $1603$  and  $1386\text{ cm}^{-1}$  for **25**;  $1609$  and  $1381\text{ cm}^{-1}$  for **26**;  $1605$  and  $1386\text{ cm}^{-1}$  for **27**; as well as  $1611$  and  $1385\text{ cm}^{-1}$  for **28**. The separations ( $\Delta$ ) between  $\nu_{\text{asym}}(\text{CO}_2)$  and  $\nu_{\text{sym}}(\text{CO}_2)$  are  $228\text{ cm}^{-1}$  for **24**,  $228\text{ cm}^{-1}$  for **25**,  $217\text{ cm}^{-1}$  for **26**,  $219\text{ cm}^{-1}$  for **27** and  $226\text{ cm}^{-1}$  for **28**, indicate the presence of monodentate coordination modes.

The solid state structures were determined by single crystal X-ray diffraction (Figure 3.39). The X-ray diffraction analysis reveals that compounds **24-28** are crystallize in the triclinic space group  $P-1$ . Compounds **24-28** are isostructural, so only the structure of **26** will be described in detail; however, it should be noted that compound **24** contains nine non-coordinating water molecules and compounds **25-28** have eight non-coordinating water molecules in the formula unit.

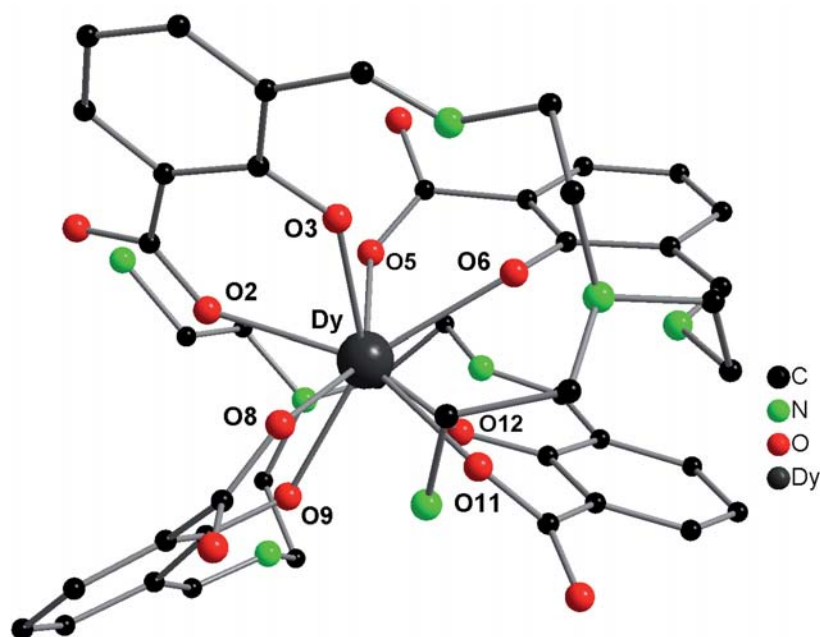


**Figure 3.39** Solid state structure of the  $[\text{Dy}(\text{H}_3\text{L}^5)_2]^+$  anion of compound **26**, omitting hydrogen atoms for clarity. Compounds **24-28** are isostructural. Selected bond lengths [ $\text{\AA}$ ] and bond angles [ $^\circ$ ]:

**24:** Eu-O1 2.372(4), Eu-O3 2.341(4), Eu-O4 2.422(4), Eu-O6 2.394(4), Eu-O7 2.390(4), Eu-O9 2.397(4), Eu-O10 2.363(4), Eu-O12 2.360(4), O1-Eu-O3 73.43(14), O1-Eu-O4 73.88(14), O1-Eu-O6 132.2814(15), O3-Eu-O4 87.15(14), O3-Eu-O9 148.67(15), O3-Eu-O12 139.71(14), O4-Eu-O6 71.96(13), O7-Eu-O9 73.26(14), O9-Eu-O10 131.54(14), O9-Eu-O12 71.23(14), O10-Eu-O12 72.02(13).

**25:** Tb-O1 2.356(2), Tb-O3 2.340(2), Tb-O4 2.371(2), Tb-O6 2.386(2), Tb-O7 2.340(2), Tb-O9 2.335(2), Tb-O10 2.398(2), Tb-O12 2.370(2), O1-Tb-O3 72.72(7), O1-Tb-O4 72.74(8), O1-Tb-O6 132.16(8), O3-Tb-O4 84.45(8), O3-Tb-O9 140.37(7), O3-Tb-O12 146.75(8), O4-Tb-O6 73.31(7), O7-Tb-O9 73.81(8), O9-Tb-O10 87.84(8), O9-Tb-O12 72.06(7), O10-Tb-O12 72.70(8).

**26:** Dy-O1 2.346(2), Dy-O3 2.325(2), Dy-O4 2.358(2), Dy-O6 2.374(2), Dy-O7 2.324(2), Dy-O9 2.324(2), Dy-O10 2.386(2), Dy-O12 2.358(2), O1-Dy-O3 73.09(8), O1-Dy-O4 72.77(9), O1-Dy-O6 132.64(8), O3-Dy-O4 84.28(9), O3-Dy-O9 140.45(8), O3-Dy-O12 146.65(8), O4-Dy-O6 73.62(8), O7-Dy-O9 74.23(8), O9-Dy-O12 72.03(8), O9-Dy-O10 87.85(9), O10-Dy-O12 73.07(8).

**27:** Er-O1 2.316(7), Er-O3 2.291(7), Er-O4 2.324(7), Er-O6 2.352(6), Er-O7 2.306(7), Er-O9 2.288(7), Er-O10 2.352(8), Er-O12 2.347(7), O1-Er-O3 74.1(2), O1-Er-O4 71.9(3), O1-Er-O6 133.4(3), O3-Er-O4 84.0(3), O3-Er-O9 141.6(3), O3-Er-O12 145.9(3), O4-Er-O6 74.7(2), O7-Er-O9 75.1(3), O9-Er-O10 86.7(3), O9-Er-O12 71.6(3), O10-Er-O12 73.8(3).

**28:** Tm-O1 2.313(2), Tm-O3 2.296(3), Tm-O4 2.323(2), Tm-O6 2.340(2), Tm-O7 2.294(2), Tm-O9 2.282(2), Tm-O10 2.357(2), Tm-O12 2.331(2), O1-Tm-O3 74.08(8), O1-Tm-O4 72.41(8), O1-Tm-O6 133.84(8), O3-Tm-O4 83.53(9), O3-Tm-O9 141.02(8), O3-Tm-O12 146.11(8), O4-Tm-O6 74.47(8), O7-Tm-O9 75.35(8), O9-Tm-O10 86.49(9), O9-Tm-O12 72.02(8), O10-Tm-O12 73.65(8).

The asymmetric unit of compound **26** contains a  $[\text{Dy}(\text{H}_3\text{L})_2]^+$  coordination cation, a  $\text{NO}_3^-$  anion, one ethanol, and eight water molecules. In order to balance the charge each ligand is singly negatively charged. Thus, the two acid groups are deprotonated forming carboxylate functions while the tethered amine is protonated giving an  $\text{NH}_3^+$  function. The  $[\text{Dy}(\text{H}_3\text{L})_2]^+$  cation contains one Dy(III) ion coordinated by two such ligands. Thus, the metal atom is

coordinated by four phenoxy oxygen atoms (O3, O6, O9 and O12) and four carboxyl oxygen atoms (O2, O5, O8 and O11) from both ligands resulting in an eight fold coordinated geometry. The coordination polyhedron can be best described as a distorted square antiprism. The Dy-O(phenoxy) and Dy-O(carboxyl) distances for the monomer are in the range of 2.324(2) Å - 2.374(2) Å and 2.324(2) Å - 2.386(2) Å, respectively. Formally each phenoxy oxygen is protonated but we could not locate the protons in the difference Fourier map. Also, there is no significant difference in the Dy-O bond lengths of the phenoxy and the carboxyl groups.

### 3.4.1 *Ab Initio* Calculation of Compound **26**

*Ab initio* calculations of **26** was performed by Prof. Liviu F. Chibotaru within CASSCF/RASSI approach using the MOLCAS package.<sup>[120]</sup> The magnetic properties have been calculated with SINGLE\_ANISO module<sup>[121],[122]</sup> recently implemented in MOLCAS-7.6.

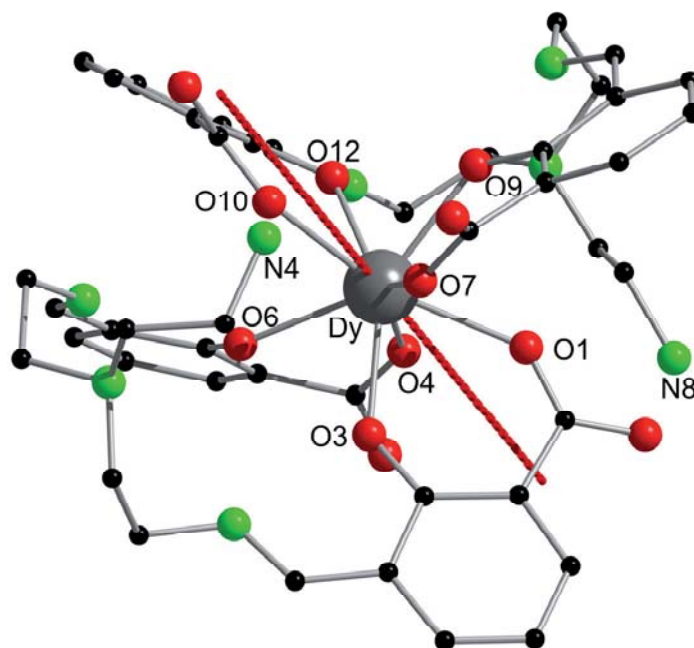


**Figure 3.40** Main anisotropy axes on Dy ion in compound **26**.

The main values of the ground state  $g$  tensors and orientations of the main magnetic axes on Dy ion in **26** are 0.0238, 0.0445 and 18.7688 for  $g_x$ ,  $g_y$  and  $g_z$ , respectively (Figure 3.40). The main magnetic axis in **26** lies almost in the O4-O7-O10 plane (Figure 3.40) close to Dy-O4 bond ( $12^\circ$ ). The positions of the hydrogen atoms close to O3, O6, O9, and O12 in **26** (Figure 3.40) are not available from structural data and have been obtained, therefore,

from molecular mechanics optimization. In order to correct the errors introduced by this procedure, the first excited Kramers doublet was slightly shifted from the calculated value.

### 3.4.2 Magnetic Properties of Compound **25** and **26**

The magnetic measurements for compounds **25** and **26** were performed by Dr. Yanhua Lan (Prof. A. K. Powell). The temperature dependence of the magnetic susceptibility measurement for compounds **25** and **26** are shown in Figure 3.41. At room temperature, the  $\chi T$  (magnetic susceptibility) product of **25** and **26** are 11.81 and 14.07  $\text{cm}^3\text{K/mol}$ , respectively. These values are in good agreement with the expected values for the presence of one Tb(III) ion ( $S = 3, L = 3, {}^7F_6, C = 11.82 \text{ cm}^3\text{K/mol}$  with  $g = 3/2$ ) for **25** as well as one Dy(III) metal ion ( $S = 5/2, L = 5, {}^6H_{15/2}, C = 14.17 \text{ cm}^3\text{K/mol}$  with  $g = 4/3$ ) for **26**.<sup>[102]</sup>

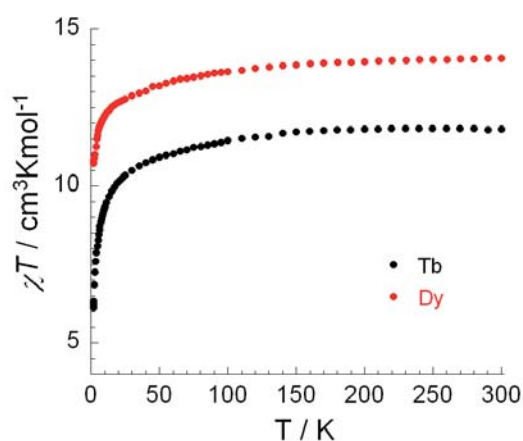


**Figure 3.41** Temperature dependence of the  $\chi T$  product for compounds **25** and **26** at 1000 Oe.

Upon cooling,  $\chi T$  for the two compounds decreases gradually but more rapidly below 50 K, which is mostly due to crystal-field effects (*i.e.* thermal depopulation of the Ln(III) Stark sublevels). The magnetizations of the two compounds from zero dc field to 50 kOe at 2-5 K are shown in the Figure 3.42, and the corresponding maximum values reached are 5.2 and 5.7  $\mu_B$ . The lack of saturation of magnetization at 50 kOe can likely be attributed to crystal-field effects and low-lying excited states, while the non-superposition of the temperature-dependence under different fields implies the presence of significant magnetic anisotropy.

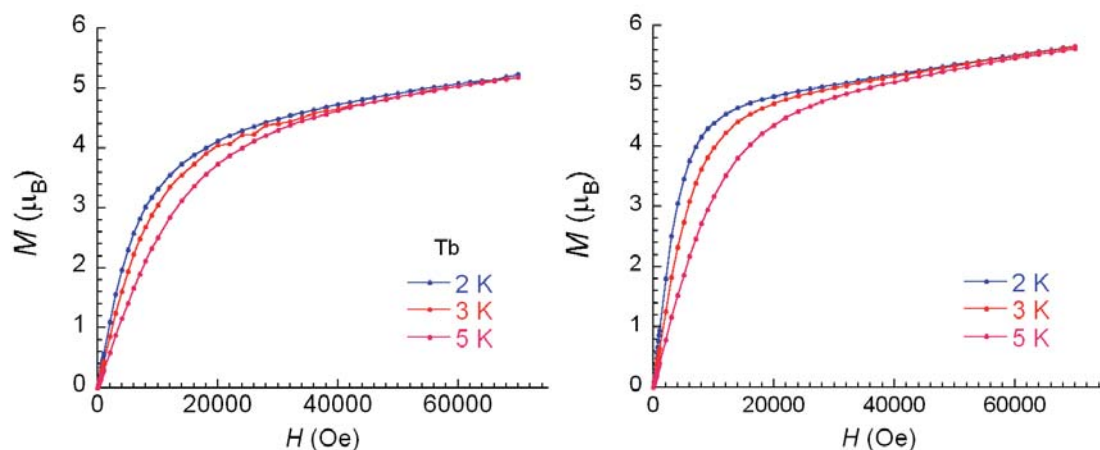


**Figure 3.42** Field dependence of magnetization for **25** (left) and **26** (right) from 2-5 K.

The magnetic relaxation of compounds **25** and **26** were tested using ac susceptibility measurements under zero dc field. For compound **25**, there was no slow relaxation; therefore, no SMM behavior was observed (Figure 4.43)

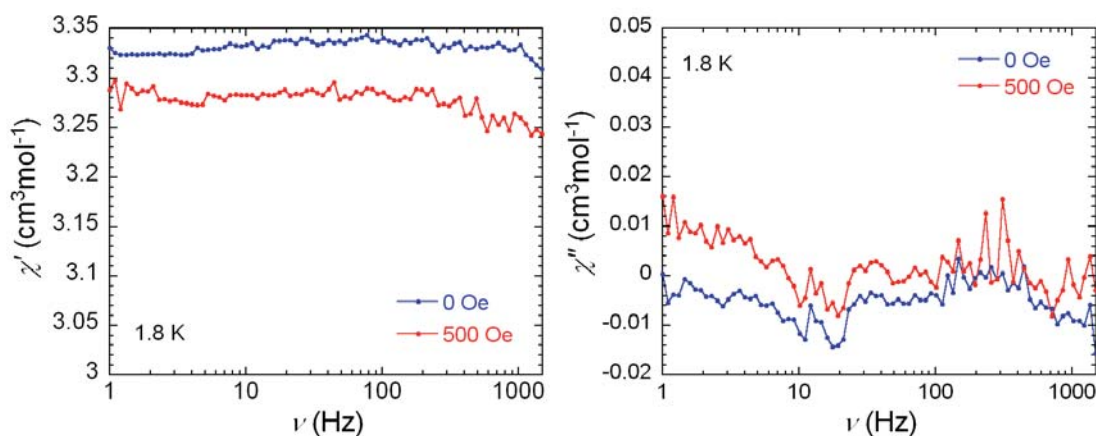


**Figure 3.43** Frequency dependence of the in-phase ( $\chi'$ ) and out-of-phase ( $\chi''$ ) ac susceptibility for compound **25**.

The ac measurements of **26** were performed in the 1.8-10 K range using a 3.0 Oe ac field oscillation in 1-1500 Hz range. In the absence of an external dc field, the out-of-phase component is almost absent. Such behavior can be due to fast zero-field tunneling of the magnetization that can be suppressed with application of a small external, dc field,<sup>[123],[124],[125],[126]</sup> which removes the state degeneracy, suppressing the relaxation *via* quantum tunnelling.<sup>[127],[128]</sup> In this way, useful information on the dynamics of the magnetization on the thermally activated regime can be extracted; therefore, ac measurements at different applied static fields less than 2500 Oe were recorded at 1.8 K (Figure 3.44).

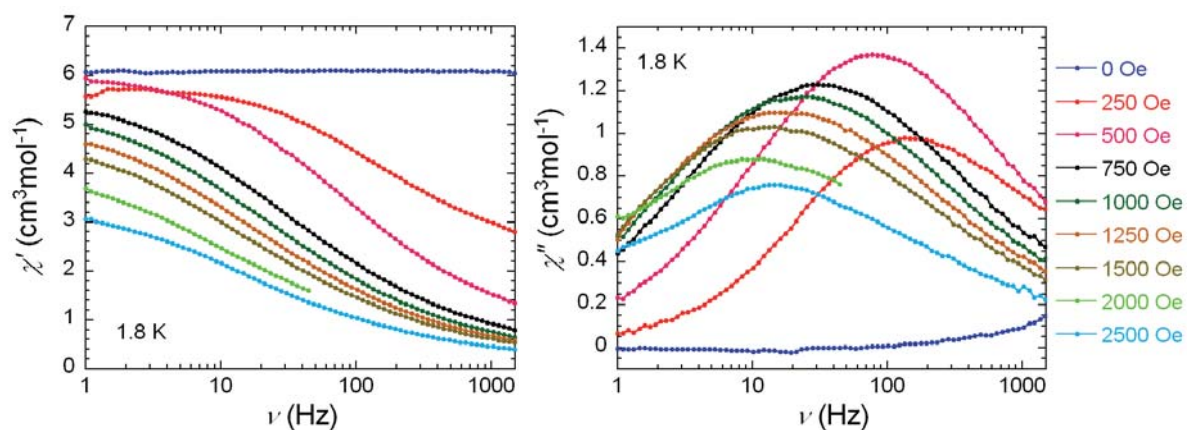


**Figure 3.44** Frequency dependence of the in-phase ( $\chi'$ ) and out-of-phase ( $\chi''$ ) ac susceptibility component under different dc fields for **26**.

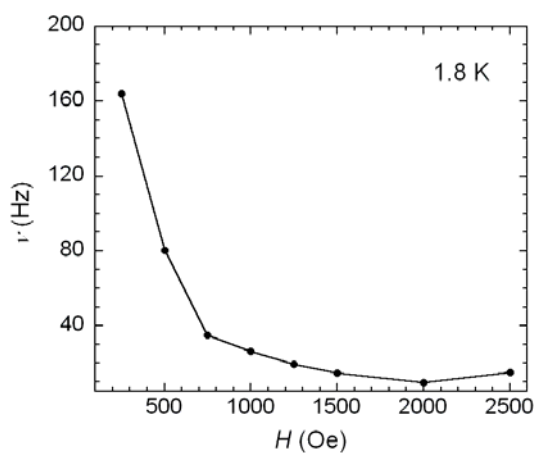


**Figure 3.45** Field dependence of the characteristic frequency as a function of the applied dc field for **26**.

With the external dc field, the intensity of out-of-phase susceptibility is dramatically enhanced and reaches the same order of the intensity observed in the in-phase component. In addition, both in-phase and out-of-phase components now become strongly field-dependent, which is characteristic of SMM behaviour.



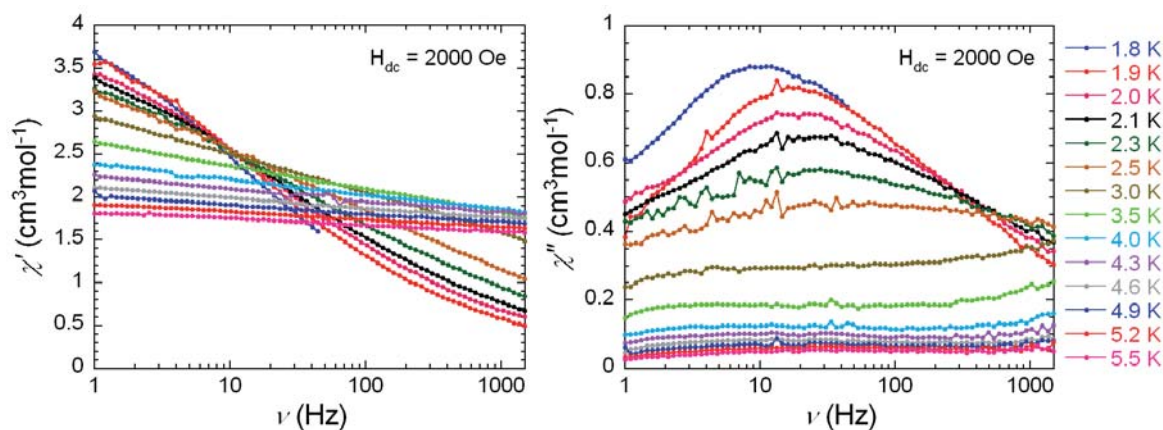


**Figure 3.46** Frequency dependence of the in-phase ( $\chi'$ ) and out-of-phase ( $\chi''$ ) ac susceptibility at different temperature under applied dc field (2000 Oe) for **26**.

As shown in Figure 3.45, the relaxation process becomes slowest at  $\sim 18$  Hz at 2000 Oe and shifts again to higher frequencies with the increase of static fields. A field of 2000 Oe was, therefore, selected to investigate the temperature dependence of the dynamic susceptibility (Figure 3.46).

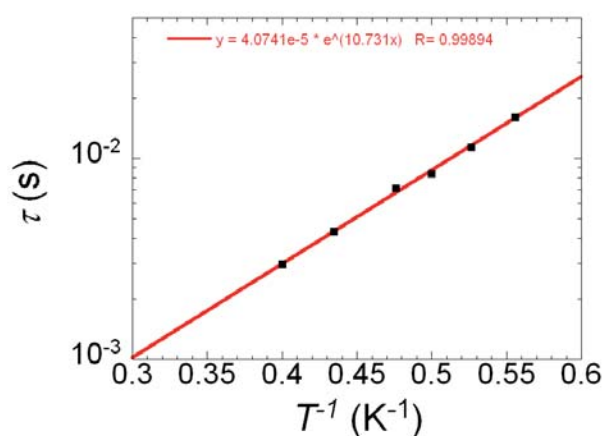


**Figure 3.47** Arrhenius plot of compound **26**.

The relaxation time of this compound extracted from the ac data is depicted in Figure 3.47 as a function of temperature. According to the Arrhenius expression,

$$\tau = \tau_0 e^{(U_{eff}/K_B T)}$$

where  $\tau_0$  is a pre-exponential factor and  $U_{eff}$  is the energy barrier to reverse the magnetization direction, a linear behavior corresponding to the thermally activated regime can only be obtained below 2.5 K. A fit to this part of data gives an effective energy barrier of

$U_{eff} = 10.7$  K and relaxation time  $\tau_0 = 4.1 \times 10^{-5}$  s (Figure 3.47). In order to evaluate the distribution of the relaxation time of **26**, a Cole-Cole plot of the in-phase versus out-of-phase susceptibilities at low temperatures was constructed. Fitting the data using a generalized Debye model gives a high  $\alpha$  value of 0.51 - 0.75 (Figure 3.48 and Table 3.2), suggesting that there is likely to be more than one relaxation process operating at low temperatures and the relaxation time has a moderate distribution.

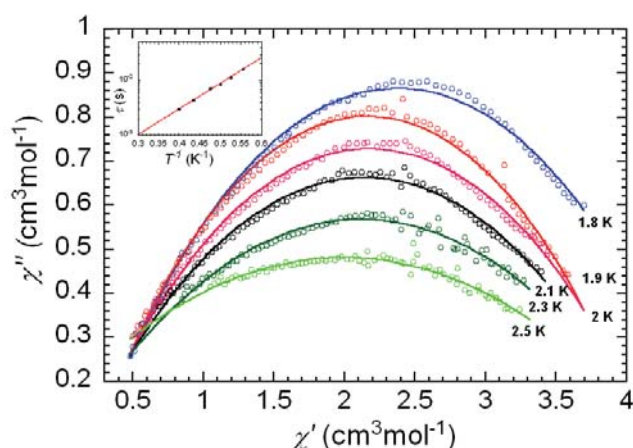


**Figure 3.48** Cole-Cole plots of **26** at indicated temperatures. The solid lines are the fittings with a generalized Debye model. The parameters are discussed in the text. Inset: The relaxation time of **26** as a function of temperature plotted against a thermally-activated Arrhenius law (solid line).

**Table 3.2** Parameters obtained from the fits of Cole-Cole diagram in **26**.

T (K)	$\alpha$	$\chi_0$ (cm <sup>3</sup> /mol)	$\chi_{inf}$ (cm <sup>3</sup> /mol)
1.8	0.524(2)	0.168(6)	4.590(14)
1.9	0.514(3)	0.162(9)	4.161(13)
2.0	0.570(3)	0.101(9)	4.256(13)
2.1	0.607(3)	0.054(11)	4.225(15)
2.3	0.678(4)	0.080(24)	4.324(28)
2.5	0.748(5)	0.0418(54)	4.404(43)

In summary, a series of mononuclear lanthanide complexes have been synthesized from *in situ* preparation of hitherto unknown cage ligand, *N,N'*-bis{2-(3-carboxysalicylidene)aminoethyl}aminoethylamine (H<sub>4</sub>L<sup>5</sup>), based on 3-formylsalicylic acid. The magnetic susceptibility measurement of complex **26** exhibits field-induced SMM

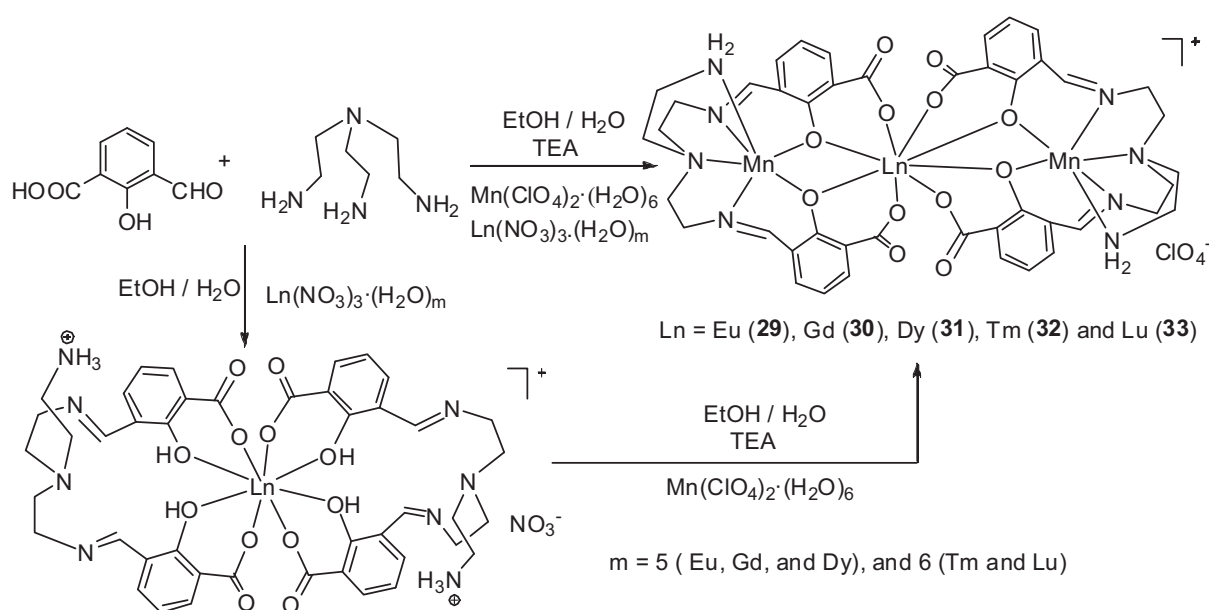
behavior. The compound **26** exhibits the very first tunneling process in the absence of a static field. Slow magnetic relaxation occurs while the application of an external field removes the degeneracy of the Dy(III) ion sublevels.

### 3.5 Heterometallic 3d-4f Metal Complexes

There has been considerable research interest in recent years for the design and construction of 3d-4f heterometallic complexes due to their excellent magnetic properties. Gatteschi *et al.* reported ferromagnetic coupling between Gd(III) and Cu(II) in two Cu<sub>2</sub>Gd trinuclear compounds.<sup>[129],[130]</sup> This ferromagnetic coupling arises from the interaction between a semi-occupied orbital, *i.e.*  $d_x^2-y^2$ , on the Cu(II) and an empty orbital on the Gd(III) center, resulting in the spin  $S = 4$ , which is possible only when the unpaired electron of Cu(II) aligns parallel to the seven 4f-electrons of Gd(III). To investigate how 3d and 4f orbitals interact, we are trying to design a novel ligand systems that can form these kinds of heterometallic complexes. Although a series of copper–lanthanide compounds<sup>[131],[132],[133],[134]</sup> have been successfully synthesized and characterized, there are only few reports on Mn–Ln complexes<sup>[135],[136],[137],[138]</sup>, complexes involving Mn(II) and Ln<sup>III</sup> are still relatively rare.<sup>[139],[140],[141]</sup> Costes *et al.* have reported the compounds, [MnL<sup>1a</sup>(H<sub>2</sub>O)<sub>2</sub>]<sub>2</sub>[Gd(NO<sub>3</sub>)<sub>5</sub>(MeOH)] (H<sub>2</sub>L<sup>1a</sup> = 1,3-bis((methoxysalicylidene)amino)-2,2'-dimethylpropane),<sup>[139]</sup> in which Gd(III) and Mn(III) are present. Recently, Wu reported a Gd<sub>2</sub>Mn<sub>3</sub> complex showing intermolecular antiferromagnetic coupling.<sup>[141]</sup> The goal of this section is to prepare new 3d-4f heterometallic complexes, mainly Mn(II)-Ln(III) and Ni(II)-Ln(III), from different ligand systems for magnetic studies. A salen-type polepodal ligand, H<sub>4</sub>L<sup>5</sup>, was prepared *in situ* (experimental section), which reacted with transition metals along with lanthanide metals to form a series of novel 3d-4f metal complexes.

### 3.5.1 Trinuclear Manganese and Lanthanide Metal Complexes

The *in situ* reaction of  $H_4L^5$ , in a ethanol / water (3:1) mixture with triethylamine,  $Mn(ClO_4)_2 \cdot (H_2O)_6$  and  $Ln(NO_3)_3 \cdot (H_2O)_m$  ( $m = 5$  (Eu, Gd and Dy) and 6 (Tm, Ho and Lu) (10:2:1) resulted in the trinuclear mixed 3d-4f complexes formulated as  $[(HNEt_3)_2[Ln\{Mn(L^5)\}_2 \cdot (H_2O)_x \cdot (ClO_4)]$  ( $x = 2$ ; Ln = Eu (**29**), Gd (**30**), Dy (**31**) and Lu (**33**) and  $x = 4$ ; Ln = Tm (**32**)) (Scheme 3.9). A slight excess of triethylamine is essential for the formation of the mixed 3d-4f metal complex because it promotes the complete deprotonation of the ligand and thus enables it to coordinate to the manganese ions. Compounds **29-33** are isolated by a reaction of their mononuclear complex with  $Mn(ClO_4)_2 \cdot (H_2O)_6$  in the presence of a base, as shown in Scheme 3.9. Compounds **29-33** were characterized by standard analytical / spectroscopic techniques. The solid state structures of compounds **29-33** were established by single crystal X-ray diffraction (Figure 3.49).



**Scheme 3.9** Synthetic scheme of compounds **29-33**.

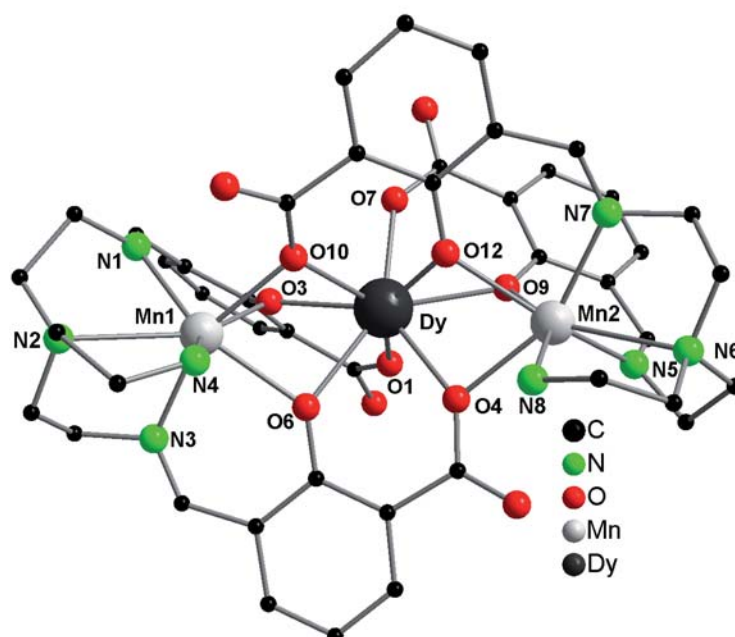


**Figure 3.49** Solid state structure of the  $[\text{Dy}\{\text{Mn}(\text{L}^5)\}_2]^-$  anion of compound **31**, omitting hydrogen atoms for clarity. Compounds **29-33** are isostructural. Selected bond lengths [ $\text{\AA}$ ] and bond angles [ $^\circ$ ]:

**29:** Mn1-N1 2.253(5), Mn1-N2 2.625(2), Mn1-N3 2.210(4), Mn1-N4 2.260(4), Mn1-O3 2.224(3), Mn1-O6 2.306(4), Mn1-O10 2.259(3), Mn2-N5 2.245(4), Mn2-N6 2.646(1), Mn2-N7 2.230(4), Mn2-N8 2.261(4), Mn2-O4 2.272(3), Mn2-O9 2.247(3), Mn2-O12 2.292(3), Eu-O1 2.349(3), Eu-O3 2.356(3), Eu-O4 2.350(3), Eu-O6 2.409(4), Eu-O7 2.350(4), Eu-O9 2.348(3), Eu-O10 2.378(3), Eu-O12 2.469(4), N1-Mn1-N2 69.24(4), N1-Mn1-N3 105.2(2), N2-Mn1-N4 71.08(4), N5-Mn2-N8 123.33(2), N7-Mn2-N8 102.3(3), N7-Mn2-O12 80.38(15), O1-Eu-O3 71.21(12), O4-Eu-O6 70.17(12), O7-Eu-O9 70.66(13).

**31:** Mn1-N1 2.256(5), Mn1-N2 2.621(1), Mn1-N3 2.208(5), Mn1-N4 2.277(5), Mn1-O3 2.231(4), Mn1-O6 2.293(4), Mn1-O10 2.247(3), Mn2-N5 2.245(5), Mn2-N6 2.652(1), Mn2-N7 2.2221(4), Mn2-N8 2.261(5), Mn2-O4 2.262(4), Mn2-O9 2.246(4), Mn2-O12 2.285(4), Dy-O1 2.321(4), Dy-O3 2.335(3), Dy-O4 2.311(3), Dy-O6 2.381(4), Dy-O7 2.311(4), Dy-O9 2.329(3), Dy-O10 2.339(4), Dy-O12 2.430(4), N1-Mn1-N2 69.06(2), N1-Mn1-N3 104.8(2), N2-Mn1-N4 71.23(2), N5-Mn2-N8 123.4(2), N7-Mn2-N8 102.1(2), N7-Mn2-O12 80.68(15), O1-Dy-O3 72.27(13), O4-Dy-O6 70.48(13), O7-Dy-O9 71.71(13).

**32:** Mn1-N1 2.252(7), Mn1-N2 2.612(6), Mn1-N3 2.209(6), Mn1-N4 2.271(7), Mn1-O3 2.245(5), Mn1-O6 2.269(5), Mn1-O10 2.249(4), Mn2-N5 2.253(7), Mn2-N6 2.649(6), Mn2-N7 2.229(6), Mn2-N8 2.267(7), Mn2-O4 2.246(5), Mn2-O9 2.243(5), Mn2-O12 2.279(5), Tm-O1 2.272(5), Tm-O3 2.292(5), Tm-O4 2.280(5), Tm-O6 2.372(5), Tm-O7 2.279(5), Tm-O9 2.298(5), Tm-O10 2.309(5), Tm-O12 2.393(5), N1-Mn1-N2 69.36(2), N1-Mn1-N3 102.7(2), N2-Mn1-N4 70.54(3), N5-Mn2-N8 123.1(3), N7-Mn2-N8 102.3(3), N7-Mn2-O12 81.1(2), O1-Tm-O3 73.4(2), O4-Tm-O6 70.8(2), O7-Tm-O9 72.0(2).

**33:** Mn1-N1 2.251(3), Mn1-N2 2.611(3), Mn1-N3 2.218(3), Mn1-N4 2.272(3), Mn1-O3 2.250(2), Mn1-O6 2.263(2), Mn1-O10 2.259(2), Mn2-N5 2.248(3), Mn2-N6 2.652(3), Mn2-N7 2.229(3), Mn2-N8 2.265(3), Mn2-O4 2.248(2), Mn2-O9 2.228(2), Mn2-O12 2.280(2), Lu-O1 2.256(2), Lu-O3 2.278(2), Lu-O4 2.262(2), Lu-O6 2.359(2), Lu-O7 2.265(2), Lu-O9 2.292(2), Lu-O10 2.285(2), Lu-O12 2.387(2), N1-Mn1-N2 69.33(11), N1-Mn1-N3 102.47(11), N2-Mn1-N4 71.87(12), N5-Mn2-N8 123.0(12), N7-Mn2-N8 102.30(12), N7-Mn2-O12 80.71(10), O1-Lu-O3 73.77(8), O4-Lu-O6 70.92(8), O7-Lu-O9 72.85(8).

The single crystal X-ray study reveals that compounds **29-33** crystallize in the triclinic space group  $P-1$ . It is worth noting that suitable yellow crystals of **29** and **31** have a crystallographic twin that was observed during the diffraction. The structure of compounds **29** and **31** were solved after twin refinement, but the data completeness was not higher than 70%. The structure of compound **30** could not be satisfactorily refined due to disorder among the metal

ions (Mn(II) and Gd(III)) as well as the counter ions ( $\text{ClO}_4^-$  and  $\text{HNEt}_3^+$ ), but we found a similar crystallographic cell corresponding to compounds **29**, **31** and **33**. Moreover, the ESI-MS analyses support the structural motif that is similar to compounds **29** and **31**. Since they are isostructural, and only the crystal structure of the compound **31** will be described in detail. The asymmetric unit contains two  $(\text{NEt}_3)^+$  cations, one  $(\text{ClO}_4)^-$ , one  $[\text{Dy}\{\text{Mn}(\text{L}^5)\}_2]^-$  coordination anion and two water molecules. Compound **32** is isostructural with compound **31** except that the number of non-coordinating water molecules / formula unit in compound **32** is higher than that in compound **31**. The solid state structure of compound **31** is illustrated in Figure 3.49, and selected bond lengths and bond angles are given in the caption for compounds **29-33**. The trimetallic  $[\text{Dy}\{\text{Mn}(\text{L}^5)\}_2]^-$  anion is build around the central Dy(III) ion, as is observed in compound **31** and two adjacent Mn(II) ions, which are coordinated in the outer cages of the anion (Figure 3.49).

In contrast to compound **26**, the two ligands are now fully deprotonated and, thus, have additional coordination sites available. The coordination mode of the Dy(III) ion is quite similar to the one observed in compound **26**: the Dy(III) ion is eight-fold coordinated and is the center of a distorted square antiprism coordination polyhedron. Although, the ligand is now fully deprotonated, there is no obvious difference in the Dy-O distances (2.311(4)-2.430(4) Å) in comparison to compound **26**. The two Mn(II) ions (Mn1 and Mn2) are seven-coordinated: they are ligated to four nitrogen atoms (around Mn1; N1-N4 and around Mn2; N5-N8) of the tris-(2-aminoethyl)amine sub-unit and three oxygen atoms, of which two are phenoxy groups (O3 and O6 for Mn1, O9 and O12 for Mn2) and the remaining one is from carboxyl group (O10 for Mn1 and O4 for Mn2) (Figure 3.49). The coordination polyhedron is best described as a distorted capped octahedron. As expected, the Mn-N bond distances of the amine nitrogen atoms (Mn1-N2 = 2.621(1) Å and Mn2-N6 = 2.652(1)) are significantly longer than those of the imine nitrogen atoms (2.208(5)-2.277(5) Å). The Dy-Mn distances of Dy-Mn1 3.4039(9) and Dy-Mn2 3.4081(8) Å show close proximity of the metal atoms.

### 3.5.1.1 ESI-MS Spectral Studies of Compounds 29-31

Electrospray ionization mass spectrometry (ESI-MS) of compounds **29-31** were performed on a Bruker Esquire 3000 plus ion trap instrument in positive and negative ionization modes in acetonitrile solution by Dr. Christoph Riehn.

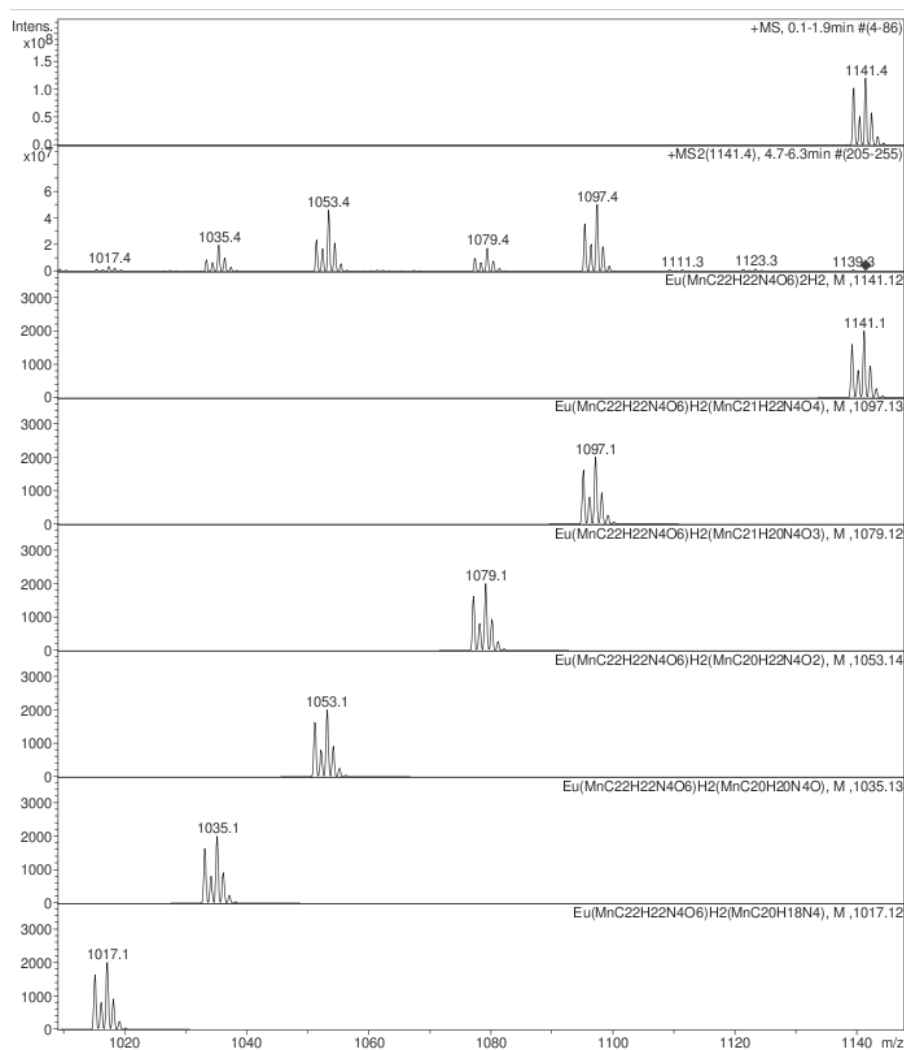


**Figure 3.50** (a) Pos. mass spectrum from 1010 to 1145 m/z. (b) MS<sup>2</sup> fragmentation of 1141.4 m/z. (c)-(h) simulated mass spectra of compound **29**.

Only one peak at m/z was detected in positive ion mode for compound **29** (Figure 3.50), corresponding to the double protonation of  $[\text{Eu}(\text{MnC}_{22}\text{H}_{22}\text{N}_4\text{O}_6)_2]^-$ , which leads to  $[\text{Eu}(\text{MnC}_{22}\text{H}_{23}\text{N}_4\text{O}_6)_2]^+$ . Simulation of the isotopic distribution shows a good match with the measured spectrum except a small shift of all peaks of 0.3 to higher m/z values (a calibration issue of the mass spectrometer). Table 3.3 shows the fragmentation of the 1141.4 m/z peak.

For the negative ion mode, a couple of peaks were detected for compound **29**. The most prominent ones are 1339.3 and 594.4 m/z. The first one is not assigned, but the latter corresponds to the species  $[(\text{MnC}_{22}\text{H}_{24}\text{N}_4\text{O}_6)(\text{ClO}_4)]^-$ . Other fragmentations are assigned in Table 3.4.

**Table 3.3** Fragmentation of the peak 1141.4 m/z.

Parent mass (m/z)	Fragment mass (m/z)	Neutral loss	Proposed fragment
1141.4	1097.4	CO <sub>2</sub>	[EuMn <sub>2</sub> C <sub>43</sub> H <sub>46</sub> N <sub>8</sub> O <sub>10</sub> ] <sup>+</sup>
1141.4	1079.4	CO <sub>2</sub> , H <sub>2</sub> O	[EuMn <sub>2</sub> C <sub>43</sub> H <sub>44</sub> N <sub>8</sub> O <sub>9</sub> ] <sup>+</sup>
1141.4	1053.4	2CO <sub>2</sub>	[EuMn <sub>2</sub> C <sub>42</sub> H <sub>46</sub> N <sub>8</sub> O <sub>8</sub> ] <sup>+</sup>
1141.4	1035.4	2CO <sub>2</sub> , H <sub>2</sub> O	[EuMn <sub>2</sub> C <sub>42</sub> H <sub>44</sub> N <sub>8</sub> O <sub>7</sub> ] <sup>+</sup>
1141.4	1017.4	2CO <sub>2</sub> , 2H <sub>2</sub> O	[EuMn <sub>2</sub> C <sub>42</sub> H <sub>42</sub> N <sub>8</sub> O <sub>6</sub> ] <sup>+</sup>

**Table 3.4** Fragmentation of negative ion mode of compound **29**.

Parent mass (m/z)	Assigned molecular formula
1293.3	[Eu(MnC <sub>22</sub> H <sub>22</sub> N <sub>4</sub> O <sub>6</sub> ) <sub>2</sub> (HClO <sub>4</sub> )] <sup>-</sup>
1202.4	[Eu(MnC <sub>22</sub> H <sub>22</sub> N <sub>4</sub> O <sub>6</sub> ) <sub>2</sub> (HNO <sub>3</sub> )] <sup>-</sup>
1139.4	[Eu(MnC <sub>22</sub> H <sub>22</sub> N <sub>4</sub> O <sub>6</sub> ) <sub>2</sub> ] <sup>-</sup>
642.5	[(C <sub>22</sub> H <sub>24</sub> N <sub>4</sub> O <sub>6</sub> )(NC <sub>6</sub> H <sub>15</sub> ) <sub>2</sub> ] <sup>-</sup>
594.4	[(MnC <sub>22</sub> H <sub>23</sub> N <sub>4</sub> O <sub>6</sub> )(HClO <sub>4</sub> )] <sup>-</sup>

Only one intense peak at 1145.7 m/z for compound **30** was detected in positive ion mode (Figure 3.51), corresponding to the doubly protonated [Gd(MnC<sub>22</sub>H<sub>22</sub>N<sub>4</sub>O<sub>6</sub>)<sub>2</sub>]<sup>-</sup>, which leads to [Gd(MnC<sub>22</sub>H<sub>23</sub>N<sub>4</sub>O<sub>6</sub>)<sub>2</sub>]<sup>+</sup>. The simulation of the isotopic distribution matches very well with the measured spectrum except a small shift of all peaks equal to or higher than 0.3 m/z (a calibration issue of the mass spectrometer). Fragmentation of the 1145.7 m/z peak leads to the same neutral losses as shown during fragmentation of the [Eu(MnC<sub>22</sub>H<sub>23</sub>N<sub>4</sub>O<sub>6</sub>)<sub>2</sub>]<sup>+</sup> parent ion. The investigation in negative ion mode gave very similar results for compound **29**.

The positive ion mode was also recorded for compound **31**, and it shows one intense peak at 1152.15 m/z. This peak corresponds to the doubly protonated [Dy(MnC<sub>22</sub>H<sub>22</sub>N<sub>4</sub>O<sub>6</sub>)<sub>2</sub>]<sup>-</sup>, leading to [Dy(MnC<sub>22</sub>H<sub>23</sub>N<sub>4</sub>O<sub>6</sub>)<sub>2</sub>]<sup>+</sup>. After recalibration of the Esquire the simulation of the isotopic distribution shows a good match with the measured spectrum except a small shift of all peaks equal to or higher than 0.3 m/z values. Fragmentation of the 1152.15 m/z peak leads to the same neutral losses as shown during fragmentation of the [Eu(MnC<sub>22</sub>H<sub>23</sub>N<sub>4</sub>O<sub>6</sub>)<sub>2</sub>]<sup>+</sup> and [Gd(MnC<sub>22</sub>H<sub>23</sub>N<sub>4</sub>O<sub>6</sub>)<sub>2</sub>]<sup>+</sup> parent ions. The composition of the solution in negative ion mode is also very similar to compounds **29** and **30**.



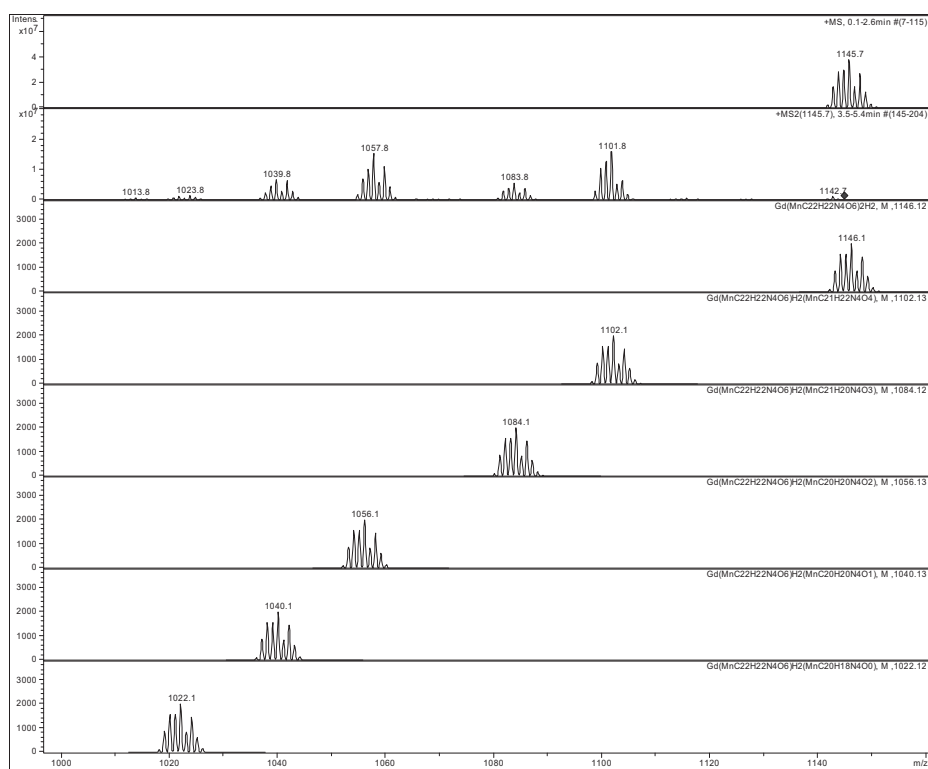


**Figure 3.51** (a) pos. mass spectrum from 1000 to 1160 m/z for compound **30**, (b) MS<sup>2</sup> fragmentation of 1146.7 m/z, (c)-(f) simulated mass spectra.

From the measurements of compounds **29-31**, a common fragmentation scheme of the positive parent ions is shown in (Figure 3.52). Each complex shows the same neutral losses in a similar intensity distribution. The loss of CO<sub>2</sub> is preferred over the loss of H<sub>2</sub>O. Additionally, some minor fragmentation paths were found, especially in the fragmentation of [LnMn<sub>2</sub>C<sub>42</sub>H<sub>42</sub>N<sub>8</sub>O<sub>6</sub>]<sup>+</sup>, e.g. the loss of 27 m/z according to HCN. These minor channels are not plotted in Figure 3.52.

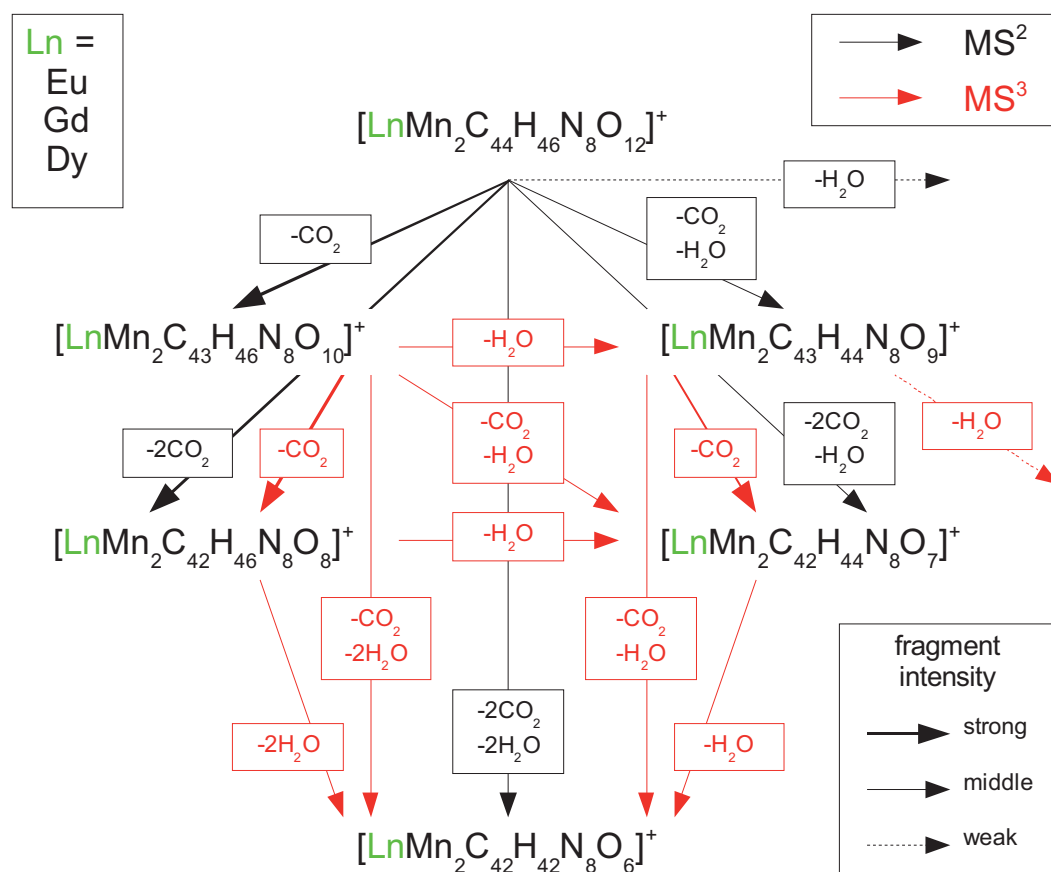


**Figure 3.52** Fragmentation scheme of  $[\text{Ln}(\text{MnC}_{22}\text{H}_{23}\text{N}_4\text{O}_6)_2]^+$  (Ln = Eu (**29**), Gd (**30**) and Dy (**31**)) according to neutral losses.

In order to further elucidate the gas phase structure of  $[\text{Dy}\{\text{Mn}(\text{HL})\}_2]^+$  in compound **31**, hydrogen/deuterium exchange (HDX) reactions with  $\text{ND}_3$  were performed in a FT-ICR Penning-trap mass spectrometer. The  $[\text{Dy}\{\text{Mn}(\text{HL})\}_2]^+$  showed only an exchange of two hydrogen atoms, even after a storage time of 960 s, although there are four more hydrogen atoms available on the amine groups (Figure 3.53). We believe that this result indicates strong coordination of the amine groups to the manganese ions. The HDX results together with the fragmentation behavior (loss of  $\text{H}_2\text{O}$ ) imply that probably the two exchangeable protons are not coordinated at the amine groups but at the carboxyl binding sites.

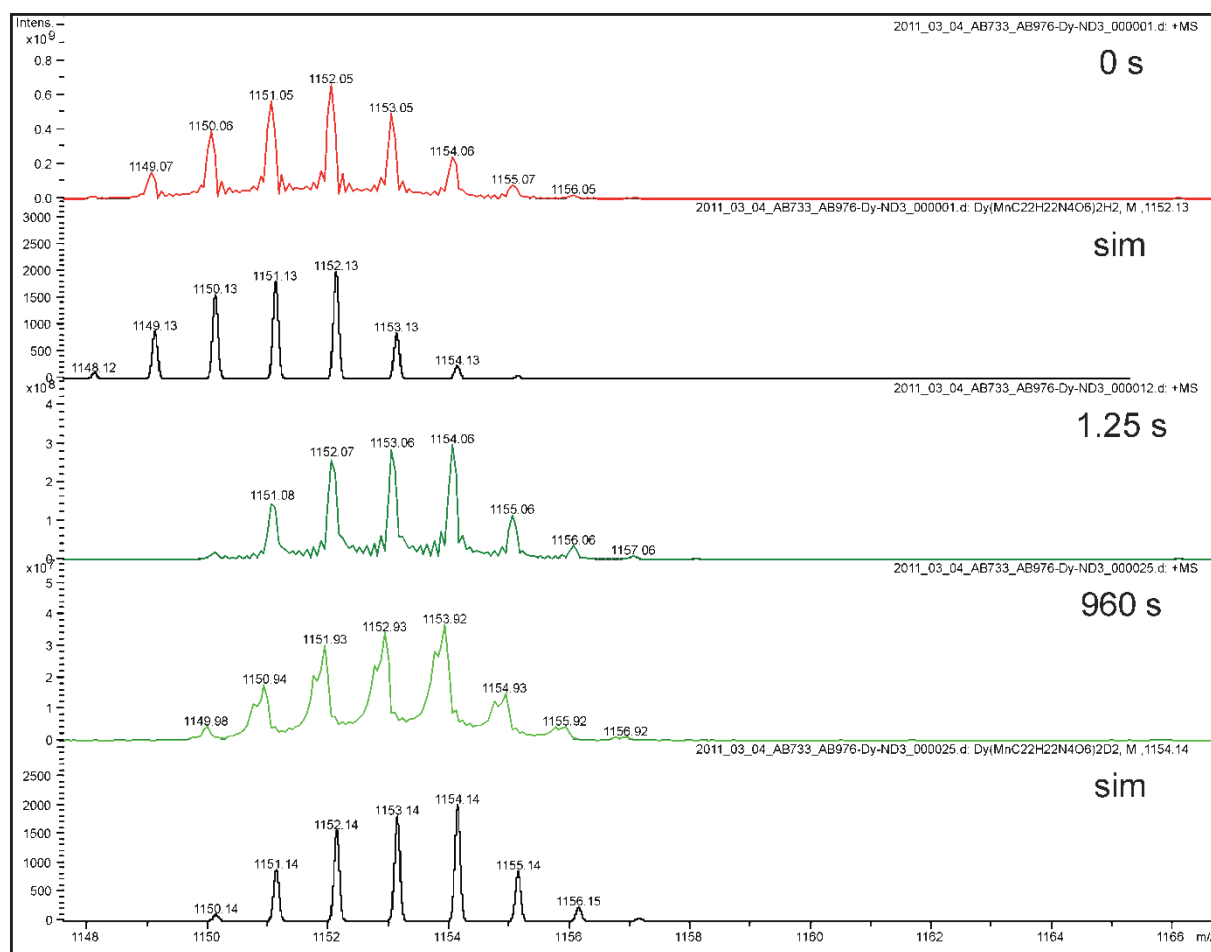


**Figure 3.53** Mass spectra of H/D exchange reactions of  $[\text{Dy}\{\text{HMn}(\text{L})\}_2]^+$  in compound **31** after 0, 1.25 and 960 seconds (first, third and fourth row) and simulated isotope patterns (second and fifth row).

### 3.5.1.2 *Ab Initio* Calculation of Compound **31**

*Ab initio* calculations of **31** was performed by Prof. Liviu F. Chibotaru within CASSCF/RASSI approach using the MOLCAS package.<sup>[120]</sup> Their magnetic properties have been calculated with SINGLE\_ANISO module<sup>[121],[122]</sup> recently implemented in MOLCAS-7.6. The main values of the ground state  $g$  tensors and orientations of the main magnetic axes on Dy ion of **31** are 0.0682, 0.1542 and 19.3367 for  $g_x$ ,  $g_y$  and  $g_z$ , respectively. In contrast to **26**, the main magnetic axis lies almost in the O4-O6-O7 plane (Figure 3.54) and makes an angle of  $81^\circ$  with the Mn1-Mn2 axis for compound **31**. The exchange spectrum in **31** has been simulated by the Lines model, as discussed in previous works, using the software POLY\_ANISO.<sup>[142]</sup> The two Lines parameters describing the Dy-Mn and Mn1-Mn2 exchange interactions have been derived from the fitting of  $\chi T(T)$  and  $M(T)$  data for **31**. The exchange

spectrum arising from the interaction of the ground Kramers doublet on Dy with  $S = 5/2$  on Mn1 and Mn2 ( $2 \times 6 \times 6 = 72$  states) has a spread of only  $1.13 \text{ cm}^{-1}$ , which is the result of a very weak Dy-Mn exchange interaction. However, the zero-field splitting obtained for the Mn sites is even smaller, *ca.*  $0.2 \text{ cm}^{-1}$ . This is the reason why the local magnetizations on Mn1 and Mn2 in exchange states are not directed along the corresponding anisotropy axes, but are tilted towards the anisotropy axis on Dy. Due to the small exchange splitting, complex **31** is found in the "paramagnetic regim", when the magnetic ions are practically uncoupled for all temperatures at which the measurements were done.

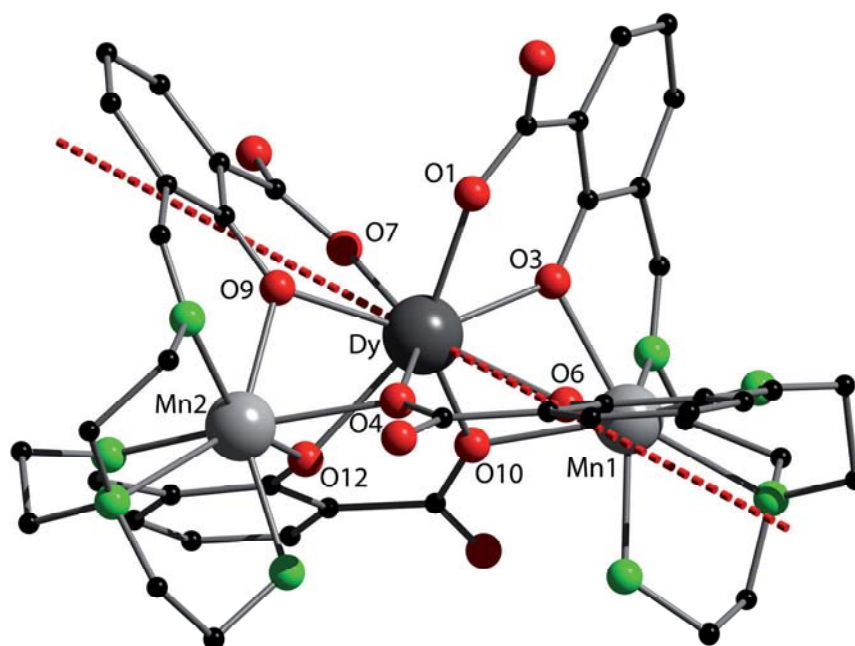


**Figure 3.54** Main anisotropy axes on Dy ion in compound **31**.

### 3.5.1.3 Magnetic Properties of Compounds **30**, **31** and **32**

The magnetic properties of compounds **30**, **31** and **32** were studied by Dr. Yanhua Lan (Prof. A. K. Powell). The magnetic susceptibility measurement of compounds **30**, **31** and **32** are shown in Figure 3.55. At room temperature, the  $\chi T$  products of **30**, **31** and **32** are 16.52, 23.26, and  $15.82 \text{ cm}^3\text{K/mol}$ , respectively. These values are in good agreement with the expected values for the presence of two  $S = 5/2$  Mn(II) ions ( $S = 5/2$ ,  $C = 4.375 \text{ cm}^3\text{K/mol}$  with  $g = 2$ ) and for **30**, one Gd(III) ion ( $S = 7/2$ ,  $L = 0$ ,  ${}^8S_{7/2}$ ,  $C = 7.875 \text{ cm}^3\text{K/mol}$  with  $g = 2$ ), for **31**, one Dy(III) metal ion ( $S = 5/2$ ,  $L = 5$ ,  ${}^6H_{15/2}$ ,  $C = 14.17 \text{ cm}^3\text{K/mol}$  with  $g = 4/3$ ), as well as for **33**, one Tm(III) ion ( $S = 1$ ,  $L = 5$ ,  ${}^3H_6$ ,  $C = 7.15 \text{ cm}^3\text{K/mol}$  with  $g = 7/6$ ).<sup>[102]</sup> The  $\chi T$  product of compound **30** is almost constant up to 60 K, after which it increases to reach  $21.79 \text{ cm}^3\text{K/mol}$

at 1.8 K (Figure 3.55), indicating ferromagnetic interaction between the neighboring Mn(II) and Gd(III) ions.

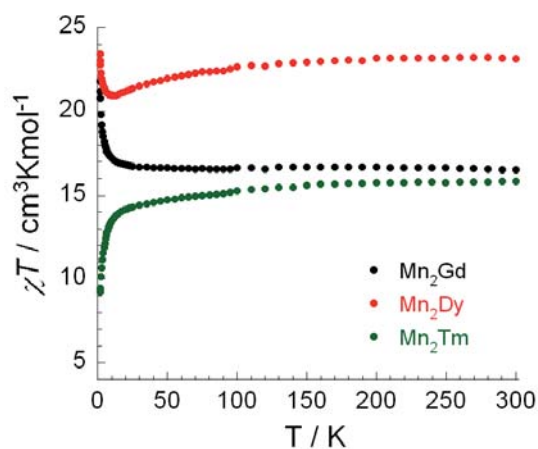


**Figure 3.55** Temperature dependence of the  $\chi T$  product for compounds **30**, **31** and **33** at 1000 Oe.

The  $M$  versus  $H$  measurements as a function of field (Figure 3.56, left) for compound **30** reveal a slow increase of the magnetization, which reaches a saturation of  $17 \mu_B$  at 7 T. The  $M$  vs  $H/T$  curves (Figure 3.56, right) at different temperatures are superposed to show the absence of magnetic anisotropy in the compound **30**. The two solid lines (Figure 3.57) correspond to the calculated curves with Brillouin functions of one  $17/2$  spin and the sum of three spins of  $5/2$ ,  $7/2$  and  $5/2$ , respectively. The magnetization is close to the latter with three isolated spins, suggesting weak ferromagnetic interactions between Mn(II) and Gd(III) ions.

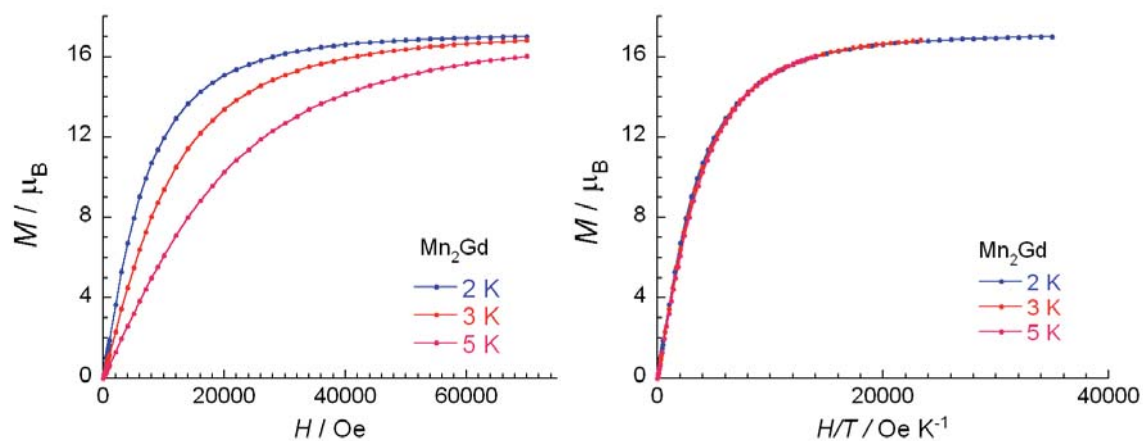


**Figure 3.56** Field dependence of magnetization (left) and  $M$  vs  $H/T$  (right), for **30** from 2-5 K.

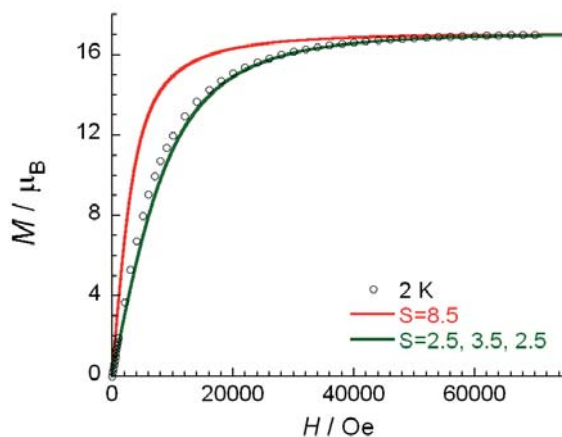


**Figure 3.57** Field dependence of magnetization for **30** at 2 K, the solid lines are calculated curves with Brillouin functions.

For compound **31**, the  $\chi T$  product slowly decreases to reach  $21 \text{ cm}^3\text{K/mol}$  at 11 K and then slightly increases to reach  $23.4 \text{ cm}^3\text{K/mol}$  at 1.8 K (Figure 3.55). This suggests the presence of weak intramolecular ferromagnetic interactions between Mn(II) and Dy(III) metal ions.

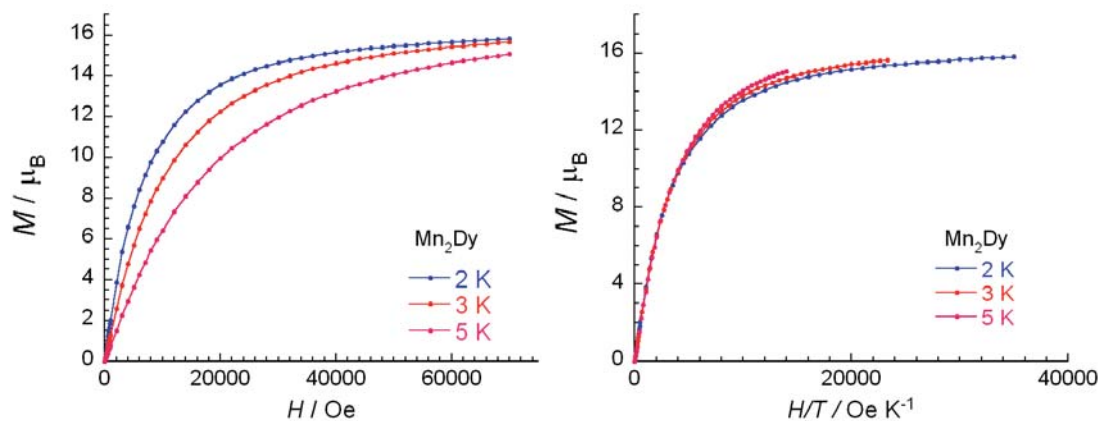


**Figure 3.58** Field dependence of magnetization (left) and  $M$  vs  $H/T$  (right), for **31** from 2-5 K.

The field dependence of the magnetization plots at different temperatures show that the magnetization is smoothly increasing with increasing applied dc field (Figure 3.58, left). At 7 T, the magnetization value is  $15.8 \mu_B$ , which is in good agreement with the expected value ( $15.23 \mu_B$ ). There is no clear saturation of magnetization, suggesting the presence of magnetic anisotropy and/or the population of low-lying excited states. Also, the plot of  $M$  vs  $H/T$  at different temperatures shows that the curves are not superposed on a single master curve (Figure 3.58 right), further indicating the presence of magnetic anisotropy and/or low-lying excited states.

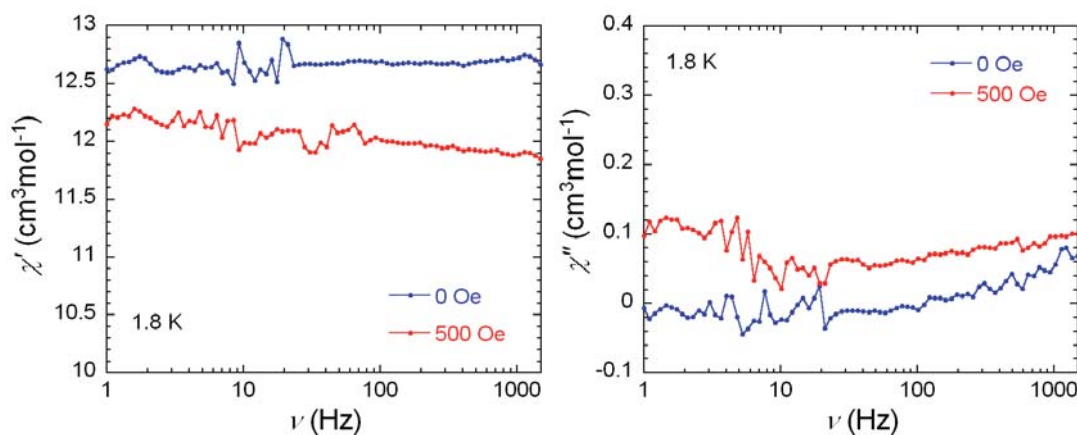


**Figure 3.59** Frequency dependence of the in-phase ( $\chi'$ ) and out-of-phase ( $\chi''$ ) susceptibilities for compound **31**.

As shown in the plots of ac susceptibilities (Figure 3.59), almost no slow magnetic relaxation is observed in the  $\text{Mn}_2\text{Dy}$  compound under zero dc field, and the slow relaxation is also not induced by applying an external dc field. This indicates that the introduction of Mn(II) into the mononuclear Dy(III) system (e.g. compound **26**) can switch off SMM behavior. These results are well explained with the help of *ab initio* calculations. Due to a very weak Dy-Mn exchange (or, generally, magnetic) interaction, the manganese ions in **31** will have independently reorienting magnetic moments already at  $T \geq 2$  K. In this "paramagnetic regim" the latter are merely sources of random magnetic field for the dysprosium ion, inducing the dynamics of its magnetic moment due to a tunneling splitting  $\Delta_{\text{tun}} = \frac{1}{2} \mu_B g_{\perp} H_{\perp}$ . This is expected to be large given the non-negligible values of  $g_X$  and  $g_Y$  for Dy in **31** (Section 3.4.1) as compared to other dysprosium complexes, and the relatively large  $H_{\perp}$  as compared to its typical values from intermolecular interactions.<sup>[143]</sup> On the contrary,  $H_{\perp}$  is much weaker in **26**, since it derives from dipolar intermolecular interactions only, while  $g_{\perp}$  is smaller than in **31** (Section 3.5.1.2). Since the tunneling rate of the magnetic moment is proportional to  $\Delta_{\text{tun}}^2$ ,<sup>[144],[145]</sup> the above estimates suggest that it will be orders of magnitude larger in **31** than in **26**, explaining why the former is not a SMM. For **32**, the  $\chi T$  product decreases upon decreasing the temperature and reach to  $9.2 \text{ cm}^3\text{K/mol}$  at 1.8 K (Figure 3.55), suggesting the presence of weak intramolecular antiferromagnetic interactions between Mn(II) and Tm(III) metal ions.

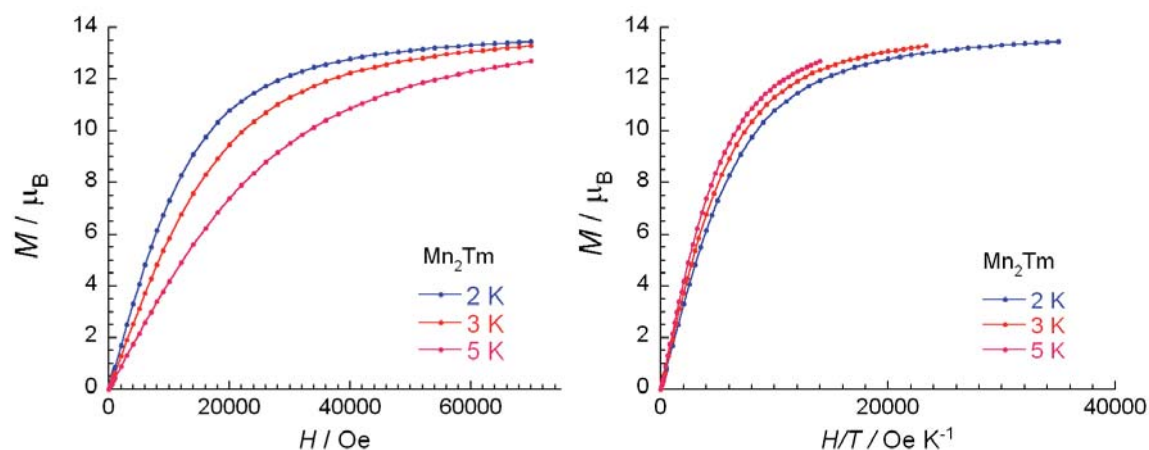


**Figure 3.60**  $M$  vs  $H$  (left) and  $M$  versus  $H/T$  (right) plots for **32** from 2 K to 5 K.

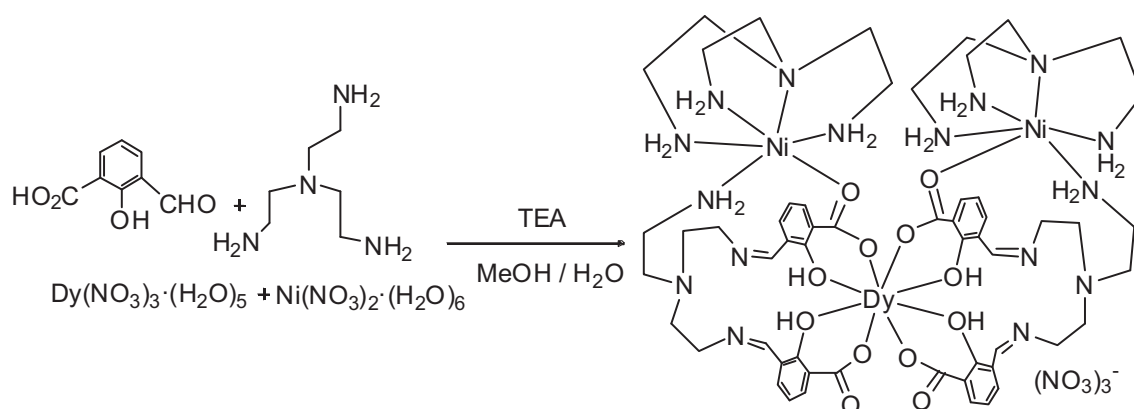
The magnetization of **32** increases with increasing dc field (Figure 3.60, left). At 7 T, the value is 13.5  $\mu_B$  (at 2 K) without a clear saturation. The plots of  $M$  vs  $H/T$  at several low temperatures show that the curves are not superposed on a single master curve (Figure 3.60, right), indicating the presence of magnetic anisotropy and/or low-lying excited states.

In summary, a series of trinuclear complexes **29-32** have been synthesized and characterized. The magnetic studies of compounds **30**, **31** and **32** show that ferromagnetic interactions exist between the metal ions (Mn(II)-Gd(III) and Mn(II)-Dy(III)), while there are antiferromagnetic interactions between the Mn(II)-Tm(III) ions.



### 3.5.2 Trinuclear Nickel and Lanthanide Metal Complexes

The treatment of 3-formylsalicylic acid, tris(2-aminoethyl)amine (tren) with  $\text{Ni}(\text{NO}_3)_2 \cdot (\text{H}_2\text{O})_6$  and  $\text{Dy}(\text{NO}_3)_3 \cdot (\text{H}_2\text{O})_m$  in the presence of triethylamine in methanol / water (15 mL / 5 mL) afforded the trinuclear 3d-4f compound formulated as  $[\text{Dy}\{\text{Ni}(\text{H}_2\text{L}^5)(\text{tren})\}_2 \cdot (\text{NO}_3)_3 \cdot (\text{H}_2\text{O})_{14}]$  (**34**) (Scheme 3.10). The base, triethylamine, plays an important role for the formation of the 3d-4f complex.



**Scheme 3.10** Synthetic scheme of compound **34**.

Compound **34** was obtained as yellow crystals and characterized by standard analytical / spectroscopic techniques. The solid state structure was established by single crystal X-ray diffraction (Figure 3.61). The *in situ* generation of  $\text{H}_4\text{L}^5$  and the free tren ligand coordinated with nickel and dysprosium ions resulted in trinuclear complexes. Although tren ligands contain transition metal complexes are known in literature, trinuclear 3d-4f complexes containing both ligands ( $\text{H}_4\text{L}^5$  and tren) are not reported in the literature. The IR spectrum of compound **34** shows characteristic bands of functional groups (see experimental section).

Compound **34** crystallizes in the triclinic space group *P*-1. The asymmetric unit of compound **34** contains a  $[\text{Dy}\{\text{Ni}(\text{H}_2\text{L}^5)(\text{tren})\}_2]^{3+}$  coordination cation, three  $\text{NO}_3^-$  anion, fourteen water molecules. Selected bond lengths and bond angles are given in the caption of Figure 3.61.

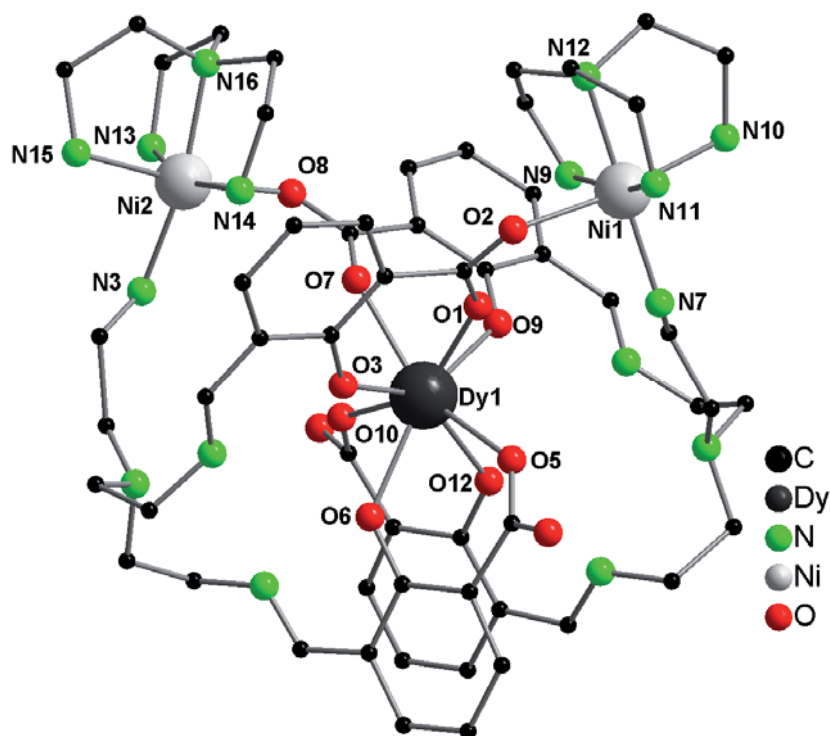


**Figure 3.61** Solid state structure of the  $[\text{Dy}\{\text{Ni}(\text{H}_2\text{L}^5)(\text{tren})\}_2]^{3+}$  cation of compound **34**, omitting hydrogen atoms for clarity. Selected bond lengths [ $\text{\AA}$ ] and bond angles [ $^\circ$ ]: Ni1-N7 2.055(7), Ni1-N9 2.105(7), Ni1-N10 2.104(7), Ni1-N11 2.126(7), Ni1-N12 2.099(7), Ni1-O2 2.160(5), Ni2-N3 2.11(2), Ni2-N13 2.090(9), Ni2-N14 2.088(10), Ni2-N15 2.108(7), Ni2-N16 2.096(8), Ni2-O8 2.092(5), Dy1-O1 2.317(6), Dy1-O3 2.333(5), Dy1-O5 2.369(6), Dy1-O6 2.358(5), Dy1-O7 2.359(5), Dy1-O9 2.312(5), Dy1-O10 2.324(5), Dy1-O12 2.368(5), N7-Ni1-N10 96.6(3), N7-Ni1-N11 95.2(3), N7-Ni1-N12 178.8(3), N9-Ni1-N10 91.5(3), N9-Ni1-N11 164.6(3), N7-Ni1-O2 91.2(2), N10-Ni1-O2 172.2(3), N13-Ni2-N16 83.1(3), N14-Ni2-N16 83.4(4), N15-Ni2-N16 83.5(3), O1-Dy1-O3 72.3(2), O1-Dy1-O5 71.6(2), O1-Dy1-O9 78.2(2), O3-Dy1-O12 145.56(2), O5-Dy1-O10 141.30(2).

The cationic  $[\text{Dy}\{\text{Ni}(\text{H}_2\text{L}^5)(\text{tren})\}_2]^{3+}$  core (Figure 3.61) contains one dysprosium ion, two nickel ions, two  $(\text{H}_2\text{L}^5)^{2-}$  ligands and two tren ligands. To balance the charge, each  $\text{H}_4\text{L}^5$  acts as a double negative charge due to the two carboxylate that are deprotonated upon crystallization. Thus, the dysprosium shows an oxidation state of +3 and nickel shows an oxidation state of +2. Both the nickel ions, Ni1 and Ni2, are surrounded by ligands, tren and  $(\text{H}_2\text{L}^5)^{2-}$ . Each nickel is six coordinated: they are ligated to five nitrogen atoms (around Ni1; N7, N9-N12 and around Ni2; N3, N13-N16) from both of the ligand and one oxygen (O2 for Ni1 and O8 for Ni2). The nickel ions Ni1 and Ni2 exhibit distorted octahedral geometry. The Ni-O and Ni-N bond lengths are in the range of 2.101(5)  $\text{\AA}$  to 2.154(5)  $\text{\AA}$  and 2.060(12)  $\text{\AA}$  to 2.139(7)  $\text{\AA}$ , respectively. The Dy(III) is situated in the center and is eight-fold coordinated: it is ligated to four phenoxy oxygen atoms (O3, O6, O9 and O12) and four carboxylate oxygen atoms (O1, O5, O7 and O10) from two different  $(\text{H}_2\text{L}^5)^{2-}$  ligands. Hence, the coordination environment of Dy(III) can be described as a distorted square-antiprism polyhedron with Dy-O bond lengths in the range of 2.313(5)  $\text{\AA}$  to 2.376(5)  $\text{\AA}$ . The distances

between dysprosium and nickel ions are Dy1-Ni1 5.473(3) Å and Dy1-Ni2 5.62(3) Å, while the distance of the two nickel ions, Ni1⋯Ni2, is 8.196(4) Å, resulting in a V-shaped structure.

### 3.5.2.1 Magnetic Properties of Compound 34

The magnetic susceptibility measurement of compound **34** is shown in Figure 3.62. At 300 K, the  $\chi T$  product is 16.11 cm<sup>3</sup>K/mol, which is in good agreement with the expected value of 16.17 cm<sup>3</sup>K/mol for two Ni(II) ( $S = 1$  and  $g = 2$ ) ions and one Dy(III) metal ions ( $S = 5/2$ ,  $L = 5$ ,  $g = 4/3$ ,  ${}^6H_{15/2}$  and  $C = 14.17$  cm<sup>3</sup>K/mol).<sup>[102]</sup> Upon decreasing the temperature, the  $\chi T$  product at 1 kOe continuously decreases to reach 11.65 cm<sup>3</sup>K/mol at 1.8 K. The profile of the  $\chi T$  product indicates that antiferromagnetic interactions may be present in this compound.

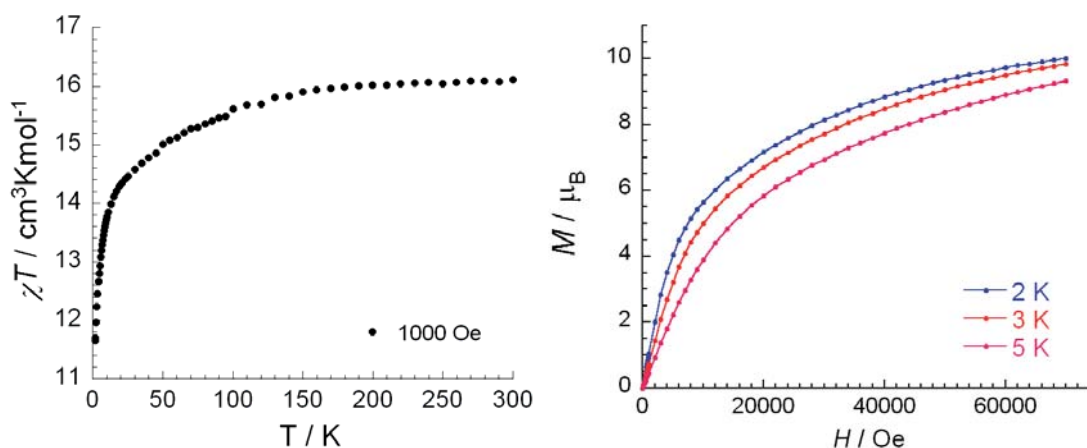


**Figure 3.62** Temperature dependence of the  $\chi T$  product for compounds **34** at 1 kOe (left); Field dependence of magnetization for **34** from 2-5 K (right).

The field dependence of magnetizations from 2-5 K for compound **36** is shown in Figure 3.62. The magnetization slowly increases to 10.0  $\mu_B$  at 2 K and 7 T without true saturation, suggesting the presence of magnetic anisotropy and/or low-lying excited states.

In summary, a new V shaped compound  $[\text{Dy}\{\text{Ni}(\text{H}_2\text{L}^5)(\text{tren})\}_2 \cdot (\text{NO}_3)_3 \cdot (\text{H}_2\text{O})_{14}]$  (**34**) has been prepared by the use of an unknown polypodal ligand ( $\text{H}_4\text{L}^5$ ), which is generated from an *in situ* reaction. The magnetic property of compound **34** suggests the presence of an antiferromagnetic interaction between neighboring metal centers.

## 4 Experimental Sections

### 4.1 Spectroscopic Studies

All compounds were characterized spectroscopically. IR were measured on a Perkin-Elmer Spectrum instrument or a Bruker IFS 113v FTIR spectrometer. NMR spectra were recorded on a Bruker Avance II 300 MHz NMR spectrometer. Chemical shifts are referenced to internal solvent resonances and are reported relative to tetramethylsilane. Deuterated solvents were obtained from Chemotrade or Euriso-Top GmbH (99 atom% D). Elemental analyses were carried out with an Elementar vario EL III. Electrospray ionization mass spectrometry (ESI-MS) was performed on a Bruker Esquire 3000plus ion trap instrument in positive and negative ionization mode. TGA measurements were made on a Netzsch STA 429 instrument. The magnetic measurements were carried out with the use of a Quantum Design SQUID magnetometer MPMS. This magnetometer works between 1.8 and 400 K for dc applied fields ranging from -7 to 7 T. Measurements were performed on the polycrystalline samples dispersed in eicosane. The magnetic data were corrected for the sample holder. N<sub>2</sub> adsorption / desorption isotherms were performed on a multi-point BELSORP-mini II from BEL. All the analytical experiments mentioned were not applied to all of the compounds due to different experimental requirements or stability considerations.

### 4.2 Syntheses

All chemicals and solvents used for synthesis were obtained from chemical sources and were used as received without further purification. All reactions were carried out in aerobic conditions.

## 4.2.1 Ligands Syntheses

### 4.2.1.1 Synthesis of *N,N'*-Bis(4-carboxysalicylidene)ethylenediamine ( $H_4L$ )

A solution of (0.13 mL, 2 mmol) ethylenediamine in 10 mL of ethanol was added dropwise to a solution of (665 mg, 4 mmol) 4-formyl-3-hydroxybenzoic acid in 20 mL ethanol. The reaction mixture was stirred for 2 hours at 60°C. The yellow solid was filtered and washed with 10 mL cold ethanol and dried in vacuo. Yield: 610 mg, 86%.  $^1H$  NMR (DMSO- $d_6$ ):  $\delta$  3.94 (m, 4H, CH<sub>2</sub>), 8.16 (s, 2H, CH=N), 7.4-7.3 (m, 6H, Ar).  $^{13}C\{^1H\}$  NMR (DMSO- $d_6$ , 300 MHz, 25°C):  $\delta$  59.3 (CH<sub>2</sub>), 117.5 (Ar), 119.7 (Ar), 119.8 (Ar), 121.5 (Ar), 131.8 (Ar), 160.5 (CH=N), 166.9 (Ar), 167.9 (COOH). EI/MS (70 ev) m/z (%): 356 ([M]<sup>+</sup>, 0.6), 179 ([M/2]<sup>+</sup>, 86), 208 ([C<sub>10</sub>H<sub>12</sub>O<sub>3</sub>N<sub>2</sub>]<sup>+</sup>, 35), 60 ([C<sub>2</sub>H<sub>8</sub>N<sub>2</sub>]<sup>+</sup>, 68), 30 ([C<sub>2</sub>H<sub>6</sub>]<sup>+</sup>, 100). IR (KBr pellet):  $\bar{\nu}$  = 3416 (m), 2969 (w), 2898 (w), 1699 (s), 1634 (s), 1535 (s), 1388 (s), 1316 (m), 1282 (s), 1214 (s), 1130 (w), 1079 (m), 1030 (s), 783 (m), 762 (s) cm<sup>-1</sup>.

### 4.2.1.2 Synthesis of *N,N'*-Bis(4-carboxysalicylidene)propanediamine ( $H_4L^2$ )

A solution of (0.17 mL, 2.3 mmol) 1,3-diaminopropane in 10 mL ethanol was added dropwise to a solution of (0.664 g, 4 mmol) 4-formyl-3-hydroxybenzoic acid in 20 mL ethanol. The reaction mixture was stirred for 2 hours at 60°C. The yellow solid was filtered and wash with 10 mL cold ethanol and dried in vacuo. Yield: 0.51 g, 69%.  $^1H$  NMR (DMSO- $d_6$ ):  $\delta$  13.6 (br, s, OH, 2H), 8.67 (s, 2H, CH=N), 7.4-7.3 (m, 6H, Ar) 3.74 (t, 4H, CH<sub>2</sub>), 2.05 (qn, 2H, CH<sub>2</sub>). IR (KBr pellet):  $\bar{\nu}$  = 3406 (w), 2963 (w), 2897 (w), 2851 (w), 1702 (m), 1634 (s), 1530 (s), 1463 (w), 1392 (s), 1335 (w), 1319 (w), 1257 (w), 1211 (m), 1138 (w), 1094 (w), 1069 (w), 982 (m), 959 (m), 931 (m), 900 (w), 813 (m), 779 (s) cm<sup>-1</sup>

### 4.2.1.3 Synthesis of *N,N'*-Bis(4-carboxysalicylidene)-1,3-diamino-2-propanol ( $H_5L^3$ )

A solution of (9 mg, 1 mmol) 1,3-diamino-2-propanol in 10 mL ethanol was added dropwise to a solution of (334 mg, 2 mmol) 4-formyl-3-hydroxybenzoic acid in 20 mL ethanol. The reaction mixture was stirred for 2 hours at 90°C. The yellow solid was filtered and wash with 10 mL cold ethanol and dried in vacuo. Yield: 315 mg, 82% (based on amine).  $^1H$  NMR (DMSO- $d_6$ ):  $\delta$  13.6 (br, s, OH), 8.63 (s, 2H, CH=N), 7.6-7.37 (m, 3H, Ar), 4.07 (pentate, 1H, CHOH), 3.82

(d, 2H, CH<sub>2</sub>). <sup>13</sup>C{<sup>1</sup>H} NMR (DMSO-*d*<sub>6</sub>, 300 MHz, 25°C): δ 63.3 (CH<sub>2</sub>), 69.6 (CHOH), 117.7 (Ar), 119.4 (Ar), 122.3 (Ar), 132.1 (Ar), 134.6 (Ar), 160.1 (CH=N), 167 (Ar), 167.3 (COOH). IR (KBr pellet):  $\bar{\nu}$  = 3406 (w), 2963 (w), 2897 (w), 2851 (w), 1702 (m), 1634 (s), 1530 (s), 1463 (w), 1392 (s), 1335 (w), 1319 (w), 1257 (w), 1211 (m), 1138 (w), 1094 (w), 1069 (w), 982 (m), 959 (m), 931 (m), 900 (w), 813 (m), 779 (s) cm<sup>-1</sup>.

#### 4.2.1.4 Synthesis of *N,N'*-bis(4-hydroxysalicylidene)-1,3-diamino-2-propa-nol (H<sub>5</sub>L<sup>4</sup>)

A solution of (361 mg, 4 mmol) 1,3-diamino 2-propanol in 10 mL of methanol was added dropwise to a solution of (1.15 g, 8.3 mmol) 2,4-dihydroxy benzaldehyde in 20 mL methanol. The reaction mixture was stirred for 2 hours at 60°C. The yellow solid was filtered and washed with 10 mL cold methanol and dried in vacuo. Yield: 1.27 gm, 92% (based on aldehyde). <sup>13</sup>C{<sup>1</sup>H} NMR (DMSO-*d*<sub>6</sub>, 300 MHz, 25°C): δ 61.68 (CH<sub>2</sub>), 70.33 (CHOH), 103.63 (Ar), 107.66 (Ar), 112.03 (Ar), 134.41 (Ar), 163.05 (CH=N), 166.71 (Ar). EI/MS (70 ev) *m/z* (%): 330 ([M]<sup>+</sup>, 0.7), 165 ([M/2]<sup>+</sup>, 8), 211 ([C<sub>10</sub>H<sub>15</sub>O<sub>3</sub>N<sub>2</sub>]<sup>+</sup>, 9). IR (KBr pellet):  $\bar{\nu}$  = 3552 (w), 3478 (w), 3414 (s), 3058 (w), 2925 (w), 2882 (w), 2468 (w), 1638 (s), 1617 (s), 1500 (m), 1438 (m), 1369 (w), 1286 (w), 1235 (s), 1191 (w), 1114 (s), 1003 (w), 977 (w), 883 (w), 839 (m), 783 (m), 751 (w), 740 (w), 678 (w), 620 (s), 465 (m), 413 (w) cm<sup>-1</sup>.

## 4.2.2 Synthesis of Novel Compounds

### 4.2.2.1 General Procedure for the Synthesis of Complexes 1-2

A solution of H<sub>4</sub>L (360 mg, 1 mmol) was dissolved in 30 mL of DMF and added a solution of NaOH (300 mg, 7.5 mmol) in 1 mL of water. The reaction mixture was stirred for 5 min and then 1 mmol of M(OAc)<sub>2</sub>·(H<sub>2</sub>O)<sub>m</sub> (m = 4; M = Ni and m = 1; M = Cu) was added. The reaction mixture was stirred for 2 h and the reaction mixture was filtered and kept for crystallization. After 2 days orange red needle shaped crystals were collected, washed with diethyl ether and dried in vacuum.

**4.2.2.1.1 [Na<sub>4</sub>(NiL)<sub>2</sub>·(H<sub>2</sub>O)<sub>9</sub>]<sub>n</sub> (1)**

Yield: = 330 mg, 67%. <sup>1</sup>H NMR (D<sub>2</sub>O, 300 MHz, 25 °C): δ 3.36 (s, 4H, CH<sub>2</sub>), 7.09 (s, 2H, CH=N), 7.1 (s, 2H, Ar), 6.82 (d, 2H, Ar) 6.74 (d, 2H, Ar). <sup>13</sup>C{<sup>1</sup>H} NMR (D<sub>2</sub>O, 300 MHz, 25°C): δ 58.4 (CH<sub>2</sub>), 115.8 (Ar), 119.4 (Ar), 122.4 (Ar), 133.2 (Ar), 141.1 (Ar), 161.7 (CH=N), 162.4 (Ar), 175.2 (COO). IR (KBr pellet):  $\bar{\nu}$  = 3240 (m), 2952 (w), 2924 (w), 1624 (s), 1571 (s), 1525 (s), 1481 (m), 1419 (m), 1390 (s), 1345 (m), 1284 (s), 1219 (s), 1139 (w), 1109 (w), 1091 (m), 1056 (m), 972 (m), 889 (w), 772 (s), 743 (w), 619 (w), 539 (w), 467 (w) cm<sup>-1</sup>. Anal. Calcd for C<sub>36</sub>H<sub>42</sub>N<sub>4</sub>Na<sub>4</sub>Ni<sub>2</sub>O<sub>21</sub>: C, 40.18; H, 3.93; N, 5.2. Found: C, 39.91; H, 3.87; N, 5.16.

**4.2.2.1.2 [Na<sub>4</sub>(CuL)<sub>2</sub>·(H<sub>2</sub>O)<sub>9</sub>]<sub>n</sub> (2)**

Yield: 38 mg, 76%. IR (KBr pellet):  $\bar{\nu}$  = 3264 (m), 2969 (w), 2947 (w), 1630 (s), 1517 (s), 1522 (s), 1478 (m), 1435 (w), 1390 (s), 1280 (m), 1195 (s), 1139 (w), 1108 (w), 1087 (w), 1046 (w), 972 (m), 895 (w), 827 (w), 797 (w), 773 (s), 633 (w), 590 (w), 521 (m) cm<sup>-1</sup>. Anal. Calcd for C<sub>36</sub>H<sub>42</sub>Cu<sub>2</sub>N<sub>4</sub>Na<sub>4</sub>O<sub>21</sub>: C, 39.82; H, 3.9; N, 5.16. Found: C, 39.30; H, 3.91; N, 4.88.

**4.2.2.2 Synthesis of [Li(NiHL)(DMSO)]<sub>n</sub> (3)**

A solution of H<sub>4</sub>L (112 mg, 0.314 mmol) was dissolved in 15 mL of DMSO and added a solution of LiOH·H<sub>2</sub>O (25 mg, 0.6 mmol) in 1 mL of water. The reaction mixture was stirring for 5 min and then Ni(OAc)<sub>2</sub>·(H<sub>2</sub>O)<sub>4</sub> (51 mg, 0.2 mmol) was added. The reaction mixture was stirred for 2 h and the reaction mixture was filtered and kept for crystallization. After 2 months orange red crystals were collected, washed with diethyl ether and dried in vacuum. Yield: 28 mg, 28%. IR (KBr Pellet):  $\bar{\nu}$  = 2986 (w), 2908 (m), 2851 (w), 1919 (br), 1686 (m), 1616 (s), 1528 (m), 1443 (w), 1420 (s), 1387 (s), 1297 (s), 1255 (m), 1221 (w), 1107 (w), 1030 (s), 970 (m), 887 (w), 814 (m), 764 (s), 615 (w), 553 (w), 463 (m) cm<sup>-1</sup>. Anal. Calcd for C<sub>20</sub>H<sub>19</sub>LiN<sub>2</sub>NiO<sub>7</sub>S: C, 48.32; H, 3.85; N, 5.63. Found: C, 48.12; H, 3.97; N, 5.41.

#### 4.2.2.3 Synthesis of $[\text{Na}_5\{(\text{NiL}^2)(\text{HCOO})(\text{H}_2\text{O})_{11}\} \cdot (\text{H}_2\text{O})_4]_n$ (4)

A solution of ligand  $\text{H}_4\text{L}^2$  (370 mg, 1 mmol) was dissolved in 20 mL DMF and added a solution of NaOH (162 mg, 4 mmol) in 1 mL water. The reaction mixture was stirred for 5 min and then  $\text{Ni}(\text{OAc})_2 \cdot (\text{H}_2\text{O})_4$  (250 mg, 1 mmol) was added. The reaction mixture was stirred for further 30 min at room temperature, filtered and kept for crystallization. After 2 days green block shaped crystal were collected, washed with diethyl ether and dried in vacuum. Yield: 142 mg, 28% (based on Ni). IR (KBr pellet):  $\bar{\nu} = 3468$  (m), 3415 (br), 3232 (w), 2941 (w), 2857 (w), 2296 (w), 1620 (s), 1572 (w), 1524 (s), 1402 (s), 1292 (s), 1197 (m), 1150 (w), 1120 (w), 1077 (w), 968 (m), 909 (w), 889 (w), 830 (w), 799 (w), 777 (s), 615 (m), 467 (w)  $\text{cm}^{-1}$ . Anal. Calcd for  $\text{C}_{39}\text{H}_{43}\text{N}_4\text{Na}_5\text{Ni}_2\text{O}_{21}$  (corresponds to loss of the eight lattices  $\text{H}_2\text{O}$ ): C, 41.23; H, 3.81; N, 4.93. Found: C, 41.19; H, 3.52; N, 4.83.

#### 4.2.2.4 Synthesis of $[\text{Na}_4(\text{CuHL}^3)_2(\text{MeOH})_2(\text{H}_2\text{O}) \cdot (\text{Et}_2\text{O})]_n$ (5)

A solution of  $\text{H}_5\text{L}^3$  (39 mg, 0.1 mmol) dissolved in 20 mL MeOH and added a solution of NaOH (16 mg, 0.4 mmol) in 1 mL water. The reaction mixture was stirred for 5 min and then  $\text{Cu}(\text{OAc})_2 \cdot \text{H}_2\text{O}$  (20 mg, 0.1 mmol) was added. The reaction mixture was stirred for further 30 min at room temperature and filtered. Diethyl ether was allowed to diffuse into the filtrate at ambient temperature. After 2 days green needle shaped crystal were collected, washed with diethyl ether and dried in vacuum. Yield: 23 mg, 22% (based on Cu). IR (KBr pellet):  $\bar{\nu} = 3415$  (s), 2920 (m), 2852 (w), 2346 (w), 1617 (s), 1574 (m), 1526 (s), 1483 (w), 1427 (w), 1386 (s), 1295 (m), 1214 (m), 1140 (w), 1126 (w), 1060 (m), 1003 (w), 969 (m), 894 (w), 807 (m), 777 (s), 743 (w), 682 (w), 613 (m), 504 (w)  $\text{cm}^{-1}$ . Anal. Calcd for  $\text{C}_{40}\text{H}_{38}\text{Cu}_2\text{N}_4\text{Na}_4\text{O}_{17}$  (corresponds to loss of one diethyl ether molecule): C, 45.08; H, 3.59; N, 5.26. Found: C, 43.91; H, 3.77; N, 5.24.

#### 4.2.2.5 General Procedure for the Synthesis of Complexes 6-9

$[\text{Na}_4(\text{LNi})_2 \cdot (\text{H}_2\text{O})_9]_n$  (1) (45 mg, 0.04 mmol) was dissolved in a few drops of water and 5 mL of DMF. Then  $\text{Ln}(\text{NO}_3)_3 \cdot (\text{H}_2\text{O})_m$  (0.16 mmol) was added and the reaction mixture was stirred



at room temperature for 30 min. After 3 months, reddish orange crystals were collected by filtration, washed with cold methanol, diethyl ether and dried in vacuum.

#### 4.2.2.5.1 [ $\{\text{Er}_2(\text{NiL})_3(\text{DMF})(\text{H}_2\text{O})_3\} \cdot (\text{DMF})_4 \cdot (\text{H}_2\text{O})_{10}\}_n$ (6)]

Yield: 22 mg, 49% (based on Ni-salen). IR (KBr pellet):  $\bar{\nu}$  = 3380 (m), 2964 (w), 2936 (w), 1664 (m), 1623 (s), 1589 (m), 1418 (w), 1390 (s), 1295 (w), 1217 (w), 1200 (w), 1137 (w), 1115 (w), 979 (m), 836 (w), 812 (w), 774 (s), 685 (w), 540 (w), 467 (w)  $\text{cm}^{-1}$ . Anal. Calcd for  $\text{C}_{69}\text{H}_{97}\text{Er}_2\text{N}_{11}\text{Ni}_3\text{O}_{36}$ : C, 38.24; H, 4.51; N, 7.11. Found: C, 38.68; H, 3.99; N, 6.92.

#### 4.2.2.5.4 [ $\{\text{Tm}_2(\text{NiL})_3(\text{DMF})(\text{H}_2\text{O})_3\} \cdot (\text{DMF})_4 \cdot (\text{H}_2\text{O})_{10}\}_n$ (7)]

Yield: 3 mg, 13% (based on Ni-salen). IR (KBr pellet):  $\bar{\nu}$  = 3422 (m), 2924 (w), 2857 (w), 1622 (s), 1505 (w), 1385 (s), 1287 (w), 1214 (w), 1194 (w), 1110 (w), 1091 (w), 979 (w), 892 (w), 848 (w), 814 (w), 774 (s), 684 (w), 618 (w), 537 (w), 470 (w)  $\text{cm}^{-1}$ . Anal. Calcd for  $\text{C}_{69}\text{H}_{97}\text{N}_{11}\text{Ni}_3\text{O}_{36}\text{Tm}_2$ : C, 38.18; H, 4.50; N, 7.10. Found: C, 37.82; H, 3.20; N, 7.16.

#### 4.2.2.5.3 [ $\{\text{Yb}_2(\text{NiL})_3(\text{DMF})(\text{H}_2\text{O})_3\} \cdot (\text{DMF})_4 \cdot (\text{H}_2\text{O})_{10}\}_n$ (8)]

Yield: 15 mg, 25% (based on Ni-salen). IR (KBr pellet):  $\bar{\nu}$  = 3435 (m), 2967 (w), 2872 (w), 2361 (m), 1655 (s), 1618 (s), 1519 (s), 1479 (m), 1420 (w), 1292 (s), 1199 (w), 1091 (w), 976 (m), 895 (w), 846 (w), 776 (s), 742 (w), 742 (w), 681 (w), 538 (w), 467 (w), 413 (w)  $\text{cm}^{-1}$ . Anal. Calcd for  $\text{C}_{69}\text{H}_{81}\text{N}_{11}\text{Ni}_3\text{O}_{28}\text{Yb}_2$  (corresponds to loss of the eight lattices  $\text{H}_2\text{O}$ ): C, 40.73; H, 4.01; N, 7.57. Found: C, 40.61; H, 3.82; N, 7.09.

#### 4.2.2.5.2 [ $\{\text{Lu}_2(\text{NiL})_3(\text{DMF})(\text{H}_2\text{O})_3\} \cdot (\text{DMF})_4 \cdot (\text{H}_2\text{O})_{10}\}_n$ (9)]

Yield: 25 mg, 55% (based on Ni-salen). IR (KBr pellet):  $\bar{\nu}$  = 3402 (m), 2963 (w), 2919 (w), 1653 (m), 1620 (s), 1580 (m), 1519 (m), 1482 (m), 1424 (s), 1387 (w), 1344 (w), 1296 (s), 1218 (w), 1202 (w), 1115 (w), 1091 (w), 1058 (w), 977 (s), 899 (w), 848 (w), 812 (w), 779 (s), 684 (w), 620 (w), 540 (w), 470 (w)  $\text{cm}^{-1}$ . Anal. Calcd for  $\text{C}_{69}\text{H}_{97}\text{Lu}_2\text{N}_{11}\text{Ni}_3\text{O}_{36}$ : C, 37.97; H, 4.48; N, 7.06. Found: C, 38.89; H, 4.08; N, 6.88.

#### 4.2.2.6 Synthesis of $[\text{Dy}\{\text{NiL}(\text{DMSO})(\text{NO}_3)\}(\text{H}_2\text{O})_2 \cdot (\text{DMSO})]_n$ (10)

$\text{H}_4\text{L}$  (109 mg, 0.3 mmol) was dissolved in DMSO / THF (25/5 mL). The resulting solution was added to a solution of NaOH (25 mg, 0.6 mmol) in 1 mL of water. The reaction mixture was stirred for 5 min and then  $\text{Ni}(\text{OAc})_2 \cdot (\text{H}_2\text{O})_4$  (52 mg, 0.2 mmol) and  $\text{Dy}(\text{NO}_3)_3 \cdot (\text{H}_2\text{O})_5$  (178 mg, 0.4 mmol) were added. The reaction mixture was then heated under reflux for 2 h, and then cooled to room temperature. Then, the mixture was filtered and kept for crystallization at room temperature. After one month, red needle shaped crystals were collected, washed with diethyl ether and dried in vacuum. Yield: 54 mg, 21% (based on  $\text{H}_4\text{L}$ ). IR (KBr pellet):  $\bar{\nu} = 3423$  (m), 2997 (w), 2919 (w), 1619 (s), 1561 (m), 1518 (s), 1483 (w), 1422 (s), 1410 (w), 1343 (w), 1294 (m), 1217 (w), 1200 (w), 1138 (w), 1092 (w), 1017 (m), 977 (m), 892 (w), 844 (w), 814 (w), 775 (s), 742 (w), 685 (w), 654 (w), 540 (w), 467 (w)  $\text{cm}^{-1}$ . Anal. Calcd for  $\text{C}_{22}\text{H}_{28}\text{DyN}_3\text{NiO}_{13}\text{S}_2$ : C, 31.92; H, 3.41; N, 5.08. Found: C, 32.48; H, 3.83; N, 4.69.

#### 4.2.2.7 Synthesis of $[\text{Na}_3\text{Yb}\{\text{NiL}(\text{H}_2\text{O})\}_3 \cdot (\text{DMF})]_n$ (11)

A solution of ligand  $\text{H}_4\text{L}$  (109 mg, 0.3 mmol) was dissolved in 30 mL DMF and added a solution of NaOH (25 mg, 0.6 mmol) in 1 mL water. The reaction mixture was stirred for 5 min and then  $\text{Ni}(\text{OAc})_2 \cdot (\text{H}_2\text{O})_4$  (52 mg, 0.2 mmol) and  $\text{Yb}(\text{NO}_3)_3 \cdot (\text{H}_2\text{O})_6$  (180 mg, 0.37 mmol) were added. The reaction mixture was heated under reflux for 3 h. Then the mixture was filtered and kept for crystallization at room temperature. After 20 days, red needle shaped crystals were collected, washed with diethyl ether and dried in vacuum. Yield: 25 mg, 4% (based on Yb). IR (KBr pellet):  $\bar{\nu} = 3411$  (m), 3249 (w), 2957 (w), 2935 (w), 1620 (s), 1576 (m), 1523 (s), 1481 (s), 1421 (w), 1387 (s), 1285 (s), 1241 (w), 1218 (m), 1137 (w), 1087 (s), 1060 (w), 973 (s), 899 (w), 837 (w), 804 (m), 772 (s), 774 (w), 689 (w), 655 (w), 612 (w), 541 (w), 466 (w)  $\text{cm}^{-1}$ . Anal. Calcd for  $\text{C}_{57}\text{H}_{49}\text{N}_7\text{Na}_3\text{Ni}_3\text{O}_{22}\text{Yb}$ : C, 42.73; H, 3.08; N, 6.12. Found: C, 43.48; H, 3.24; N, 5.81.

#### 4.2.2.8 General procedure for the synthesis of complexes 12-16

H<sub>4</sub>L (39 mg, 0.11 mmol), MnCl<sub>2</sub>·(H<sub>2</sub>O)<sub>4</sub> (27 mg, 0.1 mmol), Ln (NO<sub>3</sub>)<sub>3</sub>·(H<sub>2</sub>O)<sub>m</sub> (0.20 mmol) and pyridine (0.1 ml) were combined in 3 mL of DMF with stirring. The resulting solution was then stirred for further 3h at room temperature and then sealed in a 10 mL glass vial. The glass vial was heated at 90°C for 44 h in oven and cooled to room temperature. The red block shaped crystals were collected and washed three times with DMF followed by diethyl ether and dried in air.

##### 4.2.2.8.1 [Nd<sub>2</sub>(MnLCl)<sub>2</sub>(NO<sub>3</sub>)<sub>2</sub>(DMF)<sub>5</sub>·(DMF)<sub>4</sub>]<sub>n</sub> (12)

Yield: 52 mg, 25% (based on Mn). IR [cm<sup>-1</sup>]:  $\bar{\nu}$  = 2919 (w), 2848 (m), 1644 (s), 1593 (s), 1528 (m) (v<sub>1</sub>), 1437 (m), 1384 (w), 1385 (m), 1332 (m), 1301 (m), 1277 (m) (v<sub>2</sub>), 1253 (m), 1140 (w), 1106 (m), 1088 (m), 1033 (m) (v<sub>3</sub>), 975 (w), 903 (w), 828 (m) (v<sub>4</sub>), 796 (m), 738 (s), 672 (m), 638 (w), 611 (m), 504 (m). Anal. Calcd for C<sub>63</sub>H<sub>87</sub>Cl<sub>2</sub>Mn<sub>2</sub>N<sub>15</sub>Nd<sub>2</sub>O<sub>27</sub>: C, 38.69; H, 4.48; N, 10.74. Found: C, 37.67; H, 4.37; N, 10.39.

##### 4.2.2.8.2 [Eu<sub>2</sub>(MnLCl)<sub>2</sub>(NO<sub>3</sub>)<sub>2</sub>(DMF)<sub>5</sub>·(DMF)<sub>4</sub>]<sub>n</sub> (13)

Yield: 52 mg, 21% (based on Mn). IR [cm<sup>-1</sup>]:  $\bar{\nu}$  = 2931 (w), 2878 (w), 1645 (s), 1614 (s), 1598 (s), 1528 (m) (v<sub>1</sub>), 1476 (m), 1386 (m), 1304 (w), 1278 (m) (v<sub>1</sub>), 1196 (m), 1138 (m), 1106 (m), 1091 (s), 1036 (m) (v<sub>3</sub>), 976 (s), 902 (m), 897 (w), 829 (m) (v<sub>4</sub>), 810 (m), 797 (w), 776 (s), 739 (m), 673 (w), 639 (s), 611 (m), 555 (w), 504 (w). Anal. Calcd for C<sub>48</sub>H<sub>52</sub>Cl<sub>2</sub>Eu<sub>2</sub>Mn<sub>2</sub>N<sub>10</sub>O<sub>22</sub> (corresponds to loss of the five DMF molecules): C, 35.91; H, 3.26; N, 8.72. Found: 35.23; H, 3.78; N, 8.56.

**4.2.2.8.3 [Gd<sub>2</sub>(MnLCl)<sub>2</sub>(NO<sub>3</sub>)<sub>2</sub>(DMF)<sub>5</sub>·(DMF)<sub>4</sub>]<sub>n</sub> (14)**

Yield: 56 mg, 27% (based on Mn). IR [cm<sup>-1</sup>]:  $\bar{\nu}$  = 2940 (w), 2871 (w), 1644 (s), 1615 (s), 1599 (s), 1529 (m), 1464 (m), 1402 (m), 1385 (m), 1338 (m), 1305 (m), 1278 (m) (v<sub>1</sub>), 1251 (m), 1196 (w), 1138 (m), 1107 (w), 1090 (m), 1037 (m) (v<sub>3</sub>), 976 (m), 902 (s), 865 (m), 829 (m), 816 (m) (v<sub>4</sub>), 798 (m), 777 (m), 740 (s), 675 (s), 638 (s), 614 (m), 588 (w), 504 (w). Anal. Calcd for C<sub>51</sub>H<sub>59</sub>Cl<sub>2</sub>Gd<sub>2</sub>Mn<sub>2</sub>N<sub>11</sub>O<sub>23</sub> (corresponds to loss of the four DMF molecules): C, 36.26; H, 3.52; N, 9.12. Found: 36.05; H, 4.12; N, 9.25.

**4.2.2.8.4 [Tb<sub>2</sub>(MnLCl)<sub>2</sub>(NO<sub>3</sub>)<sub>2</sub>(DMF)<sub>5</sub>·(DMF)<sub>4</sub>]<sub>n</sub> (15)**

Yield: 53 mg, 25% (based on Mn). IR [cm<sup>-1</sup>]:  $\bar{\nu}$  = 2939 (w), 2892 (w), 1645 (s), 1617 (s), 1601 (s), 1529 (m) (v<sub>1</sub>), 1472 (m), 1386 (m), 1337 (m), 1308 (s), 1278 (m) (v<sub>2</sub>), 1197 (m), 1106 (s), 1062 (s), 1038 (s) (v<sub>3</sub>), 977 (m), 903 (m), 830 (s), 815 (m) (v<sub>4</sub>), 798 (m), 776 (s), 740 (s), 672 (s), 638 (m), 614 (m), 595 (m), 540 (m), 503 (w). Anal. Calcd for C<sub>54</sub>H<sub>66</sub>Cl<sub>2</sub>Mn<sub>2</sub>N<sub>12</sub>O<sub>24</sub>Tb<sub>2</sub> (corresponds to loss of the three DMF molecules): C, 36.73; H, 3.77; N, 9.52. Found: 36.38; H, 4.15; N, 9.59.

**4.2.2.8.5 [Dy<sub>2</sub>(MnLCl)<sub>2</sub>(NO<sub>3</sub>)<sub>2</sub>(DMF)<sub>5</sub>·(DMF)<sub>4</sub>]<sub>n</sub> (16)**

**16:** Yield: 47 mg, 22% (based on Mn). IR [cm<sup>-1</sup>]:  $\bar{\nu}$  = 2938 (w), 2894 (w), 1646 (s), 1617 (s), 1602 (s), 1529 (s) (v<sub>1</sub>), 1470 (m), 1404 (s), 1385 (s), 1337 (s), 1308 (m), 1278 (m) (v<sub>2</sub>), 1253 (m), 1196 (s), 1107 (s), 1091 (s), 1039 (m) (v<sub>3</sub>), 977 (m), 913 (s), 897 (s), 828 (s) (v<sub>4</sub>), 816 (m), 799 (s), 778 (m), 740 (m), 675 (s), 638 (m), 615 (m), 559 (w), 504 (w). Anal. Calcd for C<sub>63</sub>H<sub>87</sub>Cl<sub>2</sub>Dy<sub>2</sub>Mn<sub>2</sub>N<sub>15</sub>O<sub>27</sub>: C, 37.98; H, 4.40; N, 10.55. Found: 37.06; H, 4.25; N, 10.09.

#### 4.2.2.9 General Procedure for the Synthesis of Complexes 17-21

H<sub>4</sub>L (39 mg, 0.11 mmol), FeCl<sub>3</sub>·(H<sub>2</sub>O)<sub>6</sub> (27 mg, 0.1 mmol), Ln(NO<sub>3</sub>)<sub>3</sub>·(H<sub>2</sub>O)<sub>m</sub> (0.20 mmol) and pyridine (0.1 ml) were combined in 3 mL of DMF with stirring. The resulting solution was then stirred for further 3h at room temperature and then sealed in a 10 mL glass vial. The glass vial was heated at 90°C for 44 h in oven and cooled to room temperature. The red block shaped crystals were collected and washed three times with DMF followed by diethyl ether and dried in air.

##### 4.2.2.9.1 [Y<sub>2</sub>(FeLCl)<sub>2</sub>(NO<sub>3</sub>)<sub>2</sub>(DMF)<sub>5</sub>·(DMF)<sub>4</sub>]<sub>n</sub> (17)

Yield: 45 mg, 23% (based on Fe). IR [cm<sup>-1</sup>]:  $\bar{\nu}$  = 2929 (w), 2855 (w), 1614 (s), 1531 (m), 1476 (m) (v<sub>1</sub>), 1403 (m), 1382 (m), 1307 (w), 1278 (m) (v<sub>2</sub>), 1196 (m), 1104 (m), 1046 (m) (v<sub>3</sub>), 976 (s), 903 (m), 814 (m) (v<sub>4</sub>), 801 (m), 776 (s), 741 (m), 678 (m), 631 (m), 534 (w), 496 (w), 413 (w). Anal. Calcd for C<sub>63</sub>H<sub>87</sub>Cl<sub>2</sub>Fe<sub>2</sub>N<sub>15</sub>O<sub>27</sub>Y<sub>2</sub>: C, 40.97; H, 4.75; N, 11.38. Found: 40.18; H, 4.61; N, 10.41.

##### 4.2.2.9.2 [Eu<sub>2</sub>(FeLCl)<sub>2</sub>(NO<sub>3</sub>)<sub>2</sub>(DMF)<sub>5</sub>·(DMF)<sub>4</sub>]<sub>n</sub> (18)

Yield: 53 mg, 27% (based on Fe). IR [cm<sup>-1</sup>]:  $\bar{\nu}$  = 2931 (w), 2862 (w), 1634 (m), 1613 (s), 1597 (m), 1532 (m), 1462 (m), 1435 (m) (v<sub>1</sub>), 1401 (w), 1384 (w), 1331 (m), 1305 (m), 1281 (m), 1253 (m) (v<sub>2</sub>), 1194 (w), 1107 (m), 1093 (m), 1061 (s), 1036 (m) (v<sub>3</sub>), 978 (m), 899 (w), 816 (m) (v<sub>1</sub>), 806 (w), 778 (m), 740 (s), 676 (m), 627 (w), 612 (m), 553 (w). Anal. Calcd for C<sub>63</sub>H<sub>87</sub>Cl<sub>2</sub>Eu<sub>2</sub>Fe<sub>2</sub>N<sub>15</sub>O<sub>27</sub>: C, 38.35; H, 4.44 N, 10.65. Found: C, 37.83; H, 4.40; N, 10.27.

##### 4.2.2.9.3 [Gd<sub>2</sub>(FeLCl)<sub>2</sub>(NO<sub>3</sub>)<sub>2</sub>(DMF)<sub>5</sub>·(DMF)<sub>4</sub>]<sub>n</sub> (19)

Yield: 58 mg, 28% (based on Fe). IR [cm<sup>-1</sup>]:  $\bar{\nu}$  = 2933 (w), 2914 (w), 1674 (m), 1647 (s), 1600 (s), 1531 (m), 1477 (m) (v<sub>1</sub>), 1401 (m), 1331 (m), 1301 (w), 1281 (s) (v<sub>2</sub>), 1253 (m), 1197 (m), 1107 (m), 1033 (m) (v<sub>3</sub>), 976 (s), 903 (w), 839 (m) (v<sub>4</sub>), 811 (m), 800 (w), 776 (s),

740 (s), 675 (s), 629 (m), 526 (w). Anal. Calcd for  $C_{48}H_{52}Cl_2Fe_2Gd_2N_{10}O_{22}$  (corresponds to loss of the five DMF molecules): C, 35.63; H, 3.24; N, 8.66. Found: 35.10; H, 3.34; N, 8.32.

#### 4.2.2.9.4 $[Tb_2(FeLCl)_2(NO_3)_2(DMF)_5 \cdot (DMF)_4]_n$ (20)

Yield: 56 mg, 28% (based on Fe). IR [ $cm^{-1}$ ]:  $\bar{\nu}$  = 2933 (w), 2914 (w), 1671 (m), 1644 (s), 1600 (s), 1532 (m), 1464 (m) ( $\nu_1$ ), 1402 (s), 1384 (m), 1307 (m), 1282 (w), 1253 (m) ( $\nu_2$ ), 1194 (m), 1107 (m), 1093 (s), 1039 (s) ( $\nu_3$ ), 978 (m), 913 (w), 838 (m) ( $\nu_1$ ), 815 (m), 798 (s), 778 (m), 741 (s), 676 (s), 660 (w), 627 (s), 554 (w). Anal. Calcd for  $C_{63}H_{87}Cl_2Fe_2N_{15}O_{27}Tb_2$ : C, 38.08; H, 4.41; N, 10.57. Found: C, 37.63; H, 4.36; N, 10.01.

#### 4.2.2.9.5 $[Dy_2(FeLCl)_2(NO_3)_2(DMF)_5 \cdot (DMF)_4]_n$ (21)

Yield: 62 mg, 31% (based on Fe). IR [ $cm^{-1}$ ]:  $\bar{\nu}$  = 2925 (w), 2860 (w), 1616 (s), 1532 (w), 1475 (m) ( $\nu_1$ ), 1404 (s), 1281 (s), 1253 (m) ( $\nu_2$ ), 1198 (m), 1104 (m), 1038 (m) ( $\nu_3$ ), 978 (s), 906 (w), 802 (m) ( $\nu_1$ ), 776 (s), 740 (s), 676 (s), 629 (s), 555 (w). Anal. Calcd for  $C_{45}H_{45}Cl_2Dy_2Fe_2N_9O_{21}$  (corresponds to loss of the six DMF molecules): C, 34.75; H, 2.92; N, 8.10. Found: C, 34.63; H, 3.42; N, 8.20.

#### 4.2.2.10 Synthesis of $[Mn_3\{(H_2L^4)(HL^4)(OMe)_2(MeOH)_2\} \cdot (MeOH)_4]$ (22)

The ligand  $H_3L^4$  (34 mg, 0.1 mmol) and potassium tertiary butoxide (37 mg, 0.3 mmol) were dissolved in 15 mL methanol. To this solution  $Mn(OAc)_2 \cdot (H_2O)_4$  (51 mg, 0.2 mmol) was added. The reaction mixture was stirred for further 10 min, filtered and kept for crystallization at room temperature. After 2 days, needle shaped black crystals were collected, washed with diethyl ether and dried in vacuum. Yield: 26 mg, 38%. IR (KBr pellet):  $\bar{\nu}$  = 3436 (m), 2918 (w), 2845 (w), 2360 (w), 1583 (s), 1544 (w), 1482 (m), 1355 (w), 1301 (w), 1232 (s), 1180 (w), 1127 (s), 1009 (w), 845 (w), 802 (w), 760 (w), 720 (w), 643 (w), 603 (m), 504 (m), 451 (w)  $cm^{-1}$ . Anal. Calcd for  $C_{39}H_{53}Mn_3N_4O_{18}$  (corresponds to replacement of three lattices

MeOH by three H<sub>2</sub>O molecules): C, 45.45; H, 5.18; N, 5.44. Found: C, 45.70; H, 4.45; N, 5.77.

#### 4.2.2.11 Synthesis of [Ni<sub>3</sub>(H<sub>3</sub>L<sup>4</sup>)<sub>2</sub>(OAc)<sub>2</sub>(DMF)<sub>2</sub>·(H<sub>2</sub>O)<sub>3</sub>] (23)

The ligand H<sub>3</sub>L<sup>4</sup> (34 mg, 0.1 mmol) and LiOH·H<sub>2</sub>O (15 mg, 0.35 mmol) were dissolved in 20 mL methanol. The reaction mixture was stirred for 5 min and then Ni(OAc)<sub>2</sub>·(H<sub>2</sub>O)<sub>4</sub> (51 mg, 0.2 mmol) was added. The reaction mixture was stirred for another 10 min, filtered and kept for crystallization at room temperature. Within one week needle shaped black crystals were collected, washed with diethyl ether and dried in vacuum. Yield: 63 mg, 80%. IR (KBr pellet):  $\bar{\nu}$  = 3309 (m), 2935 (w), 2988 (w), 2353 (w), 1646 (s), 1607 (s), 1570 (w), 1489 (s), 1454 (m), 1403 (w), 1349 (w), 1277 (s), 1220 (m), 1191 (w), 1132 (w), 1057 (s), 1023 (w), 991 (s), 907(w), 851 (s), 805 (w), 759 (s), 717 (m), 673 (m), 660 (m), 636 (m), 571 (m), 476 (w), 412 (w) cm<sup>-1</sup>. Anal. Calcd for C<sub>44</sub>H<sub>58</sub>N<sub>6</sub>Ni<sub>3</sub>O<sub>19</sub>: C, 45.91; H, 5.08; N, 7.30. Found: C, 45.56; H, 5.27; N, 6.98.

#### 4.2.2.12 General Procedure for the Synthesis of Complexes 24-29

To a stirred solution of 3-formylsalicylic acid (68 mg, 0.67 mmol) in EtOH / H<sub>2</sub>O (15 mL / 5 mL) tris-(2-aminoethyl)amine (0.03 mL, 0.2 mmol) was added, followed by the addition of Ln(NO<sub>3</sub>)<sub>3</sub>·(H<sub>2</sub>O)<sub>m</sub> (m = 5 (Eu and Dy) and m = 6 (Tb, Er, Tm, and Ho)) (0.23 mmol). The resulting solution was then stirred for further 12 h at room temperature, filtered and kept for crystallization. After 2 days, yellow color block shaped crystals were collected, washed with diethyl ether and dried in vacuum.

##### 4.2.2.12.1 [Eu(H<sub>2</sub>L<sup>5</sup>)<sub>2</sub>·(EtOH)·(H<sub>2</sub>O)<sub>8</sub>·(NO<sub>3</sub>)] (24)

Yield: 47 mg, 35% (based on Eu). IR [cm<sup>-1</sup>]:  $\bar{\nu}$  = 3238 (br), 2925 (w), 2824 (w), 1647 (s), 1602 (s), 1537 (s), 1452 (m), 1374 (s), 1310 (m), 1225 (m), 1149 (m), 1020 (m), 953 (w), 870 (w), 761 (w), 643 (w), 608 (w), 489 (w), 431 (w). Anal. Calcd for C<sub>46</sub>H<sub>72</sub>EuN<sub>9</sub>O<sub>24</sub>: C, 42.93; H, 5.64 N, 9.79. Found: C, 41.28; H, 5.77; N, 10.72. ESI-MS (MeOH): For positive ion

mode- 1035.307 ( $[\text{Eu}(\text{C}_{22}\text{H}_{25}\text{N}_4\text{O}_6)_2]^+$ ). For an anionic ion mode- 1033.263 ( $[\text{Eu}(\text{C}_{22}\text{H}_{24}\text{N}_4\text{O}_6)_2]^-$ ).

#### 4.2.2.12.3 $[\text{Tb}(\text{H}_2\text{L}^5)_2 \cdot (\text{EtOH}) \cdot (\text{H}_2\text{O})_8 \cdot (\text{NO}_3)]$ (25)

Yield: 55 mg (42% based on Tb). IR [ $\text{cm}^{-1}$ ]:  $\bar{\nu}$  = 3466 (br), 2926 (w), 2815 (w), 1646 (s), 1603 (s), 1537 (s), 1478 (m), 1452 (m), 1387 (s), 1311 (m), 1247 (m), 1225 (m), 1149 (m), 1107 (m), 1067 (w), 1032 (m), 954 (w), 871 (w), 761 (w), 644 (w), 611 (w), 564 (w). Anal. Calcd for  $\text{C}_{44}\text{H}_{54}\text{N}_9\text{O}_{17}\text{Tb}$  (corresponds to loss of the six lattices  $\text{H}_2\text{O}$  and one ethanol): C, 46.36; H, 4.77; N, 11.06. Found: C, 46.15; H, 5.06; N, 10.68. ESI-MS (MeOH): For positive ion mode- 1041.311 ( $[\text{Tb}(\text{C}_{22}\text{H}_{25}\text{N}_4\text{O}_6)_2]^+$ ). For an anionic ion mode- 1039.281 ( $[\text{Tb}(\text{C}_{22}\text{H}_{24}\text{N}_4\text{O}_6)_2]^-$ ).

#### 4.2.2.12.2 $[\text{Dy}(\text{H}_2\text{L}^5)_2 \cdot (\text{EtOH}) \cdot (\text{H}_2\text{O})_8 \cdot (\text{NO}_3)]$ (26)

Yield: 53 mg, 38% (based on Dy). IR (KBr pellet):  $\bar{\nu}$  = 3420 (br), 3049 (br), 2951 (w), 2825 (w), 1650 (s), 1609 (s), 1538 (s), 1452 (m), 1381 (s), 1221 (m), 1187 (m), 1145 (m), 1031 (m), 867 (m), 762 (m), 641 (m), 628 (w), 445 (w).  $\text{cm}^{-1}$ . Anal. Calcd for  $\text{C}_{44}\text{H}_{58}\text{DyN}_9\text{O}_{19}$  (corresponds to additionally four lattices  $\text{H}_2\text{O}$  molecules): C, 44.80; H, 4.96; N, 10.69. Found: C, 44.99; H, 5.02; N, 10.61. ESI-MS (MeOH): For positive ion mode- 1046.289 ( $[\text{Dy}(\text{C}_{22}\text{H}_{25}\text{N}_4\text{O}_6)_2]^+$ ). For an anionic ion mode- 1044.287 ( $[\text{Dy}(\text{C}_{22}\text{H}_{24}\text{N}_4\text{O}_6)_2]^-$ ), 2087.531 ( $\{[\text{Dy}(\text{C}_{22}\text{H}_{24}\text{N}_4\text{O}_6)_2\text{H}]\}^-$ ).

#### 4.2.2.12.4 $[\text{Er}(\text{H}_2\text{L}^5)_2 \cdot (\text{EtOH}) \cdot (\text{H}_2\text{O})_8 \cdot (\text{NO}_3)]$ (27)

Yield: 45 mg, 35% (based on Er). IR (KBr pellet):  $\bar{\nu}$  = 3446 (br), 2964 (w), 2828 (w), 1652 (s), 1607 (s), 1544 (s), 1482 (w), 1455 (m), 1385 (s), 1315 (m), 1229 (m), 1201(w), 1152 (m), 1069 (w), 1020 (w), 956 (w), 873 (m), 764 (m), 647 (m), 619 (w), 439 (s). Anal. Calcd for  $\text{C}_{46}\text{H}_{66}\text{ErN}_9\text{O}_{21}$  (corresponds to loss of the three lattices  $\text{H}_2\text{O}$  molecules): C, 44.26; H, 5.33 N, 10.10. Found: C, 43.93; H, 4.84; N, 10.48. ESI-MS (MeOH): For positive ion mode- 1048.272 ( $[\text{Er}(\text{C}_{22}\text{H}_{25}\text{N}_4\text{O}_6)_2]^+$ ). For an anionic ion mode- 1046.261 ( $[\text{Er}(\text{C}_{22}\text{H}_{24}\text{N}_4\text{O}_6)_2]^-$ ).



**4.2.2.12.5 [Tm(H<sub>2</sub>L<sup>5</sup>)<sub>2</sub>·(EtOH)·(H<sub>2</sub>O)<sub>8</sub>·(NO<sub>3</sub>)] (28)**

Yield: 48 mg, 35% (based on Tm). IR [cm<sup>-1</sup>]:  $\bar{\nu}$  = 3470 (br), 2938 (w), 2812 (w), 1646 (s), 1604 (s), 1539 (s), 1480 (m), 1452 (s), 1391 (s), 1247 (m), 1200 (m), 1150 (m), 1107 (m), 1068 (m), 1033 (m), 954 (m), 898 (w), 873 (w), 762 (w), 645 (w), 616 (w), 520 (w), 485 (w), 432 (w). Anal. Calcd for C<sub>46</sub>H<sub>72</sub>N<sub>9</sub>O<sub>24</sub>Tm: C, 42.37; H, 5.57; N, 9.67. Found: C, 41.73; H, 5.40; N, 9.93. ESI-MS (MeOH): For positive ion mode- 1051.321 ([Tm(C<sub>22</sub>H<sub>25</sub>N<sub>4</sub>O<sub>6</sub>)<sub>2</sub>]<sup>+</sup>). For an anionic ion mode- 1049.301 ([Tm(C<sub>22</sub>H<sub>24</sub>N<sub>4</sub>O<sub>6</sub>)<sub>2</sub>]<sup>-</sup>).

**4.2.2.13 General Procedure for the Synthesis of Complexes 29-33**

3-formylsalicylic acid (67 mg, 0.4 mmol) and tris (2-aminoethyl)amine (0.03 mL, 0.2 mmol) were dissolved in ethanol / water (15 mL / 5 mL) mixture. Then triethylamine (0.14 mL, 1 mmol) was added dropwise with stirring. To the resulting solution Mn(ClO<sub>4</sub>)<sub>2</sub>·(H<sub>2</sub>O)<sub>6</sub> (75 mg, 0.2 mmol) and Ln(NO<sub>3</sub>)<sub>3</sub>·(H<sub>2</sub>O)<sub>m</sub> (m = 5 (Nd, Eu, Gd and Dy) and m = 6 (Tm and Lu)) (0.1 mmol) were added and the subsequent mixture was stirred for another 12 h. The solution was then filtered and kept for crystallization. Within one week needle shaped yellow crystals were collected, washed with diethyl ether and dried in vacuum.

**4.2.2.13.1 [HNEt<sub>3</sub>]<sub>2</sub>[Eu(MnL<sup>5</sup>)<sub>2</sub>·(H<sub>2</sub>O)<sub>2</sub>·(ClO<sub>4</sub>)] (29)**

Yield: 57 mg, 35%. (based on Eu). IR (KBr pellet):  $\bar{\nu}$  = 3447 (br), 2907 (w), 2858 (w), 1634 (s), 1594 (s), 1554 (s), 1440 (s), 1414 (s), 1373 (w), 1332 (m), 1297 (s), 1231 (m), 1193 (m), 1159 (m), 1094 (s), 1026 (m), 997 (m), 986 (m), 962 (m), 877 (m), 832 (m), 801 (m), 764 (s), 667 (m), 624 (m), 600 (w), 483 (w), 457 (w) cm<sup>-1</sup>. Anal. Calcd for C<sub>56</sub>H<sub>80</sub>ClEuMn<sub>2</sub>N<sub>10</sub>O<sub>18</sub>: C, 45.49; H, 5.45; N, 9.47. Found: C, 45.41; H, 5.34; N, 9.44.

**4.2.2.13.2 [HNEt<sub>3</sub>]<sub>2</sub>[Gd(MnL<sup>5</sup>)<sub>2</sub>·(H<sub>2</sub>O)<sub>2</sub>·(ClO<sub>4</sub>)] (30)**

Yield: 45 mg, 29%. (based on Gd). IR (KBr pellet):  $\bar{\nu}$  = 3415 (br), 3293 (w), 3246 (w), 2923 (m), 2864 (w), 2360 (m) 1635(s), 1558 (s), 1440 (s), 1406 (m), 1295 (s), 1233 (w), 1094 (s), 1028 (m), 986 (w), 961 (w), 876 (m), 833 (w), 803 (w), 765 (w), 666 (w), 624 (w), 480 (w) cm<sup>-1</sup>. Anal. Calcd for C<sub>56</sub>H<sub>80</sub>ClGdMn<sub>2</sub>N<sub>10</sub>O<sub>18</sub>: C, 45.33; H, 5.43; N, 9.44. Found: C, 44.87; H, 5.43; N, 9.39.

**4.2.2.13.3 [HNEt<sub>3</sub>]<sub>2</sub>[Dy(MnL<sup>5</sup>)<sub>2</sub>·(H<sub>2</sub>O)<sub>2</sub>·(ClO<sub>4</sub>)] (31)**

**31:** Yield: 48 mg, 30% (based on Dy). IR (KBr pellet):  $\bar{\nu}$  = 3451 (w), 3480 (w), 3415 (br), 3283 (w), 3232 (w), 2906 (w), 2857 (w), 1637 (s), 1594 (m), 1553 (s), 1440 (m), 1416 (s), 1405 (w), 1332 (w), 1298 (m), 1227 (m), 1194 (w), 1159 (m), 1093 (s), 1026 (m), 962 (m), 878 (s), 832 (m), 802 (m), 764 (s), 666 (w), 623 (s), 476 (w) cm<sup>-1</sup>. Anal. Calcd for C<sub>56</sub>H<sub>80</sub>ClDyMn<sub>2</sub>N<sub>10</sub>O<sub>18</sub>: C, 45.17; H, 5.41; N, 9.41. Found: C, 44.71; H, 5.34; N, 9.26.

**4.2.2.13.5 [HNEt<sub>3</sub>]<sub>2</sub>[Tm(MnL<sup>5</sup>)<sub>2</sub>·(H<sub>2</sub>O)<sub>4</sub>·(ClO<sub>4</sub>)] (32)**

Yield: 62 mg, 41% (based on Tm). IR (KBr pellet):  $\bar{\nu}$  = 3448 (w), 2906 (w), 2857 (w), 1635 (s), 1596 (w), 1555 (s), 1453 (m), 1416 (w), 1405 (w), 1375 (w), 1300 (s), 1231 (m), 1195 (w), 1159 (m), 1094 (m), 1027 (m), 963 (m), 878 (s), 833 (w), 803 (m), 764 (m), 669 (w), 624 (s), 601 (w), 482 (w), 459 (w) cm<sup>-1</sup>. Anal. Calcd for C<sub>56</sub>H<sub>84</sub>ClMn<sub>2</sub>N<sub>10</sub>O<sub>20</sub>Tm: C, 43.90; H, 5.53; N, 9.15. Found: C, 44.80; H, 5.43; N, 9.30.

**4.2.2.13.4 [HNEt<sub>3</sub>]<sub>2</sub>[Lu(MnL<sup>5</sup>)<sub>2</sub>·(H<sub>2</sub>O)<sub>2</sub>·(ClO<sub>4</sub>)] (33)**

Yield: 59 mg, 40%. (based on Lu). IR (KBr pellet):  $\bar{\nu}$  = 3438 (br), 2902 (w), 2857 (w), 1630 (s), 1594 (m), 1552 (m), 1462 (s), 1440 (m), 1414 (m), 1335 (w), 1301 (m), 1231 (m), 1194 (w), 1162 (w), 1096 (s), 1026 (w), 986 (w), 966 (m), 960 (m), 878 (m), 833 (w), 805 (w), 761 (m), 669 (m), 624 (m), 603 (w), 551 (w), 482 (w), 455 (w), 409 (w) cm<sup>-1</sup>. Anal.

Calcd for  $C_{56}H_{80}ClLuMn_2N_{10}O_{18}$ : C, 44.79; H, 5.37; N, 9.33. Found: C, 45.40; H, 5.44; N, 9.17.

#### 4.2.2.14 Synthesis of $[Dy\{Ni(H_2L^5)\}_2 \cdot (H_2O)_{14} \cdot (NO_3)_3]$ (34)

3-formylsalicylic acid (67 mg, 0.4 mmol), tris (2-aminoethyl)amine (0.03 mL, 0.2 mmol) were dissolved in methanol / water (15 mL / 5 mL) mixture and then triethylamine (0.14 mL, 1 mmol) was added dropwise with stirring. To this solution  $Ni(NO_3)_2 \cdot (H_2O)_6$  (60 mg, 0.2 mmol) and  $Dy(NO_3)_3 \cdot (H_2O)_5$  (46 mg, 0.1 mmol) were added and reflux at  $65^\circ C$  for 3h. The solution was then filtered and kept for crystallization. Within one week, the yellow crystals were collected, washed with little amount of methanol and dried in vacuum. Yield: 68 mg, 36% (based on Dy). IR [ $cm^{-1}$ ]:  $\bar{\nu} = 3334, 3270$  (br), 2923 (w), 2857 (w), 1651 (s), 1604 (s), 1541 (s), 1477(w), 1453 (s), 1371 (m), 1308 (s), 1226 (s), 1150 (m), 1121(m), 1072 (m), 1016 (s), 980 (m), 873 (s), 829 (m), 799 (m), 765 (s), 616 (w), 541 (w). Anal. Calcd for  $C_{56}H_{92}DyNi_2N_{19}O_{25}$  (corresponds to loss of the ten water molecules): C, 39.30; H, 5.42; N, 15.55. Found: 39.55; H, 5.61; N, 15.70.

## 5 Crystal Structure Measurements

### 5.1 Data Collection with Refinement

The measurement for the structure analyses of this thesis were done with STOE IPDS 2. A suitable crystal was covered in mineral oil (Aldrich) and mounted on a glass fiber. The crystal was transferred directly to the cold N<sub>2</sub> stream of a STOE IPDS 2 diffractometer (MoK $\alpha$  radiation;  $\lambda = 0.71073 \text{ \AA}$ ). Subsequent computations were carried out on an Intel Pentium IV or on a Core2Duo PC. All structures were solved by the Patterson method (SHELXS-97).<sup>[146]</sup> The refinements were carried out by using full-matrix least-squares techniques on  $F$ , minimizing the function  $(F_o - F_c)^2$ , where the weight is defined as  $4F_o^2/2(F_o^2)$  and  $F_o$  and  $F_c$  are the observed and calculated structure factor amplitudes using the program SHELXL-97.<sup>[146]</sup> For this, the following equations are used.

$$\frac{1}{W} = \sigma^2 F_o^2 + (aP)^2 + bP \quad \text{with} \quad P = \frac{\max(F_o^2, 0) + 2F_c^2}{3}$$

The values proposed by the SHELXL were accepted as the coefficients  $a$  and  $b$ . With this the determined optimum values are

$$R_1 = \frac{\sum ||F_o| - |F_c||}{\sum |F_o|} \quad \text{and} \quad wR_2 = \left[ \frac{\sum [w(F_o^2 - F_c^2)^2]}{\sum [w(F_o^2)^2]} \right]^{0.5}$$

The Goodness of Fit is another important factor for the quality of the structural analysis, and is defined as:

$$\text{Goof} = S = \left[ \frac{\sum [w(F_o^2 - F_c^2)^2]}{(n - p)} \right]^{0.5}$$

Where  $n$  is the number of reflections and  $p$  is the total number of parameters refined. The graphical representation was done using the program DIAMOND. Carbon-bound hydrogen atom positions were calculated. The hydrogen atom contributions were calculated, but not refined. The locations of the largest peaks in the final difference Fourier map calculation as

---

well as the magnitude of the residual electron densities in each case were of no chemical significance.

## 5.2 Crystallographic Data

### 5.2.1 [Na<sub>4</sub>(NiL)<sub>2</sub>·(H<sub>2</sub>O)<sub>9</sub>]<sub>n</sub> (1)

Chemical formula	C <sub>36</sub> H <sub>42</sub> N <sub>4</sub> Na <sub>4</sub> Ni <sub>2</sub> O <sub>21</sub>
Formula mass	1076.12
Crystal system	Triclinic
Space group	<i>P</i> -1
<i>a</i> /Å, <i>b</i> /Å, <i>c</i> /Å	8.860(2), 14.699(3), 17.013(3).
$\alpha$ /°, $\beta$ /°, $\gamma$ /°	83.43(3), 77.74(3), 79.98(3).
Unit cell volume/Å <sup>3</sup>	2120.7(7)
Temperature/K	173(2)
No. of formula units per unit cell, <i>Z</i>	2
Absorption correction	Integration
Absorption coefficient, $\mu$ /mm <sup>-1</sup>	1.019
No. of reflections measured	15591
No. of independent reflections	8576
<i>R</i> <sub>int</sub>	0.0583
Final <i>R</i> <sub>1</sub> values ( <i>I</i> > 2σ( <i>I</i> ))	0.0440
Final <i>wR</i> <sub>2</sub> values (all data)	0.1134
Goodness of fit	0.976

### 5.2.2 [Na<sub>4</sub>(CuL)<sub>2</sub>·(H<sub>2</sub>O)<sub>9</sub>]<sub>n</sub> (2)

Chemical formula	C <sub>36</sub> H <sub>42</sub> Cu <sub>2</sub> N <sub>4</sub> Na <sub>4</sub> O <sub>21</sub>
Formula mass	1085.78
Crystal system	Triclinic
Space group	<i>P</i> -1
<i>a</i> /Å, <i>b</i> /Å, <i>c</i> /Å	8.860(2), 14.669(3), 17.013(3).
$\alpha$ /°, $\beta$ /°, $\gamma$ /°	83.43(3), 77.74(3), 79.98(3).
Unit cell volume/Å <sup>3</sup>	2120.7(7)
Temperature/K	173(2)
No. of formula units per unit cell, <i>Z</i>	2
Absorption correction	Integrationl
Absorption coefficient, $\mu$ /mm <sup>-1</sup>	1.134
No. of reflections measured	37382
No. of independent reflections	8458
<i>R</i> <sub>int</sub>	0.1083
Final <i>R</i> <sub>1</sub> values ( <i>I</i> > 2σ( <i>I</i> ))	0.0440
Final <i>wR</i> <sub>2</sub> values (all data)	0.1226
Goodness of fit	1.041

**5.2.3 [Li(NiHL)(DMSO)]<sub>n</sub> (3)**

Chemical formula	C <sub>20</sub> H <sub>19</sub> LiN <sub>2</sub> NiO <sub>7</sub> S
Formula mass	497.08
Crystal system	Monoclinic
Space group	<i>P21/n</i>
a/Å, b/Å, c/Å	16.234(3), 8.1754(16), 17.328(3).
β/°	111.16(3)
Unit cell volume/Å <sup>3</sup>	2020.9(7)
Temperature/K	200(2)
No. of formula units per unit cell, Z	4
Absorption correction	Integration
Absorption coefficient, μ/mm <sup>-1</sup>	1.111
No. of reflections measured	15178
No. of independent reflections	4124
R <sub>int</sub>	0.0598
Final R <sub>1</sub> values (I > 2σ(I))	0.0414
Final wR <sub>2</sub> values (all data)	0.1000
Goodness of fit	1.058

**5.2.4 [Na<sub>5</sub>{(NiL<sup>2</sup>)(HCOO)(H<sub>2</sub>O)<sub>11</sub>}·(H<sub>2</sub>O)<sub>4</sub>]<sub>n</sub> (4)**

Chemical formula	C <sub>39</sub> H <sub>59</sub> N <sub>4</sub> Na <sub>5</sub> Ni <sub>2</sub> O <sub>29</sub>
Formula mass	1280.27
Crystal system	Monoclinic
Space group	<i>P21/m</i>
a/Å, b/Å, c/Å	23.2692(10), 18.0786(8), 10.5869(4).
β/°	96.936(3)
Unit cell volume/Å <sup>3</sup>	4421.1(3)
Temperature/K	200(2)
No. of formula units per unit cell, Z	2
Absorption correction	Integration
Absorption coefficient, μ/mm <sup>-1</sup>	1.08
No. of reflections measured	24687
No. of independent reflections	5611
R <sub>int</sub>	0.0749
Final R <sub>1</sub> values (I > 2σ(I))	0.0399
Final wR <sub>2</sub> values (all data)	0.1174
Goodness of fit	1.050

**5.2.5 [Na<sub>4</sub>{(CuHL<sup>3</sup>)<sub>2</sub>(MeOH)<sub>2</sub>(Et<sub>2</sub>O)(H<sub>2</sub>O)]<sub>n</sub> (5)**

Chemical formula	C <sub>44</sub> H <sub>48</sub> Cu <sub>2</sub> N <sub>4</sub> Na <sub>4</sub> O <sub>18</sub>
Formula mass	1139.90
Crystal system	Monoclinic
Space group	<i>C2/c</i>
<i>a</i> /Å, <i>b</i> /Å, <i>c</i> /Å	23.2692(10), 18.0786(8), 10.5869(4).
$\beta$ /°	96.936(3)
Unit cell volume/Å <sup>3</sup>	4421.1(3)
Temperature/K	200(2)
No. of formula units per unit cell, <i>Z</i>	4
Absorption correction	Integration
Absorption coefficient, $\mu$ /mm <sup>-1</sup>	1.08
No. of reflections measured	22542
No. of independent reflections	5052
<i>R</i> <sub>int</sub>	0.0587
Final <i>R</i> <sub>1</sub> values ( <i>I</i> > 2σ( <i>I</i> ))	0.0458
Final <i>wR</i> <sub>2</sub> values (all data)	0.1100
Goodness of fit	1.109

**5.2.6. [{Er<sub>2</sub>(NiL)<sub>3</sub>(DMF)(H<sub>2</sub>O)<sub>3</sub>}·(DMF)<sub>4</sub>·(H<sub>2</sub>O)<sub>10</sub>]<sub>n</sub> (6)**

Chemical formula	C <sub>69</sub> H <sub>97</sub> Er <sub>2</sub> N <sub>11</sub> Ni <sub>3</sub> O <sub>36</sub>
Formula mass	2167.23
Crystal system	Triclinic
Space group	<i>P</i> -1
<i>a</i> /Å, <i>b</i> /Å, <i>c</i> /Å	14.682(3), 15.347(3), 19.140(4).
$\alpha$ /°, $\beta$ /°, $\gamma$ /°	95.82(3), 100.58(3), 94.33(3).
Unit cell volume/Å <sup>3</sup>	4197.9(14)
Temperature/K	150(2)
No. of formula units per unit cell, <i>Z</i>	2
Absorption correction	Integration
Absorption coefficient, $\mu$ /mm <sup>-1</sup>	2.732
No. of reflections measured	32757
No. of independent reflections	16656
<i>R</i> <sub>int</sub>	0.1229
Final <i>R</i> <sub>1</sub> values ( <i>I</i> > 2σ( <i>I</i> ))	0.0765
Final <i>wR</i> <sub>2</sub> values (all data)	0.1994
Goodness of fit	0.987



**5.2.9**  $[\{\text{Tm}_2(\text{NiL})_3(\text{DMF})(\text{H}_2\text{O})_3\} \cdot (\text{DMF})_4 \cdot (\text{H}_2\text{O})_{10}]_n$  (7)

Chemical formula	$\text{C}_{69}\text{H}_{97}\text{N}_{11}\text{Ni}_3\text{O}_{36}\text{Tm}_2$
Formula mass	2170.57
Crystal system	Triclinic
Space group	$P-1$
$a/\text{\AA}$ , $b/\text{\AA}$ , $c/\text{\AA}$	14.681(3), 15.356(3), 19.139(3).
$\alpha/^\circ$ , $\beta/^\circ$ , $\gamma/^\circ$	95.72(3), 100.67(3), 94.37(3).
Unit cell volume/ $\text{\AA}^3$	4199.2(14)
Temperature/K	150(2)
No. of formula units per unit cell, $Z$	2
Absorption correction	Integration
Absorption coefficient, $\mu/\text{mm}^{-1}$	2.846
No. of reflections measured	44991
No. of independent reflections	17776
$R_{\text{int}}$	0.0873
Final $R_1$ values ( $I > 2\sigma(I)$ )	0.487
Final $wR_2$ values (all data)	0.1116
Goodness of fit	1.029

**5.2.8**  $[\{\text{Yb}_2(\text{NiL})_3(\text{DMF})(\text{H}_2\text{O})_3\} \cdot (\text{DMF})_4 \cdot (\text{H}_2\text{O})_{10}]_n$  (8)

Chemical formula	$\text{C}_{69}\text{H}_{97}\text{N}_{11}\text{Ni}_3\text{O}_{36}\text{Yb}_2$
Formula mass	2178.72
Crystal system	Triclinic
Space group	$P-1$
$a/\text{\AA}$ , $b/\text{\AA}$ , $c/\text{\AA}$	14.642(1), 15.392(1), 19.100(1).
$\alpha/^\circ$ , $\beta/^\circ$ , $\gamma/^\circ$	95.70(5), 100.47(5), 94.24(5).
Unit cell volume/ $\text{\AA}^3$	4193.2(5)
Temperature/K	150(2)
No. of formula units per unit cell, $Z$	2
Absorption correction	Integration
Absorption coefficient, $\mu/\text{mm}^{-1}$	2.964
No. of reflections measured	35333
No. of independent reflections	17599
$R_{\text{int}}$	0.2218
Final $R_1$ values ( $I > 2\sigma(I)$ )	0.1365
Final $wR_2$ values (all data)	0.3685
Goodness of fit	1.111

**5.2.7 [ $\{\text{Lu}_2(\text{NiL})_3(\text{DMF})(\text{H}_2\text{O})_3\} \cdot (\text{DMF})_4 \cdot (\text{H}_2\text{O})_{10}\}_n$  (9)**

Chemical formula	$\text{C}_{69}\text{H}_{97}\text{Lu}_2\text{N}_{11}\text{Ni}_3\text{O}_{36}$
Formula mass	2182.65
Crystal system	Triclinic
Space group	$P\bar{1}$
$a/\text{\AA}$ , $b/\text{\AA}$ , $c/\text{\AA}$	14.637(1), 15.373(1), 19.098(1).
$\alpha/^\circ$ , $\beta/^\circ$ , $\gamma/^\circ$	95.65(6), 100.61(6), 94.39(6).
Unit cell volume/ $\text{\AA}^3$	4183.5(5)
Temperature/K	150(2)
No. of formula units per unit cell, $Z$	2
Absorption correction	Integration
Absorption coefficient, $\mu/\text{mm}^{-1}$	3.095
No. of reflections measured	30288
No. of independent reflections	16731
$R_{\text{int}}$	0.0837
Final $R_1$ values ( $I > 2\sigma(I)$ )	0.0594
Final $wR_2$ values (all data)	0.1326
Goodness of fit	1.031

**2.10 [ $\text{Dy}\{(\text{NiL})(\text{DMSO})(\text{NO}_3)\}(\text{H}_2\text{O})_2 \cdot (\text{DMSO})_n$  (10)**

Chemical formula	$\text{C}_{22}\text{H}_{28}\text{DyN}_3\text{NiO}_{13}\text{S}_2$
Formula mass	827.80
Crystal system	Monoclinic
Space group	$P2_1/n$
$a/\text{\AA}$ , $b/\text{\AA}$ , $c/\text{\AA}$	7.523(1), 22.668(5), 17.349(4).
$\beta/^\circ$	95.88(3)
Unit cell volume/ $\text{\AA}^3$	2942.9(10)
Temperature/K	200(2)
No. of formula units per unit cell, $Z$	4
Absorption correction	Integration
Absorption coefficient, $\mu/\text{mm}^{-1}$	3.369
No. of reflections measured	20559
No. of independent reflections	6252
$R_{\text{int}}$	0.0891
Final $R_1$ values ( $I > 2\sigma(I)$ )	0.582
Final $wR_2$ values (all data)	0.1424
Goodness of fit	1.040

**5.2.11 [Na<sub>3</sub>Yb{(NiL)(H<sub>2</sub>O)}<sub>3</sub>DMF]<sub>n</sub> (11)**

Chemical formula	C <sub>57</sub> H <sub>49</sub> N <sub>7</sub> Na <sub>3</sub> Ni <sub>3</sub> O <sub>22</sub> Yb
Formula mass	1602.17
Crystal system	Hexagonal
Space group	<i>P</i> 6 <sub>3</sub> / <i>m</i>
<i>a</i> /Å, <i>b</i> /Å, <i>c</i> /Å	14.052(2), 14.052(2), 16.522(3).
$\gamma$ /°	120
Unit cell volume/Å <sup>3</sup>	2825.5(8)
Temperature/K	203(2)
No. of formula units per unit cell, <i>Z</i>	2
Absorption correction	Integration
Absorption coefficient, $\mu$ /mm <sup>-1</sup>	2.739
No. of reflections measured	14745
No. of independent reflections	2080
<i>R</i> <sub>int</sub>	0.0896
Final <i>R</i> <sub>1</sub> values ( <i>I</i> > 2σ( <i>I</i> ))	0.0567
Final <i>wR</i> <sub>2</sub> values (all data)	0.1596
Goodness of fit	1.098

**5.2.11 [Nd<sub>2</sub>(MnLCl)<sub>2</sub>(NO<sub>3</sub>)<sub>2</sub>(DMF)<sub>5</sub>·(DMF)<sub>4</sub>]<sub>n</sub> (12)**

Chemical formula	C <sub>63</sub> H <sub>87</sub> Cl <sub>2</sub> Mn <sub>2</sub> N <sub>15</sub> Nd <sub>2</sub> O <sub>27</sub>
Formula mass	1955.74
Crystal system	Triclinic
Space group	<i>P</i> -1
<i>a</i> /Å, <i>b</i> /Å, <i>c</i> /Å	13.767(3), 14.726(3), 21.486(4).
$\alpha$ /°, $\beta$ /°, $\gamma$ /°	88.19(3), 74.15(3), 76.57(3).
Unit cell volume/Å <sup>3</sup>	4073.4(14)
Temperature/K	200(2)
No. of formula units per unit cell, <i>Z</i>	2
Absorption correction	Integration
Absorption coefficient, $\mu$ /mm <sup>-1</sup>	1.706
No. of reflections measured	41925
No. of independent reflections	21440
<i>R</i> <sub>int</sub>	0.0694
Final <i>R</i> <sub>1</sub> values ( <i>I</i> > 2σ( <i>I</i> ))	0.0516
Final <i>wR</i> <sub>2</sub> values (all data)	0.1401
Goodness of fit	0.997

**5.2.13 [Eu<sub>2</sub>(MnLCl)<sub>2</sub>(NO<sub>3</sub>)<sub>2</sub>(DMF)<sub>5</sub>·(DMF)<sub>4</sub>]<sub>n</sub> (13)**

Chemical formula	C <sub>63</sub> H <sub>87</sub> Cl <sub>2</sub> Eu <sub>2</sub> Mn <sub>2</sub> N <sub>15</sub> O <sub>27</sub>
Formula mass	1971.18
Crystal system	Triclinic
Space group	<i>P</i> -1
<i>a</i> /Å, <i>b</i> /Å, <i>c</i> /Å	13.678(3), 14.648(3), 21.363(4).
$\alpha$ /°, $\beta$ /°, $\gamma$ /°	88.07(3), 74.02(3), 76.52(3).
Unit cell volume/Å <sup>3</sup>	3999.3(14)
Temperature/K	150(2)
No. of formula units per unit cell, <i>Z</i>	2
Absorption correction	Integration
Absorption coefficient, $\mu$ /mm <sup>-1</sup>	2.008
No. of reflections measured	78278
No. of independent reflections	21555
<i>R</i> <sub>int</sub>	0.1154
Final <i>R</i> <sub>1</sub> values ( <i>I</i> > 2σ( <i>I</i> ))	0.0423
Final <i>wR</i> <sub>2</sub> values (all data)	0.1147
Goodness of fit	1.002

**5.2.14 [Gd<sub>2</sub>(MnLCl)<sub>2</sub>(NO<sub>3</sub>)<sub>2</sub>(DMF)<sub>5</sub>·(DMF)<sub>4</sub>]<sub>n</sub> (14)**

Chemical formula	C <sub>63</sub> H <sub>87</sub> Cl <sub>2</sub> Gd <sub>2</sub> Mn <sub>2</sub> N <sub>15</sub> O <sub>27</sub>
Formula mass	1981.76
Crystal system	Triclinic
Space group	<i>P</i> -1
<i>a</i> /Å, <i>b</i> /Å, <i>c</i> /Å	13.725(3), 14.716(3), 21.451(4).
$\alpha$ /°, $\beta$ /°, $\gamma$ /°	88.22(3), 74.06(3), 76.58(3).
Unit cell volume/Å <sup>3</sup>	4049.8(14)
Temperature/K	200(2)
No. of formula units per unit cell, <i>Z</i>	2
Absorption correction	Integration
Absorption coefficient, $\mu$ /mm <sup>-1</sup>	2.072
No. of reflections measured	150550
No. of independent reflections	21850
<i>R</i> <sub>int</sub>	0.0621
Final <i>R</i> <sub>1</sub> values ( <i>I</i> > 2σ( <i>I</i> ))	0.0308
Final <i>wR</i> <sub>2</sub> values (all data)	0.0784
Goodness of fit	1.059

**5.2.15 [Tb<sub>2</sub>(MnLCl)<sub>2</sub>(NO<sub>3</sub>)<sub>2</sub>(DMF)<sub>5</sub>·(DMF)<sub>4</sub>]<sub>n</sub> (15)**

Chemical formula	C <sub>63</sub> H <sub>87</sub> Cl <sub>2</sub> Mn <sub>2</sub> N <sub>15</sub> O <sub>27</sub> Tb <sub>2</sub>
Formula mass	1985.10
Crystal system	Triclinic
Space group	<i>P</i> -1
<i>a</i> /Å, <i>b</i> /Å, <i>c</i> /Å	13.665(3), 14.642(3), 21.663(4).
$\alpha$ /°, $\beta$ /°, $\gamma$ /°	88.06(3), 74.08(3), 76.44(3).
Unit cell volume/Å <sup>3</sup>	3994.1(14)
Temperature/K	150(2)
No. of formula units per unit cell, <i>Z</i>	2
Absorption correction	Integration
Absorption coefficient, $\mu$ /mm <sup>-1</sup>	2.211
No. of reflections measured	58668
No. of independent reflections	16949
<i>R</i> <sub>int</sub>	0.1675
Final <i>R</i> <sub>1</sub> values ( <i>I</i> > 2σ( <i>I</i> ))	0.0436
Final <i>wR</i> <sub>2</sub> values (all data)	0.1146
Goodness of fit	0.922

**5.2.16 [Dy<sub>2</sub>(MnLCl)<sub>2</sub>(NO<sub>3</sub>)<sub>2</sub>(DMF)<sub>5</sub>·(DMF)<sub>4</sub>]<sub>n</sub> (16)**

Chemical formula	C <sub>63</sub> H <sub>87</sub> Cl <sub>2</sub> Dy <sub>2</sub> Mn <sub>2</sub> N <sub>15</sub> O <sub>27</sub>
Formula mass	1992.26
Crystal system	Triclinic
Space group	<i>P</i> -1
<i>a</i> /Å, <i>b</i> /Å, <i>c</i> /Å	13.704(3), 14.709(3), 21.449(4).
$\alpha$ /°, $\beta$ /°, $\gamma$ /°	88.21(3), 74.23(3), 76.63(3).
Unit cell volume/Å <sup>3</sup>	4045.8(14)
Temperature/K	200(2)
No. of formula units per unit cell, <i>Z</i>	2
Absorption correction	Integration
Absorption coefficient, $\mu$ /mm <sup>-1</sup>	2.281
No. of reflections measured	61665
No. of independent reflections	21454
<i>R</i> <sub>int</sub>	0.0985
Final <i>R</i> <sub>1</sub> values ( <i>I</i> > 2σ( <i>I</i> ))	0.0574
Final <i>wR</i> <sub>2</sub> values (all data)	0.1227
Goodness of fit	0.922

**5.2.17 [Y<sub>2</sub>(FeLCl)<sub>2</sub>(NO<sub>3</sub>)<sub>2</sub>(DMF)<sub>5</sub>·(DMF)<sub>4</sub>]<sub>n</sub> (17)**

Chemical formula	C <sub>63</sub> H <sub>87</sub> Cl <sub>2</sub> Fe <sub>2</sub> N <sub>15</sub> O <sub>27</sub> Y <sub>2</sub>
Formula mass	1846.90
Crystal system	Triclinic
Space group	<i>P</i> -1
<i>a</i> /Å, <i>b</i> /Å, <i>c</i> /Å	13.430(3), 14.799(3), 21.553(4).
$\alpha$ /°, $\beta$ /°, $\gamma$ /°	87.39(3), 74.19(3), 77.21(3).
Unit cell volume/Å <sup>3</sup>	4018.9(14)
Temperature/K	150(2)
No. of formula units per unit cell, <i>Z</i>	2
Absorption correction	Integration
Absorption coefficient, $\mu$ /mm <sup>-1</sup>	1.935
No. of reflections measured	42870
No. of independent reflections	21161
<i>R</i> <sub>int</sub>	0.1309
Final <i>R</i> <sub>1</sub> values ( <i>I</i> > 2σ( <i>I</i> ))	0.0869
Final <i>wR</i> <sub>2</sub> values (all data)	0.2457
Goodness of fit	0.930

**5.2.18 [Eu<sub>2</sub>(FeLCl)<sub>2</sub>(NO<sub>3</sub>)<sub>2</sub>(DMF)<sub>5</sub>·(DMF)<sub>4</sub>]<sub>n</sub> (18)**

Chemical formula	C <sub>63</sub> H <sub>87</sub> Cl <sub>2</sub> Eu <sub>2</sub> Fe <sub>2</sub> N <sub>15</sub> O <sub>27</sub>
Formula mass	1973.00
Crystal system	Triclinic
Space group	<i>P</i> -1
<i>a</i> /Å, <i>b</i> /Å, <i>c</i> /Å	13.616(3), 14.823(3), 21.566(4).
$\alpha$ /°, $\beta$ /°, $\gamma$ /°	87.36(3), 74.47(3), 76.62(3).
Unit cell volume/Å <sup>3</sup>	4078.5(14)
Temperature/K	200(2)
No. of formula units per unit cell, <i>Z</i>	2
Absorption correction	Integration
Absorption coefficient, $\mu$ /mm <sup>-1</sup>	2.015
No. of reflections measured	48395
No. of independent reflections	21451
<i>R</i> <sub>int</sub>	0.0593
Final <i>R</i> <sub>1</sub> values ( <i>I</i> > 2σ( <i>I</i> ))	0.0430
Final <i>wR</i> <sub>2</sub> values (all data)	0.1055
Goodness of fit	0.932

**5.2.19 [Gd<sub>2</sub>(FeLCl)<sub>2</sub>(NO<sub>3</sub>)<sub>2</sub>(DMF)<sub>5</sub>·(DMF)<sub>4</sub>]<sub>n</sub> (19)**

Chemical formula	C <sub>63</sub> H <sub>87</sub> Cl <sub>2</sub> Gd <sub>2</sub> Fe <sub>2</sub> N <sub>15</sub> O <sub>27</sub>
Formula mass	1983.58
Crystal system	Triclinic
Space group	<i>P</i> -1
<i>a</i> /Å, <i>b</i> /Å, <i>c</i> /Å	13.614(3), 14.830(3), 21.566(4).
$\alpha$ /°, $\beta$ /°, $\gamma$ /°	87.37(3), 74.37(3), 76.58(3).
Unit cell volume/Å <sup>3</sup>	4078.0(14)
Temperature/K	200(2)
No. of formula units per unit cell, <i>Z</i>	2
Absorption correction	Integration
Absorption coefficient, $\mu$ /mm <sup>-1</sup>	2.103
No. of reflections measured	42702
No. of independent reflections	21638
<i>R</i> <sub>int</sub>	0.0809
Final <i>R</i> <sub>1</sub> values ( <i>I</i> > 2σ( <i>I</i> ))	0.0505
Final <i>wR</i> <sub>2</sub> values (all data)	0.1321
Goodness of fit	0.947

**5.2.20 [Tb<sub>2</sub>(FeLCl)<sub>2</sub>(NO<sub>3</sub>)<sub>2</sub>(DMF)<sub>5</sub>·(DMF)<sub>4</sub>]<sub>n</sub> (20)**

Chemical formula	C <sub>63</sub> H <sub>87</sub> Cl <sub>2</sub> Fe <sub>2</sub> N <sub>15</sub> O <sub>27</sub> Tb <sub>2</sub>
Formula mass	1986.92
Crystal system	Triclinic
Space group	<i>P</i> -1
<i>a</i> /Å, <i>b</i> /Å, <i>c</i> /Å	13.603(3), 14.829(3), 21.588(4)
$\alpha$ /°, $\beta$ /°, $\gamma$ /°	87.40(3), 74.33(3), 76.73(3).
Unit cell volume/Å <sup>3</sup>	4080.3(14)
Temperature/K	200(2)
No. of formula units per unit cell, <i>Z</i>	2
Absorption correction	Integration
Absorption coefficient, $\mu$ /mm <sup>-1</sup>	2.210
No. of reflections measured	57316
No. of independent reflections	27298
<i>R</i> <sub>int</sub>	0.0695
Final <i>R</i> <sub>1</sub> values ( <i>I</i> > 2σ( <i>I</i> ))	0.0401
Final <i>wR</i> <sub>2</sub> values (all data)	0.1059
Goodness of fit	1.019

**5.2.21 [Dy<sub>2</sub>(FeLCl)<sub>2</sub>(NO<sub>3</sub>)<sub>2</sub>(DMF)<sub>5</sub>·(DMF)<sub>4</sub>]<sub>n</sub> (21)**

Chemical formula	C <sub>63</sub> H <sub>87</sub> Cl <sub>2</sub> Dy <sub>2</sub> Fe <sub>2</sub> N <sub>15</sub> O <sub>27</sub>
Formula mass	1994.08
Crystal system	Triclinic
Space group	<i>P</i> -1
<i>a</i> /Å, <i>b</i> /Å, <i>c</i> /Å	13.582(3), 14.723(3), 21.432(4).
$\alpha$ /°, $\beta$ /°, $\gamma$ /°	87.03(3), 74.25(3), 76.10(3).
Unit cell volume/Å <sup>3</sup>	4003.7(14)
Temperature/K	150(2)
No. of formula units per unit cell, <i>Z</i>	2
Absorption correction	Integration
Absorption coefficient, $\mu$ /mm <sup>-1</sup>	2.352
No. of reflections measured	32415
No. of independent reflections	14243
<i>R</i> <sub>int</sub>	0.1392
Final <i>R</i> <sub>1</sub> values ( <i>I</i> > 2σ( <i>I</i> ))	0.0678
Final <i>wR</i> <sub>2</sub> values (all data)	0.1768
Goodness of fit	0.999

**5.2.22 [Mn<sub>3</sub>{(H<sub>2</sub>L<sup>4</sup>)(HL<sup>4</sup>)(OMe)<sub>2</sub>(MeOH)<sub>2</sub>}·(MeOH)<sub>4</sub>] (22)**

Chemical formula	C <sub>42</sub> H <sub>59</sub> Mn <sub>3</sub> N <sub>4</sub> O <sub>18</sub>
Formula mass	1072.75
Crystal system	Tetragonal
Space group	<i>P</i> 41
<i>a</i> /Å, <i>b</i> /Å, <i>c</i> /Å	13.735(2), 13.735(2), 24.967(5).
$\alpha$ /°, $\beta$ /°, $\gamma$ /°	90
Unit cell volume/Å <sup>3</sup>	4710.0(13)
Temperature/K	200(2)
No. of formula units per unit cell, <i>Z</i>	4
Absorption correction	Integration
Absorption coefficient, $\mu$ /mm <sup>-1</sup>	0.870
No. of reflections measured	36699
No. of independent reflections	9989
<i>R</i> <sub>int</sub>	0.1054
Final <i>R</i> <sub>1</sub> values ( <i>I</i> > 2σ( <i>I</i> ))	0.0518
Final <i>wR</i> <sub>2</sub> values (all data)	0.1033
Goodness of fit	0.883



**5.2.23 [Ni<sub>3</sub>(H<sub>3</sub>L<sup>4</sup>)<sub>2</sub>(OAc)<sub>2</sub>(DMF)<sub>2</sub>·(H<sub>2</sub>O)<sub>3</sub>] (23)**

Chemical formula	C <sub>44</sub> H <sub>58</sub> N <sub>6</sub> Ni <sub>3</sub> O <sub>19</sub>
Formula mass	1151.09
Crystal system	Monoclinic
Space group	<i>P</i> 2 <sub>1</sub> / <i>n</i>
<i>a</i> /Å, <i>b</i> /Å, <i>c</i> /Å	10.890(2), 18.070(4), 13.073(3).
β/°	105.49(3).
Unit cell volume/Å <sup>3</sup>	2479.2(9)
Temperature/K	150(2)
No. of formula units per unit cell, <i>Z</i>	2
Absorption correction	Integration
Absorption coefficient, μ/mm <sup>-1</sup>	1.08
No. of reflections measured	49446
No. of independent reflections	6558
R <sub>int</sub>	0.2126
Final R <sub>1</sub> values ( <i>I</i> > 2σ( <i>I</i> ))	0.0704
Final wR <sub>2</sub> values (all data)	0.2061
Goodness of fit	1.059

**5.2.24 [Eu(H<sub>2</sub>L<sup>5</sup>)<sub>2</sub>·(EtOH)·(H<sub>2</sub>O)<sub>9</sub>·(NO<sub>3</sub>)] (24)**

Chemical formula	C <sub>46</sub> H <sub>74</sub> EuN <sub>9</sub> O <sub>25</sub>
Formula mass	1305.10
Crystal system	Triclinic
Space group	<i>P</i> -1
<i>a</i> /Å, <i>b</i> /Å, <i>c</i> /Å	12.9856(3), 15.1302(4), 16.3921(4).
α/°, β/°, γ/°	75.195(2), 66.686(2), 71.861(2).
Unit cell volume/Å <sup>3</sup>	2778.19(12)
Temperature/K	150(2)
No. of formula units per unit cell, <i>Z</i>	2
Absorption correction	Integration
Absorption coefficient, μ/mm <sup>-1</sup>	1.219
No. of reflections measured	21184
No. of independent reflections	11305
R <sub>int</sub>	0.0994
Final R <sub>1</sub> values ( <i>I</i> > 2σ( <i>I</i> ))	0.0616
Final wR <sub>2</sub> values (all data)	0.1607
Goodness of fit	0.961

**5.2.24 [Tb(H<sub>2</sub>L<sup>5</sup>)<sub>2</sub>·(EtOH)·(H<sub>2</sub>O)<sub>8</sub>·(NO<sub>3</sub>)] (25)**

Chemical formula	C <sub>46</sub> H <sub>72</sub> N <sub>9</sub> O <sub>24</sub> Tb
Formula mass	1294.05
Crystal system	Triclinic
Space group	<i>P</i> -1
<i>a</i> /Å, <i>b</i> /Å, <i>c</i> /Å	12.9690(3), 15.2260(4), 16.5079(4).
$\alpha$ /°, $\beta$ /°, $\gamma$ /°	74.873(2), 66.826(2), 71.571(2).
Unit cell volume/Å <sup>3</sup>	2807.99(12)
Temperature/K	200(2)
No. of formula units per unit cell, <i>Z</i>	2
Absorption correction	Integration
Absorption coefficient, $\mu$ /mm <sup>-1</sup>	1.348
No. of reflections measured	27791
No. of independent reflections	12774
<i>R</i> <sub>int</sub>	0.0494
Final <i>R</i> <sub>1</sub> values ( <i>I</i> > 2σ( <i>I</i> ))	0.0350
Final <i>wR</i> <sub>2</sub> values (all data)	0.0970
Goodness of fit	0.941

**5.2.26 [Dy(H<sub>2</sub>L<sup>5</sup>)<sub>2</sub>·(EtOH)·(H<sub>2</sub>O)<sub>8</sub>·(NO<sub>3</sub>)] (26)**

Chemical formula	C <sub>46</sub> H <sub>72</sub> DyN <sub>9</sub> O <sub>24</sub>
Formula mass	1297.63
Crystal system	Triclinic
Space group	<i>P</i> -1
<i>a</i> /Å, <i>b</i> /Å, <i>c</i> /Å	12.9580(3), 15.2000(4), 16.4680(4).
$\alpha$ /°, $\beta$ /°, $\gamma$ /°	74.850(2), 66.944(2), 71.621(2).
Unit cell volume/Å <sup>3</sup>	2796.72(12)
Temperature/K	220(2)
No. of formula units per unit cell, <i>Z</i>	2
Absorption correction	Integration
Absorption coefficient, $\mu$ /mm <sup>-1</sup>	1.425
No. of reflections measured	30623
No. of independent reflections	12726
<i>R</i> <sub>int</sub>	0.0979
Final <i>R</i> <sub>1</sub> values ( <i>I</i> > 2σ( <i>I</i> ))	0.0429
Final <i>wR</i> <sub>2</sub> values (all data)	0.1199
Goodness of fit	1.063

**5.2.27 [Er(H<sub>2</sub>L<sup>5</sup>)<sub>2</sub>·(EtOH)·(H<sub>2</sub>O)<sub>8</sub>·(NO<sub>3</sub>)] (27)**

Chemical formula	C <sub>46</sub> H <sub>72</sub> N <sub>9</sub> O <sub>24</sub> Er
Formula mass	1302.39
Crystal system	Triclinic
Space group	<i>P</i> -1
<i>a</i> /Å, <i>b</i> /Å, <i>c</i> /Å	12.9060(3), 15.1407(4), 16.4050(4).
$\alpha$ /°, $\beta$ /°, $\gamma$ /°	74.779(2), 66.829(2), 71.728(2).
Unit cell volume/Å <sup>3</sup>	2762.66(12)
Temperature/K	150(2)
No. of formula units per unit cell, <i>Z</i>	2
Absorption correction	Integration
Absorption coefficient, $\mu$ /mm <sup>-1</sup>	1.609
No. of reflections measured	23936
No. of independent reflections	12407
<i>R</i> <sub>int</sub>	0.0755
Final <i>R</i> <sub>1</sub> values ( <i>I</i> > 2σ( <i>I</i> ))	0.0880
Final <i>wR</i> <sub>2</sub> values (all data)	0.2382
Goodness of fit	1.261

**5.2.28 [Tm(H<sub>2</sub>L<sup>5</sup>)<sub>2</sub>·(EtOH)·(H<sub>2</sub>O)<sub>8</sub>·(NO<sub>3</sub>)] (28)**

Chemical formula	C <sub>46</sub> H <sub>72</sub> N <sub>9</sub> O <sub>24</sub> Tm
Formula mass	1304.06
Crystal system	Triclinic
Space group	<i>P</i> -1
<i>a</i> /Å, <i>b</i> /Å, <i>c</i> /Å	12.951(3), 15.136(4), 16.459(4).
$\alpha$ /°, $\beta$ /°, $\gamma$ /°	90.99(3), 113.00(3), 108.31(3).
Unit cell volume/Å <sup>3</sup>	2783.1(10)
Temperature/K	207(2)
No. of formula units per unit cell, <i>Z</i>	2
Absorption correction	Integration
Absorption coefficient, $\mu$ /mm <sup>-1</sup>	1.684
No. of reflections measured	53357
No. of independent reflections	15000
<i>R</i> <sub>int</sub>	0.0847
Final <i>R</i> <sub>1</sub> values ( <i>I</i> > 2σ( <i>I</i> ))	0.0373
Final <i>wR</i> <sub>2</sub> values (all data)	0.1019
Goodness of fit	1.051

**5.2.29 [NHEt<sub>3</sub>]<sub>2</sub>[Eu(MnL<sup>5</sup>)<sub>2</sub>·(H<sub>2</sub>O)<sub>2</sub>·(ClO<sub>4</sub>)] (29)**

Chemical formula	C <sub>56</sub> H <sub>80</sub> ClEuMn <sub>2</sub> N <sub>10</sub> O <sub>18</sub>
Formula mass	1478.59
Crystal system	Triclinic
Space group	<i>P</i> -1
<i>a</i> /Å, <i>b</i> /Å, <i>c</i> /Å	10.8515(5), 15.9218(7), 19.7737(10).
$\alpha$ /°, $\beta$ /°, $\gamma$ /°	77.689(4), 85.253(4), 73.277(4).
Unit cell volume/Å <sup>3</sup>	3195.8(3)
Temperature/K	200(2)
No. of formula units per unit cell, <i>Z</i>	2
Absorption correction	Integration
Absorption coefficient, $\mu$ /mm <sup>-1</sup>	1.476
No. of reflections measured	48202
No. of independent reflections	11949
<i>R</i> <sub>int</sub>	0.0818
Final <i>R</i> <sub>1</sub> values ( <i>I</i> > 2σ( <i>I</i> ))	0.0476
Final <i>wR</i> <sub>2</sub> values (all data)	0.1156
Goodness of fit	0.931

**5.2.30 [HNEt<sub>3</sub>]<sub>2</sub>[Dy(MnL<sup>5</sup>)<sub>2</sub>·(H<sub>2</sub>O)<sub>2</sub>·(ClO<sub>4</sub>)] (31)**

Chemical formula	C <sub>56</sub> H <sub>80</sub> ClDyMn <sub>2</sub> N <sub>10</sub> O <sub>18</sub>
Formula mass	1489.13
Crystal system	Triclinic
Space group	<i>P</i> -1
<i>a</i> /Å, <i>b</i> /Å, <i>c</i> /Å	10.825(3), 15.910(5), 19.856(3)
$\alpha$ /°, $\beta$ /°, $\gamma$ /°	77.33(3), 85.55(3), 73.0(2).
Unit cell volume/Å <sup>3</sup>	3190.3(16)
Temperature/K	200(2)
No. of formula units per unit cell, <i>Z</i>	2
Absorption correction	Integration
Absorption coefficient, $\mu$ /mm <sup>-1</sup>	1.667
No. of reflections measured	49900
No. of independent reflections	7909
<i>R</i> <sub>int</sub>	0.0737
Final <i>R</i> <sub>1</sub> values ( <i>I</i> > 2σ( <i>I</i> ))	0.0384
Final <i>wR</i> <sub>2</sub> values (all data)	0.1013
Goodness of fit	1.058

**5.2.31 [HNEt<sub>3</sub>]<sub>2</sub>[Tm(MnL<sup>5</sup>)<sub>2</sub>·(H<sub>2</sub>O)<sub>4</sub>·(ClO<sub>4</sub>)] (32)**

Chemical formula	C <sub>56</sub> H <sub>84</sub> ClMn <sub>2</sub> N <sub>10</sub> O <sub>20</sub> Tm
Formula mass	1531.59
Crystal system	Triclinic
Space group	<i>P</i> -1
<i>a</i> /Å, <i>b</i> /Å, <i>c</i> /Å	10.833(3), 15.795(5), 20.169(6).
$\alpha$ /°, $\beta$ /°, $\gamma$ /°	76.45(3), 86.42(3), 72.08(2).
Unit cell volume/Å <sup>3</sup>	3192.09(16)
Temperature/K	200(2)
No. of formula units per unit cell, <i>Z</i>	2
Absorption correction	Integration
Absorption coefficient, $\mu$ /mm <sup>-1</sup>	1.890
No. of reflections measured	122656
No. of independent reflections	17229
<i>R</i> <sub>int</sub>	0.1120
Final <i>R</i> <sub>1</sub> values ( <i>I</i> > 2σ( <i>I</i> ))	0.0783
Final <i>wR</i> <sub>2</sub> values (all data)	0.2270
Goodness of fit	1.061

**5.2.32 [HNEt<sub>3</sub>]<sub>2</sub>[Lu(MnL<sup>5</sup>)<sub>2</sub>·(H<sub>2</sub>O)<sub>2</sub>·(ClO<sub>4</sub>)] (33)**

Chemical formula	C <sub>56</sub> H <sub>80</sub> ClLuMn <sub>2</sub> N <sub>10</sub> O <sub>18</sub>
Formula mass	1501.60
Crystal system	Triclinic
Space group	<i>P</i> -1
<i>a</i> /Å, <i>b</i> /Å, <i>c</i> /Å	10.841(3), 15.795(5), 20.249(6).
$\alpha$ /°, $\beta$ /°, $\gamma$ /°	76.40(3), 86.68(3), 71.99(2).
Unit cell volume/Å <sup>3</sup>	3204.63(16)
Temperature/K	200(2)
No. of formula units per unit cell, <i>Z</i>	2
Absorption correction	Integration
Absorption coefficient, $\mu$ /mm <sup>-1</sup>	2.034
No. of reflections measured	33484
No. of independent reflections	16960
<i>R</i> <sub>int</sub>	0.0594
Final <i>R</i> <sub>1</sub> values ( <i>I</i> > 2σ( <i>I</i> ))	0.0406
Final <i>wR</i> <sub>2</sub> values (all data)	0.1109
Goodness of fit	1.035

**5.2.33 [Dy{Ni(H<sub>2</sub>L<sup>5</sup>)(tren)}<sub>2</sub>·(H<sub>2</sub>O)<sub>14</sub>·(NO<sub>3</sub>)<sub>3</sub>] (34)**

Chemical formula	C <sub>56</sub> H <sub>112</sub> DyN <sub>19</sub> Ni <sub>2</sub> O <sub>35</sub>
Formula mass	1891.57
Crystal system	Triclinic
Space group	<i>P</i> -1
<i>a</i> /Å, <i>b</i> /Å, <i>c</i> /Å	14.879(9), 16.092(8), 18.612(10).
$\alpha$ /°, $\beta$ /°, $\gamma$ /°	102.70(4), 106.78(5), 103.58(4).
Unit cell volume/Å <sup>3</sup>	3944.0(4)
Temperature/K	100(2)
No. of formula units per unit cell, <i>Z</i>	2
Absorption correction	Integration
Absorption coefficient, $\mu$ /mm <sup>-1</sup>	1.509
No. of reflections measured	25544
No. of independent reflections	13541
<i>R</i> <sub>int</sub>	0.0860
Final <i>R</i> <sub>1</sub> values ( <i>I</i> > 2σ( <i>I</i> ))	0.0754
Final <i>wR</i> <sub>2</sub> values (all data)	0.1225
Goodness of fit	0.855

## 6 Summary / Zusammenfassung

### 6.1 Summary

This research work deals with the synthesis of heterobimetallic coordination compounds composed of transition metal ions and rare earth elements that are supported by salen ligands. These compounds offer opportunities to study areas such as gas adsorption, catalysis and magnetic properties. Generally, a salen ligand is synthesized from an amine and a carbonyl compound (*e.g.* aldehydes, ketones) *via* a condensation reaction to give an imine. For this purpose, the salen ligands, *N,N'*-bis(4-carboxysalicylidene)ethylenediamine ( $H_4L$ ), *N,N'*-bis(4-carboxysalicylidene)propanediamine ( $H_4L^2$ ), *N,N'*-bis(4-carboxysalicylidene)-1,3-diamino-2-propanol ( $H_5L^3$ ), *N,N'*-bis(4-hydroxysalicylidene)-1,3-diamino-2-propanol ( $H_5L^4$ ), were initially synthesized *via* a condensation reaction. The hitherto unknown cage compound *N,N'*-bis{[2-hydroxy-3-carboxybenzylidene]aminoethyl}aminoethylamine ( $H_4L^5$ ) was prepared *in situ* as a proligand.

The treatment of  $H_4L$  with transition metal salts in the presence of NaOH or LiOH leads to the 2D ICPs,  $[Na_4(ML)_2 \cdot (H_2O)_9]_n$  ( $M = Ni$  (**1**),  $Cu$  (**2**)), and 1D ICP,  $[Li\{(NiHL)\}(DMSO)]_n$  (**3**). The nickel and copper metal atoms show square planer geometry. The structures of **1** and **2** are built from 1D zig-zag chains along the *c* axis through metal salen (ML) and sodium atoms. The second sodium atom incorporates in such a way as to extend the structure along the *a* axis, forming a 2D layer. In contrast, the structure of **3** is based on 1D chains that interact with each other through hydrogen bonding and  $\pi$ - $\pi$ -stacking interactions, resulting in a 3D supramolecular structure. Compounds **1-3** are thermally robust, as proved by thermogravimetric analysis (TGA). The magnetic studies of compound **2** suggest that weak antiferromagnetic interactions are present in each dinuclear motif. The slightly modified  $H_4L^2$  and  $H_5L^3$  ligands were reacted with transition metal salts, which, in the presence of NaOH, give the novel 2D polymeric compounds,  $[Na_5\{(NiL^2)(HCOO)(H_2O)_{11}\} \cdot (H_2O)_4]_n$  (**4**) and  $[Na_4(CuHL^3)_2MeOH)_2(H_2O) \cdot (Et_2O)]_n$  (**5**). Compound **4**, has both square pyramidal geometry and distorted octahedral coordination environment around the Ni(II) ions, while the Cu(II) ion in compound **5** is exclusively coordinated in a square pyramidal fashion. The magnetic properties of compound **4** reveal antiferromagnetic interactions between the metal centers. The treatment of  $[Na_4(NiL)_2 \cdot (H_2O)_9]_n$  (**1**) with  $Ln(NO_3)_3 \cdot (H_2O)_m$  ( $m = 4$  (Lu), 5 (Er, Dy), 6 (Tm, Yb)) afforded the microporous lanthanide-nickel-based metal organic frameworks,  $[\{Ln_2(NiL)_3(DMF)(H_2O)_3\} \cdot (DMF)_4 \cdot (H_2O)_{10}]_n$  ( $Ln = Er$  (**6**), Tm (**7**), Yb (**8**) and Lu (**9**)).

Moreover, aqueous lanthanide nitrate (Ln = Dy and Yb) was added to the *in situ* reaction used to prepare compound **1**, resulting in the polymeric compounds,  $[\text{Dy}\{(\text{NiL})(\text{DMSO})(\text{NO}_3)\}(\text{H}_2\text{O})_2 \cdot (\text{DMSO})]_n$  (**10**) and  $[\text{Na}_3\text{Yb}\{(\text{NiL})(\text{H}_2\text{O})\}_3 \cdot (\text{DMF})]_n$  (**11**). In these complexes, the nickel-salen unit acts as flexible strut. The shape of the network is strongly influenced by the ionic radius of the lanthanide element as well as the reaction conditions. The thermogravimetric analysis of compound **6-11** shows that the compounds are stable, but thermal removal of the solvent molecules leads to decomposition of the frameworks. The magnetic susceptibility studies of compounds **6**, **9** and **10** suggest the presence of weak antiferromagnetic interactions between the lanthanide ions. The magnetic relaxation of compounds **6**, **9** and **10** were tested using ac susceptibility measurements under zero dc field, but only compound **10** exhibited a non-zero frequency dependence of out-of-phase components below 12 K, indicating slow relaxation of magnetization under zero dc field.

The reaction of  $\text{H}_4\text{L}$ ,  $\text{MnCl}_2 \cdot (\text{H}_2\text{O})_4$  and  $\text{Ln}(\text{NO}_3)_3 \cdot (\text{H}_2\text{O})_m$  ( $m = 5$  (Nd, Eu, Gd, Dy), 6 (Tb)) in DMF / Py gave the lanthanide-manganese-based metal organic frameworks,  $[\text{Ln}_2(\text{MnLCl})_2(\text{NO}_3)_2(\text{DMF})_5 \cdot (\text{DMF})_4]_n$  ((Ln = Nd (**12**), Eu (**13**), Gd (**14**), Tb (**15**) and Dy (**16**)). The structures of **12-16** are 1D chains along the *a* axis through manganese-salen moiety and lanthanide ions, which also interact with neighboring chains along the *c* axis by  $\pi$ - $\pi$ -stacking to form 2D polymers. The thermogravimetry studies of compounds **12-16** suggest that all the compounds are very robust. Guest solvent molecules are present in the void space, which was observed from thermogravimetric analysis.

Using  $\text{FeCl}_3 \cdot (\text{H}_2\text{O})_6$  instead of  $\text{MnCl}_2 \cdot (\text{H}_2\text{O})_4$  afforded the compounds,  $[\text{Ln}_2(\text{FeLCl})_2(\text{NO}_3)_2(\text{DMF})_5 \cdot (\text{DMF})_4]_n$  (Ln = Y (**17**), Eu (**18**), Gd (**19**), Tb (**20**) and Dy (**21**)). The repeating unit of the polymeric compounds,  $[\text{Ln}_2(\text{FeLCl})_2(\text{NO}_3)_2(\text{DMF})_5 \cdot (\text{DMF})_4]_n$ , consist of two iron and two lanthanide ions. The structure of **17-21** consists of 1D chains along the *a* axis. The 1D chains is also interact with neighboring chains along *c* axis by  $\pi$ - $\pi$ -stacking, to form 2D iron-lanthanide based polymers. The magnetic susceptibilities of compounds **19-21** at room temperature are 25.30, 33.06 and 37.67  $\text{cm}^3\text{K/mol}$ , respectively. The observed decrease of the  $\chi T$  value with decreasing temperature is due to weak antiferromagnetic interactions between the lanthanide ions.

By using the  $\text{H}_5\text{L}^4$  ligand, the trinuclear Mn(III) and Ni(II) complexes of composition  $[\text{Mn}_3\{(\text{H}_2\text{L}^4)(\text{HL}^4)(\text{OMe})_2(\text{MeOH})_2\} \cdot (\text{MeOH})_4]$  (**22**) and  $[\text{Ni}_3(\text{H}_3\text{L}^4)_2(\text{OAc})_2(\text{DMF})_2 \cdot (\text{H}_2\text{O})_3]$



(**23**) were prepared. It was observed that compound **22** has three Mn(III) ion that form a triangle, and compound **23** contains a linear nickel trimer unit. The magnetic measurement of the two trinuclear complexes show that an antiferromagnetic interaction is present due to close proximity of the neighboring metal centers.

The *in situ* formation of the hitherto unknown cage  $H_4L^5$  ligand with  $Ln(NO_3)_3 \cdot (H_2O)_m$  ( $m = 5$  (Eu, Dy),  $6$  (Tb, Er, Ho)) afforded the mononuclear lanthanide compounds,  $[Ln(H_2L^5)_2 \cdot (EtOH) \cdot (H_2O)_x \cdot (NO_3)]$  ( $x = 9$ ; Ln = Eu (**24**) and  $x = 8$ ; Ln = Tb (**25**), Dy (**26**), Er (**27**), Tm (**28**)). In these compounds, the geometry around the eight-fold coordinated lanthanides is a distorted square antiprism. Magnetic properties of compounds **25** and **26** show different kind of magnetic behavior: compound **26** exhibits slow relaxation of magnetization as a SMM, but for compound **25** shows no magnetic slow relaxation.

The treatment of  $H_4L^5$  (*in situ* generation),  $Mn(ClO_4)_2 \cdot (H_2O)_6$  with  $Ln(NO_3)_3 \cdot (H_2O)_m$  ( $m = 5$  (Eu, Gd, Dy),  $6$  (Tm, Lu)) in the presence of triethylamine afforded the trinuclear compounds,  $[HNEt_3]_2[Ln(MnL^5)_2 \cdot (H_2O)_x \cdot (ClO_4)]$  ( $x = 2$ ; Ln = Eu (**29**), Gd (**30**), Dy (**31**), Lu (**33**) and  $x = 4$ ; Ln = Tm (**32**)). Compounds **29-33** were also synthesized from isolated mononuclear lanthanide complexes  $[\{Ln(H_2L^5)_2\} \cdot (NO_3) \cdot (H_2O)_8 \cdot (EtOH)]$  by simply reacting with  $Mn(ClO_4)_2 \cdot (H_2O)_6$  in the presence of TEA, forming mononuclear to linear trinuclear 3d-4f complexes. Magnetic measurements of compounds **30-31** indicate the presence of ferromagnetic interactions within the heterometallic core. In contrast to compounds **30-31**, compound **32** shows antiferromagnetic interaction within the heterometallic core.

The treatment of 3-formylsalicylic acid, tris(2-aminoethyl)amine (tren) with  $Ni(NO_3)_2 \cdot (H_2O)_6$  and  $Dy(NO_3)_3 \cdot (H_2O)_5$  in the presence of triethylamine in methanol / water afforded the trinuclear mixed 3d-4f complex,  $[Dy\{Ni(H_2L^5)(tren)\}_2 \cdot (NO_3)_3 \cdot (H_2O)_{14}]$  (**34**). In this complex, the Dy(III) is present in the center and two Ni(II) are on the two sides. Magnetic studies show that there are weak antiferromagnetic interactions between Ni(II) and Dy(III) ions.

## 6.2 Zusammenfassung

Die vorliegende Arbeit befasst sich mit der Synthese von heterobimetallischen Koordinationsverbindungen, die sich aus Übergangsmetallen und Seltenen Erden zusammensetzen, welche durch Salenliganden zusammengehalten werden. Diese Verbindungen ermöglichen unter anderem die Untersuchungen von Gas Adsorption, Katalyse und magnetischer Eigenschaften. Im Allgemeinen werden Salene über eine Kondensationsreaktion zwischen einem Amin und einer Carbonylverbindung (z.B. Aldehyde, Ketone) synthetisiert. Auf diesem Weg konnten die Salenliganden *N,N'*-bis(4-carboxysalicyliden)ethylendiamin ( $H_4L$ ), *N,N'*-Bis(4-carboxy-salicyliden)propandiamin ( $H_4L^2$ ), *N,N'*-Bis(4-carboxysalicyliden)-1,3-diamino-2-propanol ( $H_5L^3$ ), *N,N'*-Bis(4-hydroxysalicyliden)-1,3-diamino-2-propanol ( $H_5L^4$ ) erhalten werden. Die bisher unbekannte Käfigverbindung *N,N'*-Bis{[2-hydroxy-3-carboxybenzyliden]aminoethyl}-aminoethylamine) ( $H_4L^5$ ) wurde zur Verwendung als Proligand *in situ* dargestellt.

Die Umsetzung von  $H_4L$  mit Übergangsmetallen in Anwesenheit von NaOH oder LiOH führt zu zweidimensionalen ICPs des Typs  $[Na_4(ML)_2 \cdot (H_2O)_9]_n$  ( $M = Ni$  (**1**),  $Cu$  (**2**)), und dem eindimensionalen ICP,  $[Li\{(NiHL)\}(DMSO)]_n$  (**3**), in welchen die Nickel- und Kupferatome quadratisch-planar koordiniert sind. Die Strukturen von **1** und **2** setzen sich aus eindimensionalen Zick-Zack-Ketten, bestehend aus Metallsalenen (ML) und Natriumatomen, entlang der *c*-Achse zusammen. Das zweite Natriumatom wird so eingelagert, dass die Struktur entlang der *a*-Achse erweitert und somit eine zweidimensionale Schicht gebildet wird. Im Gegensatz dazu basiert die Struktur von **3** auf eindimensionalen Ketten, welche über Wasserstoffbrücken und  $\pi$ - $\pi$ -Stacking wechselwirken, woraus eine dreidimensionale supramolekulare Struktur resultiert. Die Verbindungen **1-3** sind thermisch robust, was durch thermogravimetrische Analysen (TGA) nachgewiesen wurde. Die magnetischen Eigenschaften von **2** deuten auf eine schwach antiferromagnetische Wechselwirkung in jedem dinuklearen Motiv hin. Die geringfügig modifizierten Liganden  $H_4L^2$  und  $H_5L^3$  wurden ebenfalls mit Übergangsmetallsalzen in Anwesenheit von NaOH und LiOH umgesetzt. Dies führte zu neuartigen zweidimensionalen Polymeren der Zusammensetzung  $[Na_5\{(NiL^2)(HCOO)(H_2O)_{11}\} \cdot (H_2O)_4]_n$  (**4**) und  $[Na_4(CuHL^3)_2(MeOH)_2(H_2O) \cdot (Et_2O)]_n$  (**5**). In Verbindung **4** sind die Ni(II)-Ionen quadratisch-pyramidal und verzerrt oktaedrisch koordiniert, wogegen die Cu(II)-Ionen in **5** ausschließlich eine quadratisch-pyramidale Koordinationsgeometrie aufweisen. Die magnetischen Eigenschaften von **4** zeigen eine

antiferromagnetische Kopplung zwischen den Metallzentren. Die Umsetzung von  $[\text{Na}_4(\text{NiL})_2 \cdot (\text{H}_2\text{O})_9]_n$  (**1**) mit  $\text{Ln}(\text{NO}_3)_3 \cdot (\text{H}_2\text{O})_m$  ( $m = 4$  (Lu), 5 (Er, Dy), 6 (Tm, Yb)) führte zu mikroporigen lanthanoid-nickel-basierten metallorganischen Netzwerken (MOFs),  $[\{\text{Ln}_2(\text{NiL})_3(\text{DMF})(\text{H}_2\text{O})_3\} \cdot (\text{DMF})_4 \cdot (\text{H}_2\text{O})_{10}]_n$  ( $\text{Ln} = \text{Er}$  (**6**), Tm (**7**), Yb (**8**), and Lu (**9**)). Zudem wurden durch Zugabe von wasserhaltigen Lanthanoidnitraten ( $\text{Ln} = \text{Dy}$  und Yb) zu der *in situ* dargestellten Verbindung **1** die polymeren Verbindungen  $[\text{Dy}\{(\text{NiL})(\text{DMSO})(\text{NO}_3)\}(\text{H}_2\text{O})_2 \cdot (\text{DMSO})]_n$  (**10**) und  $[\text{Na}_3\text{Yb}\{(\text{NiL})(\text{H}_2\text{O})\}_3 \cdot (\text{DMF})]_n$  (**11**) erhalten. In diesen Komplexen dient die Nickel-Salen-Einheit als flexibler Linker. Die Struktur des Netzwerkes ist stark durch den Ionenradius des Lanthanoids, sowie die Reaktionsbedingungen beeinflusst. Die thermogravimetrischen Analysen der Verbindungen **6-11** zeigen, dass die Verbindungen zwar stabil sind, die Netzwerke jedoch bei Erhitzen die Lösungsmittelmoleküle abgeben und sich dadurch zersetzen. Die magnetischen Suszeptibilitäten der Verbindungen **6**, **9** und **10** weisen auf eine schwache antiferromagnetische Kopplung zwischen den Lanthanoidionen hin. Die magnetischen Relaxationen von **6**, **9** und **10** wurden mittels AC-Suszeptibilitätsmessungen bei DC-Nullfeld bestimmt. Dabei zeigte jedoch nur die Verbindung **10** eine Frequenzabhängigkeit der gegenphasigen Komponenten unter 12 K, was auf eine langsame Relaxation der Magnetisierung unter DC-Nullfeld hinweist.

Die reaktion von  $\text{H}_4\text{L}$ ,  $\text{MnCl}_2 \cdot (\text{H}_2\text{O})_4$  und  $\text{Ln}(\text{NO}_3)_3 \cdot (\text{H}_2\text{O})_m$  ( $m = 5$  (Nd, Eu, Gd, Dy), 6 (Tb)) in einem DMF-Pyridin-Gemisch führte zu lanthanoid-mangan-basierten MOFs,  $[\text{Ln}_2(\text{MnLCl})_2(\text{NO}_3)_2(\text{DMF})_5 \cdot (\text{DMF})_4]_n$  ( $\text{Ln} = \text{Nd}$  (**12**), Eu (**13**), Gd (**14**), Tb (**15**) und Dy (**16**)). Die Verbindungen **12-16** bilden entlang der *a*-Achse eindimensionale Ketten aus Mangan-Salen-Einheiten und Lanthanoid-Ionen, welche mit den benachbarten Schichten entlang der *c*-Achse durch  $\pi$ - $\pi$ -Wechselwirkung zu zweidimensionalen Polymere verbunden werden. Thermogravimetrische Studien von **12-16** deuten auf eine hohe thermische Stabilität hin und zeigen, dass sich in den vorhandenen Hohlräumen noch Lösungsmittelmoleküle befinden.

Verwendet man  $\text{FeCl}_3 \cdot (\text{H}_2\text{O})_6$  anstatt des  $\text{MnCl}_2 \cdot (\text{H}_2\text{O})_4$  erhält man die Verbindungen  $[\text{Ln}_2(\text{FeLCl})_2(\text{NO}_3)_2(\text{DMF})_5 \cdot (\text{DMF})_4]_n$  ( $\text{Ln} = \text{Y}$  (**17**), Eu (**18**), Gd (**19**), Tb (**20**) and Dy (**21**)). Die sich wiederholende Einheit der polymeren Verbindungen,  $[\text{Ln}_2(\text{FeLCl})_2(\text{NO}_3)_2(\text{DMF})_5 \cdot (\text{DMF})_4]_n$ , besteht aus zwei Eisen- und zwei Lanthanoid-Ionen. Die Strukturen von **17-21** bestehen aus eindimensionalen Ketten entlang der *a*-Achse. Diese Ketten wechselwirken entlang der *c*-Achse mit Nachbarketten über  $\pi$ - $\pi$ -Stacking, wodurch zweidimensionale eisen-

lanthanoid-basierte Polymere entstehen. Die magnetischen Suszeptibilitäten der Verbindungen **19-21** bei Raumtemperatur betragen 25.30, 33.06, bzw. 37.76 cm<sup>3</sup>K/mol. Die beobachtete Erhöhung der  $\chi T$ -Werte mit steigender Temperatur ist durch schwache antiferromagnetische Wechselwirkung zwischen den Lanthanoid-Ionen bedingt.

Durch Verwendung des H<sub>5</sub>L<sup>4</sup>-Liganden konnten die trinuklearen Mn(III)- und Ni(II)-Komplexe der Zusammensetzung [Mn<sub>3</sub>{(H<sub>2</sub>L<sup>4</sup>)(HL<sup>4</sup>)(OMe)<sub>2</sub>(MeOH)<sub>2</sub>}(MeOH)<sub>4</sub>] (**22**) und [Ni<sub>3</sub>(H<sub>3</sub>L<sup>4</sup>)<sub>2</sub>(OAc)<sub>2</sub>(DMF)<sub>2</sub>(H<sub>2</sub>O)<sub>3</sub>] (**23**) erhalten werden. Es wurde beobachtet, dass in Verbindung **22** drei Mn(III)-Ionen ein Dreieck bilden, während in Verbindung **23** eine lineares Nickel-Trimer vorliegt. Die magnetischen Messungen der beiden trinuklearen Komplexe weisen aufgrund der direkten Nachbarschaft der Metallzentren antiferromagnetische Wechselwirkung auf.

Bei der Umsetzung des *in situ*-gebildeten, bisher unbekanntes Käfig-Liganden H<sub>4</sub>L<sup>5</sup> mit Ln(NO<sub>3</sub>)<sub>3</sub>·(H<sub>2</sub>O)<sub>m</sub> (m = 5 (Eu, Dy), 6 (Tb, Er, Ho)) führte zur Bildung mononuklearer Lanthanoid-Verbindungen, [Ln(H<sub>2</sub>L<sup>5</sup>)<sub>2</sub>·(EtOH)·(H<sub>2</sub>O)<sub>x</sub>·(NO<sub>3</sub>)<sub>3</sub>] (x = 9; Ln = Eu (**24**) und x = 8; Ln = Tb (**25**), Dy (**26**), Er (**27**), Tm (**28**)). In diesen Verbindungen sind die Lanthanoid-Ionen verzerrt quadratisch antiprismatisch umgeben. Die magnetischen Eigenschaften der Verbindungen **25** und **26** zeigen unterschiedliches magnetisches Verhalten: Verbindung **26** weist wie ein SMM eine langsame Relaxation der Magnetisierung auf, Verbindung **25** zeigt keine langsame magnetische Relaxation.

Die Reaktion von H<sub>4</sub>L<sup>5</sup>, Mn(ClO<sub>4</sub>)<sub>2</sub>·(H<sub>2</sub>O)<sub>6</sub> und Ln(NO<sub>3</sub>)<sub>3</sub>·(H<sub>2</sub>O)<sub>m</sub> (m = 5 (Eu, Gd, Dy), 6 (Tm, Lu)) in Gegenwart von Triethylamin führte zu den trinuklearen Verbindungen [HNEt<sub>3</sub>]<sub>2</sub>[Ln(MnL<sup>5</sup>)<sub>2</sub>·(H<sub>2</sub>O)<sub>x</sub>·(ClO<sub>4</sub>)<sub>4</sub>] (x = 2; Ln = Eu (**29**), Gd (**30**), Dy (**31**), Lu (**33**) und x = 4; Ln = Tm (**32**)). Die Verbindungen **29-33** konnten auch aus dem isolierten mononuklearen Lanthanoidkomplex [Ln(H<sub>2</sub>L<sup>5</sup>)<sub>2</sub>·(NO<sub>3</sub>)·(H<sub>2</sub>O)<sub>8</sub>·(EtOH)] durch einfache Umsetzung mit Mn(ClO<sub>4</sub>)<sub>2</sub>·(H<sub>2</sub>O)<sub>6</sub> in Gegenwart von TEA, unter Bildung mononuklearer bis linear trinuklearer 3d-4f-Komplexe, synthetisiert werden. Magnetische Messungen der Verbindungen **30-31** weisen auf ferromagnetische Wechselwirkungen im heterometallischen Kern hin. Im Gegensatz dazu liegt in Verbindung **32** eine antiferromagnetische Wechselwirkung zwischen den Metallatomen vor.

Die Umsetzung von 3-Formylsalicylsäure und Tris-(2-aminoethyl)amin (tren) mit Ni(NO<sub>3</sub>)<sub>2</sub>·(H<sub>2</sub>O)<sub>6</sub> und Dy(NO<sub>3</sub>)<sub>2</sub>·(H<sub>2</sub>O)<sub>5</sub> in Anwesenheit von Triethylamin in einem Methanol / Wasser-Gemisch führt zum trinuklearen 3d-4f-Komplex,

---

[Dy{Ni(H<sub>2</sub>L<sup>5</sup>)(tren)}<sub>2</sub>·(NO<sub>3</sub>)<sub>3</sub>·(H<sub>2</sub>O)<sub>14</sub>] (**34**). In diesem Komplex liegen das Dy(III)-Ion im Zentrum und die beiden Nickelatome an den beiden Seiten. Magnetische Untersuchungen zeigen, dass eine schwache antiferromagnetische Kopplung zwischen den Ni(II)- und Dy(III)-Ionen vorliegt.

## 7 References

- [1] K. H. Wedepohl, *Geochim. Cosmochim. Acta* **1995**, *59*, 1217.
- [2] Y. U. Tang, X. Gan, W. Liu, N. Tang, M. Tan, K. Yu, *Polyhedron* **1996**, *15*, 2607.
- [3] G. Meyer, *Chem. Rev.* **1988**, *88*, 93.
- [4] D. A. Johnson, *J. Chem. Ed.* **1980**, *57*, 475.
- [5] B. E. Douglas, *J. Chem. Ed.* **1954**, *31*, 598.
- [6] J.-C. G. Bünzli, in *Rare Earths* (Eds.: R. Saez-Puche, P. Caro), Editorial Complutense, Madrid, **1998**, 223.
- [7] G. E. Buono-core, H. Li, B. Marciniak, *Coord. Chem. Rev.* **1990**, *99*, 55.
- [8] W. D. Horrocks, D. R. Sudnick, *Acc. Chem. Res.* **1981**, *14*, 384.
- [9] N. Sabbatini, M. Guardigli, J.-M. Lehn, *Coord. Chem. Rev.* **1993**, *123*, 201.
- [10] D. Parker, *Chem. Rev.* **1991**, *91*, 1441.
- [11] P. Caravan, J. J. Ellison, T. J. McMurry, R. B. Lauffer, *Chem. Rev.* **1999**, *99*, 2293.
- [12] F. Edelmann, *Top. Curr.* **1996**, *179*, 247.
- [13] M. Komiyama, N. Takeda, H. Shigekawa, *Chem. Commun.* **1999**, 1443.
- [14] S. Qiu, G. Zhu, *Coord. Chem. Rev.* **2009**, *253*, 2891.
- [15] R. Sessoli, A. K. Powell, *Coord. Chem. Rev.* **2009**, *253*, 2328.
- [16] R. L. Griffith, *J. Chem. Phys.* **1943**, *11*, 499.
- [17] E. A. Tomic, *J. Appl. Poly. Sci.* **1965**, *9*, 3745.
- [18] R. Robson, *J. Chem. Soc., Dalton Trans.* **2000**, 3735.
- [19] M. Eddaoudi, J. Kim, N. Rosi, D. Vodak, J. Wachter, M. O'Keeffe, O. M. Yaghi, *Science* **2002**, *295*, 469.
- [20] H. K. Chae, D. Y. Siberio-Perez, J. Kim, Y. Go, M. Eddaoudi, A. J. Matzger, M. O'Keeffe, O. M. Yaghi, *Nature* **2004**, *427*, 523.
- [21] B. Moulton, J. Lu, A. Mondal, M. Z. Zaworotko, *Chem. Commun.* **2001**, 863.
- [22] G. Férey, C. Mellot-Draznieks, C. Serre, F. Millange, *Acc. Chem. Res.* **2005**, *38*, 217.
- [23] O. M. Yaghi, M. O'Keeffe, N. W. Ockwig, H. K. Chae, M. Eddaoudi, J. Kim, *Nature* **2003**, *423*, 705.
- [24] R. J. Hill, D.-L. Long, N. R. Champness, P. Hubberstey, M. Schröder, *Acc. Chem. Res.* **2005**, *38*, 335.
- [25] D. Bradshaw, J. E. Warren, M. J. Rosseinsky, *Science* **2007**, *315*, 977.
- [26] N. L. Rosi, J. Kim, M. Eddaoudi, B. Chen, M. O'Keeffe, O. M. Yaghi, *J. Am. Chem. Soc.* **2005**, *127*, 1504.

- [27] M. Eddaoudi, *J. Am. Chem. Soc.* **2001**, *123*, 4368.
- [28] H. Li, M. Eddaoudi, M. O'Keeffe, O. M. Yaghi, *Nature* **1999**, *402*, 276.
- [29] S. S. Kaye, A. Dailly, O. M. Yaghi, J. R. Long, *J. Am. Chem. Soc.* **2007**, *129*, 14176.
- [30] L. Ma, D. J. Mihalcik, W. Lin, *J. Am. Chem. Soc.* **2009**, *131*, 4610.
- [31] S. Shimomura, M. Higuchi, R. Matsuda, K. Yoneda, Y. Hijikata, Y. Kubota, Y. Mita, J. Kim, M. Takata, S. Kitagawa, *Nat Chem* **2010**, *2*, 633.
- [32] J.-R. Li, R. J. Kuppler, H.-C. Zhou, *Chem. Soc. Rev.* **2009**, *38*, 1477.
- [33] M. Kurmoo, *Chem. Soc. Rev.* **2009**, *38*, 1353.
- [34] M. D. Allendorf, C. A. Bauer, R. K. Bhakta, R. J. T. Houk, *Chem. Soc. Rev.* **2009**, *38*, 1330.
- [35] P. Horcajada, C. Serre, M. Vallet-Regí, M. Sebban, F. Taulelle, G. Férey, *Angew. Chem. Int. Ed.* **2006**, *118*, 6120.
- [36] P. Horcajada, C. Serre, G. Maurin, N. A. Ramsahye, F. Balas, M. a. Vallet-Regí, M. Sebban, F. Taulelle, G. r. Férey, *J. Am. Chem. Soc.* **2008**, *130*, 6774.
- [37] W.-X. Zhang, Y.-Y. Yang, S.-B. Zai, S. Weng Ng, X.-M. Chen, *Eur. J. Inorg. Chem.* **2008**, *2008*, 679.
- [38] Q.-R. Fang, G.-S. Zhu, Z. Jin, Y.-Y. Ji, J.-W. Ye, M. Xue, H. Yang, Y. Wang, S.-L. Qiu, *Angew. Chem. Int. Ed.* **2007**, *46*, 6638.
- [39] X. Shi, G. Zhu, S. Qiu, K. Huang, J. Yu, R. Xu, *Angew. Chem. Int. Ed.* **2004**, *43*, 6482.
- [40] Z. Ni, R. I. Masel, *J. Am. Chem. Soc.* **2006**, *128*, 12394.
- [41] M. D. Hobday, T. D. Smith, *Coord. Chem. Rev.* **1973**, *9*, 311.
- [42] V. K. Gupta, A. K. Singh, B. Gupta, *Anal. Chim. Acta* **2006**, *575*, 198.
- [43] E. N. Jacobsen, *Acc. Chem. Res.* **2000**, *33*, 421.
- [44] S. B. Ogunwumi, T. Bein, *Chem. Commun.* **1997**, 901.
- [45] T. D. Pasatoiu, A. M. Madalan, M. U. Kumke, C. Tiseanu, M. Andruh, *Inorg. Chem.* **2010**, *49*, 2310.
- [46] C. Coulon, H. Miyasaka, R. Clérac, *Top. Curr.* **2006**, *122*, 163.
- [47] R. Kitaura, G. Onoyama, H. Sakamoto, R. Matsuda, S.-i. Noro, S. Kitagawa, *Angew. Chem. Int. Ed.* **2004**, *43*, 2684.
- [48] S.-i. Noro, S. Kitagawa, M. Yamashita, T. Wada, *Chem. Commun.* **2002**, 222.
- [49] Y.-M. Jeon, J. Heo, C. A. Mirkin, *J. Am. Chem. Soc.* **2007**, *129*, 7480.
- [50] J. Heo, Y.-M. Jeon, C. A. Mirkin, *J. Am. Chem. Soc.* **2007**, *129*, 7712.
- [51] G. Yuan, C. Zhu, W. Xuan, Y. Cui, *Chem. Eur. J.* **2009**, *15*, 6428.

- [52] S.-S. Sun, C. L. Stern, S. T. Nguyen, J. T. Hupp, *J. Am. Chem. Soc.* **2004**, *126*, 6314.
- [53] Kathryn E. Splan, Aaron M. Massari, Gregory A. Morris, S.-S. Sun, E. Reina, SonBinh T. Nguyen, Joseph T. Hupp, *Eur. J. Inorg. Chem.* **2003**, *2003*, 2348.
- [54] S.-H. Cho, B. Ma, S. T. Nguyen, J. T. Hupp, T. E. Albrecht-Schmitt, *Chem. Commun.* **2006**, 2563.
- [55] B. Chen, X. Zhao, A. Putkham, K. Hong, E. B. Lobkovsky, E. J. Hurtado, A. J. Fletcher, K. M. Thomas, *J. Am. Chem. Soc.* **2008**, *130*, 6411.
- [56] F. Song, C. Wang, J. M. Falkowski, L. Ma, W. Lin, *J. Am. Chem. Soc.* **2010**, *132*, 15390.
- [57] D. Gatteschi, R. Sessoli, *Angew. Chem. Int. Ed.* **2003**, *42*, 268.
- [58] P. D. W. Boyd, Q. Li, J. B. Vincent, K. Folting, H. R. Chang, W. E. Streib, J. C. Huffman, G. Christou, D. N. Hendrickson, *J. Am. Chem. Soc.* **1988**, *110*, 8537.
- [59] W. Wernsdorfer, R. Sessoli, *Science* **1999**, *284*, 133.
- [60] M. N. Leuenberger, D. Loss, *Nature* **2001**, *410*, 789.
- [61] S. M. J. Aubin, N. R. Dilley, L. Pardi, J. Krzystek, M. W. Wemple, L.-C. Brunel, M. B. Maple, G. Christou, D. N. Hendrickson, *J. Am. Chem. Soc.* **1998**, *120*, 4991.
- [62] R. Bircher, G. Chaboussant, C. Dobe, H. U. Güdel, S. T. Ochsenbein, A. Sieber, O. Waldmann, *Adv. Funct. Mater.* **2006**, *16*, 209.
- [63] T. Lis, *Acta Crystallogr. Sec. B* **1980**, *36*, 2042.
- [64] R. Sessoli, D. Gatteschi, A. Caneschi, M. A. Novak, *Nature* **1993**, *365*, 141.
- [65] R. Sessoli, H. L. Tsai, A. R. Schake, S. Wang, J. B. Vincent, K. Folting, D. Gatteschi, G. Christou, D. N. Hendrickson, *J. Am. Chem. Soc.* **1993**, *115*, 1804.
- [66] L. Thomas, F. Lioni, R. Ballou, D. Gatteschi, R. Sessoli, B. Barbara, *Nature* **1996**, *383*, 145.
- [67] R. Bagai, G. Christou, *Chem. Soc. Rev.* **2009**, *38*, 1011.
- [68] P.-H. Lin, T. J. Burchell, R. Clérac, M. Murugesu, *Angew. Chem. Int. Ed.* **2008**, *47*, 8848.
- [69] Y. Ma, G.-F. Xu, X. Yang, L.-C. Li, J. Tang, S.-P. Yan, P. Cheng, D.-Z. Liao, *Chem. Commun.* **2010**, *46*, 8264.
- [70] P.-H. Lin, T. J. Burchell, L. Ungur, L. F. Chibotaru, W. Wernsdorfer, M. Murugesu, *Angew. Chem. Int. Ed.* **2009**, *48*, 9489.
- [71] T. Yamaguchi, J.-P. Costes, Y. Kishima, M. Kojima, Y. Sunatsuki, N. Bréfuel, J.-P. Tuchagues, L. Vendier, W. Wernsdorfer, *Inorg. Chem.* **2010**, *49*, 9125.



- [72] T. C. Stamatatos, S. J. Teat, W. Wernsdorfer, G. Christou, *Angew. Chem. Int. Ed.* **2009**, *121*, 529.
- [73] (a) V. M. Mereacre, A. M. Ako, R. Clérac, W. Wernsdorfer, G. Filoti, J. Bartolomé, C. E. Anson, A. K. Powell, *J. Am. Chem. Soc.* **2007**, *129*, 9248. (b) G. Abbas, Y. Lan, V. Mereacre, W. Wernsdorfer, R. Clérac, G. Buth, M. T. Sougrati, F. Grandjean, G. J. Long, C. E. Anson, A. K. Powell, *Inorg. Chem.* **2009**, *48*, 9345.
- [74] (a) F. Mori, T. Nyui, T. Ishida, T. Nogami, K.-Y. Choi, H. Nojiri, *J. Am. Chem. Soc.* **2006**, *128*, 1440. (b) H. L. C. Feltham, R. Clérac, A. K. Powell, S. Brooker, *Inorg. Chem.* **2011**, *50*, 4232.
- [75] M. Oh, C. A. Mirkin, *Nature* **2005**, *438*, 651.
- [76] A. M. Spokoyny, D. Kim, A. Sumrein, C. A. Mirkin, *Chem. Soc. Rev.* **2009**, *38*, 1218.
- [77] B. F. Hoskins, R. Robson, *J. Am. Chem. Soc.* **1990**, *112*, 1546.
- [78] R. Robson, *Dalton Trans.* **2008**, 5113.
- [79] D. J. Tranchemontagne, J. L. Mendoza-Cortes, M. O'Keeffe, O. M. Yaghi, *Chem. Soc. Rev.* **2009**, *38*, 1257.
- [80] B. F. Hoskins, R. Robson, *J. Am. Chem. Soc.* **1989**, *111*, 5962.
- [81] M. Dincă, J. R. Long, *Angew. Chem. Int. Ed.* **2008**, *47*, 6766.
- [82] J. Lee, O. K. Farha, J. Roberts, K. A. Scheidt, S. T. Nguyen, J. T. Hupp, *Chem. Soc. Rev.* **2009**, *38*, 1450.
- [83] M. Oh, C. A. Mirkin, *Angew. Chem. Int. Ed.* **2006**, *45*, 5492.
- [84] X. Liu, *Angew. Chem. Int. Ed.* **2009**, *48*, 3018.
- [85] S. S. Kaye, J. R. Long, *J. Am. Chem. Soc.* **2007**, *130*, 806.
- [86] S. Jung, M. Oh, *Angew. Chem. Int. Ed.* **2008**, *47*, 2049.
- [87] S. J. Wezenberg, A. W. Kleij, *Angew. Chem. Int. Ed.* **2008**, *47*, 2354.
- [88] E. M. McGarrigle, D. G. Gilheany, *Chem. Rev.* **2005**, *105*, 1563.
- [89] Y.-M. Jeon, J. Heo, C. A. Mirkin, *Tetrahedron Lett.* **2007**, *48*, 2591.
- [90] R. C. Lochan, M. Head-Gordon, *Phys. Chem. Chem. Phys.* **2006**, *8*, 1357.
- [91] A. Mavrandonakis, W. Klopper, *J. Phys. Chem. C* **2008**, *112*, 11580.
- [92] S. N. Poddar, *Z. Anorg. Allg. Chem.* **1963**, 322, 326.
- [93] O. Kahn, *Molecular Magnetism*, VCH Publishers Inc.: New York, **1993**.
- [94] P. W. Roesky, A. Bhunia, Y. Lan, A. K. Powell, S. Kureti, *Chem. Commun.* **2011**, *47*, 2035.
- [95] G. B. Deacon, M. Forsyth, P. C. Junk, S. G. Leary, G. J. Moxey, *Polyhedron* **2006**, *25*, 379.

- [96] Y. Wan, L. Jin, K. Wang, L. Zhang, X. Zheng, S. Lu, *New J. Chem.* **2002**, *26*, 1590.
- [97] H.-L. Jiang, N. Tsumori, Q. Xu, *Inorg. Chem.* **2010**, *49*, 10001.
- [98] A. W. Addison, T. N. Rao, J. Reedijk, J. van Rijn, G. C. Verschoor, *Journal of the Chemical Society, Dalton Trans.* **1984**, 1349.
- [99] T. Akitsu, Y. Hiroshima, S. Komorita, Y. Kushi, *Bull. Chem. Soc. Jpn.* **2001**, *74*, 507.
- [100] S. Sarkar, M. Nayak, M. Fleck, S. Dutta, U. Flörke, R. Koner, S. Mohanta, *Eur. J. Inorg. Chem.* **2010**, *2010*, 735.
- [101] Y. Huang, T. Liu, J. Lin, J. Lü, Z. Lin, R. Cao, *Inorg. Chem.* **2011**, *50*, 2191.
- [102] C. Benelli, D. Gatteschi, *Chem. Rev.* **2002**, *102*, 2369.
- [103] G. Abbas, Y. Lan, G. E. Kostakis, W. Wernsdorfer, C. E. Anson, A. K. Powell, *Inorg. Chem.* **2010**, *49*, 8067.
- [104] A. Thirumurugan, S. K. Pati, M. A. Green, S. Natarajan, *J. Mater. Chem.* **2003**, *13*, 2937.
- [105] J.-W. Ye, J. Wang, J.-Y. Zhang, P. Zhang, Y. Wang, *CrystEngComm* **2007**, *9*, 515.
- [106] A. Ouchi, Y. Suzuki, Y. Ohki, Y. Koizumi, *Coord. Chem. Rev.* **1988**, *92*, 29.
- [107] Y.-Y. Yang, W.-T. Wong, *Chem. Commun.* **2002**, 2716.
- [108] X. Guo, G. Zhu, F. Sun, Z. Li, X. Zhao, X. Li, H. Wang, S. Qiu, *Inorg. Chem.* **2006**, *45*, 2581.
- [109] S.-P. Chen, Y.-X. Ren, W.-T. Wang, S.-L. Gao, *Dalton Trans.* **2010**, *39*, 1552.
- [110] R. Hernández-Molina, A. Mederos, S. Dominguez, P. Gili, C. Ruiz-Pérez, A. Castiñeiras, X. Solans, F. Lloret, J. A. Real, *Inorg. Chem.* **1998**, *37*, 5102.
- [111] X. Wang, W. T. Pennington, D. L. Ankers, J. C. Fanning, *Polyhedron* **1992**, *11*, 2253.
- [112] I. D. Brown, D. Altermatt, *Acta Crystallogr. Sect. B* **1985**, *41*, 244.
- [113] H. H. Thorp, *Inorg. Chem.* **1992**, *31*, 1585.
- [114] P. Chaudhuri, R. Wagner, T. Weyhermüller, *Eur. J. Inorg. Chem.* **2010**, *2010*, 1339.
- [115] P. Chaudhuri, *Coord. Chem. Rev.* **2003**, *243*, 143.
- [116] C. Lampropoulos, K. A. Abboud, T. C. Stamatatos, G. Christou, *Inorg. Chem.* **2009**, *48*, 813.
- [117] P. L. Feng, D. N. Hendrickson, *Inorg. Chem.* **2010**, *49*, 6393.
- [118] S. Akine, T. Nabeshima, *Inorg. Chem.* **2005**, *44*, 1205.
- [119] D. J. Mackey, R. L. Martin, *J. Chem. Soc., Dalton Trans.* **1978**, 702.
- [120] F. Aquilante, L. De Vico, N. Ferré, G. Ghigo, P.-å. Malmqvist, P. Neogrady, T. B. Pedersen, M. Pitoňák, M. Reiher, B. O. Roos, L. Serrano-Andrés, M. Urban, V. Veryazov, R. Lindh, *J. Comput. Chem.* **2010**, *31*, 224.

- [121] L. F. Chibotaru, L. Ungur, C. Aronica, H. Elmoll, G. Pilet, D. Luneau, *J. Am. Chem. Soc.* **2008**, *130*, 12445.
- [122] L. Ungur, W. Van den Heuvel, L. F. Chibotaru, *New J. Chem.* **2009**, *33*, 1224.
- [123] N. Ishikawa, M. Sugita, W. Wernsdorfer, *J. Am. Chem. Soc.* **2005**, *127*, 3650.
- [124] M. Ferbinteanu, T. Kajiwara, K.-Y. Choi, H. Nojiri, A. Nakamoto, N. Kojima, F. Cimpoesu, Y. Fujimura, S. Takaishi, M. Yamashita, *J. Am. Chem. Soc.* **2006**, *128*, 9008.
- [125] F. Pointillart, K. Bernot, R. Sessoli, D. Gatteschi, *Chem. Eur. J.* **2007**, *13*, 1602.
- [126] N. Ishikawa, M. Sugita, W. Wernsdorfer, *Angew. Chem. Int. Ed.* **2005**, *117*, 2991.
- [127] S. Koizumi, M. Nihei, T. Shiga, M. Nakano, H. Nojiri, R. Bircher, O. Waldmann, S. T. Ochsenein, H. U. Güdel, F. Fernandez-Alonso, H. Oshio, *Chem. Eur. J.* **2007**, *13*, 8445.
- [128] D. Gatteschi, R. Sessoli, J. Villain, *Molecular Nanomagnets*, Oxford University Press, **2006**.
- [129] A. Bencini, C. Benelli, A. Caneschi, R. L. Carlin, A. Dei, D. Gatteschi, *J. Am. Chem. Soc.* **1985**, *107*, 8128.
- [130] A. Bencini, C. Benelli, A. Caneschi, A. Dei, D. Gatteschi, *Inorg. Chem.* **1986**, *25*, 572.
- [131] A. J. Stemmler, J. W. Kampf, M. L. Kirk, B. H. Atasi, V. L. Pecoraro, *Inorg. Chem.* **1999**, *38*, 2807.
- [132] M. Andruh, I. Ramade, E. Codjovi, O. Guillou, O. Kahn, J. C. Trombe, *J. Am. Chem. Soc.* **1993**, *115*, 1822.
- [133] A. Jana, S. Majumder, L. Carrella, M. Nayak, T. Weyhermueller, S. Dutta, D. Schollmeyer, E. Rentschler, R. Koner, S. Mohanta, *Inorg. Chem.* **2010**, *49*, 9012.
- [134] F. Z. C. Fella, J.-P. Costes, F. O. Dahan, C. Duhayon, G. Novitchi, J.-P. Tuchagues, L. Vendier, *Inorg. Chem.* **2008**, *47*, 6444.
- [135] A. M. Ako, V. Mereacre, R. Clérac, I. J. Hewitt, Y. Lan, G. Buth, C. E. Anson, A. K. Powell, *Inorg. Chem.* **2009**, *48*, 6713.
- [136] M. N. Akhtar, Y.-Z. Zheng, Y. Lan, V. Mereacre, C. E. Anson, A. K. Powell, *Inorg. Chem.* **2009**, *48*, 3502.
- [137] V. M. Mereacre, A. M. Ako, R. Clérac, W. Wernsdorfer, G. Filoti, J. Bartolomé, C. E. Anson, A. K. Powell, *J. Am. Chem. Soc.* **2007**, *129*, 9248.
- [138] A. Mishra, W. Wernsdorfer, K. A. Abboud, G. Christou, *J. Am. Chem. Soc.* **2004**, *126*, 15648.

- 
- [139] J.-P. Costes, F. Dahan, B. Donnadieu, M.-I. Fernandez-Garcia, M.-J. Rodriguez-Douton, *Dalton Trans.* **2003**, 3776.
- [140] B. Wu, *Dalton Trans.* **2006**, 5113.
- [141] J.-P. Costes, J. Garcia-Tojal, J.-P. Tuchagues, L. Vendier, *Eur. J. Chem.* **2009**, 2009, 3801.
- [142] The program POLY ANISO, L. F. Chibotaru, University of Leuven, **2006**.
- [143] Beside the dipolar magnetic contribution from  $S = 5/2$  of Mn1 and Mn2, there is also a contribution of the superexchange Mn1-Dy and Mn2-Dy interaction to  $\Delta_{nm}$ .
- [144] N. V. Prokofev, P. C. E. Stamp, *Phys. Rev. Lett.* **1998**, 80, 5794.
- [145] N. V. Prokofev, P. C. E. Stamp, *Rep. prog. Phys.* **2000**, 63, 669.
- [146] G. Sheldrick, *Acta Crystallogr. Sec. A* **2008**, 64, 112.

## 8 Appendices

### A.1 Directory of Abbreviations

#### A.1.1 General

Ar	Aryl group
Me	Methyl
Py	Pyridine
Et	Ethyl
Ph	Phenyl
THF	Tetrahydrofuran
DMF	Dimethylformamide
DMSO	Dimethyl sulfoxide
en	Ethylenediamine
tren	Tris(2-aminoethyl)amine
R	Organic group
calcd	Calculated
obsd	Observed
M	Metal atom
Ln	Lanthanide
L	Ligand
ML	Metalloligand
NMR	Nuclear magnetic resonance
EI-MS	Electron-ionization mass spectrometry
IR	Infrared
TGA	Thermogravimetric analysis
MOFs	Metal organic frameworks
CMOFs	Chiral metal organic frameworks
MCPs	Microporous coordination polymers

---

UMCs	Unsaturated metal centers
ICPs	Infinite coordination polymers
SMMs	Single molecule magnets

### A.1.1 NMR Abbreviations

$\delta$	Chemical shift
ppm	Parts per million
s	Singlet
d	Doublet
t	Triplet
m	Multiplet

### A.1.2 IR Abbreviations

br	Broad
w	Weak
m	Medium
s	Strong
vs	Very strong
sh	Shoulder

### A.1.2 Magnetic Abbreviations

SQUID	Super-conducting quantum interference device
ac	Alternating current
dc	Direct current
$D$	zero-field splitting parameter
K	Kelvin
Oe	Oersted
$H$	Field

---

Hz	Hertz
$M$	Magnetisation
T	Tesla
$T_b$	Blocking temperature
$T_c$	Critical temperature
h	Hour
$\chi$	Molar magnetic susceptibility
$\chi'$	In-phase magnetic susceptibility
$\chi''$	Out-of-phase magnetic susceptibility
$\tau$	Relaxation rate
$\mu_B$	Bohr magneton
$U_{eff}$	Effective energy barrier
$\text{cm}^3$	Cubic centimeters

## A.2 Directory of Compounds

- 1  $[\text{Na}_4(\text{NiL})_2 \cdot (\text{H}_2\text{O})_9]_n$
- 2  $[\text{Na}_4(\text{CuL})_2 \cdot (\text{H}_2\text{O})_9]_n$
- 3  $[\text{Li}(\text{NiHL})(\text{DMSO})]_n$
- 4  $[\text{Na}_5\{(\text{NiL}^2)(\text{HCOO})(\text{H}_2\text{O})_{11}\} \cdot (\text{H}_2\text{O})_4]_n$
- 5  $[\text{Na}_4\{(\text{CuHL}^3)_2(\text{MeOH})_2(\text{H}_2\text{O}) \cdot (\text{Et}_2\text{O})\}]_n$
- 6  $[\{\text{Er}_2(\text{NiL})_3(\text{DMF})(\text{H}_2\text{O})_3\} \cdot (\text{DMF})_4 \cdot (\text{H}_2\text{O})_{10}]_n$
- 7  $[\{\text{Tm}_2(\text{NiL})_3(\text{DMF})(\text{H}_2\text{O})_3\} \cdot (\text{DMF})_4 \cdot (\text{H}_2\text{O})_{10}]_n$
- 8  $[\{\text{Yb}_2(\text{NiL})_3(\text{DMF})(\text{H}_2\text{O})_3\} \cdot (\text{DMF})_4 \cdot (\text{H}_2\text{O})_{10}]_n$
- 9  $[\{\text{Lu}_2(\text{NiL})_3(\text{DMF})(\text{H}_2\text{O})_3\} \cdot (\text{DMF})_4 \cdot (\text{H}_2\text{O})_{10}]_n$
- 10  $[\text{Dy}\{(\text{NiL})(\text{DMSO})(\text{NO}_3)\} \cdot (\text{H}_2\text{O})_2 \cdot (\text{DMSO})]_n$
- 11  $[\text{Na}_3\text{Yb}\{(\text{NiL})(\text{H}_2\text{O})\}_3 \cdot (\text{DMF})]_n$
- 12  $[\text{Nd}_2(\text{MnLCl})_2(\text{NO}_3)_2(\text{DMF})_5 \cdot (\text{DMF})_4]_n$
- 13  $[\text{Eu}_2(\text{MnLCl})_2(\text{NO}_3)_2(\text{DMF})_5 \cdot (\text{DMF})_4]_n$
- 14  $[\text{Gd}_2(\text{MnLCl})_2(\text{NO}_3)_2(\text{DMF})_5 \cdot (\text{DMF})_4]_n$
- 15  $[\text{Tb}_2(\text{MnLCl})_2(\text{NO}_3)_2(\text{DMF})_5 \cdot (\text{DMF})_4]_n$
- 16  $[\text{Dy}_2(\text{MnLCl})_2(\text{NO}_3)_2(\text{DMF})_5 \cdot (\text{DMF})_4]_n$
- 17  $[\text{Y}_2(\text{FeLCl})_2(\text{NO}_3)_2(\text{DMF})_5 \cdot (\text{DMF})_4]_n$
- 18  $[\text{Eu}_2(\text{FeLCl})_2(\text{NO}_3)_2(\text{DMF})_5 \cdot (\text{DMF})_4]_n$
- 19  $[\text{Gd}_2(\text{FeLCl})_2(\text{NO}_3)_2(\text{DMF})_5 \cdot (\text{DMF})_4]_n$
- 20  $[\text{Tb}_2(\text{FeLCl})_2(\text{NO}_3)_2(\text{DMF})_5 \cdot (\text{DMF})_4]_n$
- 21  $[\text{Dy}_2(\text{FeLCl})_2(\text{NO}_3)_2(\text{DMF})_5 \cdot (\text{DMF})_4]_n$
- 22  $[\text{Mn}_3(\text{H}_2\text{L}^4)(\text{HL}^2)(\text{OMe})_2 \cdot (\text{MeOH})_2 \cdot (\text{MeOH})_4]$
- 23  $[\text{Ni}_3(\text{L}^4)_2(\text{OAc})_2(\text{DMF})_2 \cdot (\text{H}_2\text{O})_3]$
- 24  $[\text{Eu}(\text{H}_2\text{L}^5)_2 \cdot (\text{EtOH}) \cdot (\text{H}_2\text{O})_9 \cdot (\text{NO}_3)]$
- 25  $[\text{Tb}(\text{H}_2\text{L}^5)_2 \cdot (\text{EtOH}) \cdot (\text{H}_2\text{O})_8 \cdot (\text{NO}_3)]$
- 26  $[\text{Dy}(\text{H}_2\text{L}^5)_2 \cdot (\text{EtOH}) \cdot (\text{H}_2\text{O})_8 \cdot (\text{NO}_3)]$
- 27  $[\text{Er}(\text{H}_2\text{L}^5)_2 \cdot (\text{EtOH}) \cdot (\text{H}_2\text{O})_8 \cdot (\text{NO}_3)]$



- 
- 28  $[\text{Tm}(\text{H}_2\text{L}^5)_2 \cdot (\text{EtOH}) \cdot (\text{H}_2\text{O})_8 \cdot (\text{NO}_3)]$
- 29  $[\text{HNEt}]_2[\text{Eu}(\text{MnL}^5)_2 \cdot (\text{H}_2\text{O})_2 \cdot (\text{ClO}_4)]$
- 30  $[\text{HNEt}]_2[\text{Gd}(\text{MnL}^5)_2 \cdot (\text{H}_2\text{O})_2 \cdot (\text{ClO}_4)]$
- 31  $[\text{HNEt}]_2[\text{Dy}(\text{MnL}^5)_2 \cdot (\text{H}_2\text{O})_2 \cdot (\text{ClO}_4)]$
- 32  $[\text{HNEt}]_2[\text{Tm}(\text{MnL}^5)_2 \cdot (\text{H}_2\text{O})_4 \cdot (\text{ClO}_4)]$
- 33  $[\text{HNEt}]_2[\text{Lu}(\text{MnL}^5)_2 \cdot (\text{H}_2\text{O})_2 \cdot (\text{ClO}_4)]$
- 34  $[\text{Dy} \{ \text{Ni}(\text{H}_2\text{L}^5)(\text{tren}) \}_2 \cdot (\text{H}_2\text{O})_{14} \cdot (\text{NO}_3)_3]$

## Acknowledgements

The work described in this doctoral thesis has been carried out under the guidance and supervision of Prof. Dr. Peter Roesky at the Institute of Inorganic chemistry, Karlsruhe Institute of Technology (KIT). I consider myself to be very lucky to have had the opportunity to work under his supervision. I would like to take the opportunity to convey my sincere thanks and heartfelt gratitude to my supervisor, Prof. Roesky for his excellent guidance, constant encouragement, constructive criticism, and continuous support throughout the course of this work. In addition, his friendly nature and easy-going attitude made my stay pleasant here.

I would like to express my thanks to Dr. Michael Gamer for measuring and solving the crystal structure and for his invaluable suggestions and corrections during writing of my thesis.

I appreciate Petra for measuring the crystals and providing valuable tips on solving my crystal structures.

I would like to thank Sibylle for measuring the single crystals and thermogravimetric analysis.

Thanks to Dr. Christoph Riehn for his help with the ESI-MS spectrum.

I would like to thank Dr. Yanhua Lan for performing the SQUID measurements of my compounds and for their magnetic studies, Prof. Liviu F. Chibotaru for *ab initio* calculations, Prof. Sven Kureti for studies the gas adsorption properties and Dr. Marco Neumaier for his help with the ESI-MS spectrum.

I am grateful to Partha Pratim Jana and Dr. Klaus Harms for providing the single crystal data.

Thanks to various staff members of this university, Frau Kayas and Frau Pendl (Paper work) Frau Berberich (NMR), Frau Lude (Elemental analysis), Herr Müller (Mass spectra) Herr Rieß, Herr Lampert and Herr Kastner (Mechanical workshop), Herr Schlachter (Electrical workshop), Frau Leichle, Frau Böcker (Chemical store), Herr Munshi (Glassblowing) and Frau Maurer for their kind help.

I would like to thank Dr. Murugesapandian Balasubramanian, Dr. Paul Benndorf, Dr. Jelena Jenter, Dr. Ralf Köppe, Dr. Tianshu Li, Dr. Karolin Löhnwitz, Dr. Sebastian Marks, Dr. Hari Pada Nayek, Dr. Dominique Thielemann, Dr. Michal Wiecko, Nicholas Arleth, Denise Girnt, Claude Kiefer, Jochen Kratsch, Magdalena Kuzdrowska, Anja Lühl, Tanja Sanden, Christian Sarcher, Matthias Schmid and Larissa Zielke help with various parts of this work.

I am grateful to Dr. George Kostakis and Christine Morrison for their help with my thesis corrections.

Thanks to Dr. Kartik Mondal for his all kind help.

My sincere thanks to all the faculty members of chemistry department of IIT Bombay for their guidance, constant encouragement and help, without which, I would not have been able to pursue my research.

I would like to thank Prof. B. D. Gupta. Without his help, it would not have been possible to pursue my research in Germany.

Finally, my whole hearted thanks to my parents, my brothers and my whole family for their continuous support and encouragement which made my work possible. At the same time, my deepest gratitude goes to my friend Subarna for her continuous support. Thanks also to Arnab, Anupam, Manas, Mrinal, Samir, Sandip, Prasad and Souvik for their friendship.

---

## Curriculum Vitae

Name	Asamanjoy Bhunia
Date of Birth	9 <sup>th</sup> July, 1982
Place of Birth	Midnapore, West Bengal, India
Sex	Male
Marital Status	Single
Nationality	Indian

### Education

Ph. D. in Chemistry	(2008-present) Department of Chemistry, Karlsruhe Institute of Technology, Germany.
Thesis Supervisor	Prof. Dr. Peter Roesky
Thesis Title	Functionalized 3d/4f Coordination Oligomers and Polymers
Master of Science	(2007) Department of Chemistry, Indian Institute of Technology Bombay, India.
Bachelor of Science	(2005) Chemistry (Honors), Vidyasagar University, Midnapore, India.

### Publications

- 1) Salen-Based Infinite Coordination polymers of Nickel and Copper. Asamanjoy Bhunia, Peter W. Roesky, Yanhua Lan, Annie K. Powell, *Inorg.Chem.* **2009**, *48*, 10483-10485.
- 2) Salen-based metal organic frameworks of nickel and the lanthanides. Peter W. Roesky, Asamanjoy Bhunia, Yanhua Lan, Annie K. Powell and the Sven Kureti, *Chem. Commun.* **2011**, *47*, 2035-2037.

- 3) From a Dy(III) Mononuclear Single Molecule Magnet (SMM) to a Ferromagnetic [Mn(II)Dy(III)Mn(II)] Trinuclear Complex: 3d-4f Exchange Induced Quenching of SMM Behavior. Asamanjoy Bhunia, Michael T. Gamer, Liviu Ungur, Liviu F. Chibotaru, Annie K. Powell, Yanhua Lan, Peter W. Roesky, Fabian Menges, Christoph Riehn, and Gereon Niedner-Schatteburg, *Submitted*.
- 4) Salen-Based Metal Organic Frameworks of Iron and the Lanthanides. Asamanjoy Bhunia, Yanhua Lan, Valeriu Mereacre, Michael T. Gamer, Annie K. Powell,\* and Peter W. Roesky, *Submitted*.

